PYROLYSIS OF DIFFERENT COAL TYPES

by

Glen H. Ko

B.A.Sc in Chemical Engineering
The University of British Columbia (1984)

Submitted to the Department of Chemical Engineering
in Partial Fulfillment of the Requirements for the
Degree of

DOCTOR OF PHILOSOPHY

at the

MASSACHUSETTS INSTITUTE OF TECHNOLOGY

August, 1988

Signature of Author _____
Department of Chemical Engineering
August, 1988

Certified by _____
Prof. Jack B. Howard
Thesis Supervisor

Certified by _____
Dr. William A. Peters
Thesis Supervisor

Accepted by _____
Prof. Robert G. Armstrong
Chairman, Departmental Graduate Committee

by

Glen H. Ko

Submitted to the Department of Chemical Engineering at the Massachusetts Institute of Technology in August 1988, in partial fulfillment of the requirements for the degree of Doctor of Philosophy in Chemical Engineering.

Abstract

Coal-type effects on rapid pyrolysis behavior were investigated. The experimental phase of this study examined the pyrolysis behavior of six (6) selected coals ranging from lignites to low-volatile bituminous coals, and under conditions where mass transport resistances are small (1 atm and $\tilde{<}$ 100 μm particle dia.). To experimentally establish coal-type effects, time-resolved product evolution measurements were made for tars, gases and total volatiles using a constant heating rate of 1000 C/s up to a maximum temperature of 1050 C. The modeling phase of this work derived kinetic information from the experimental data, using the multiple independent parallel reaction (MIPR) and extended MIPR models, and attempted to relate the kinetic information to measurable properties of the coal.

Among the six coals studied, higher rank coals generally produced tars at higher temperatures, and over a narrower range of temperatures. Consequently, a larger mean and a narrower distribution of global activation energies were obtained using the MIPR model for coals of increasing rank. Predicted tar yields from the extended MIPR model agreed well with experimental values for a wide range of coal types (lignites to low-volatile bituminous coal; non-softening and softening) and pressures (0.001-10 atm). The parameter values used to make predictions are within the range of expected values. A quantitative correlation, developed to independently relate tar yield limits to coal type and pressure, was tested against a large set of experimental data representing a wide range of coals and pressures. Good agreement between the predicted and experimental yields were obtained for all coals and pressures, with a standard error of estimate of ±3wt% dmmf.

In general, no discernable coal-type effects on the apparent rate of gas production was observed. Consequently, kinetic parameters of the MIPR model for measured gas species were only slightly affected by coal type. Higher rank coals generally produced less carbon oxides and pyrolytic water, but more methane. The ethylene and ethane yields are small and their absolute yields were less affected by coal type.

Total volatiles evolve at higher temperatures and over a narrower range of temperatures for higher rank coals. Thus as expected, a larger mean and a narrower distribution of global activation energies were obtained using the MIPR model for coals of increasing rank. The total volatiles yield limit is fairly constant among the lignites,

subbituminous and high-volatile bituminous coals, but is significantly less for low-volatile bituminous coal. The high-volatile bituminous coals produced significantly more reactive volatiles (total volatiles-H_2O and CO_2) than other coals.

Thesis supervisors:
Professor Jack B. Howard, Department of Chemical Engineering
Dr. William A. Peters, Energy Laboratory

Acknowledgements

My supervisors, Prof. J.B. Howard and Dr. W.A. Peters, have generously provided many hours of valuable discussions and suggestions. Their always careful guidance and constant encouragement during this work are deeply appreciated.

Helpful comments from my thesis committee members, Profs. J.M. Beér, J.P. Longwell and A.F. Sarofim, are gratefully acknowledged.

Several M.I.T. undergraduate students have made valuable contributions in this work: Thomas Kronenberger - coal structure study, Steve Beaudoin - experimental set-up, Jefferey Hwang - computer modeling, and Debbie Sanchez - experimental runs. Special thanks to Debbie for the help during the many months of collecting data.

Sharing ideas, friendship, and many other things with colleagues and friends met during my stay at M.I.T. have been a very valuable part of my learning experience here - B.Barat, Dr.M.Boroson, A.Bouhris, S.Choi, G.Darivakas, Dr.W.Fong, T.Griffin, Dr.M.Hajaligol, P.Kwon, F.Lam, T.McKinnon, D.Mess, Dr.C.Vaughn, P.Utthoff, H.Yoon, and J.Xiao- thanks.

The financial support provided by the 1967 Natural Sciences and Engineering Research Council Scholarship, and by the U.S. Department of Energy under Contract No. DE-RA21-85MC-22049 are gratefully acknowledged.

My family and family-in-law-to-be have given me a lot of support. My fiancée, Susie, has been very understanding and patient. Thanks for all your love, help, and encouragement.

Table of Contents

List of Figures

List of Tables

1. Summary

1.1. Introduction

Investigation of the pyrolysis behavior of different coal types is important as the vast coal reserves in the U.S. consist of many different coal types with widely varying chemical and physical properties, and since pyrolysis occurs during initial stages of almost all coal conversion processes, including combustion, gasification and liquefaction. Coal pyrolysis involves complex thermal decomposition reactions coupled with multicomponent mass transport in a molten liquid or porous solid depending on whether the coal is a softening type or not.

Understanding the influence of coal type on pyrolysis behavior requires a reliable experimental data base to determine the kinds and extents of coal-type effects, and a mathematical model to explain the observed behavior. Quantitative time-resolved product evolution measurements for a wide range of coal types are needed to experimentally establish coal-type effects, but such data are currently lacking. In response, the experimental phase of this study examines the pyrolysis behavior of six coals ranging from low-rank lignites to very high-rank bituminous coals. Attempts are made to relate the observed behavior to measurable properties of the coal. The modeling phase of this work derives kinetic information from the experimental data using the multiple independent parallel reaction (MIPR) model and the extended MIPR model. The former model describes the kinetics of product evolution under conditions where the effects of physical transport are relatively unimportant, whereas the latter model explicitly includes approximate descriptions of transport effects, and

Table 1.2-1: Ultimate and proximate analysis of the six selected coals in this study[a]

coal	Lower Wilcox	Beulah Zap	Smith Roland	Blue	Illinois #6	Lower Kittanning
coal-rank[b]	L	L	SB	HVB	HVB	LVB
Ultimate analysis wt%,dry						
C	56.0	60.2	62.0	74.9	67.4	82.5
H	4.2	4.0	4.6	5.0	4.4	4.5
N	1.1	1.0	1.0	1.4	1.3	1.3
S	0.7	1.1	1.1	0.8	3.9	1.2
O	19.9	21.6	19.5	13.7	8.7	2.4
ash	20.3	15.0	13.0	4.5	15.6	8.9
Proximate analysis wt%,dry						
moisture[c]	3.0	3.0	3.0	4.0	4.0	1.0
volatile matter	45.3	42.0	45.2	43.3	35.7	16.3
fixed carbon	34.4	43.0	41.8	52.2	48.7	74.8
ash	20.3	15.0	13.0	4.5	15.6	8.9

[a] analyzed by Huffman Laboratories, Inc.
[b] L = lignite, SB = subbituminous, HVB = high-volatile bituminous, LVB = low-volatile bituminous.
[c] partially vacuum dried.

Table 1.2-2: Summary of experimental conditions employed in this study

reactor variables:	coal type	temperature-time history	pressure	particle size
varied (v) or fixed (f)	v	f	v	f
range covered	lignites to low-volatile bituminous coals, elemental carbon content ranges 72-92 wt% dmmf.	1000 C/s heat-up, 200-1000 C/s cool-down, 1050 C max. temperature.	10^{-3}-10 atm	75-90 μm dia.

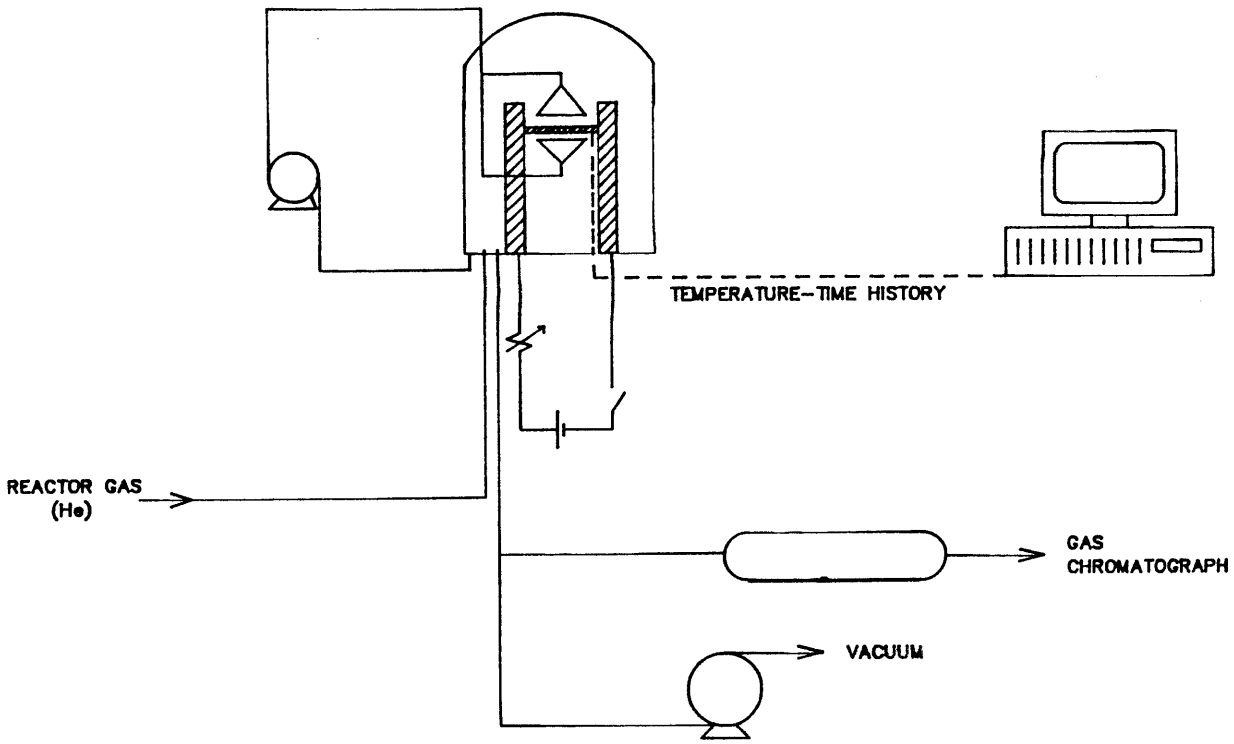

Figure 1.2-1 The reactor assembly, product collection, and data acquisition system.

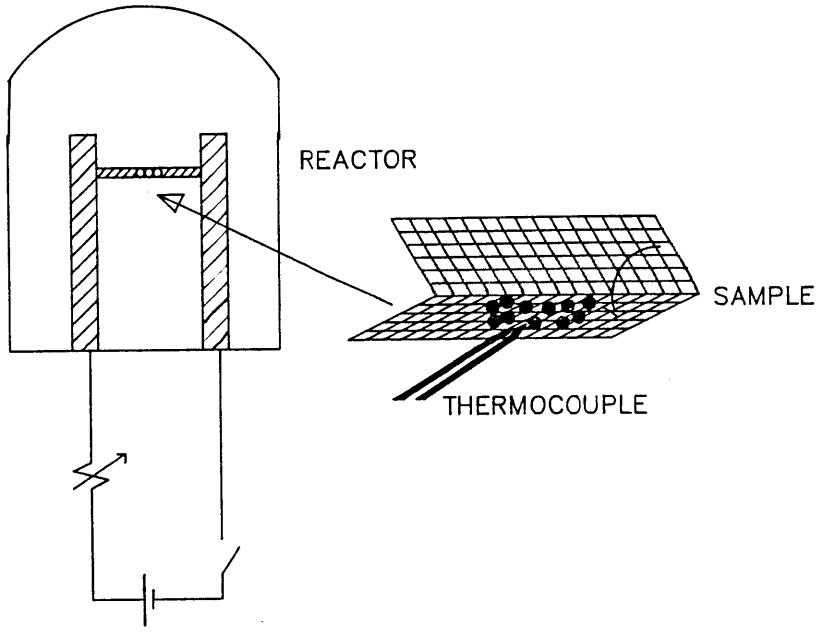

Figure 1.2-2 Details of the electrical screen-heater reactor.

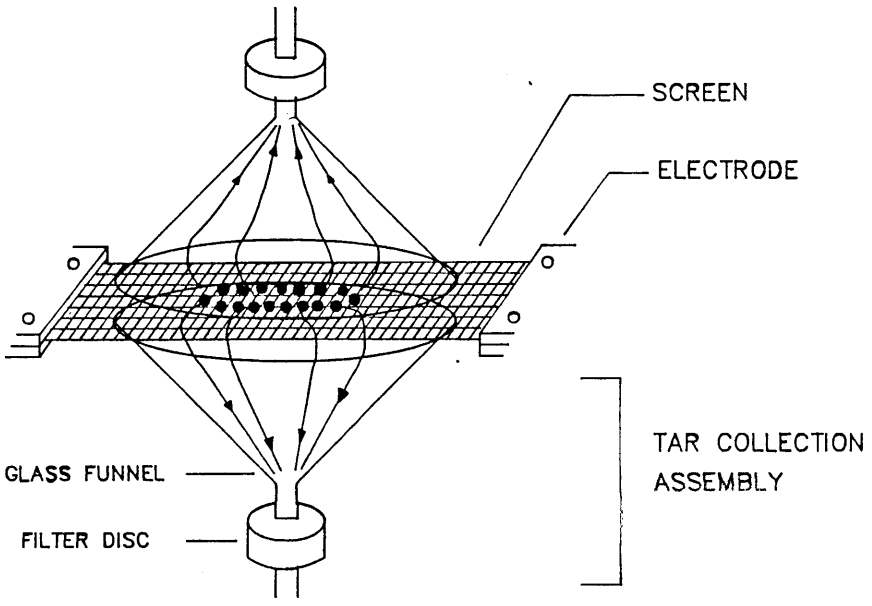

Figure 1.2-3 Tar collection assembly

thus is applicable over a wider range of operating conditions.

1.2. Experimental studies

1.2.1. Experimental procedures

The six chosen coals for this study are: Beulah Zap, ND (lignite A); Lower Wilcox, TX (lignite A); Smith Roland, WY (subbituminous B); Blue, NM (high-volatile bituminous C); Illinois #6, IL (high-volatile bituminous A); and Lower Kittanning, PA (low-volatile bituminous). Table 1.2-1 gives the ultimate and proximate analysis of the selected coals. The experimental conditions employed in this study are summarized in Table 1.2-2.

An electrically heated screen-heater type reactor (Fig.1.2-1) was used to measure the apparent evolution kinetics and the yield limit of volatile products for the six coals. This reactor type has been extensively used in past pyrolysis studies (Anthony et al., 1974; Suuberg, 1977; Fong, 1986), as it offers many advantages important in kinetic studies including reliable temperature measurement of the sample over a wide range of heating rates, rapid quenching and dilution of volatile products upon leaving the coal particle surface, and ability to work over a wide range of pressures. In a typical low pressure run (10^{-3} to 1 atm), about 20 mg of 75-90 μm diameter particles spread thinly in the central region of 10 cm x 5 cm, folded 400 mesh stainless steel screen (Fig.1.2-2) are pyrolyzed under a controlled temperature-time history. To ensure thin well dispersed coal particles, smaller sample sizes ($\approx$5 mg) had to be used in high pressure runs (10 atm) since smaller screens are used in the high pressure reactor. The sample temperature is measured using a very thin

Chromel-Alumel thermocouple (0.0005 in. foil) placed within the folded screen near the coal particles. The reactor gas, ultra high purity He (99.999%), remains near room temperature, and provides rapid dilution and quenching of volatiles as soon as they are evolved from the coal surface, thus presenting minimal opportunity for further reactions of volatiles outside the particle.

Tars, light hydrocarbon gases, carbon oxides, and water are the major volatile products from coal pyrolysis. Tars are operationally defined as the sum of all volatile products (except water) that condense in the reactor at room temperature, and were collected using the tar trap assembly shown in Fig.1.2-3. The gas yields were measured using a Perkin Elmer Sigma 2B Gas Chromatograph equipped with thermal conductivity and flame ionization detectors.

1.2.2. Experimental results and discussion

Coal-type effects on tar production. Figure 1.2-4 shows the atmospheric pressure tar yield versus peak temperatures for the six coals studied. Heating and cooling rates in these runs were respectively 1000 and 200-1000 C/s with no holding time at peak temperatures, and with a maximum peak temperature of 1050 C. The lines through the data points in Fig.1.2-4 were hand-drawn to indicate trends. Individual plots with model predictions are given in Fig.1.3-3. Qualitatively, the figure shows that there is a clear effect of coal type on both the apparent rate of tar production and the yield limit, defined as the asymptotic yield at high peak temperatures ($\tilde{>}$ 800 C). Low-rank coals (ZP,LW,SR) tend to initiate and achieve given extents of tar production at lower temperatures compared to higher rank

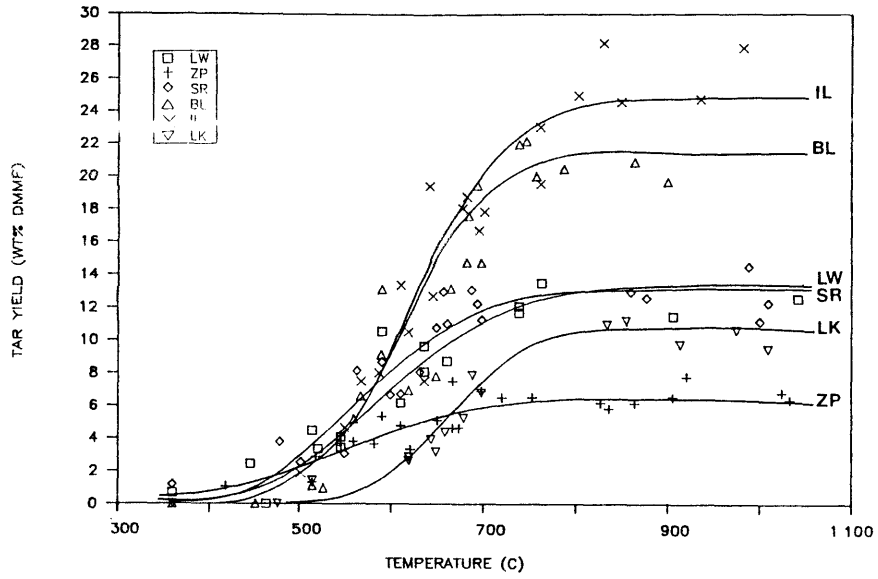

Figure 1.2-4 Experimental yields of pyrolysis tar versus peak temperature for the six selected coals in this study. Carbon: LW < ZP < SR < BL < IL < LK. Abbreviations: LW = Lower Wilcox lignite, ZP = Beulah Zap lignite, SR = Smith Roland subbit., BL = Blue high-volatile bit., IL = Illinois high-volatile bit., LK = Lower Kittanning low-volatile bit.

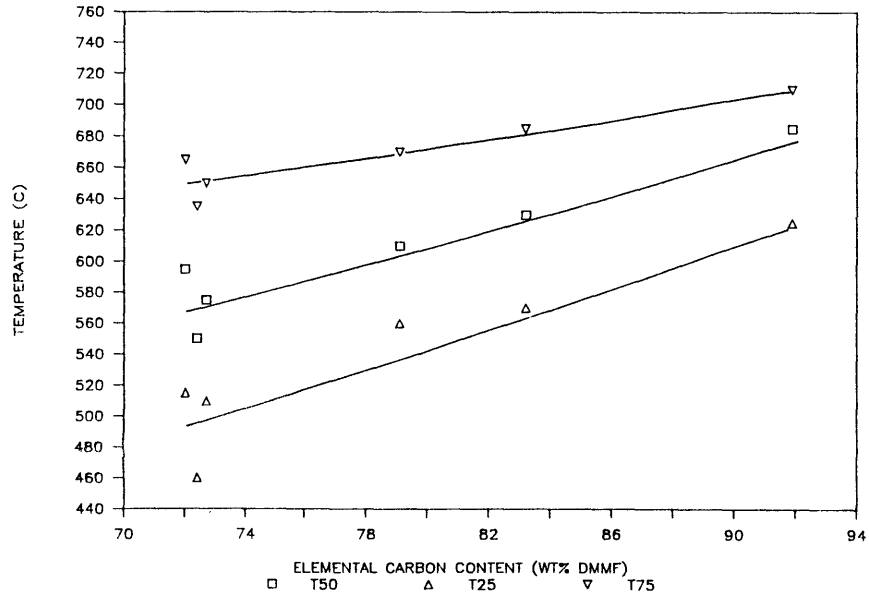

Figure 1.2-5 Characteristic yield temperatures for tar production versus elemental carbon content for the six coals studied (Tx denotes the temperature at which the yield reaches x% of the maximum yield). Carbon: LW < ZP < SR < BL < IL < LK. Abbreviations: see Fig.1.2-4.

coals (BL,IL,LK); abbreviations are defined in Fig.1.2-4. These points are reinforced by quantitative observations on the apparent rate of tar production presented in Fig.1.2-5, which compares the temperatures at which the tar yield reaches 25% (T25), 50% (T50), and 75% (T75) of the yield limit for the six coals represented by their elemental carbon contents in wt% dmmf. The three characteristic temperatures were determined from the tar data fitted with the MIPR model (see Fig.1.3-3). The difference between T75 and T25 (T75-T25) represents an approximate spread of the yield curve, whereas T50 roughly corresponds to the temperature at which the observed tar evolution rate is maximum. Comparing T50 shows almost a monotonic increase with coal rank represented by the elemental carbon content of the coal, indicating a shift in the yield curve to higher temperatures for higher rank coals. T50 ranges from 550 C for ZP to 685 C for LK, an increase in the maximum difference of about 135 C among the coals studied. Comparing (T75-T25) shows a decreasing trend for higher rank coals, indicating less spread in the yield curve for higher rank coals. The difference ranges from 175 C for ZP to 85 C for LK, a reduction in the maximum difference of about 90 C.

An exact description of the complex reaction chemistry and transport phenomena involved in tar production is currently not available. Thus, interpretation of the observed tar evolution rate behavior for different coal types, depends on the assumed mechanism for tar formation. A frequently assumed mechanism is the decomposition of 'tar precursors' in the coal via multiple first-order independent parallel reactions (Serio, 1984; Ko et al., 1988a)

$$\text{Tar precursors in coal} \xrightarrow[\text{transport}]{\text{first-order decomposition}} \text{Tar}$$

The model parameters for this global decomposition reaction are influenced by physical transport effects. Under such a global description and with the further assumption that all coals have the same preexponential factor in the Arrhenius rate constant, a higher T50 implies that tars are produced from reactions with greater apparent activation energies. Similarly, a larger (T75-T25) implies a wider distribution of apparent activation energies. Thus, under the assumptions of this global description, higher rank coals appear to produce tars from reactions with apparent activation energies that have a higher mean but a narrower distribution.

The tar yield limit data from this study and from the literature indicate that coal-rank information alone is not enough to quantitatively explain the observed trend. A new approach to quantitatively relate the tar yield to measurable properties of the coal is given below (Ko et al., 1987, 1988b). The predictive capability of the new correlation is tested against a large set of experimental data from this study and the literature, representing a wide range of coals (37 coals, ranging from lignites to anthracites) and pressures ('vacuum' to 90 atm). Table 1.2-3 gives the elemental analysis and measured tar yield under a specified pressure for each coal. The data represent the maximum amount of tar generated during rapid devolatilization (heating rate = 100-1500 C/s, max. T $\approx$ 1000 C) with minimal influence from secondary reactions outside the coal particle (small sample mass and particle sizes).

Table 1.2-3 Characteristics of coals and experimental tar yields used in the tar yield limit correlation.

Investigator	Coal[a]	Elemental Analysis (wt% dmmf) C	O[b]	H	So[c]	Tar yield (wt% dmmf; symbols used in Figs. 5.1-4 and 5.1-5) at pressures (MPa) of 10^{-4}-10^{-5}	0.01	0.1	1	6.9	9
Freihaut and Seery (1981)	Montana L	68.3	25.5	4.6	0.7	▲18.0[f]					
	Wyodak SB 1	75.4	18.1	4.9	0.4	▲20.0					
	Wyodak SB 2	75.5	17.0	5.2	0.6	▲21.0					
	Utah B	78.2	13.9	5.5	0.8	▲27.0					
	Colorado B	81.0	11.2	5.5	0.6	▲26.0[f]					
	Pittsburgh B	82.0	9.4	5.4	1.9	▲39.0					
	Alabama B	85.0	8.2	4.6	0.5	▲25.0					
	Anthricite	93.7	1.9	2.6	0.7	▲ 2.0					
Freihaut et al. (1982)	Colorado B	81.0	11.2	5.5	0.6		△19.8[d,f]	△19.2[f]			
	Pittsburgh B	82.0	9.4	5.4	1.9		△28.1[d]	△26.0			
Loison and Chauvin (1964)	Faulquemont B	80.8	12.8	5.1	0.5	◥20.0					
	Wendel III B	86.1	8.3	5.3	0.3	◥24.3					
	Lens-Lievin B	88.4	6.4	5.0	0.6	◥27.0					
	Emma B	88.5	5.4	4.7	0.5	◥20.5					
	Bergmannsgluck B	89.0	5.2	4.6	0.7	◥17.6					
	Maigre Oignies B	91.9	4.4	3.8	0.4	◥15.1					
	Flenus de Bruay B	86.7	6.4	5.1	0.5	◥ 2.1					
Oh (1985)	Pittsburgh B	82.2	10.0	5.9	1.9	◥39.8		◺29.3			
Arendt and van Heek (1981)	Prosper II B	91.5	2.7	4.4	0.7		⊙ 9.9		⊕ 6.6		⊙ 3.7
	Schlaegel u. Eisen B	90.1	3.7	4.3	0.5		⊙17.7		⊕12.2		⊙ 7.5
	Wulfen B	87.6	5.7	4.7	0.6		⊙26.5		⊕19.3		⊙14.1
	Leopold B	84.2	8.4	5.7	0.9		⊙28.4	○25.7	⊕19.8		⊙15.2
Suuberg (1977)	Pittsburgh B	81.0	9.7	5.7	1.9	▼37.0		▽26.5		▽13.8	
Cosway (1981)	Montana L	72.2	22.0	4.6	0.8	▼ 8.4		▽ 6.5		▽ 3.2	
Reitzen (1978)	Wyodak SB	73.1	19.8	6.1	0.4			◸19.3			
	Sesser SB	82.9	10.3	5.4	0.4			◸21.5[e]			
	Colstrip L	76.8	17.4	4.9	0.5			◸11.5			
This Study	Lower Wilcox L	72.0	20.9	5.6	0.4	■16.8		□13.1	⊞ 9.9		
	Illinois B	83.2	9.8	5.4	2.0	■30.1		□24.8	⊞15.0		
	Blue SB	79.1	14.1	5.3	0.4	■27.7		□21.2	⊞14.5		
	Beulah Zap L	72.4	21.6	4.8	0.6	■ 9.1		□ 7.2	⊞ 4.1		
	Lower Kittanning B	91.9	1.7	5.0	0.6	■14.0		□10.7	⊞ 6.5[h]		
	Smith Roland L	72.7	20.9	5.3	0.5	■14.8		□12.9	⊞11.1		
Suuberg et al. (1987)	Pocahantas B	91.3	4.1	4.6	0.2			◸ 9.9			
	North Dakota L	74.5	20.5	4.1	0.5			◸ 5.6			
	Illinois B	78.6	14.6	5.4	2.0			◸22.8			
	Bruceton B	85.1	7.6	5.6	0.5			◸26.5			
Suuberg et al. (1985)	North Dakota L	75.4	19.1	4.1	0.5	◢ 6.7					
	Bruceton B	85.1	7.6	5.6	0.5	◢37.7					
Bautista (1984)	Pittsburgh B	84.7	7.9	5.8	0.7	◆38.6		◇30.0	◇29.7(0.2)[g]		
									◇26.5(0.4)		
									◇25.2(0.7)		
									◇23.7(1.0)[d]		
									◇21.1(1.5)		
									◇20.6(2.4)		

[a] B-bituminous; L-lignite; SB-subbituminous
[b] By Difference
[c] Estimated as half the total sulphur content when organic sulphur not reported (Loison and Chauvin, 1964; Arendt and van Heek, 1981; Cosway, 1981; Reitzen, 1978; Suuberg et al., 1985, 1987; Bautista, 1984; this study).
[d] Obtained by interpolation between 0.0007 and 0.013 MPa in Freihaut et al. (1982), and between 0.7 and 1.5 MPa in Bautista (1984).
[e] The tar yield (6.5 wt% dmmf) reported for Sesser SB seemed low and was substituted by the 21.5 wt% dmmf measured in this study.
[f] Colorado B and Montana L from Freihaut and Seery (1981), and Freihaut et al. (1982) were not used because possible errors in tar yield measurement are suspected.
[g] Indicates pressure in MPa.
[h] This value is slightly lower than the previously reported value (7.2 wt% dmmf) in Ko et al. (1988b)

Formulation of correlation: treatment of coal-type effects.

(1) Chemical and physical mechanism of tar production. Tar is assumed to be generated via the global mechanism first suggested by van Krevelen (1961):

$$\text{Coal} \xrightarrow[\text{of bridges}]{\text{[1] thermolysis}} \text{Metaplast} \xrightarrow{\text{[2] transport}} \text{Tar}$$

(2) Important chemical structures. The identities and numbers of bridges between aromatic clusters of the coal and the concentration of hydrogen available to stabilize the free radicals created by bridge scission reactions are important structural chemical factors in tar generation without transport effects. Since the structural features important in the transport process, [2] in the assumed mechanism, are not easily identifiable, the transport effect is correlated via empirical parameters obtained from best-fit analyses of existing data.

(3) Formulation of coal-specific parameter. A coal-specific parameter, X_{TAR}, proposed to correlate tar yields with coal type is

$$X_{TAR} = \frac{(\text{no. of labile bridges})(\text{amt. of abstractable hydrogen})}{(\text{no. of cross-linked bridges})} \qquad (1.2\text{-}1)$$

(4) Estimation of identified structures. Since the necessary molecular structures are generally unavailable for most coals, reasonable estimates were made for each quantity based on currently available information. Table 1.2-4 gives procedures to estimate the three quantities in X_{TAR}.

Formulation of correlation: treatment of pressure effects.

Tar yield limit at a given pressure is linearly correlated with the coal-type parameter derived above:

$$\text{Tar yield limit (wt\% dmmf)} = \alpha(P) + \beta(P)X_{TAR} \qquad (1.2\text{-}2)$$

The pressure dependent coefficients α and β are obtained by best

Table 1.2-4 Equations to compute X_{TAR}

- number of labile bridges = $\{(1-f_a)[C]/12\}^{1.8}$

assumption: Labile bridges are only aliphatic, and their concentration is assumed to be proportional to the aliphatic carbon content of of the raw coal. The fraction $(1-f_a)$ also contains contributions from carboxyl, carbonyl and ether carbons, but these are assumed to be small. The exponent 1.8 is a best-fit parameter obtained by applying multivariable fitting routines to obtain the best correlation between tar yields and X_{TAR}.

- number of cross-linked bridges = $\begin{cases} [O]/16 + [So]/32.066 & \text{if } [O] > 3.5 \text{ wt\% dmmf} \\ 3.5/16 + [So]/32.066 & \text{if } [O] \leq 3.5 \text{ wt\% dmmf} \end{cases}$

assumption: Cross-linked bridges consist only of ether and thioether structures, whose concentration is assumed to be proportional to the sum of elemental oxygen and organic sulphur contents of the raw coal. A constant [O] was needed for coals with low elemental oxygen contents because the number of cross-linked bridge is highly sensitive to coal elemental oxygen contents below about 4 wt% dmmf, and uncertainties in oxygen measurement can easily exceed ±1 wt% dmmf.

- amount of abstractable hydrogen = $[H]/1 - [OH]/17$

assumption: Abstractable hydrogen is the hydrogen attached to aliphatic carbons. Its concentration is proportional to the amount of elemental hydrogen in the raw coal, minus a slight correction to account for experimental observations that OH groups may compete for the abstractable hydrogen (Suuberg, 1977).

Notations:
[C] = the elemental carbon content (wt% dmmf)
[O] = the elemental oxygen content (wt% dmmf)
[So] = the organic sulphur content (wt% dmmf)
[H] = the elemental hydrogen content (wt% dmmf)
f_a = aromaticity
= $0.830526 - 2.008147([C]/100) + 2.241218\ ([C]/100)^2$
(polynomial best-fit of f_a versus [C] using data from Gerstein et al., 1982)
[OH] = the hydroxyl group content (wt% dmmf)
= 33.2 - 0.35 [C] (Given, 1976)

fitting experimental tar yield data either for a specified pressure or pressure range (Table 1.2-5a), or for all pressures (Table 1.2-5b). Figure 1.2-6 compares measured maximum tar yields with those predicted using the pressure-specific coefficients [Eq.(1.2-2), Table 1.2-5a]. The predicted yields are within ± 5 wt% dmmf of the observed values for all coals tested at the four pressures and pressure ranges. The standard error of estimate of the prediction was 2.8 wt% dmmf. The standard error of estimate was computed using the definition

$$\text{standard error of estimate} = \sum_{j=1}^{n} \left[\frac{(\text{Yield,j,exp'l} - \text{Yield,j,pre'd})^2}{n-k} \right]^{1/2} \qquad (1.2\text{-}3)$$

where n is the number of data points (j), and k the number of best-fitted parameters used in the correlation. Figure 1.2-7 compares experimental data for all pressures with predictions obtained using the pressure-correlated parameters [Eq.(1.2-2), Table 1.2-5b]. The predicted yields are within ±6 wt% dmmf for all coals. Use of the pressure-correlated parameters has the advantage that it is applicable for all pressures between 10 Pa to 9 MPa, but suffers from a slightly greater standard error of estimate of 3.1 wt% dmmf.

Coal-type effects on gas production. Figure 1.2-8 compares the yield limit of gaseous products versus the elemental carbon content for the six coals investigated in this study, and the two coals studied by Suuberg (1977) under similar but not identical experimental conditions. Higher rank coals generally produce less carbon oxides and pyrolytic water, but more methane; the ranges for CO, CO_2, H_2O, CH_4 are 0.9-11.0, 0.4-9.9, 2.4-16, 1.6-4.3 wt% dmmf respectively. The ethylene and ethane yields are small and their absolute yield values are less

Table 1.2-5 Best-fit parameters of pressure dependent coefficients α and β for use in Eq.(1.2-2)

(a) pressure-specific coefficients (α / β)

	$X_{TAR} < 15$	$15 \leq X_{TAR} \leq 31$	$X_{TAR} > 31$
10-100 Pa	2 / 0	-30.8125 / 2.1825	37 / 0
0.1 MPa	2 / 0	-22.375 / 1.625	28 / 0
1 MPa	2 / 0	-16.75 / 1.25	22 / 0
2.5-9 MPa	2 / 0	-10.1875 / 0.8125	15 / 0

(b) pressure-correlated coefficients

	$X_{TAR} < 15$	$15 \leq X_{TAR} \leq 31$	$X_{TAR} > 31$
α	2	$1/(0.021533 + 0.028651L_p) - 36$	$11.24071 + 9.743707L_p - 0.91326L_p^2$
β	0	$0.508030 + 0.696487L_p - 0.06959L_p^2$	0

$$L_p = -\log_{10}P + 1$$

$$P = \begin{cases} \text{reactor pressure in MPa for } P \leq 2.5 \text{ MPa (1 MPa} \approx \text{10 atm)} \\ \text{fixed at 2.5 MPa for reactor pressure above 2.5 MPa}^a. \end{cases}$$

[a] This was justified since pressure has negligible effects on tar yield above 2.5 MPa. Bautista (1984) observed that tar yield did not decline with increasing pressure above ≈2 MPa, and the present work (Fig.1.2-6) found a close agreement between predictions and data using 2.5 MPa to represent pressures from 2.5-9 MPa.

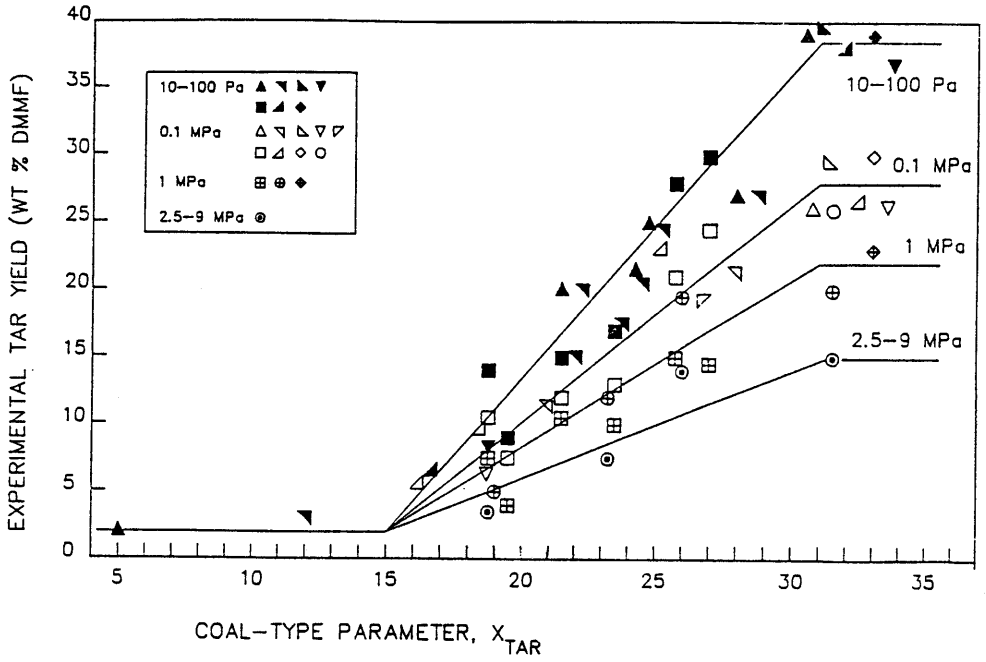

Figure 1.2-6 Correlation of tar yields at different pressures with X_{TAR}. Symbols: see Table 1.2-3. Lines are from Eq.(1.2-2) and Table 1.2-5a.

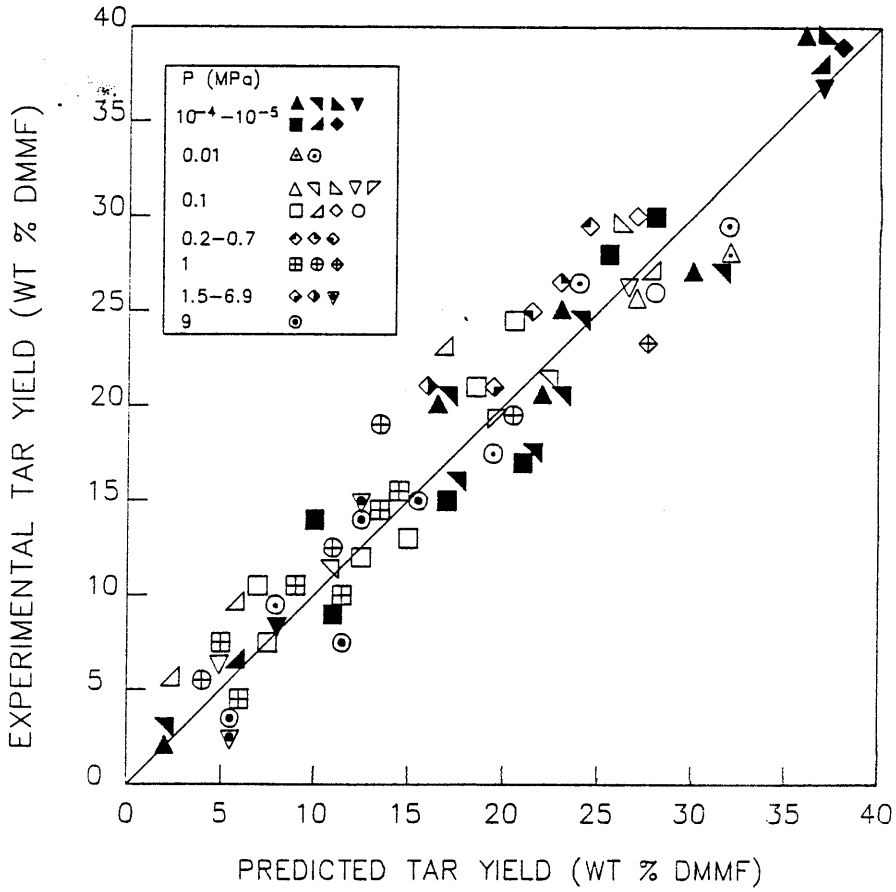

Figure 1.2-7 Comparison of experimental tar yields with those predicted by Eq.(1.2-2) and Table 1.2-5b. Symbols: see Table 1.2-3.

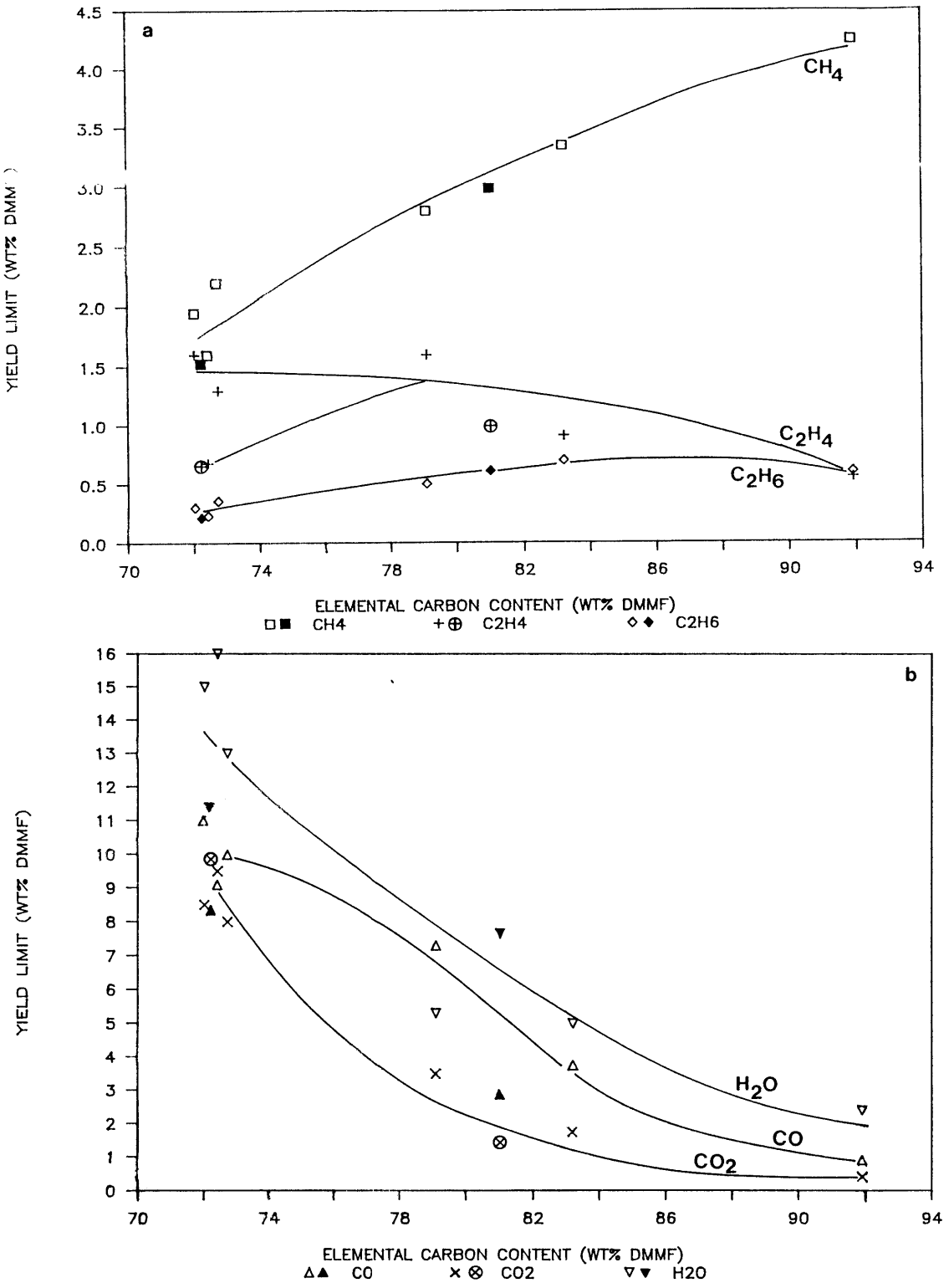

Figure 1.2-8 Comparison of the yield limit of gaseous products versus the elemental carbon content: (a) hydrocarbons; (b) carbon oxides and pyrolytic water. Open or non-circled symbols are from this study; closed or circled symbols are from Suuberg (1977). Carbon: LW < ML < ZP < SR < BL < PB < IL < LK. Abbreviations: ML = Montana lignite, PB = Pittsburgh Seam bituminous, see Fig.1.2-4 for others.

affected by coal type; they range from 0.6 to 1.6 wt% dmmf for ethylene and from 0.2 to 0.7 wt% dmmf for ethane. The higher carbon oxides and water yields have been associated with higher concentrations of carboxyl and hydroxyl groups respectively in lower rank coals (Suuberg, 1977). However, an exact reaction mechanism is not yet available to quantitatively rationalize the relationship. Methane production has been postulated to occur via bond dissociation of alkyl groups to yield methyl radicals, which upon abstracting hydrogen form methane (Gavalas et al., 1981). But applying such a mechanism to explain the observed trend for methane yields is difficult due to the lack of the necessary quantitative structural information, e.g., in particular the concentration of alkyl groups.

Figure 1.2-9 compares the apparent evolution rates of (a) CH_4, (b) C_2H_4, (c) C_2H_6, (d) CO, and (e) CO_2 for the six coals investigated. Each figure shows three characteristic yield temperatures (T25, T50, and T75) obtained from the experimental data (Figs. 1.3-5 to 1.3-9 respectively) versus the elemental carbon content of the coal. Comparing T50 shows a slightly increasing trend with coal rank for methane and ethane (Fig.1.2-9a,c), but almost no observable effect for ethylene and carbon oxides (Fig.1.2-9b,d,e). The spread of the yield curve as indicated by (T75-T25) appears to be unaffected by coal type for all gases, except for carbon dioxide, which shows a decreasing trend for higher rank coals.

Reasons for the lack of observable coal-type effects on the apparent rate of gas production are currently unclear. One hypothesis is that the kinetics of gas production are unaffected by coal type (Solomon and Hamblen, 1985). Gaseous products are claimed to evolve

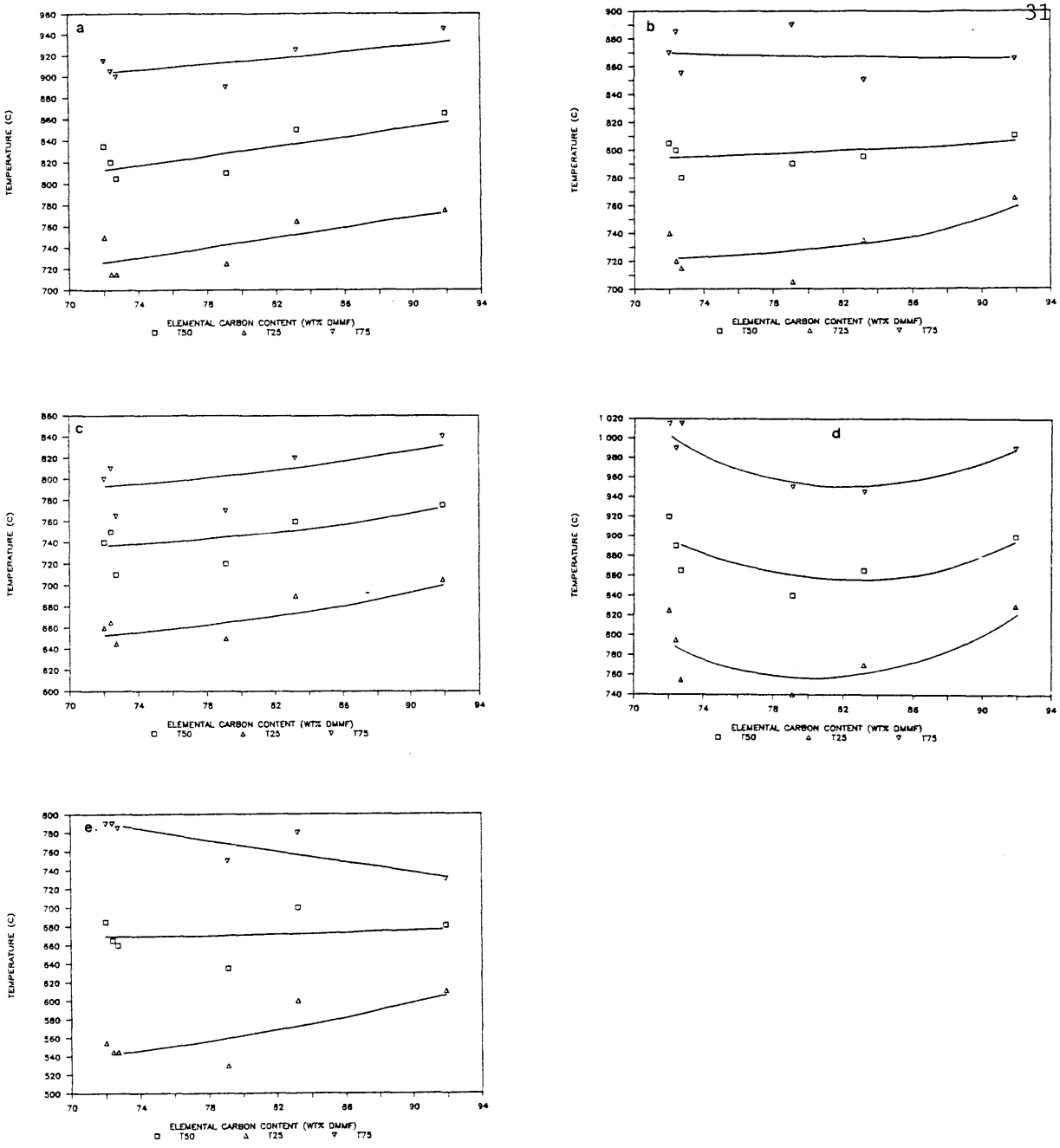

Figure 1.2-9 Comparison of characteristic yield temperatures versus the elemental carbon content: (a) CH_4, (b) C_2H_4, (c) C_2H_6, (d) CO, (e) CO_2. Carbon: LW < ZP < SR < BL < IL < LK. Abbreviations: see Fig.1.2-4.

from decomposition of specific functional groups, e.g., carbon monoxide is assumed to be produced from ether groups in the coal. The rate of gas production is assumed to depend only on the type of functional group, and thus is asserted to be independent of coal type. But a problem in such a simple picture is illustrated in the following example. Upon rapid pyrolysis at temperatures above 750 C, phenol decomposes along two parallel pathways, one of which gives CO and a C_5 moiety, and the other H_2O and benzene [Cypres and Bettens (1974), (1975a,b)]. The former pathway is a base-catalyzed reaction, and thus is expected to be promoted by strong solid base materials from minerals in the coal such as CaO generated by calcite decomposition (Franklin et al., 1981).

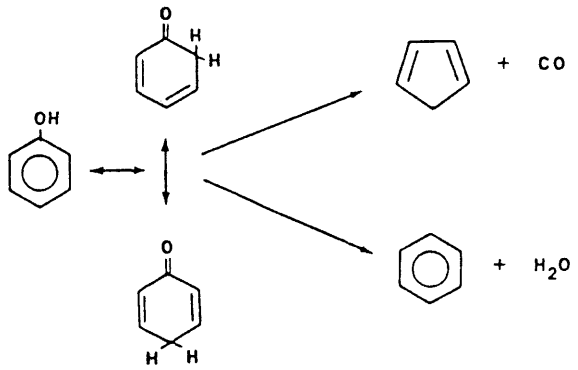

Thus, assuming this mechanism applies for the decomposition of phenolic groups in coal, the phenol group can produce several different gas species, and the concentration of base-catalysts in minerals can strongly influence the relative extent of the two reaction paths.

An alternative and more plausible explanation for the lack of observable coal-type effects in this study, is that differences in the apparent gas production rates are less than or comparable to scatter in the data caused by experimental uncertainties. A supporting evidence for this explanation comes from a recent study of Burnham et al.

(1988), in which eight coals ranging from lignites to low-volatile bituminous coals were pyrolyzed at low heating rates ($\tilde{<}$ 1 C/s) under atmospheric pressure. They observed that T_{max} (T at which the evolution rate is maximum) generally increases with coal rank, with maximum differences ranging from 18 to 33 C among light hydrocarbons (CH_4, C_2H_4, C_2H_6). Such differences are more clearly resolved in the slow heating apparatus which is able to measure the sample temperature within ±5 C (Burnham et al., 1988). In rapid heating studies such as the present one, uncertainties in the temperature measurement are much higher (≈±25 C), and are comparable to the reported differences caused by coal-type effects in the low-heating experiment.

Coal-type effects on total volatiles production. Figure 1.2-10 compares the yield limit of total and 'reactive' volatiles versus the elemental carbon content for the six coals investigated in this study and the two coals studied by Suuberg (1977). Reactive volatiles are defined as total volatiles minus water and carbon dioxide yields. The total yield limit ranges from 41 to 55 wt% dmmf among lignites, and subbituminous and high-volatile bituminous coals, but drops to 22 wt% dmmf for the low-volatile bituminous coal. A useful quantity to compare is reactive volatile yields, which show that high-volatile bituminous coals (BL,PB,IL) produce significantly more than other coal types.

Figure 1.2-11 compares the characteristic yield temperatures of total volatiles production at atmospheric pressure for the six coals. Plots of the total yield versus temperature for individual coals are shown in Fig.1.3-11. The characteristic temperatures tend to increase for higher rank coals, indicating a shift in the yield curve to higher

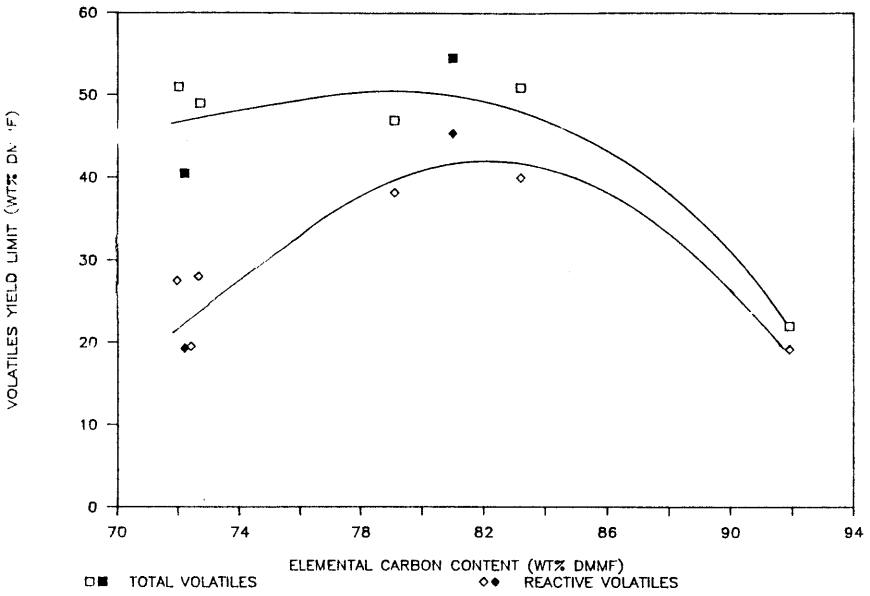

Figure 1.2-10 Comparison of total and reactive volatiles yield limit versus the elemental carbon content. Open symbols are from this study; closed symbols from Suuberg (1977). Carbon: LW < ML < ZP < SR < BL < PB < IL < LK. Abbreviations: see Figs. 1.2-4 and 1.2-8.

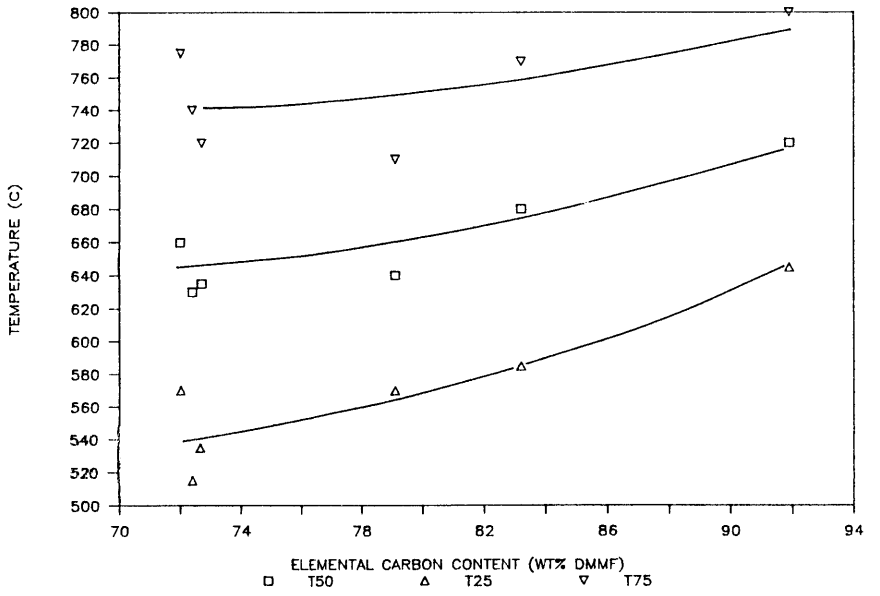

Figure 1.2-11 Comparison of characteristic yield temperatures for total volatiles production at 1 atm. Carbon: LW < ZP < SR < BL < IL < LK. Abbreviations: see Fig.1.2-4.

temperatures. Comparing the spread of the yield curve, measured by (T75-T25), shows a small decreasing trend with increasing rank. These trends are consistent with the expected behavior from combining the observed coal-type effects on the rate of tar and gas production. Such a consistency together with a good product mass balance (90-110 %) helps to verify the experimentally observed coal-type effects on the apparent rate of product evolution.

1.3. Modeling studies

1.3.1. Model description

The MIPR model has been widely used to describe the evolution rate of tar (Serio, 1984; Ko et al., 1988a), gaseous products (Weimer and Ngan, 1979), and total volatiles (Anthony et al., 1974; Ciuryla et al., 1979; Sprouse and Schuman, 1981). The rate of volatiles evolution in the MIPR model is expressed as the sum of the contributions from a large number of first-order independent parallel reactions,

$$dY/dt = \sum k_{o\,i} \exp(-E_i/RT) \; (Y^*_i - Y_i) \qquad (1.3\text{-}1)$$

where i denotes one reaction. The same preexponential factor is used for all reactions, i.e., $k_{o\,i} = k_o$, and the activation energies are described by a Gaussian distribution function f(E) with mean E_o and standard deviation σ

$$f(E) = [\sigma(2\pi)^{1/2}]^{-1} \exp[-(E-E_o)^2/2\sigma^2] \qquad (1.3\text{-}2)$$

The probability of finding a reaction with activation energy between E and E+dE is given by f(E)dE, where for a large number of reactions, $f(E) = Y^*_i/Y^*$ and Y^* is equal to the sum of the Y^*_i for all i. The input parameters required in the model are Y^*, E_o, σ, and k_o. The notation 'Y' here is equivalent to 'V' in earlier descriptions of this

model (Anthony et al., 1974; Howard, 1981).

The extended MIPR model increases the range of applicability of the MIPR model by explicitly including descriptions of mass transport and secondary reactions. The main objective in formulating this model was to be able to describe tar production over a wide range of operating conditions (coal type, heating rate, pressure, and particle size), using as few difficult-to-obtain physical parameters as possible and requiring a minimal computational effort. The chemistry of the model assumes a hypothetical molecular structure of coal shown in Fig.1.3-1. Figure 1.3-2 gives a schematic diagram of the proposed mechanism where the tar is produced via the sequential steps of **bridge scission**, **hydrogenation** and **transport**. Competing with the tar production pathway are **cross-linking**, **polymerization**, and **tar cracking reactions**, all of which lead to the formation of char + gas. As will be shown below, each or a combination of these three competing reactions uniquely describes and explains the experimentally observed effects of main operating variables - coal type, heating rate, pressure, and particle size. This proposed mechanism is assumed in the mathematical formulation of the extended MIPR model described below.

For non-softening coals, the rate of tar (Y) leaving the particle of radius R is

$$dY/dt = \sum E_{p,i}\ E_{c,ns}\ k_{t,i}(V^*_i - V_i) \qquad (1.3\text{-}3)$$

where

$$dV_i/dt = k_{t,i}(V^*_i - V_i) \qquad (1.3\text{-}4)$$

$$E_{p,i} = \frac{\text{rate of scission}}{\text{rate of scission + polymerization}}$$

$$= k_{s,i} \,/\, (k_{s,i}+k_p) \qquad (1.3\text{-}5)$$

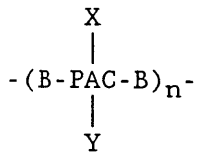

PAC = represents repeating nuclear units of polyaromatic and hydroaromatic clusters

B = bridging molecules

X = side groups suspected to be responsible for cross-linking

Y = non-cross-linking side groups

n = number of repeating units

Figure 1.3-1 Hypothetical molecular structure of coal assumed in formulating the extended MIPR model.

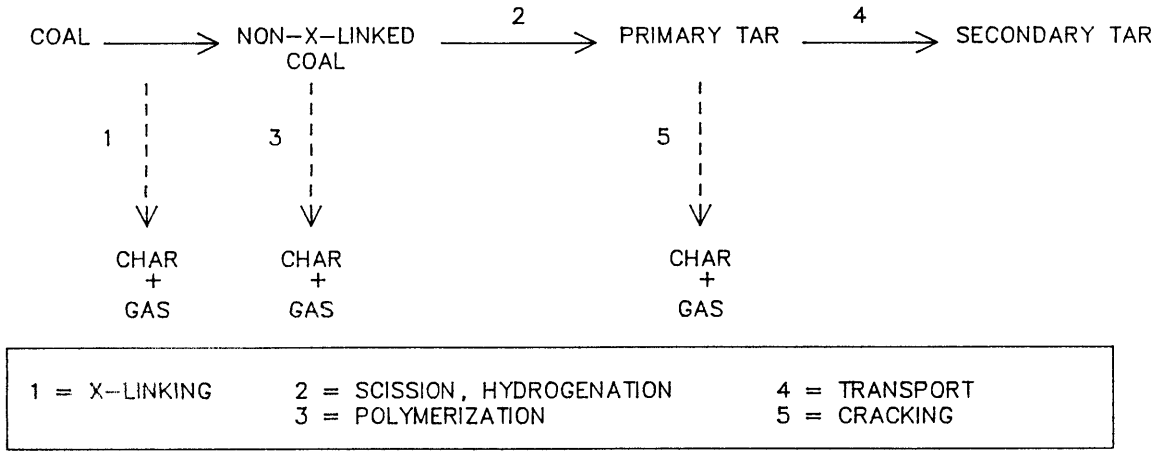

Figure 1.3-2 Chemical and physical mechanism of tar formation.

$$E_{c,ns} = \frac{\text{rate of tar production with transport limitation}}{\text{rate without transport limitation}}$$

$$= 2\exp(-m_{ns}R)/[1+\exp(-2m_{ns}R)] \qquad (1.3\text{-}6)$$

For a component i, Eq.(1.3-4) describes the rate at which the non-x-linked fraction of coal (V^*_i) reacts, where V_i represents the cumulative amount of the reacted material. The subscript i denotes one reaction in a multiple independent parallel reaction scheme, in which each reaction describes the thermal scission of a bridge bond with its specific chemical bond strength. The activation energies for these scission reactions are described by a Gaussian distribution with mean E_{os} and standard deviation σ_s.

Equations (1.3-5) and (1.3-6) represent the fraction of the reacted coal [Eq.(1.3-4)] which survives polymerization and cracking reactions respectively. The values of each of these two quantities are bound between 0 and 1, where 0 represents the most severe limitation on tar production and 1 represents no limitation. The first-order Arrhenius rate constants, k_s, k_p, k_c are for scission, polymerization, tar cracking reactions respectively, and $k_{t,i} = k_{s,i} + k_p$. The kinetics of cross-linking are not considered here since this process is assumed to occur at relatively mild temperatures before other reactions proceed to any appreciable extent. The dimensionless quantity $m_{ns}R$ in Eq. (1.3-6) is the Thiele modulus for non-softening coals, where $m_{ns} = (k_c/D_{g,eff})^{1/2}$ and $D_{g,eff}$ is the effective gas phase binary diffusivity of tar. The transport description assumed in deriving $E_{c,ns}$ considers steady-state transport in macropores where the tar enters the pore from the center of the particle, and neglects external transport resistance and convective contributions. A characteristic time analysis supports

the steady-state and negligible external transport resistance assumptions. The assumption that tars enter the pore from the center of the particle is not strictly valid, but making this approximation considerably simplifies the mathematics without seriously hindering the model's ability to capture the effects of the main operating variables.

Applying a similar derivation procedure for softening coals gives the rate of tar leaving the particle surface as

$$dY/dt = \sum E_{p,i}\ E_{c,s}\ k_{t,i}(V^*_i - V_i) \qquad (1.3\text{-}7)$$

where

$$E_{c,s} = 2\exp(-m_s R_{eff})/[1+\exp(-2m_s R_{eff})] \qquad (1.3\text{-}8)$$

The quantity $m_s R_{eff}$ is the Thiele modulus for softening coals, where $m_s = (k_c/D_L)^{1/2}$; D_L represents the liquid phase diffusivity of tar in the molten coal; and V_i and $E_{p,i}$ are the same as those for non-softening coals given in Eqs.(1.3-4) and (1.3-5) respectively. The molten coal is assumed to have a shape of a cenospherical shell (Sung, 1978), and thus R_{eff}, the effective diffusion length scale, is assumed to be half of the shell thickness (Griffin, 1988; Hsu, 1988). Based on recent data from ≈40 μm rad. particles pyrolyzed at 1 atm (Griffin, 1988), the shell thickness is assumed to be roughly 20% of the radius of the raw coal. An exact explanation for the experimentally observed pressure and particle-size effect on tar production for softening coals, is currently not established due to large uncertainties in physical property values of the molten coal (Oh, 1985). In this formulation, excluding external and bubble transport effects leaves the possibility that the shell thickness is a function of pressure and particle size as the only viable explanation to describe the observed behavior. Thus until more conclusive explanation becomes available, the present model

will assume that the shell thickness is related to the pressure and particle size in the form of

$$R_{eff} = 0.1\ R \times 10^{-4}\ (P/1)^{1/3}(R/40)^{1/3}\ cm \qquad (1.3\text{-}9)$$

where R is the particle radius in μm, and P the reactor pressure in atm. The work of Griffin (1988) is currently seeking to provide quantitative experimental data to examine the effect of pressure and particle size on the shell thickness.

For a given coal, the extended MIPR model requires a total of 9 input parameters: V^*_{max} ($\sum V^*_i$), k_{os}, E_{os}, σ_s, k_{op}, E_p, k_{oc}, E_c, and $D_{g,eff}$ or D_L. Table 1.3-1 gives the estimated values of model parameters used to predict tar evolution rates for the six coals studied (see below, Fig.1.3-13). V^*_{max} is the experimental tar yield limit obtained with rapid heating under low pressures (vacuum). The values of k_{os}, k_{op}, E_p, k_{oc} and E_c are obtained either from experimental data found in the literature (Serio, 1984), or from estimates (Gavalas, 1984) using thermochemical methods, although such estimates are strictly valid for gas-phase reactions only. These parameters were assumed not to vary significantly among different coal types. This assumption was mainly made because information necessary to assign coal-type dependent values for these parameters is presently not available, but we do not imply that these parameters are truly constant for all coal types. Any errors generated from this assumption will affect the values of best-fitted parameters. If the error cannot be sufficiently compensated by the fitted parameters, then the error will be reflected in the model's predictive capability. The remaining parameters, E_{os}, σ_s, and $D_{g,eff}$ or D_{oL} were best-fitted from experimental tar data.

Table 1.3-1 Model parameters for the extended MIPR model.

(a) Coal-type dependent parameters[a]:

Coal[b]	V^*_{max} wt% dmmf	E_{os} kcal/mole	σ_s kcal/mole	e/τ[c] or	D_{oL}[d]
Lower Wilcox L	16.8	53.8	7.0	$10^{-2.81}$	-
Beulah Zap L	9.1	52.8	9.4	$10^{-3.23}$	-
Smith Roland SB	14.8	51.7	6.3	$10^{-2.70}$	-
Blue HVB	27.7	54.6	5.3	$10^{-2.90}$	-
Illinois HVB	30.1	54.4	4.4	-	$10^{-5.67}$
Lower Kittanning LVB	14.0	56.8	3.5	-	$10^{-5.41}$

(b) Fixed parameters[e]:

scission	k_{os}, s^{-1}	10^{14}	-	
polymerization	k_{op}, s^{-1}	10^{7}	E_p, kcal/mole	35.5
cracking	k_{oc}, s^{-1}	10^{14}	E_c, kcal/mole	55.0

[a] V^*_{max} is obtained from vacuum tar yield data; E_{os}, σ_s, e/τ or D_{oL} are best-fitted from the data.
[b] Coals are listed in the order of increasing elemental carbon contents in dmmf basis. Elemental analysis is given in Table 1.2-1.
[c] Geometrical factor in $D_{g,eff} = (e/\tau)\ 0.1\ (T/273)^{1.5}\ (1/P)\ cm^2/s$.
[d] Liquid phase diffusivity, $D_L = D_{oL}\ (T/298)\ cm^2/s$.
[e] See text for sources.

Modeling results and discussion

MIPR model. Figure 1.3-3 compares the experimental and predicted tar yields from the MIPR model for the six coals investigated in this study. The model predictions were made with k_o fixed at 10^{14} s^{-1}, Y^* obtained from the measured maximum tar yield, and E_o and σ best-fitted to the experimental data using a multivariable non-linear regression routine. In all cases, the predicted yields agree well with the experimental values; the standard error of the estimate [Eq.(1.2-3)] ranges from 6.5 to 10 % of the maximum tar yield.

Figure 1.3-4 plots the best-fitted values of E_o and σ for tar production versus the elemental carbon contents of the coal. Higher rank coals, indicated by higher elemental carbon contents, generally gave greater values of E_o and smaller values of σ. Maximum differences in E_o and σ are 7.1 and 3.6 kcal/mole respectively. Such differences far exceed the variation explainable by experimental uncertainties, estimated to be $\approx \pm 1$ kcal/mole for both E_o and σ. Therefore, under the conditions employed in this study, there appears to be a convincing coal-type effect on the MIPR model rate parameters for tar production. The trends for both E_o and σ in Fig.1.3-4 appear to be more scattered among low-rank coals, where the Beulah Zap lignite shows a considerably lower E_o and higher σ compared to the Lower Wilcox lignite and Smith Roland subbituminous coal. One property that appears to distinguish the different behavior of the low-rank coals is the elemental hydrogen content; in dmmf basis, the Zap has 4.8 wt% whereas the Lower Wilcox and Smith Roland have noticeably larger values of 5.6 and 5.3 wt% respectively. Therefore in estimating E_o and σ from Fig.1.3-4 in the

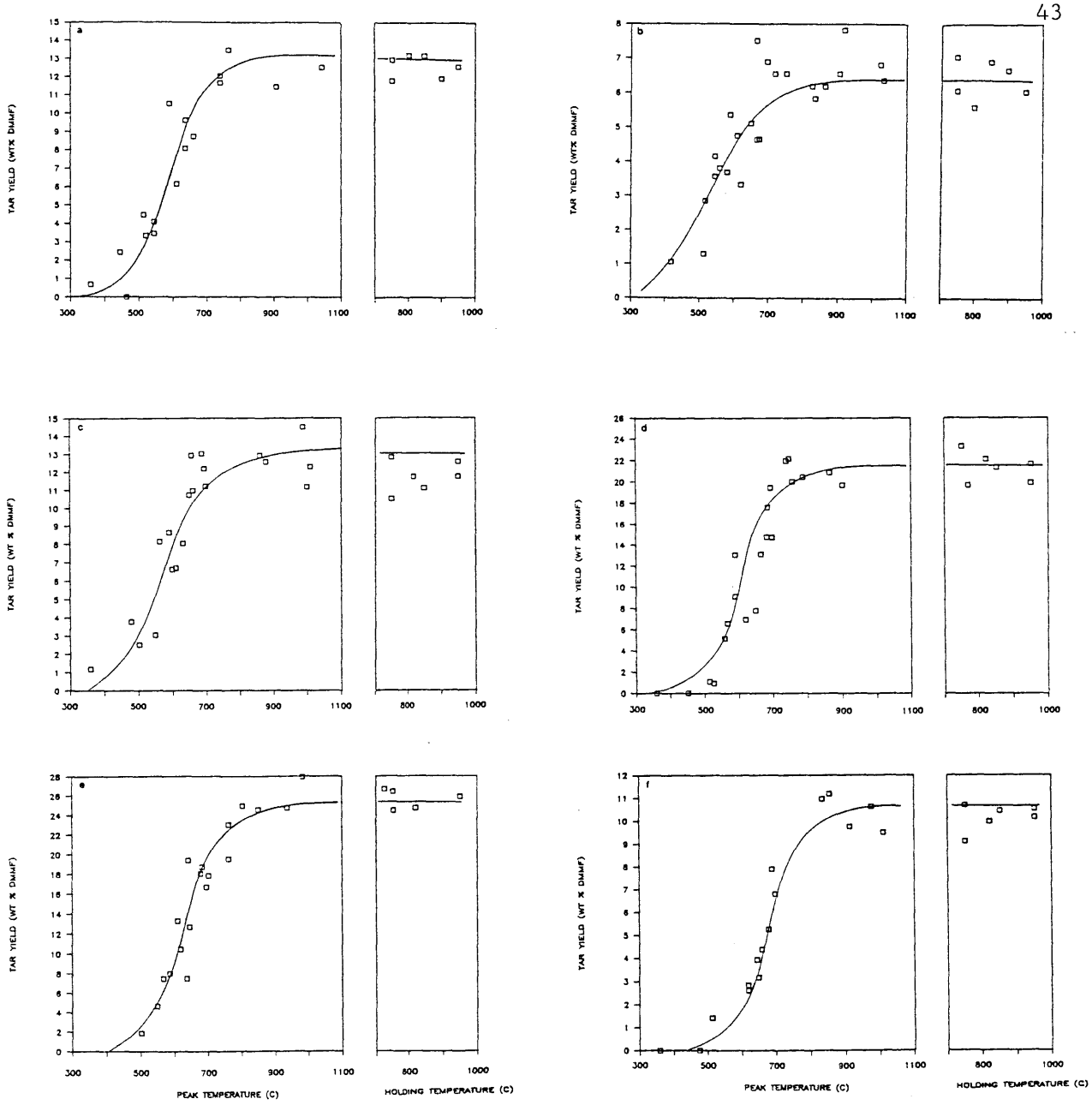

Figure 1.3-3 Tar yields versus peak and holding temperatures (5 s hold). Symbols represent experimental data; lines represent MIPR model predictions. (a) LW, (b) ZP, (c) SR, (d) BL, (e) IL, (f) LK. Abbreviations: see Fig.1.2-4.

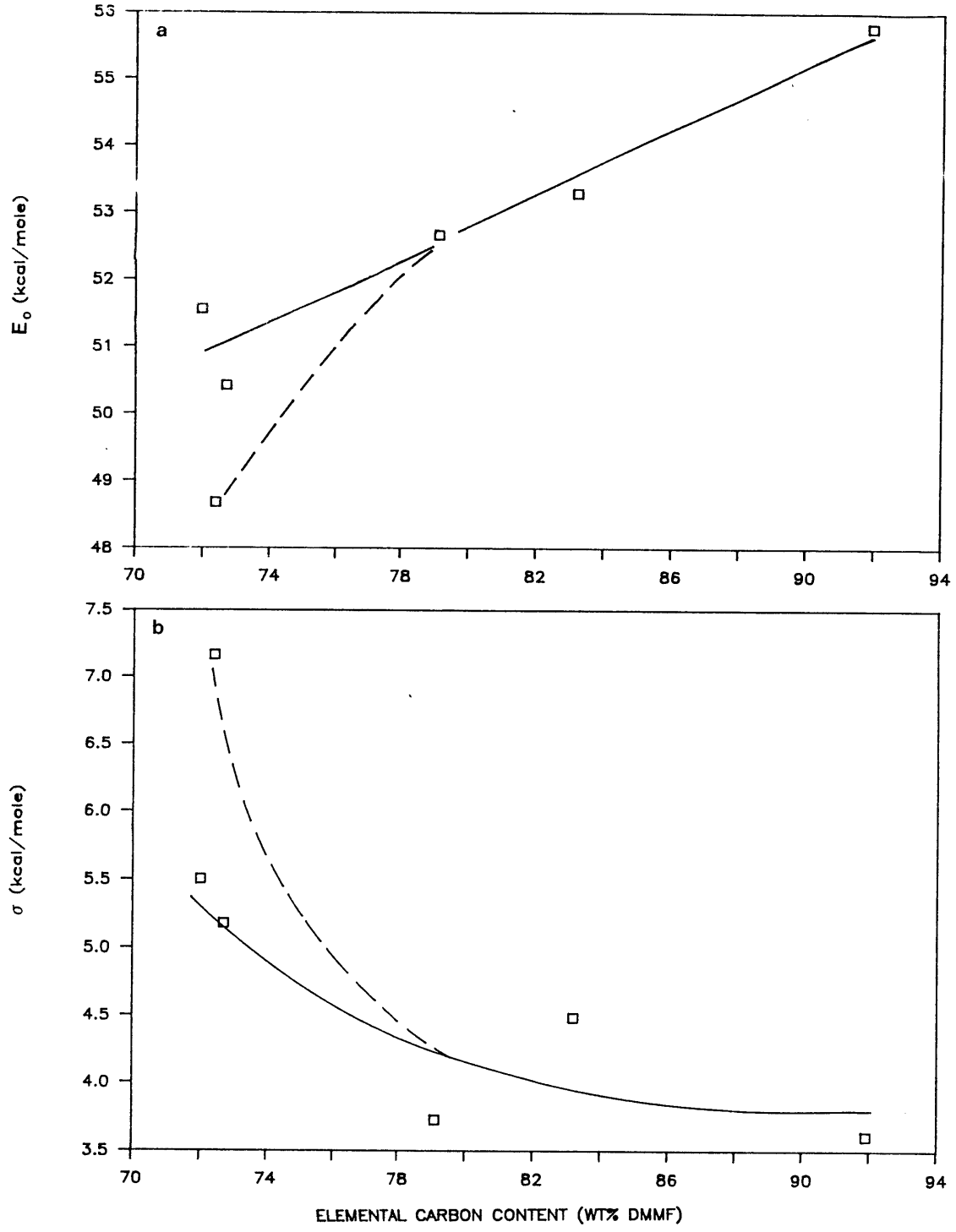

Figure 1.3-4 Best-fitted values of (a) E_o and (b) σ for predicting atmospheric tar production using the MIPR model, versus the elemental carbon content of the coal. k_o was fixed at 10^{14} s^{-1} for all coals; Y^* was obtained from experimental data for each coal. Dashed lines are for coals with [H] < 5 wt% dmmf; solid lines for [H] ≥ 5 wt% dmmf. Carbon: LW < ZP < SR < BL < IL < LK. Abbreviations: see Fig.1.2-4.

low-rank region, the dashed lines are recommended for coals with the elemental hydrogen content of < 5 wt% dmmf, and the solid lines for coals with the elemental hydrogen of ≥ 5 wt% dmmf.

Figures 1.3-5 through 1.3-9 compare the experimental and predicted gas yields from the MIPR model for the six coals investigated in this study. The model predictions were made using the same procedure as above for tar. For all gas species, the agreement between the predicted and experimental yields is generally good; the standard error of estimate ranges from 4 to 15 % of the maximum yield. Figure 1.3-10 plots the best-fitted values of E_o and σ for the measured gas species versus the elemental carbon contents of the coal. Coal-type effects on E_o range from almost none for C_2H_4 and CO_2, to a slightly increasing trend for higher rank coals in cases of CH_4 and C_2H_6. The E_o of CO shows a concave downward trend with a minimum near high-volatile bituminous range. However, these variations are small and are comparable to estimated errors produced from experimental uncertainties, which range from ± 0.5 to 1 kcal/mole. The general trend for σ is decreasing values for higher rank coals. The coal-type effect is strong for CO_2, but for other gas species the effect is much weaker. Except for CO_2, variations in σ are comparable to estimated errors produced from experimental uncertainties, which range from ± 1 to 1.5 kcal/mole.

Figure 1.3-11 compares the experimental and predicted total volatile yields from the MIPR model for the six coals studied. In all cases, the predicted yields agree well with experimental values; the standard error of the estimate ranges from 6 to 10 % of the maximum yield. Figure 1.3-12 plots the best-fitted values of E_o and σ versus

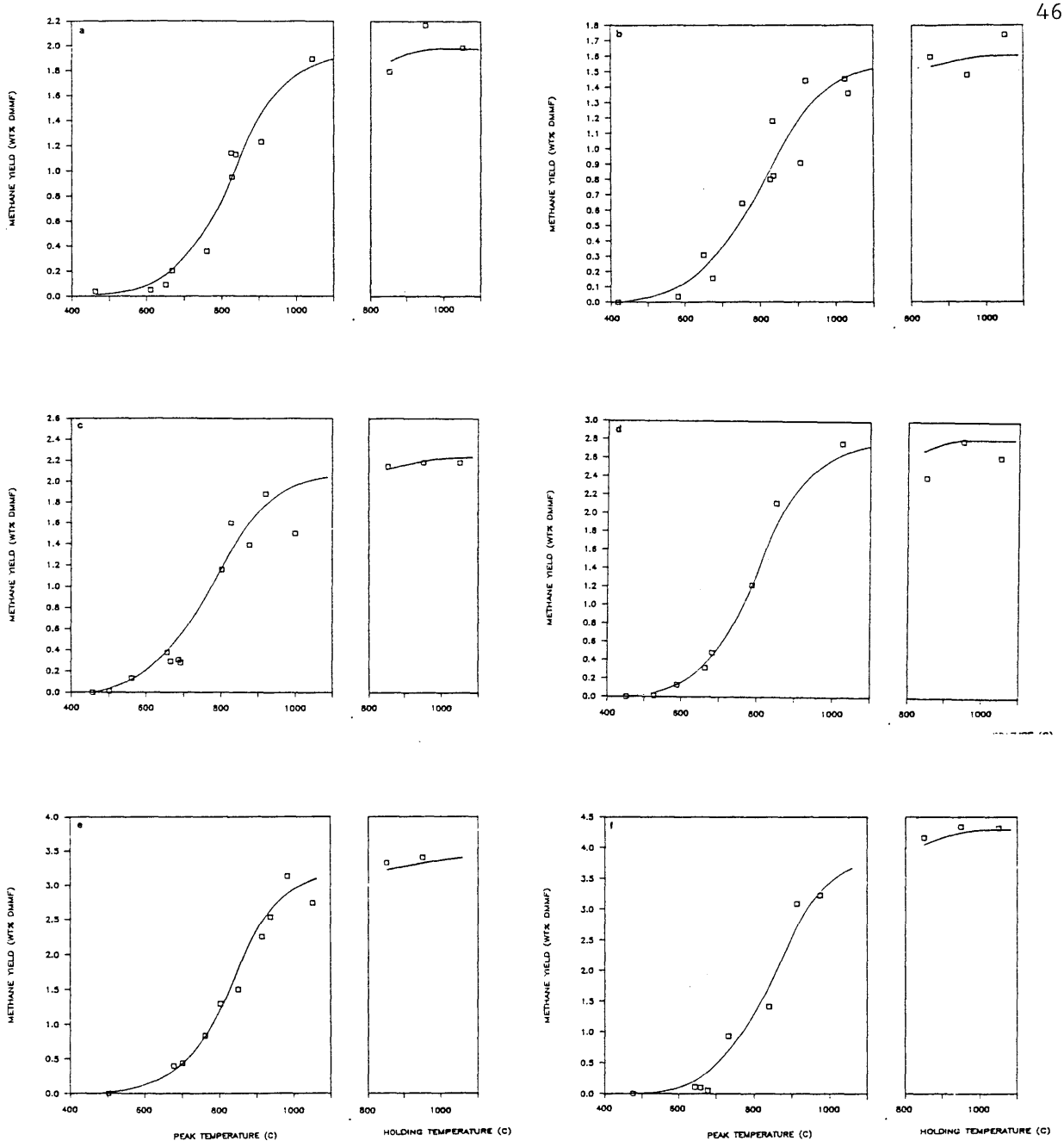

Figure 1.3-5 Methane yields versus peak and holding temperatures (5 s hold). Symbols represent experimental data; lines represent MIPR model predictions. (a) LW, (b) ZP, (c) SR, (d) BL, (e) IL, (f) LK. Abbreviations: see Fig.1.2-4.

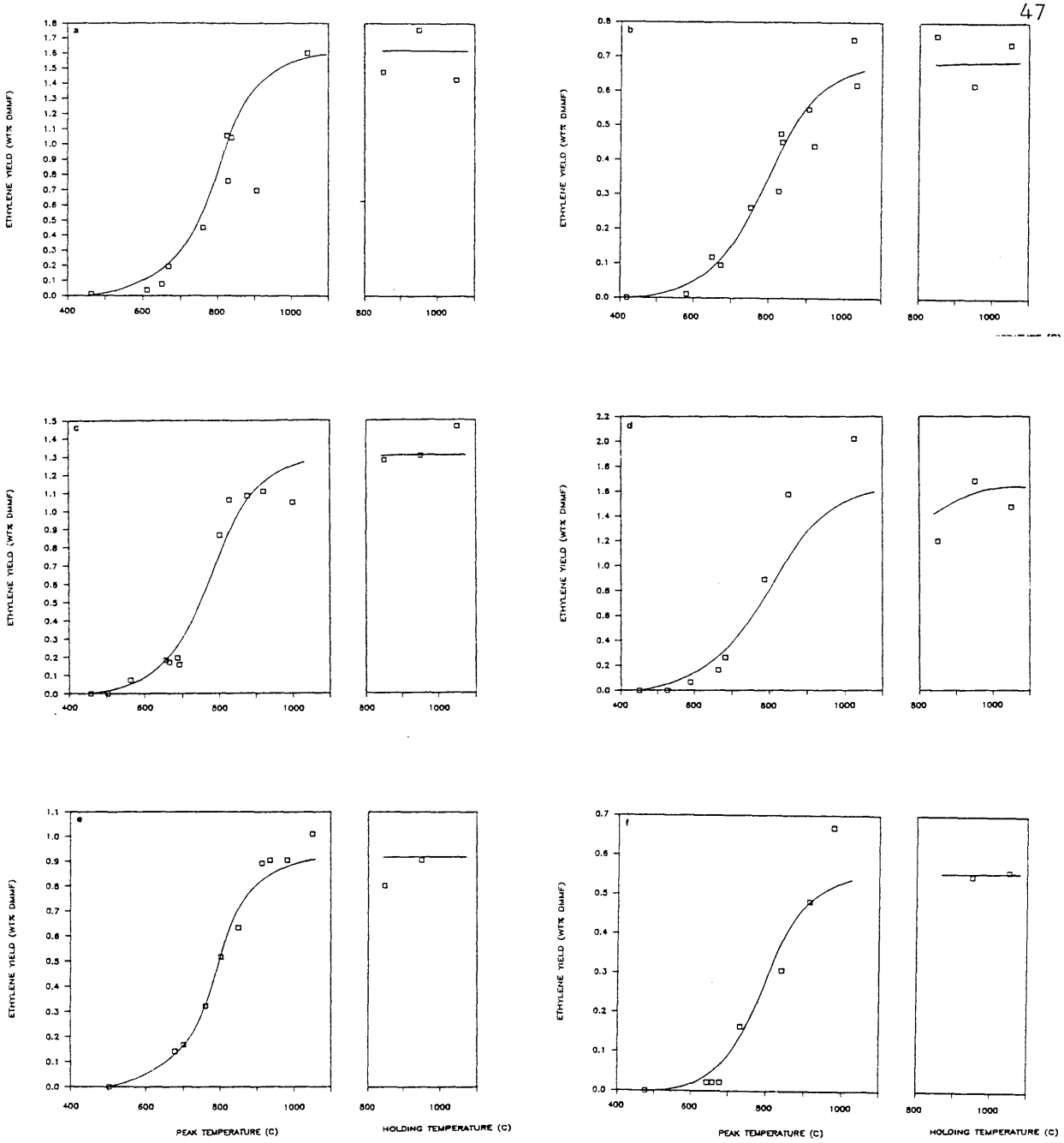

Figure 1.3-6 Ethylene yields versus peak and holding temperatures (5 s hold). Symbols represent experimental data; lines represent MIPR model predictions. (a) LW, (b) ZP, (c) SR, (d) BL, (e) IL, (f) LK. Abbreviations: see Fig.1.2-4.

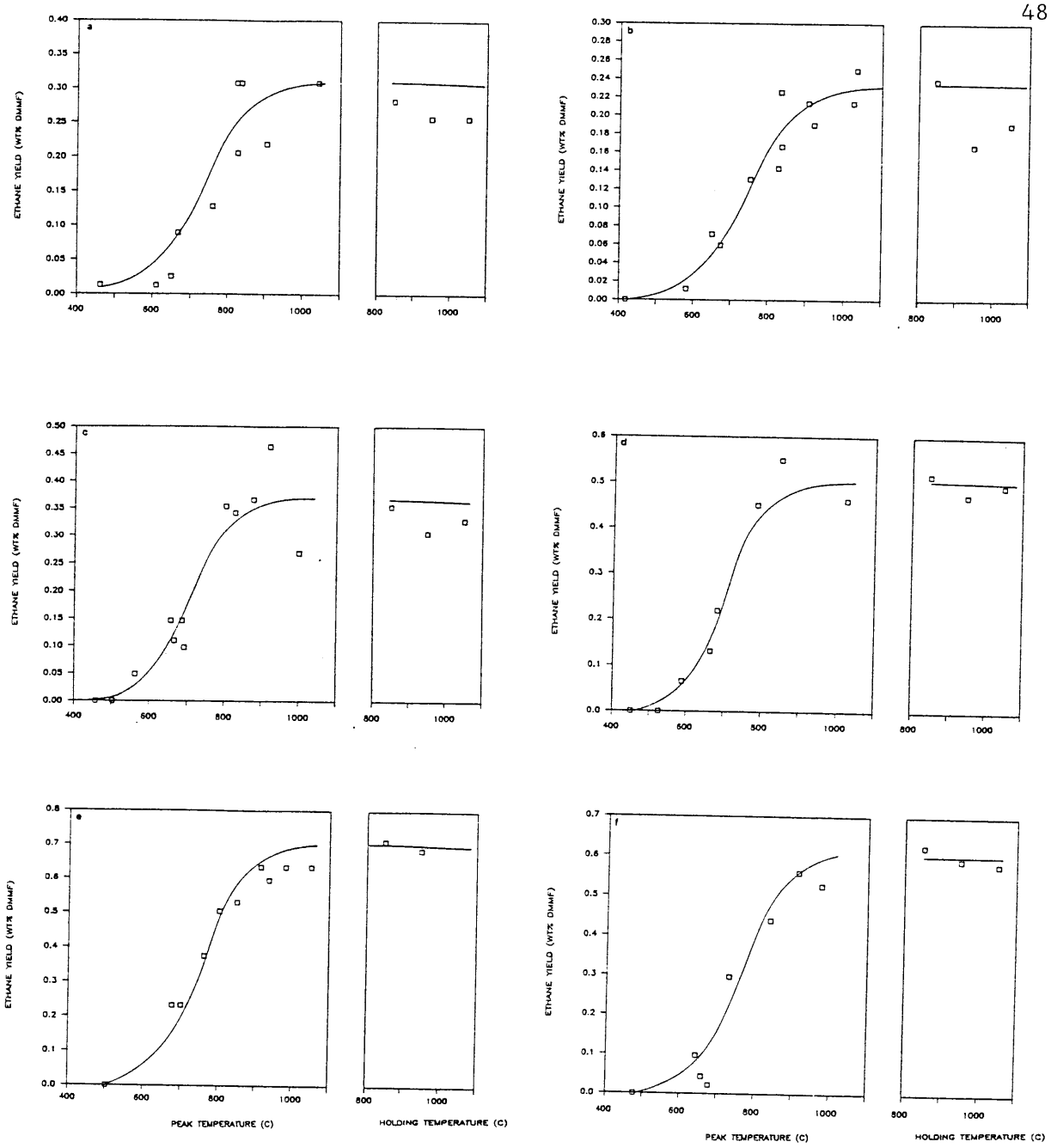

Figure 1.3-7 Ethane yields versus peak and holding temperatures (5 s hold). Symbols represent experimental data; lines represent MIPR model predictions. (a) LW, (b) ZP, (c) SR, (d) BL, (e) IL, (f) LK. Abbreviations: see Fig.1.2-4.

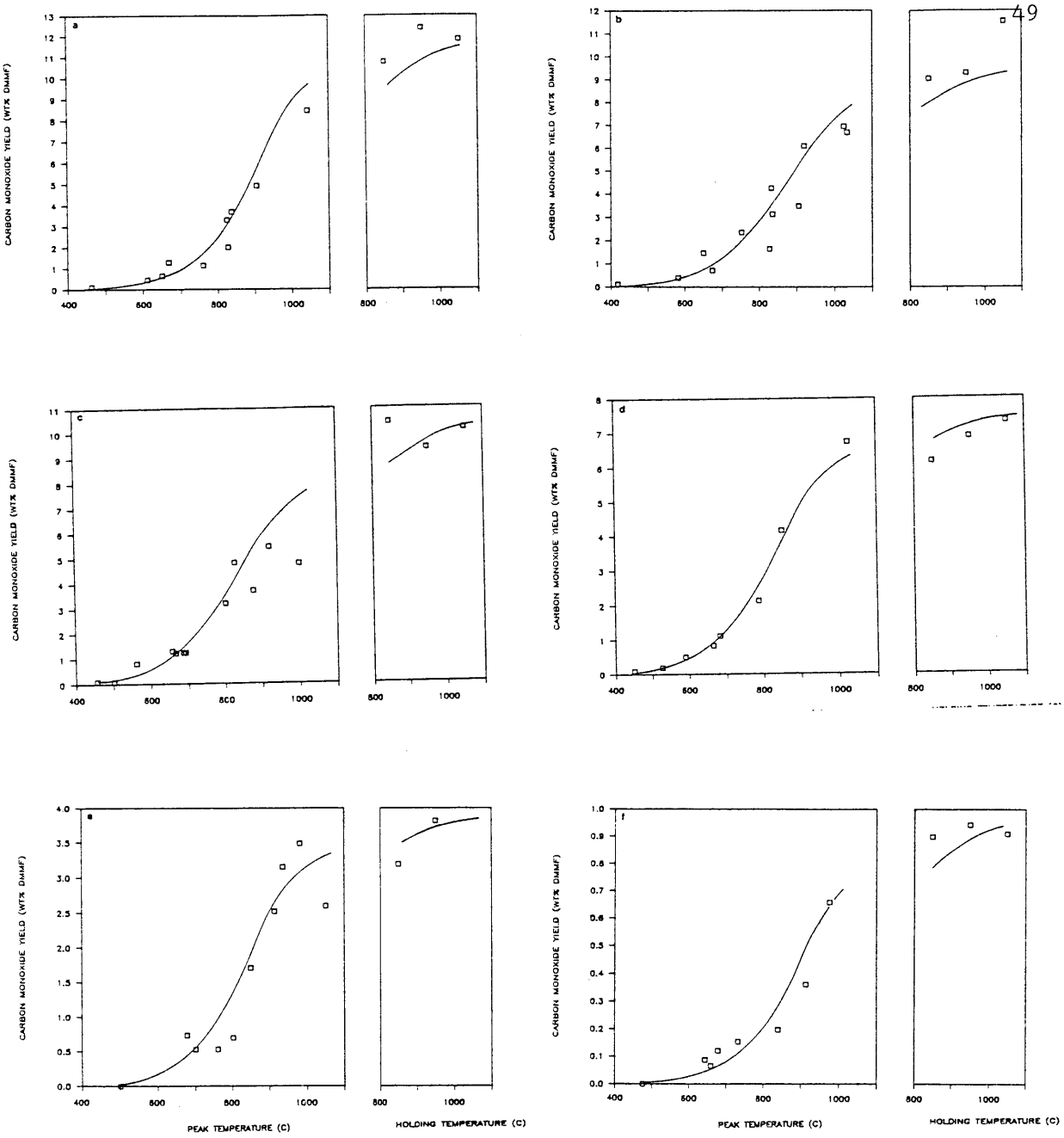

Figure 1.3-8 Carbon monoxide yields versus peak and holding temperatures (5 s hold). Symbols represent experimental data; lines represent MIPR model predictions. (a) LW, (b) ZP, (c) SR, (d) BL, (e) IL, (f) LK. Abbreviations: see Fig.1.2-4.

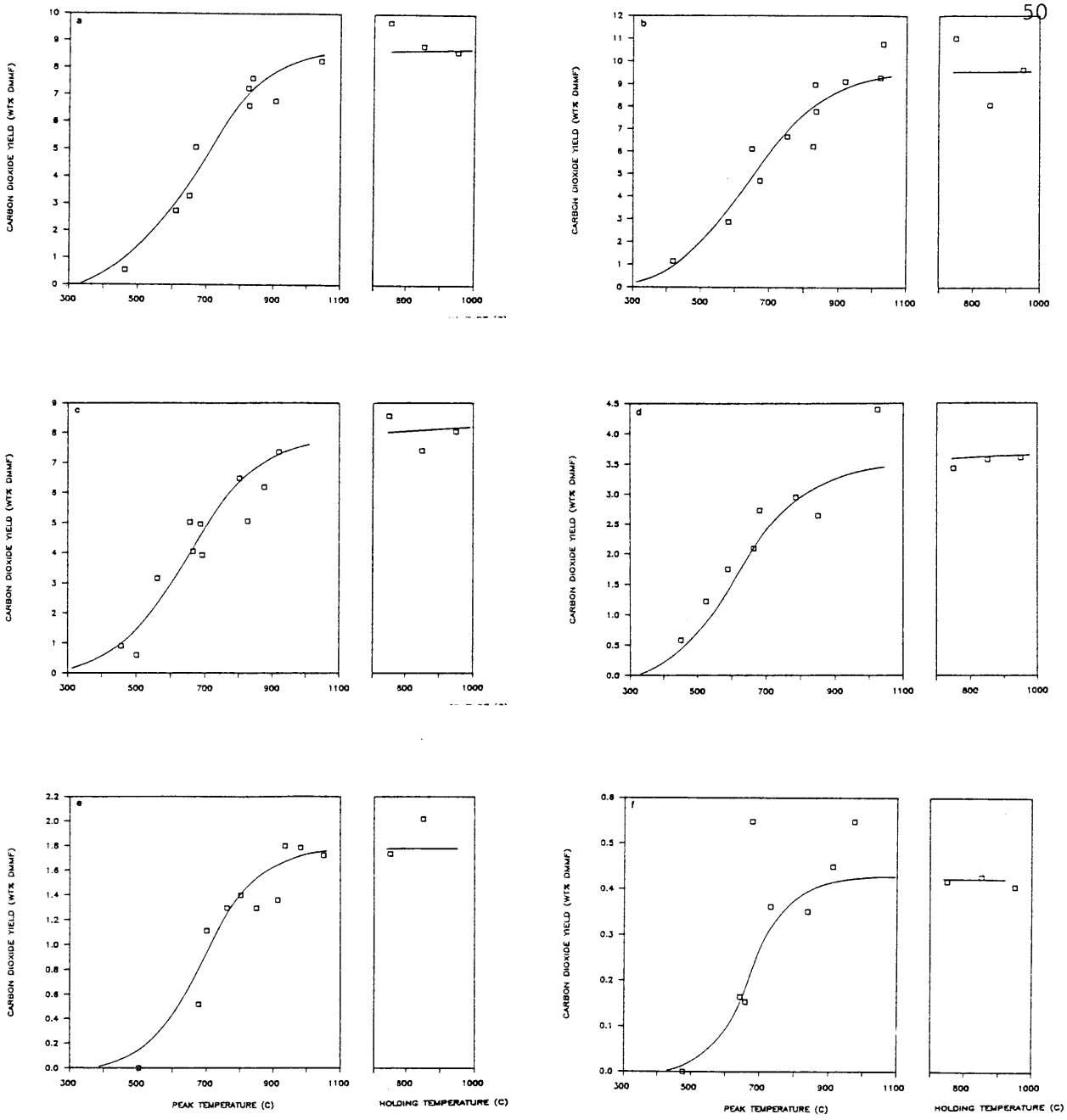

Figure 1.3-9 Carbon dioxide yields versus peak and holding temperatures (5 s hold). Symbols represent experimental data; lines represent MIPR model predictions. (a) LW, (b) ZP, (c) SR, (d) BL, (e) IL, (f) LK. Abbreviations: see Fig.1.2-4.

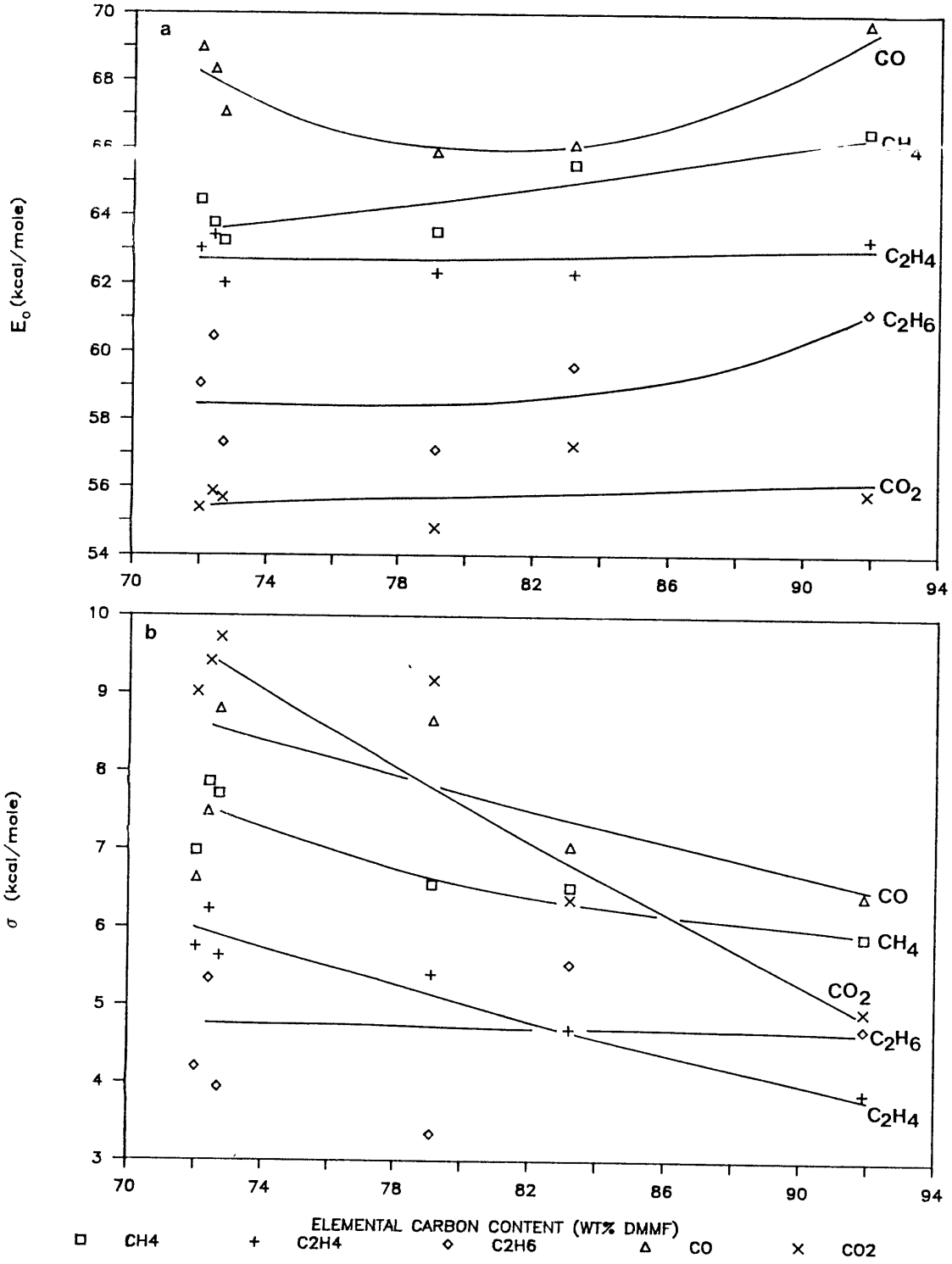

Figure 1.3-10 Best-fitted values of (a) E_o and (b) σ for predicting gas evolution rates at 1 atm using the MIPR model, versus elemental carbon contents of the coal. k_o was fixed at 10^{14} s^{-1} in all cases, and Y^* was obtained from experimental data for each coal. Carbon: LW < ZP < SR < BL < IL < LK. Abbreviations: see Fig.1.2-4.

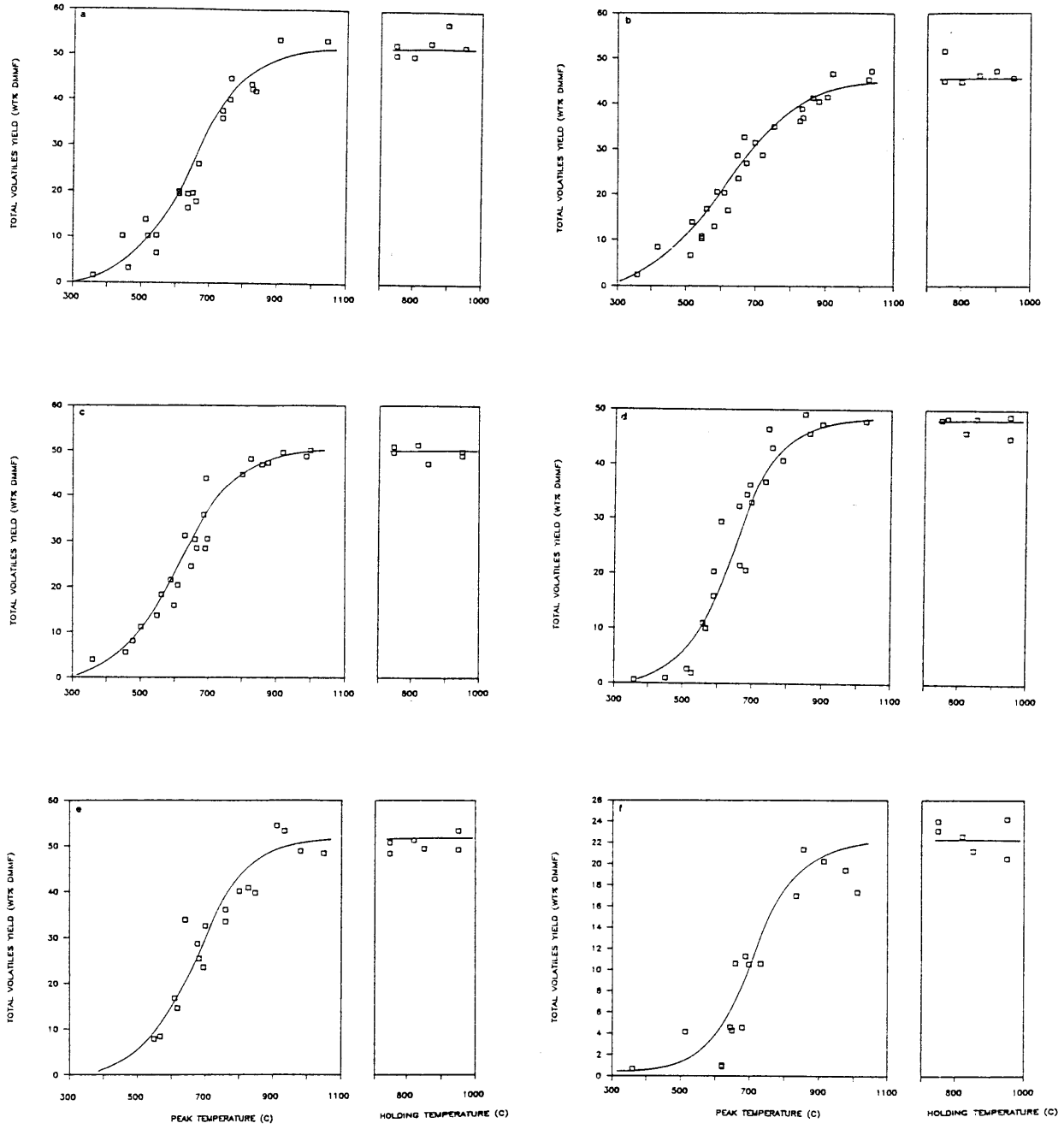

Figure 1.3-11 Total volatiles yield versus peak and holding temperatures (5 s hold). Symbols represent experimental data; lines represent MIPR model predictions. (a) LW, (b) ZP, (c) SR, (d) BL, (e) IL, (f) LK. Abbreviations: see Fig.1.2-4.

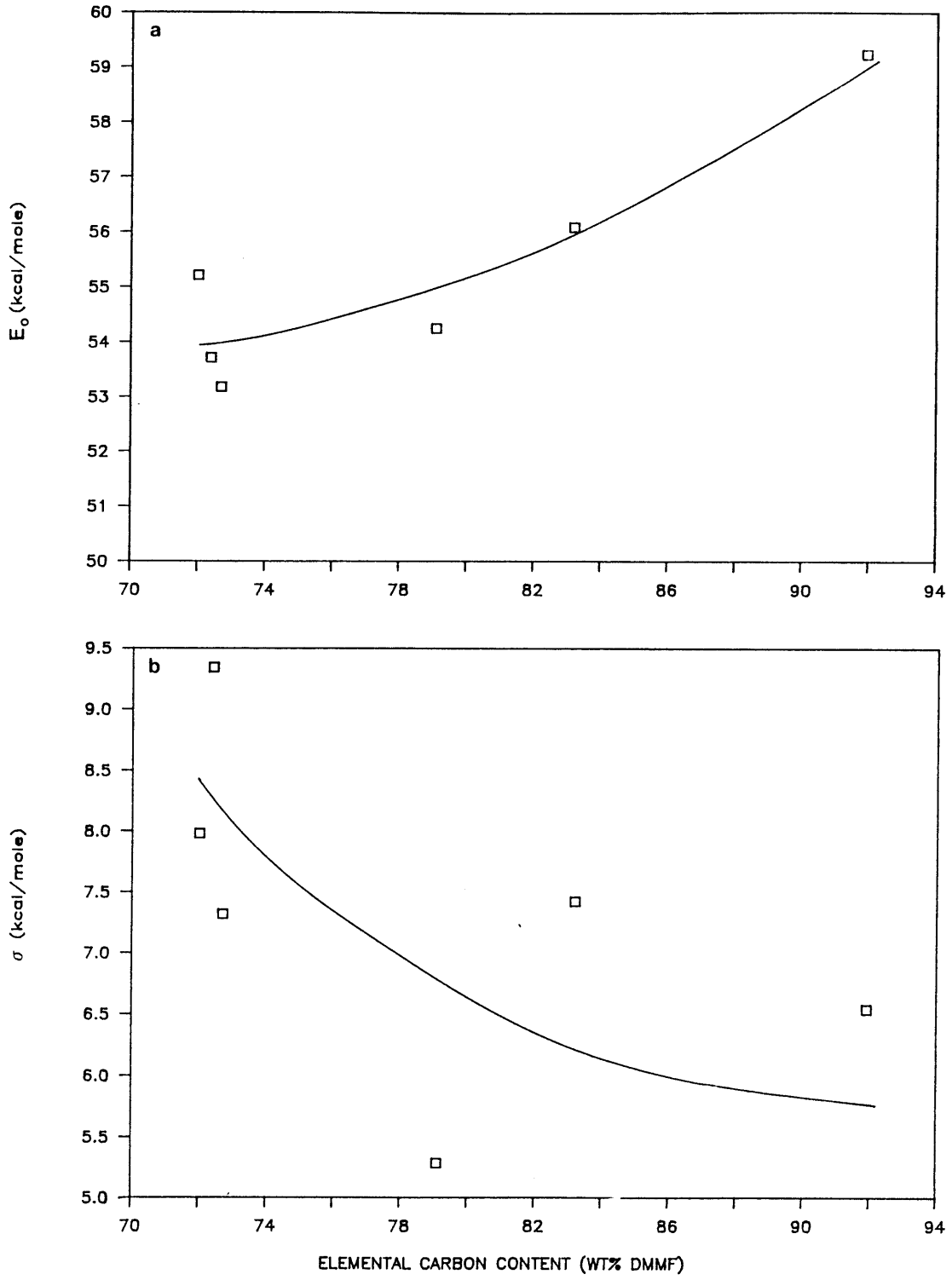

Figure 1.3-12 Best-fitted values of (a) E_o and (b) σ for predicting atmospheric pressure total volatiles evolution using the MIPR model, versus the elemental carbon contents of the coal. k_o was fixed at 10^{14} s^{-1} in all cases, and Y^* was obtained from experimental data for each coal Carbon: LW < ZP < SR < BL < IL < LK.

the elemental carbon contents of the coal. Generally, higher rank coals show increasing values of E_o with a maximum difference of about 6 kcal/mole. The E_o of Lower Wilcox lignite appears to be high compared to the other two low-rank coals, but is within estimated uncertainties of ±1 kcal/mole. Comparing the σ shows a decreasing trend for higher rank coals, but with much scatter. A maximum difference of 4 kcal/mole in σ is moderately greater than the estimated uncertainty of ±1.5 kcal/mole. The trends in the rate parameters for independently measured total volatiles production confirm the trends observed for individual products. The relatively modest coal-type dependence of the MIPR rate parameters for total volatiles reflect the combined effects of a strong coal-type dependence for tars and a much weaker dependence for gases. Also, the general trend for all products are always consistent - higher E_o and lower σ for increasing coal rank.

Extended MIPR model. Figure 1.3-13 shows a good agreement between the experimental and predicted tar yields at all three pressures- 0.001, 1 and 10 atm. The accurate prediction of the yield limits over a wide range of pressures is especially encouraging since, unlike the MIPR model, the yield limits were predicted without having to rely on experimentally measured values at different pressures. Also, the predicted behavior in which the rate is unaffected by pressure at fairly low temperatures ($\lesssim$ 550 C), and that the yields 'level-off' earlier (i.e., at lower temperatures) as pressure is increased, closely resembles the experimentally observed behavior reported by Suuberg (1977).

Figure 1.3-14 helps to illustrate how the model works. The figure plots (a) $E_{p,avg}$, $E_{c,ns}$ and (b) $E_{p,avg}$, $E_{c,s}$ versus temperature, where

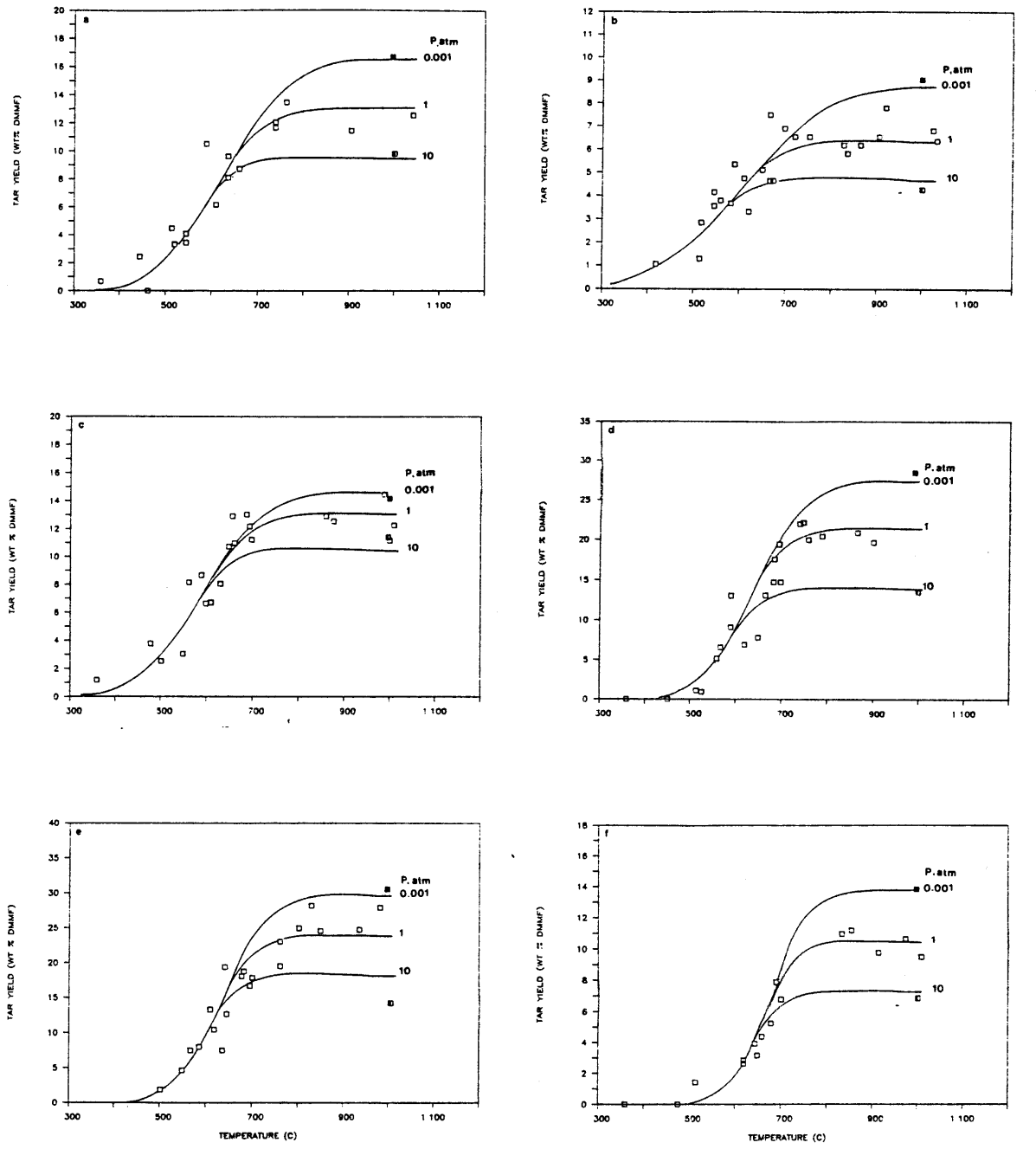

Figure 1.3-13 Tar yields versus peak temperatures. Symbols represent experimental data: ■ - 0.001 atm, □ - 1 atm, ◧ - 10 atm. Lines represent extended MIPR model predictions. Coals: (a) LW, (b) ZP, (c) SR, (d) BL, (e) IL, (f) LK. 0.001 and 10 atm data points represent averaged values from 1-3 runs. Abbreviations: see Fig.1.2-4.

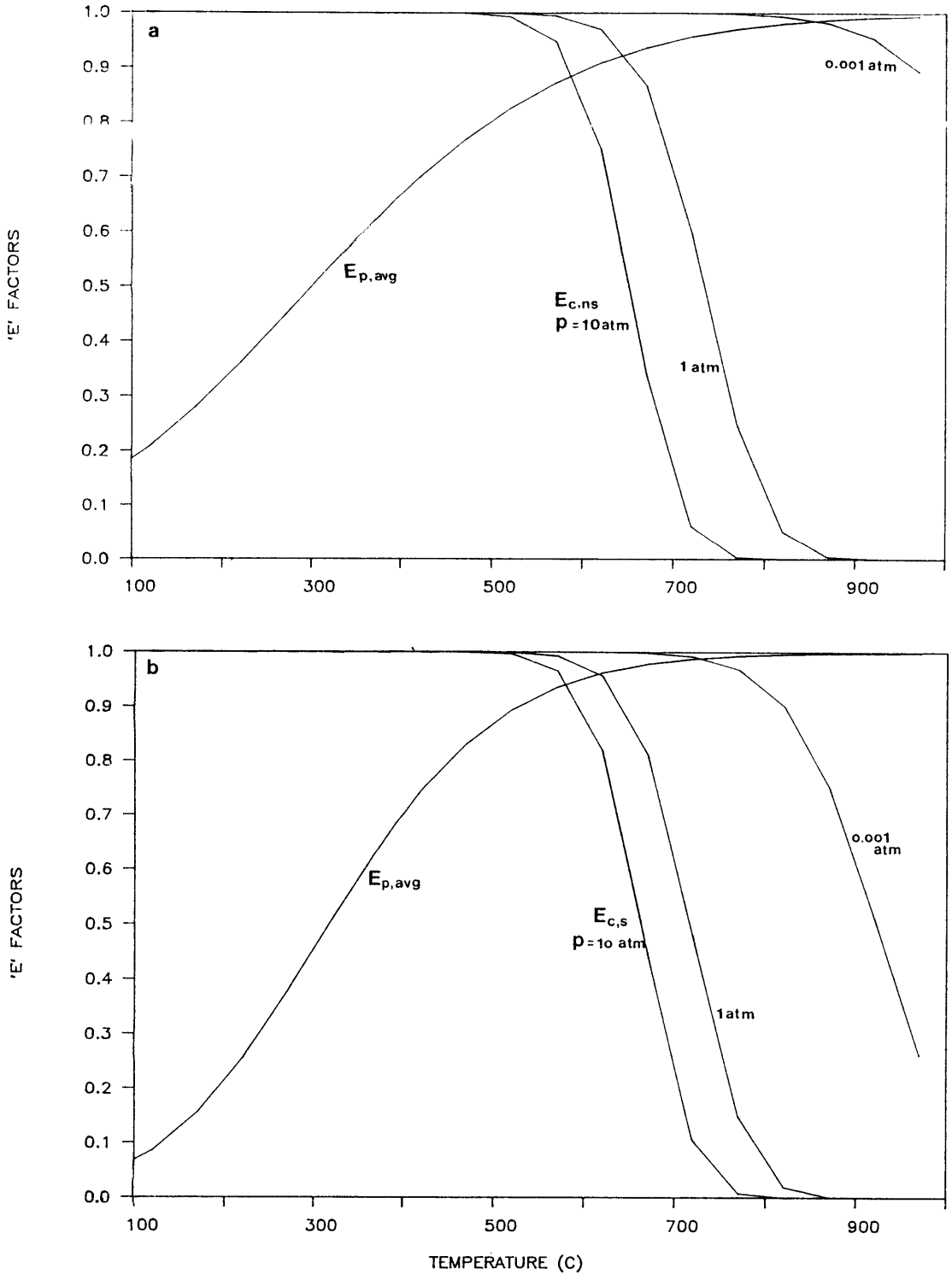

Figure 1.3-14 (a) $E_{p,avg}$ and $E_{c,ns}$ versus temperature for a non-softening coal (LW). (b) $E_{p,avg}$ and $E_{c,s}$ versus temperature for a softening coal (IL). $E_{p,avg} = \sum E_{p,i} f(E)\Delta E$, $E_{p,i}$ from Eq.(1.3-5), $E_{c,ns}$ and $E_{c,s}$ from Eqs. (1.3-6) and (1.3-8) respectively. Abbreviations: see Fig.1.2-4.

$E_{p,avg} = \sum E_{p,i}\ f(E)\Delta E$. Recall that the rate of tar production for both non-softening and softening coals is represented as the product of the total rate at which the non-x-linked fraction reacts and the two 'E' factors, and that the values of these E factors range between 0 and 1. The decrease in tar production at higher pressures is explained by the smaller $E_{c,ns}$ or $E_{c,s}$ as the pressure increases. At vacuum, $E_{c,ns}$ and $E_{c,s}$ are near 1 indicating negligible mass transport resistance; at high pressures ($\tilde{>}$ 10 atm), the values are much lower, indicating a substantial transport resistance.

Another important feature of this model is that it is able to explain the experimentally observed heating-rate effects at vacuum and 1 atm. Niksa (1981) observed an increasing volatiles (implying tar) production at higher heating rates under vacuum, whereas Anthony et al. (1974) and Suuberg (1977) observed negligible heating-rate effects on product yields at 1 atm. The two sets of results first appear contradictory, but this model can explain the results. Figure 1.3-14 shows that the polymerization effect, indicated by $E_{p,avg}$, is more severe at lower temperatures. The non-x-linked fraction of coal reacts at higher temperatures as the heating rate is increased. Thus without mass transport effects, higher heating rates enhance tar production. At 1 atm, where mass-transport effects are not negligible, tars produced at higher temperatures experience a greater extent of secondary tar cracking reactions. Thus, the increased tar production at higher temperatures is 'off-set' by more cracking reactions.

Figure 1.3-15 plots the best-fitted values of E_{o_s} and σ_s versus the elemental carbon contents of the coal. As before for the MIPR model (Fig.1.3-4), higher rank coals generally gave greater values of E_{o_s} and

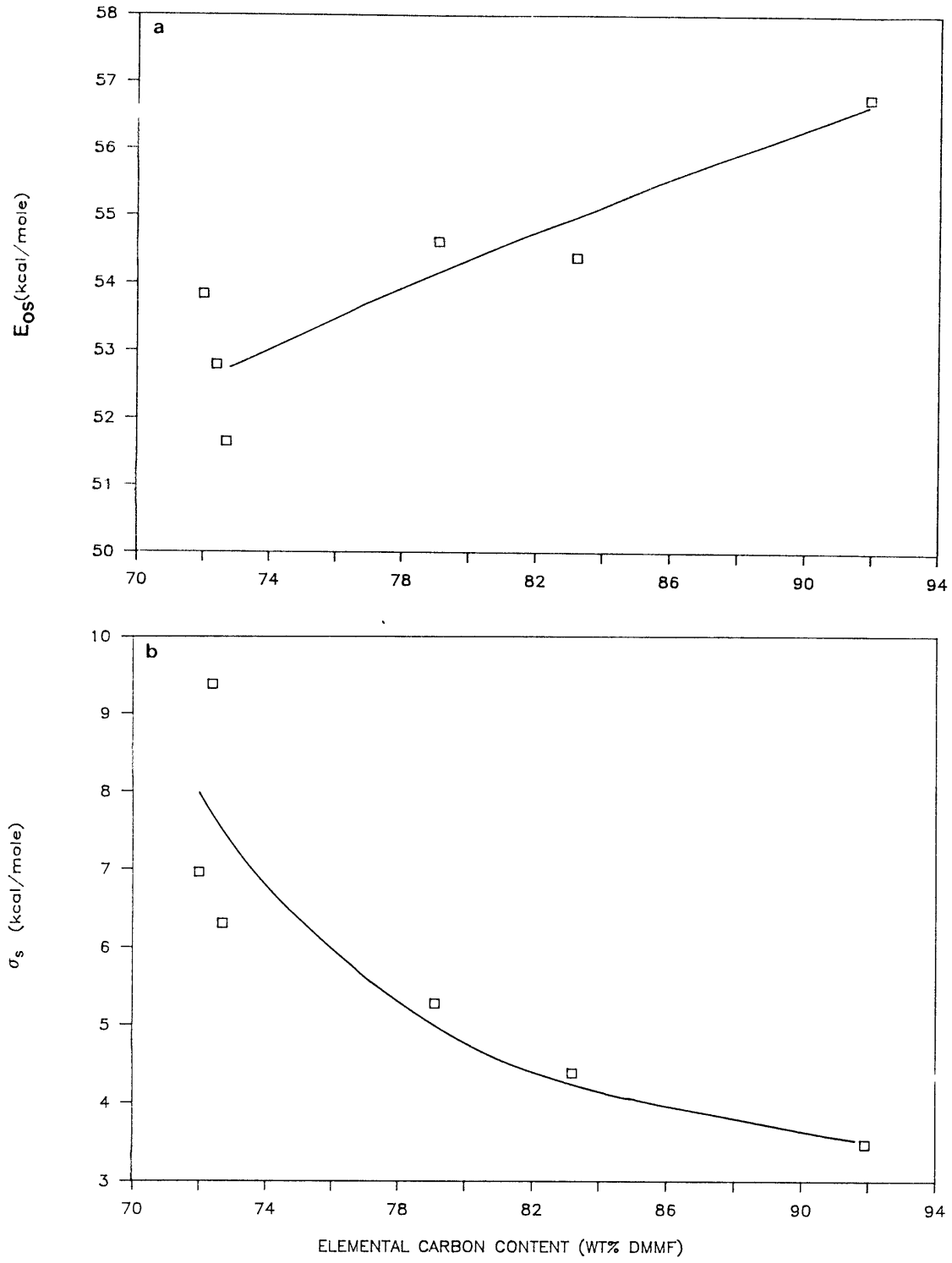

Figure 1.3-15 Best-fitted values of (a) E_{os} and (b) σ_s for predicting tar evolution using the extended MIPR model versus the elemental carbon content of the coal. Carbon: LW < ZP < SR < BL < IL < LK. Abbreviations: see Fig.1.2-4. Other model parameters are given in Table 1.3-1.

smaller values of σ_s, implying that bridging molecules of higher rank coals have bond dissociation energies with a greater mean and a narrower distribution. The best fitted values of E_{os} and σ_s are within the range of expected values for the scission of bibenzyl type bridges ($Ph\text{-}CH_2\text{-}CH_2\text{-}Ph$).

Figure 1.3-16 plots the best-fitted values of e/τ or D_{oL} versus the elemental carbon contents of the coal. For non-softening coals (LW,ZP, SR,BL), the best-fitted values of e/τ range from $10^{-3.23}$ to $10^{-2.70}$. These values imply that the tortuosity (τ) is about 100 assuming that the void fraction (e) is around 0.1. Such values for τ are at least an order of magnitude higher than typical values reported for porous solids (Froment and Bischoff, 1979). For softening coals (IL,LK), the best-fitted values of D_{oL} are between $10^{-5.41}$ and $10^{-5.67}$, which are within the range of expected values of $10^{-6\pm1}$ (Oh, 1985; Suuberg and Sezen, 1985). Changing the value of k_{oc} will directly influence the values of the fitted transport parameters since the quantity that is actually fitted is the ratio $k_{oc}/(e/\tau)$ or k_{oc}/D_{oL}.

In applications employing coals other than those studied here, use of the model parameters obtained from the experimental data specific to the coal of interest would give the most reliable performance. If such experimental information is not available, use of the parameter values estimated from the coal-type dependent trends established in this study is expected to give the next best performance. A note of caution in using the estimated values is that the trends were established from a fairly small number of coals (6), and thus there is a possibility that some 'unusual' coals may behave very differently from those studied here.

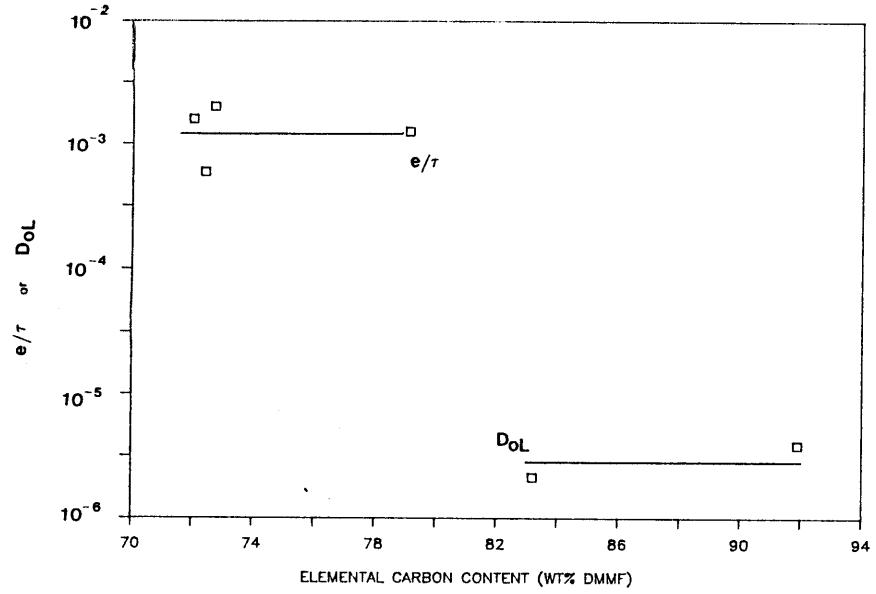

Figure 1.3-16 Best-fitted values of transport parameters for predicting tar evolution using the extended MIPR model versus the elemental carbon content of the coal. e/τ is for non-softening coals (LW,ZP,SR,BL), and D_{oL} is for softening coals (IL,LK). Carbon: LW < ZP < SR < BL < IL < LK. Abbreviations: see Fig.1.2-4. Other model parameters are given in Table 1.3-1.

1) Among the six coals studied, higher rank coals generally produced tars at higher temperatures, and over a narrower range of temperatures. Consequently, a larger mean and a narrower distribution of global activation energies were obtained using the MIPR model for coals of increasing rank.

2) A quantitative correlation, developed to independently relate tar yield limits to coal type and pressure, was tested against a large set of experimental data representing a wide range of coals (37 coals, ranging from lignites to anthracites) and pressures ('vacuum' to 90 atm). A good agreement between the predicted and experimental yields was obtained for all coals and pressures, with a standard error of estimate of ±3 wt% dmmf.

3) In general, no discernable coal-type effects on the apparent rate of gas production were observed. A probable explanation for this is that variations in the rate caused by different coal types are comparable to those caused by uncertainties in experimental measurements. Consequently, the kinetic parameters of the MIPR model for measured gas species were only slightly affected by coal type.

4) Higher rank coals generally produced less carbon oxides and pyrolytic water, but more methane. The ethylene and ethane yields were small and their absolute yield values were less affected by coal type.

5) Total volatiles evolve at higher temperatures and over a narrower range of temperatures for higher rank coals. Thus for coals of increasing rank, a larger mean and a narrower distribution of global activation energies were obtained using the MIPR model. These trends are consistent with the expected behavior from combining the observed coal-type effects on the rate of tar and gas production.

6) The total volatiles yield limit is fairly constant among the lignites, and subbituminous and high-volatile bituminous coals (41-55 wt% dmmf), but is significantly less for the low-volatile bituminous coal (22 wt% dmmf). The high-volatile bituminous coals produced significantly more reactive volatiles than other coals (38-45 versus 19-28 wt% dmmf); reactive volatiles are defined as total volatiles minus water and carbon dioxide yields.

7) Predicted tar yields from the extended MIPR model agreed well with experimental values for a wide range of coal types (lignites to low-volatile bituminous coal; non-softening and softening) and pressures (0.001-10 atm).

8) The best-fitted values of $E_{o s}$ and σ_s for bridge scission are within the range of expected values for the scission of bibenzyl type bridges ($Ph\text{-}CH_2\text{-}CH_2\text{-}Ph$). The best-fitted values of e/τ imply a tortuosity (τ) that is about an order of magnitude greater than typical values reported for porous solids, and those of D_{oL} are within the range of values reported in the literature.

Anthony, D.B., Howard, J.B., Hottel, H.C., and Meissner, H.P., "Rapid Devolatilization of Pulverized Coal," Fifteenth Symp. (Int.) on Combustion, The Combustion Institute, Pittsburgh, 1303, 1974.

Arendt, P.A. and van Heek, K.J., "Comparative Investigations of Coal Pyrolysis Under Inert Gas and Hydrogen at Low and High Heating Rates and Pressures Up to 10 MPa," Fuel, 60, 779, 1981.

Bautista, J.R, "Time-Resolved Pyrolysis Product Distributions of Softening Coals," Ph.D. Thesis, Dept. Chem. Eng., Princeton University, Princeton, NJ, 1984

Burnham, A.K., Oh, M.S., and Crawford, R.W., "Activation Energy Distributions and Related Chemistry for Pyrolysis of the Argonne Premium Coals," submitted for publication in Energy and Fuels, 1988.

Ciuryla, V.T., Weimer, R.F., Bivans, D.A., and Motika, S.A., "Ambient-pressure thermogravimetric characterization of four different coals and their chars," Fuel, 58, 748, 1979.

Cosway, R.G., S.M. Thesis, Dept. Chem. Eng., M.I.T., Cambridge, MA, 1981.

Cypres, R. and Bettens, B., Tetrahedron, 1253, 30, 1974.

Cypres, R. and Bettens, B., Tetrahedron, 353, 31, 1975a.

Cypres, R. and Bettens, B., Tetrahedron, 359, 31, 1975b.

Fong, W.S., "Plasticity and Agglomeration in Coal Pyrolysis," Sc.D. Thesis, Dept. Chem. Eng., M.I.T., Cambridge, MA, 1986.

Franklin, H.D., Peters, W.A., Cariello, F., and Howard, J.B., "Effects of Calcium Minerals on the Rapid Pyrolysis of a Bituminous Coal," Ind. Eng. Chem. Proc. Des. & Dev., 20, 670, 1981.

Freihaut, J.D. and Seery, D.J., "An Investigation of Yields and Characteristics of Tars Released During the Thermal Decomposition of Coal," Am. Chem. Soc. Div. Fuel Chem. Prepr., 26 (2), 133. 1981.

Freihaut, J.D., Zabielski, M.F., and Seery, D.J., "A Parametric Investigation of Tar Release in Coal Devolatilization," Nineteenth Symposium (Int.) on Combustion, The Combustion Institute, Pittsburgh, 1159, 1982.

Froment, G.F. and Bischoff, K.B., Chemical Reactor Analysis and Design, J. Wiley & Sons, New York, 1979.

Gavalas, G.R., Cheong, P.H.K., and Jain, R., "Model of Coal Pyrolysis. 1.Qualitative Development," Ind. Eng. Chem. Fundam., 20, 113, 1981.

Gavalas, G.R., Coal Pyrolysis, Elsevier Scientific Publishing Co.,

Amsterdam, 1984.

Gerstein, B.C., Murphy, P.D., and Ryan, L.M., "Aromaticity in Coal," in Coal Structure, R.A. Meyers, ed., Academic Press, New York, 1982.

Given, P.H., "The Organic Chemistry of Coal Macerals," Penn State Short Course on Coal, The Pennsylvania State University, June 1976.

Griffin, T.P., "Intra-Particle Secondary Reactions in Coal Pyrolysis," Ph.D. Thesis, Dept. Chem. Eng., M.I.T., Cambridge, MA, in preparation 1988.

Howard, J.B., "Fundamentals of Coal Pyrolysis and Hydropyrolysis," in Chemistry of Coal Utilization, 2nd Suppl. Vol., M.A. Elliott, ed., J. Wiley & Sons, New York, 1981.

Hsu, J., Ph.D. Thesis, Dept. Chem. Eng., M.I.T., Cambridge, MA, in preparation 1988.

Ko, G.H., Peters, W.A., and Howard, J.B., "Correlation of Tar Yields from Rapid Pyrolysis with Coal Type and Pressure," Fuel, 66, 1118, 1987.

Ko, G.H., Peters, W.A., and Howard, J.B., "Comparison of Tar Evolution Rate Predictions in Coal Pyrolysis from Multiple Independent Parallel Reaction Model and Functional Group Model Over a Wide Range of Heating Rates," Energy and Fuels, in press 1988a.

Ko, G.H., Sanchez, D.M., Peters, W.A., and Howard, J.B., "Correlations for Effects of Coal Type and Pressure on Tar Yields from Rapid Devolatilization," Twenty-Second Symposium (Int.) on Combustion, in press 1988b.

Loison, R. and Chauvin, F., "Pyrolyse Rapide Du Charbon," Chem. Ind., (Paris), 91, 269, 1964.

Niksa, S., "Time-Resolved Kinetics of Rapid Coal Devolatilization," Ph.D. Thesis, Dept. Chem. Eng., Princeton University, Princeton, NJ, 1981.

Oh, M.S., "Softening Coal Pyrolysis," Sc.D. Thesis, Dept. Chem. Eng., M.I.T., Cambridge, MA, 1985.

Reitzen, R.G., S.M. Thesis, Dept. Chem. Eng., M.I.T., Cambridge, MA, 1978.

Serio, M.A., "Secondary Reactions of Tar in Coal Pyrolysis," Ph.D. Thesis, Dept. Chem. Eng., M.I.T., Cambridge, MA, 1984.

Solomon, P.R. and Hamblen, D.G., Pyrolysis, in Chemistry of Coal Conversion, R.H. Schlosberg, ed., Plenum Press, N.Y., 1985.

Sprouse, K.M. and Schuman, M.D., "Predicting Lignite Devolatilization with the Multiple Parallel and Two-Competing Reaction Models,"

Combustion and Flame, 43, 265-271, 1981.

Sung, W.F., "The Study of the Swelling Property of Bituminous Coal," S.M. Thesis, Dept. Chem. Eng., M.I.T., Cambridge, 1978.

Suuberg, E.M., "Rapid Pyrolysis and Hydropyrolysis of Coal," Sc.D. Thesis, Dept. Chem. Eng., M.I.T., Cambridge, MA, 1977.

Suuberg, E.M. and Sezen, Y., "Competitive Reaction and Transport Processes in Coal Pyrolysis," Proc. 1985 Int. Conf. Coal Science, Sydney, 913, 1985.

Suuberg, E.M., Lee, D., and Larsen, J.W., "Temperature dependence of crosslinking processes in pyrolysing coals," Fuel, 64, 1668, 1985.

Suuberg, E.M., Unger, P.E., and Larsen, P.E., "Relation between Tar and Extractables Formation and Cross-Linking during Coal Pyrolysis," Energy and Fuels, 1, 305, 1987.

Van Krevelen, , D.W., Coal, Elsevier Publishing Co., Amsterdam, 1961.
Weimer, R.F. and Ngan, D.Y., "Rates of Light Gas Production by Devolatilization of Coal and Lignite," Am. Chem. Soc. Div. Fuel Chem. Prepr., 24 (3), 129, 1979.

Coal is projected to be an important source of energy in the future. The vast coal reserve in the U.S. consists of many different coal types with widely varying chemical and physical properties. Understanding the relationship between the coal properties and its conversion behavior is essential for efficient utilization of the coal.

Combustion, gasification and liquefaction are main routes for coal utilization. Coal pyrolysis occurs during initial stages in all of these conversion processes, and thus impacts the course of subsequent processing steps. For instance, tars generated from coal devolatilization influence combustion behavior since they affect ignition and flame stability, soot and PAH formation, heat release, and overall burning efficiency. In coal gasification, the heating value and composition of the product gas depend on the yields and distributions of pyrolysis products.

Coal pyrolysis involves complex thermal decomposition reactions coupled with multicomponent mass transport in a molten liquid or porous solid depending on whether the coal is a softening type or not. The decomposition reactions are generally distinguished as primary and secondary reactions (Serio, 1984). The former refers to reactions that produce volatile products directly from the coal, while the latter refers to further reactions of primary products. In addition to the mass transport, coal type exerts a significant influence on the extent of both primary and secondary reactions (Howard, 1981).

The focus of this study is to improve the understanding of coal-type effects under conditions of practical interest. Many modern coal conversion processes rapidly heat small coal particles under

atmospheric or higher reactor pressures. Low pressures and small particle sizes minimize mass transport resistances, and thus the extent of secondary reactions within or immediately adjacent to the pyrolyzing coal particle. The effect of heating rate on the extent primary and secondary reactions remains to be established as sufficient intrinsic kinetic information on the relative rates of the two reaction types is not available. For this reason, extrapolating kinetic measurements over a wide range of heating rates can be a difficult procedure (Ko et al., 1988a). Therefore, in this study, coal-type effects are investigated using small particles under rapid heating rates over a wide range of pressures.

Understanding the pyrolysis behavior among different coal types requires a reliable experimental data base to determine the kinds and extents of coal-type effects, and a mathematical model to explain the observed behavior. Quantitative time-resolved product evolution measurements for a wide range of coal types under conditions of minimal mass transport limitations, are needed to experimentally establish coal-type effects, but such data are currently lacking. In response, the experimental phase of this study examines the pyrolysis behavior of six coals ranging from low-rank lignites to very high-rank bituminous coals under conditions where mass transport resistances are small.

The modeling phase of this work derives kinetic information from the experimental data, and attempts to relate the kinetic information to measurable properties of the coal. Two different models are utilized in this study: the multiple independent parallel reaction model (MIPR) model and the extended MIPR model. The former model describes kinetics of product evolution under conditions where the

effects of physical transport processes and secondary reactions are relatively unimportant. The latter model explicitly includes approximate descriptions of transport and secondary reaction effects, and thus is applicable over a wider range of operating conditions. More rigorous models often require detailed information on chemical and physical properties of the coal, many of which are difficult to estimate or experimentally measure with currently available techniques. Such limitations are greatly magnified when one needs to consider many different coals.

This chapter provides selected background information pertinent to the main focus of this study - investigating the effect of coal type on pyrolysis behavior. Section 3.1 discusses chemical and physical structural properties among different coal types, noting wherever possible, trends that relate the structural properties to coal type. Section 3.2 describes the current understanding of the reaction chemistry and mass transport phenomena relevant to coal pyrolysis. Section 3.3 reviews experimental data on coal pyrolysis, specifically the effect of main operating variables on pyrolysis behavior. Efforts to quantitatively model the experimentally observed behavior are described in Section 3.4.

3.1. Coal characteristics

According to the A.S.T.M. classification scheme shown in Table 3.1-1, coals are ranked as lignites, subbituminous, bituminous, or anthracites, depending on the fixed carbon and volatile matter contents, and the heating value of the coal. Coals within each rank are further classified into different groups, e.g., low-volatile bituminous, medium-volatile bituminous, and high-volatile bituminous A,B,C. Table 3.1-2 shows variations in some frequently used chemical and physical properties among different coal types. Coals of increasing rank (lignites --→ anthracites) tend to have higher values of elemental carbon, aromaticity, average number of benzene rings/layer, reflectance, and calorific value; and lower amounts of elemental oxygen, carboxyl, hydroxyl, and volatile matter. High-volatile

Table 3.1-1 A.S.T.M. classification of coals by rank[a]. [Reproduced from Singer, 1981.]

Class and Group	Fixed Carbon Limits, % (Dry, Mineral-Matter-Free Basis)		Volatile Matter Limits, % (Dry, Mineral-Matter-Free Basis)		Calorific Value Limits, Btu/lb (Moist,[b] Mineral-Matter-Free Basis)		Agglomerating Character
	Equal or Greater Than	Less Than	Equal or Greater Than	Less Than	Equal or Greater Than	Less Than	
I. Anthracitic							
1. Meta-anthracite	98	...	...	2	...	...	nonagglom-
2. Anthracite	92	98	2	8	...	...	erating
3. Semianthracite[c]	86	92	8	14	...	...	
II. Bituminous							
1. Low-volatile bituminous coal	78	86	14	22	...	...	
2. Medium volatile bituminous coal	69	78	22	31	...	...	
3. High-volatile A bituminous coal	...	69	31	...	14,000[d]	...	commonly agglomerating[c]
4. High-volatile B bituminous coal	...	...	...	...	13,000[d]	14,000	
5. High-volatile C bituminous coal	...	...	...	...	11,500	13,000	
					10,500	11,500	agglomerating
III. Subbituminous							
1. Subbituminous A coal	...	...	...	...	10,500	11,500	
2. Subbituminous B coal	...	...	...	...	9,500	10,500	nonagglom-
3. Subbituminous C coal	...	...	...	...	8,300	9,500	erating
IV. Lignitic							
1. Lignite A	...	...	...	...	6,300	8,300	
2. Lignite B	...	...	...	...	...	6,300	

[a] This classification does not include a few coals, principally nonbanded varieties, which have unusual physical and chemical properties and which come within the limits of fixed carbon or calorific value of the high-volatile bituminous and subbituminous ranks. All of these coals either contain less than 48% dry, mineral-matter-free fixed carbon or have more than 15,500 moist, mineral-matter-free Btu per pound.

[b] Moist refers to coal containing its natural inherent moisture but not including visible water on the surface of the coal.

[c] If agglomerating, classify in low-volatile group of the bituminous class.

[d] Coals having 69% or more fixed carbon on the dry, mineral-matter-free basis shall be classified by fixed carbon, regardless of calorific value.

[e] It is recognized that there may be nonagglomerating varieties in these groups of the bituminous class, and there are notable exceptions in high-volatile C bituminous group.

Reprinted from *ASTM Standards* D 388, Classification of Coals by Rank.

Table 3.1-2 Approximate values of some coal properties in different rank ranges. [Reproduced from Franklin, 1980; data from Given, 1977.]

			High Vol. Bit.			Bituminous		
	Lignite	Subbit.	C	B	A	Medium Vol.	Low Vol.	Anthracite
%C (min. matter free)	65-72	72-76	76-78	78-80	80-87	89	90	93
% H	4.5	5	5.5	5.5	5.5	4.5	3.5	2.5
% O	30	18	13	10	10-4	3-4	3	2
% O as COOH	13-10	5-2	0	0	0	0	0	0
% O as OH	15-10	12-10	9	?	7-3	1-2	0-1	0
Aromatic C atoms % of total C	50	65	?	?	75	80-85	85-90	90-95
Av. no. benz. rings/layer	1-2	?	←	2-3	→		5?	>25?
Volatile matter, %	40-50	35-50	35-45	?	31-40	31-20	20-10	<10
Reflectance, %, Vitrinite	0.2-0.3	0.3-0.4	0.5	0.6	0.6-1.0	1.4	1.8	4
Density	←				minimum			→
Total surface area	←				minimum			→
Plasticity and coke formation			←		only		→	
Calorific value, moist, min. matter free, BTU/lb.	7000	10,000	12,000	13,500	14,500	15,000	15,800	15,200

bituminous coals have maximum values of elemental hydrogen. More detailed descriptions of chemical and physical properties of coal are given below.

3.1.1 Chemical structure

Detailed chemical structure of coal is reviewed in many books on coal utilization (e.g., Given, 1976; Whitehurst et al., 1980; Gavalas, 1984). Tingey and Morrey (1973) have compiled chemical structural data reported in the literature up to 1973, and Suuberg (1977) has done similar work up to 1977. Much more data have accumulated since then as a result of improvements made in analytical techniques and a resurgence of scientific and commercial interest in coal utilization during the 70's and early 80's. A brief survey of more recent literature was done by Ko (Howard et al., 1987a).

Figure 3.1-1 gives a molecular description of coal inferred from the literature survey, where the coal is postulated to be made-up of clusters of condensed and hydroaromatic rings (nuclei) held together by bridge groups. Peripheral groups are attached to the nuclei. This postulated structure identifies (1) nuclei, (2) bridge groups, and (3) peripheral groups as main building-units of a coal molecule. Differences within each of these three components reflect variations in chemical properties among different coal types. Such a unitary description is convenient in explaining the effect of coal type on the pyrolysis behavior (Chapter 5), and in formulating a quantitative model (Chapter 6).

Within nuclei, structural features reckoned to play an important role in pyrolysis are the aromaticity, nucleus size, and heteroatom

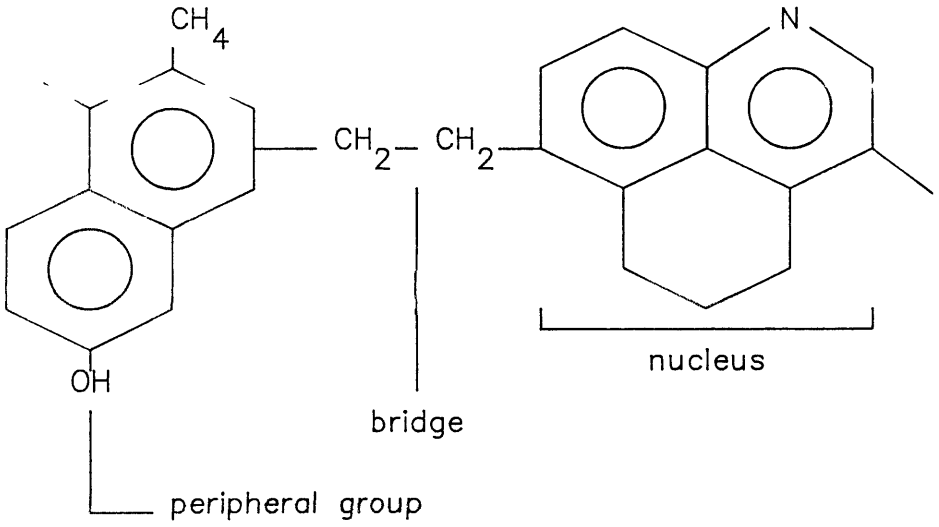

Figure 3.1-1 Hypothetical coal structure.

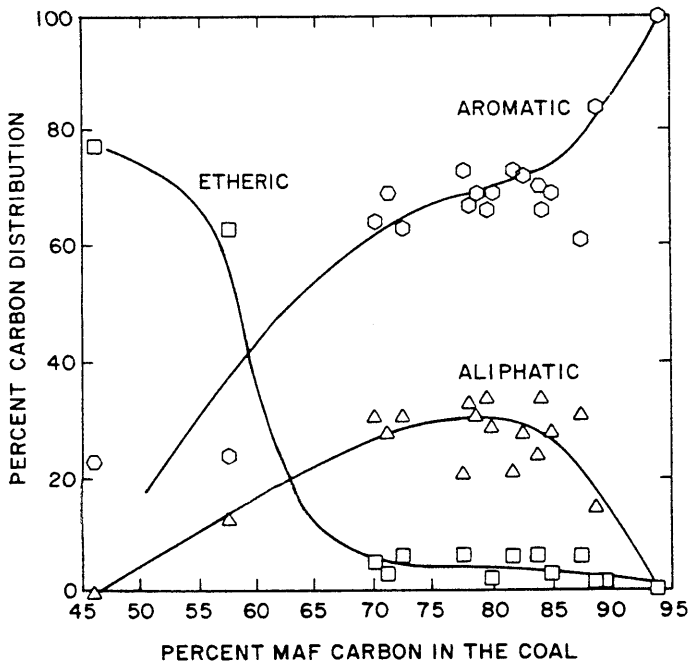

Figure 3.1-2 Aromatic carbon, aliphatic carbon, and etheric carbon versus elemental carbon content. [Reproduced from Whitehurst et al. (1980).]

content. Aromaticity is a measure of the amount of aromatic carbon in coal, and is defined as

$$fa = \text{aromaticity} = \frac{\text{number of aromatic carbon atoms}}{\text{total number of carbon atoms}} \qquad (3.1\text{-}1)$$

Table 3.1-3 lists different methods to probe the aromatic structure of nuclei and gives a brief description of each method. Despite some scatter, Figure 3.1-2 shows that higher rank coals tend to be more aromatic. From the aromaticity information, one can infer how many aliphatic carbons and hydrogens are present. These aliphatic quantities are believed to play key roles in thermal scission and free-radical stabilization type reactions. The nucleus size is often expressed as number of rings per nucleus. Rough estimates of the ring size are 1-2 for lignites, 3-4 for bituminous coals, and > 4 for anthracites (Given, 1977). Winans et al. (1988) recently suggested that the ring size of bituminous coals could be as low as 1 or 2, and that growth during thermal degradation reactions may be a possible reason for observing larger ring sizes for these coals. The ring size is an important property in determining bond dissociation energies of bridging molecules because it affects the degree of resonance stabilization of benzyl radicals formed from typical bridge scission reactions. But, a simple correlation between the ring size and the extent of resonance stabilization is difficult to observe since the stabilization is also influenced by other factors, e.g., the position of a $CH_2\cdot$ radical on the ring structure (Stein and Golden, 1977). Heteroatoms within the aromatic rings include N, S, and O. Pyrolysis studies of coal tars (Wornat, 1988) and model compounds (Briunsma et al., 1988) containing nitrogen heteroatoms indicate that the heteroatom enhances the reactivity. Unfortunately, data on the types and amounts

Table 3.1-3 Aromaticity measurement techniques.

(1) NMR
Nuclear magnetic resonance arises from the interaction of the magnetic component of electromagnetic radiation with the very small magnetic moments possessed by certain nuclei (^{13}C, ^{1}H). Structural information is obtained from measuring the magnetic field required to resonate and the number of resonating nuclei. For more information see Bartle and Jones (1978), Retcofsky (1982).

(2) IR and FTIR
Infrared spectroscopic techniques measure the frequency and intensity of light reflection emission and absorption due to the stretching and bending motions of molecules. Fourier Transform techniques improve the resolution and sensitivity of this technique.

(3) ESR
Electron spin resonance spectroscopy is based upon the absorption of microwave radiation by an unpaired electron when it is exposed to a strong magnetic field. The unpaired electrons of free radicals in coals are related to the condensed aromatic system. This method has provided only qualitative information on the aromatic coal structure. For more information see Retcofsky et al. (1981).

(4) X-Ray Diffraction
Structural information is inferred by comparing the x-ray spectrum of coal to x-ray spectra of known aromatic crystallites. For more information see Hirsch (1954), and Kwan and Yen (1976).

(5) Chemical Methods
Fluorination of aromatic rings (Huston and Studier, 1981) appears to be the only reliable chemical method for measuring aromaticity.

(6) Optical Methods
Aromaticity is measured by comparing reflectance of coal macerals to those of model compounds (Van Krevelen, 1961).

(7) Density Methods
The distance between C-C bonds is related to aromaticty as well as the density. Empirical correlations between the density and aromaticity of known compounds are used to measure the aromaticity of coal.

of heteroatom functionalities in coals are very scarce.

Many pyrolysis models either explicitly or implicitly assume that the scission of bridge groups is the main route for thermal decomposition of coal (Niksa and Kerstein, 1985; Unger and Suuberg, 1981; Gavalas et al., 1981a,b; extended multiple independent parallel reaction model, see Chapter 6). Further degradation of thermolyzed bridges may contribute in light gas production. Various chemical and spectroscopic studies have produced evidence that a wide range of bridge types are present in the coal. Oxidative degradation studies indicate the presence of ethylene, butyl ether or polymethyl (>4 carbons) linkages (Deno et al., 1981). Reductive alkylation studies of Ignasiak and Gawlak (1977) support the presence of ether type bridges. From C^{13} CP/MAS NMR and acetylation measurements, Yoshida et al. (1984) report higher concentrations of ether type bridges for lower rank coals. The presence of methylene, ethylene, aliphatic ether, and ether linkages has been inferred from liquefaction studies (Mayo et al., 1978; Whitehurst, 1978; Poutsma, 1980; Benjamin et al., 1978). However based on currently available data, no reliable quantitative trends can be observed on types and amounts of bridge groups among different coal types.

Peripheral groups are postulated to contribute in light gas production and to influence the stability of nuclei. Evidence for the latter postulate comes from the recent work of Wornat (1988), which indicates that substituted coal tars (i.e., tars with peripheral groups) are less stable than unsubstituted tars when subjected to thermal degradation. A further observation from Wornat (1988) is that there is little difference in the stability of substituted tars of the

same ring number (or size). It is convenient to subdivide the peripheral group into (1) oxygen containing species, e.g., -OH, -COOH, C=O, $-OCH_3$; (2) alkyl chains, $-CH_3$, $-C_2H_5$; and (3) N or S containing species, $-NH_2$, -SH. Reasonable estimates of the amount of -OH and -COOH groups present in different coals, can be made respectively from the data of Yarzab et al. (1980) and Blom (1960). Based on product yield data from coal pyrolysis, pyrolytic water is often hypothesized to be produced from -OH groups, and carbon dioxide from -COOH groups. Higher rank coals generally have less oxygen containing groups. The only work found in the literature on peripheral alkyl groups is from Deno et al. (1981). Their study shows that aryl-methyl and aryl-ethyl groups account for approximately 1% and 0.1-0.3% of the total carbon respectively. Larger alkyl groups were not detected. Although four different coals were used, no information on effects of coal type can be inferred. Discussions on the subgroup (3) will be omitted here since the experimental program of this study excludes measuring gaseous nitrogen and sulphur compounds.

3.1.2 Physical structure

Distribution of pore sizes is an important physical property in coal pyrolysis. In non-softening coals, the pore size is a key parameter in describing the transport of volatiles (see Section 3.4.3). In softening coals, the 'melting' destroys much of the initial pore structure. But, porosity information can still be valuable for these coals. For example, Oh et al. (1988) utilized the macropore volume data to estimate the initial number density of bubbles in their bubble transport model of softening coal pyrolysis.

Literature data on coal pore structure (Gan et al., 1972) show that all three pore types, micropores (pore dia. <12 Å), transitional pores (12-300 Å) and macropores (300 Å - 1 μm), are present in raw coal. Table 3.1-4 gives initial pore-size distributions for various ranks of coal. In general, micro- and macropores appear to dominate the pore structure in lignites and medium-volatile and low-volatile bituminous coals, whereas transitional pores are most abundant in high-volatile bituminous coals. Upon pyrolysis at relatively mild temperatures (500 C), Gavalas and Wilks (1980) report that the coal retains its general structure, though they observed a slight increase of pores above 0.015 μm and an elimination of pores below that size. A review by Suuberg (1985) report that apparent porosity may increase from an initial value of 10% to a final value of 50% at the end of pyrolysis, and that this may be attributed to increases in micro- and macropores.

3.2. Reaction chemistry and mass transport

3.2.1. Reaction chemistry

The reaction chemistry of coal pyrolysis is extremely complex. A complete quantitative description of reaction mechanisms remains to be established. However, recent reviews by Stein (1981, 1985) provide valuable semi-quantitative analysis of reaction chemistry pertinent to coal conversion. This section discusses Stein's reviews in the context of coal pyrolysis.

Free-radical reaction path

Free-radical reactions are believed to be the primary path for

Table 3.1-4 Initial pore-size distributions for various ranks of coals[a].

Sample	Rank	V_T[b] (cm³/g)	V_1[c] (cm³/g)	V_2[d] (cm³/g)	V_3[e] (cm³/g)	V_3(%)	V_2(%)	V_1(%)
PSOC-80	Anthracite	0.076	0.009	0.010	0.057	75.0	13.1	11.9
PSOC-127	LVB	0.052	0.014	0.000	0.038	73.0	0	27.0
PSOC-135	MVB	0.042	0.016	0.000	0.026	61.9	0	38.1
PSOC-4	HVA bituminous	0.033	0.017	0.000	0.016	48.5	0	51.5
PSOC-105A	HVB bituminous	0.144	0.036	0.065	0.043	29.9	45.1	25.0
Rand	HVC bituminous	0.083	0.017	0.027	0.039	47.0	32.5	20.5
PSOC-26	HVC-bituminous	0.158	0.031	0.061	0.066	41.8	38.6	19.6
POC-197	HVB bituminous	0.105	0.022	0.013	0.070	66.7	12.4	20.9
PSOC-190	HCV bituminous	0.232	0.040	0.122	0.070	30.2	52.6	17.2
PSOC-141	Lignite	0.114	0.088	0.004	0.022	19.3	3.5	77.2
PSOC-87	Lignite	0.105	0.062	0.000	0.043	40.9	0	59.1
PSOC-89	Lignite	0.073	0.064	0.000	0.009	12.3	0	87.7

[a] Data from Gan et al. (1972); Table reproduced from Suuberg (1985).
[b] V_T = total porosity.
[c] V_1 = macroporosity (300 Å - 1 μm).
[d] V_2 = transitional porosity (12-300 Å).
[e] V_3 = microporosity (4-12 Å).

thermal decomposition of coal (Stein, 1985). Supporting evidence for this view comes from the general observation that free-radical reactions control the pyrolysis chemistry of most organic substances. In addition, resonance-stabilized aromatic and hydroaromatic units derived from coal tars and liquids are formed and react readily at coal decomposition temperatures ($\tilde{>}$ 350 C). Gavalas (1984) has reviewed some organic model compound studies that suggest concerted reaction mechanisms as possible pathways to explain the results. But he also points out that results from other studies have been explained solely by free-radical mechanisms. Thus, he concludes that "more experimental work is needed to determine which of the pyrolysis reactions proceed by concerted mechanisms and which by the more widely accepted free-radical mechanisms". In this study, all reactions in coal pyrolysis are assumed to occur via the latter mechanism.

Applying gas-phase rate constants to condensed-phase reactions

Most of the reaction in primary coal pyrolysis occurs in condensed-phase (liquid or solid), whereas much of the experimental kinetic information as well as rate estimation methods [e.g., thermo-chemical kinetic methods, Benson (1976)] are for gas-phase reactions. Thus, the question on the applicability of gas-phase reaction rates to condensed-phase reactions needs to be examined.

Stein (1981) states that using gas-phase rate constants for liquid-phase reactions is a good approximation in the absence of "significant differences in solvent-molecule interactions between reactants and products". Such conditions closely resemble those of softening coals during the 'liquid-like' phase. For non-softening and softening coals

during the solid phase, applying the analysis is less valid due to possible "cage" effects, where the restricted mobility hinders the product species from diffusing apart. But Stein (1981) points out that this effect can be significant only for bond homolysis reactions (R1-R2 $\rightarrow$ R1$\cdot$ + R2$\cdot$). If R1$\cdot$ and R2$\cdot$ radicals are relatively large in size, a slower net homolysis reaction rate is expected since the "cage" effect would enhance the rate of reverse recombination reaction. Stein's evidence on the applicability of gas-phase thermochemistry and kinetics to liquid phase is based on the comparison of equilibrium constants in the two phases. First consider unimolecular reactions of type A $\rightarrow$ B, involving no change in the number of moles (i.e., $\Delta n = 0$), and without "cage" and solvation effects. Examples of such reactions pertinent to coal pyrolysis include bond homolysis and free-radical beta-bond scission reactions (within the framework of transition-state theory, see below). On the basis of available experimental data, Stein (1981) concludes that the equilibrium constants for these reactions can be assumed to be nearly the same for the gas and liquid phase. The equilibrium condition can be related to reaction rates from the transition-state theory. Represent a unimolecular homolysis reaction as

$$AB \text{ -------} \rightarrow AB^{\#} \text{ -------} \rightarrow A + B$$

where # indicates the transition state. Then, the rate constant for decomposition of AB is

$$k_{AB} = (kT/h)K^{\#}_{AB}$$

where $K^{\#}_{AB}=[AB]^{\#}/[AB]$ and (kT/h) is a universal frequency factor with a value of 6.3×10^{12} s^{-1} at 300 K. If one assumes that the comparable equilibrium condition between the two phases for "normal" species holds

for transition-state species, the rate constants in the two phases should also be about the same.

Similar analysis can be made for bimolecular reactions in the absence of substantial solvation differences between reactants and products (or transition state), and diffusion limitations. Hydrogen abstraction and molecule-radical addition reactions are examples of such reactions believed to be important in coal pyrolysis. For reactions involving two large reactant molecules (e.g., n-paraffins), Stein concludes that $K_l \approx K_g$, and therefore $k_l \approx k_g$. However, when one of the reactants is a small molecule (e.g., methane, $H\cdot$), the value of K_l/K_g considerably exceeds unity implying that the liquid phase reaction rate is much greater than that of the gas phase.

Under conditions where solvation and diffusion limiting effects are non-negligible, using gas-phase reaction constants in coal pyrolysis is not strictly valid. However, at coal conversion temperatures, the former effect is expected to be far smaller due to reduced hydrogen bonding, polar, and charge-transfer interactions. A decrease in the latter effect is also expected since the rate of diffusion increases at higher temperatures, whereas the rate of recombination is relatively independent of temperature.

To summarize, in the absence of significant solvation and diffusion effects, liquid-phase reaction constants can be adequately estimated from gas-phase reaction kinetic data or from thermochemical estimation methods. Applying the gas-phase rate information to solid-phase reaction is less valid, especially for bond homolysis reactions involving large molecules, and bimolecular reactions involving molecules of widely different size. The solvation and diffusion

effects are less at higher temperatures, and thus the above approximation becomes more valid.

Elementary reactions

1. Unimolecular reactions

Bond-homolysis. Rates of homolysis reactions, (3.2-1), may be estimated relative to bibenzyl homolysis, (3.2-2), whose rates and thermodynamics are well established.

$$\text{R-X} \xrightarrow{k_1} \text{R}\cdot + \text{X}\cdot \qquad (3.2\text{-}1)$$

$$\phi\text{CH}_2\text{-CH}_2\phi \xrightarrow{k_2} 2\ \phi\text{CH}_2\cdot \qquad (3.2\text{-}2)$$

Assuming that recombination rate constants are the same for all radicals in a given fluid, the rate of (3.2-1) is

$$k_1 = k_2 \exp[-(\Delta H_1 - \Delta H_2)/RT + (\Delta S_{i1} - \Delta S_{i2})/R] \qquad (3.2\text{-}3)$$

where S_i is intrinsic entropy (excludes rotational symmetry), ΔH and ΔS are obtained from gas-phase data or estimation methods (Benson, 1976), and $k_2 = 10^{16.6} \exp(-66.8 \text{ kcal mol}^{-1}/RT)\ \text{s}^{-1}$ in tetralin (Stein, 1985). Due to "cage" effects, the rate of bond homolysis declines with increasing fluid viscosity with an approximate relationship, $k \propto \eta^{-0.4\pm0.1}$ (Stein, 1981). Also, an appreciable decrease in the ethylene bond strength, and hence an increase in the rate, is expected if benzyl rings are more heavily substituted (e.g., -OH, -COOH), or if they are replaced by polyaromatic clusters. Such effects can create a spread in bond strengths of "at least" 10 kcal mol^{-1}.

Beta-bond scission. An example of beta-scission reaction ($\cdot$X-Y-Z $\rightarrow$ X=Y + Z$\cdot$) in coal pyrolysis is

$$\phi CH_2CH_2CH_2\cdot \text{ ----------} \rightarrow \phi CH{=}CH_2 + CH_3\cdot \qquad (3.2\text{-}4)$$

Preexponential factors for beta-scission reactions are typically $10^{14.5\pm1}$ s^{-1} compared $10^{15.5\pm1}$ s^{-1} for homolysis reactions. Activation energies are given by ΔH + intrinsic activation energy (equal to the activation energy for the reverse addition reaction). Intrinsic activation energies range from 1-4 kcal mol^{-1} for β C-H dissociation to 6-12 kcal mol^{-1} for β C-C dissociation, all of which are significantly lower than those of homolysis reactions. The ΔH of the reaction is most easily computed from appropriate nonradical reactions

$$\Delta H(\cdot XYZ \rightarrow XY+Z\cdot) = \Delta H(H\text{-}XYZ \rightarrow XY+Z\text{-}H) + D(Z\text{-}H) - D(H\text{-}XYZ) \qquad (3.2\text{-}5)$$

where D(Z-H) and D(H-XYZ) represent bond strengths of Z-H and H-XYZ respectively.

2. Bimolecular reactions

Radical-molecule reactions. H-atom abstraction and radical addition are examples of radical-molecule reactions. Rate constants for the abstraction reaction are sensitive to reaction thermochemistry and heteroatom (polar) effects, but are not strongly affected by steric factors. The Polyani relation applies for H abstraction for homologous series of H donors. Thus, for exothermic abstraction, $E_{act} = E_o - \alpha |\Delta H|$, and for endothermic abstraction, $E_{act} = E_o + (1-\alpha)|\Delta H|$, where the constant α ranges from 0 to 1. Kerr and Parsonage (1976) report E_o = 15 kcal mol^{-1} and α = 0.5 for methyl radical abstraction from acyclic paraffins; Stein (1985) believes that this value of α may be considered typical for H-abstraction. Generally, intrinsic activation energies of reactions involving carbon-centered radicals are $\approx$15 kcal mol^{-1}, whereas they may be significantly lower for oxygen- and sulphur-

centered radicals. Preexponential factors are typically $10^{8.5}$ $M^{-1}s^{-1}$ for polyatomic species, and higher for smaller species.

Radical addition to unsaturated structures compete with H-abstraction reactions. Preexponential factors for carbon-centered radicals are $10^{7.5\pm1}$ $M^{-1}s^{-1}$, and they also tend to be larger for smaller species. For olefinic compounds, activation energies are often lower for addition than abstraction. The Polanyi relation is expected to hold for addition of reactive radicals $C_6H_5\cdot$ and $CH_3\cdot$ to polyaromatics, and an α of $\approx$ 0.25 appears to be a typical value for these reactions (Stein, 1985). At coal pyrolysis temperatures, redissociation of radical/molecule adducts is also expected to be very fast. Thus, for addition to be effective, rapid irreversible reactions of the adducts are important.

Molecule-molecule reactions. An example of this reaction type is a molecular disproportionation, where two radicals are formed from a transfer of a H atom from one molecule to another. This reaction may serve as an important source of free radicals, particularly after weak covalent bonds have decomposed, but no quantitative information is available.

Radical-radical reactions. These reactions occur via recombination or disproportionation. At low temperatures, the former is the dominant mode of radical termination. Without severe steric effects, Stein reports that radicals recombine with a "near-diffusion-controlled" rate constant of 10^9-10^{10} $M^{-1}s^{-1}$. The latter is only significant for radicals with weak β-H bonds ($\lesssim$ 50 kcal mol^{-1}).

3.2.2. Mass Transport

Mass transport limitations can significantly alter the pyrolysis behavior predicted from considering just the chemical decomposition. Suuberg (1985) gives the most comprehensive review to date on mass transfer effects in coal pyrolysis. The discussion below considers only the transport of high molecular weight volatiles (tars). Low molecular weight volatiles (gases) generally escape rapidly and are relatively unreactive.

Internal mass transport

Distinctions need to be made between non-softening and softening coals as their mode of volatiles transport are radically different. Consider the non-softening case first. Porosity characteristics among different coal types have been discussed in Section 3.1.2. Table 3.1-4 gives initial pore-size distributions for various ranks of coals. Pores are generally classified, according to their pore sizes, as micropores, transitional pores, or macropores. The mode of diffusive transport differs significantly in the three pore regimes. In addition, depending on the regime, diffusivity values vary many orders of magnitude (Fig.3.2-1).

Configurational diffusion is the dominant mode of transport in micropores. Since the size of pore diameter and diffusing tar molecules is comparable in this regime, the configurational diffusivity (assumed binary), D_C, is expected to be activated, and is in the form of

$$D_C = D_{C\,o} \exp(-E_C/RT) \qquad (3.2\text{-}6)$$

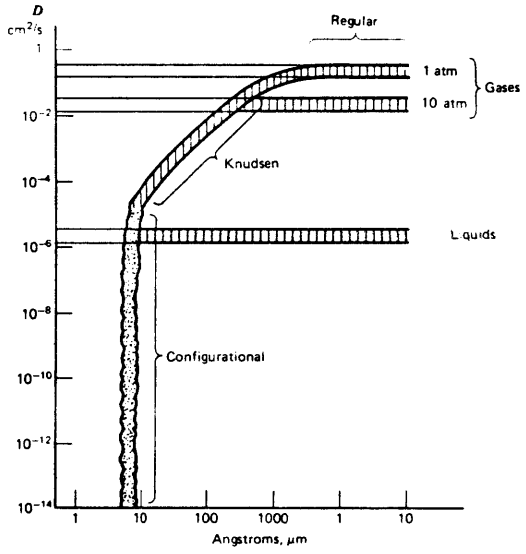

Figure 3.2-1 Diffusivity versus pore size for regimes of configurational, Knudsen, and regular diffusion. [Reproduced from Froment and Bischoff (1979).]

where D_{Co} and E_C represent preexponential factor and activation energy respectively. Knudsen diffusive transport is dominant in transitional pores, a regime where collision between pore walls and diffusing species is important. Knudsen diffusivity, D_K, is of the form

$$D_K = 4r/3\ (2RT/\pi M_A)^{1/2} \qquad (3.2\text{-}7)$$

where r is the pore radius and M_A is the molecular weight of diffusing molecule. "Regular" molecular diffusion dominates in macropores, a regime where intermolecular collisions are important. Molecular diffusivity, D_M, is of the form

$$D_M = D_{Mo}\ (T/273)^{1.5}\ (1/P) \qquad (3.2\text{-}8)$$

where D_{Mo} is the reference molecular diffusivity at T = 273 K and P = 1 atm, and is inversely correlated with a fractional power of the molecular weight of diffusing species [e.g., see Fuller, Schettler and Giddings method given in Reid et al. (1977)]. Convective transport contributions can also be important in this pore regime.

In <u>softening coals</u>, liquid-phase molecular diffusion and volatile "bubble" growth/escape are believed to be the main modes of tar transport. Diffusivity in the molten coal, D_L, is (Oh, 1985)

$$D_L = C_D\ T/\mu^{2/3} \qquad (3.2\text{-}9)$$

where C_D is a constant estimated to be $\approx 10^{-5}$ cm^2/s for molten coal, and μ is the viscosity of the coal melt with a minimum value of $\approx 10^4$ poise (Oh, 1985). Based on the particle radius length scale, Oh (1985) asserts that the characteristic time for liquid phase diffusion is too slow to explain experimentally observed tar release rates in pyrolysis. She proposes an alternative mechanism whereby most of the volatiles transport occurs via the following sequential steps: (1) volatiles diffuse into many small bubbles distributed throughout the molten coal,

(2) bubbles grow as more volatiles diffuse-in, and (3) volatiles are released outside the particle when a growing bubble bursts upon contacting the particle surface.

Another postulated mechanism for volatiles transport in softening coals proposes that most of the bubbling phenomena occur before most tars are evolved (Griffin, 1988; Hsu, 1988). Quantitative information on the degree of overlap between the two processes is currently being gathered by the two investigators. Implicit in this mechanism is that, in computing the characteristic time scale for intra-particle mass transport, the 'shell' thickness is the more appropriate length scale than the particle radius. The particle shape, after bubbling, resembles a cenospherical shell. For $\approx$40 μm radius particles of Pittsburgh Seam bituminous coal pyrolyzed at 1000 C/s at atmospheric pressure, Griffin (1988) estimates the shell thickness to be approximately 20% of the particle radius. The diffusion time scale based on the shell thickness is comparable to observed characteristic times for pyrolysis at the heating rate of approximately 1000 C/s.

External mass transport

For non-softening coals, molecular diffusion and convective flow are the main modes of external transport, whereas for softening coals, surface evaporation is also important. The molecular diffusivity is of the same form as that in macropore transport [Eq.(3.2-8)]. From comparing rates of pure diffusive flux and convection enhanced diffusive flux, as in Eq.(3.2-10), Suuberg (1985) concludes that convective enhancement is insignificant for small particles ($\tilde{<}$ 100 μm).

$$\text{pure diffusion/convective enhancement} = \phi/[1-\exp(-\phi)] \qquad (3.2\text{-}10)$$

where $\phi = NR/D_V C_V$, N = total molar surface flux, R = particle radius, D_V = diffusivity of tar in the surrounding gas, and C_V = molar density of the gas phase.

Experimental evidence that surface evaporation is an important factor in determining the mechanism of tar transport is based on Suuberg and co-workers' (Unger and Suuberg, 1984; Suuberg, 1985) molecular-weight (MW) distribution measurements on tar and extract (which is speculated to be the precursor of tar). For tars and extracts produced from pyrolyzing a HVB softening coal in the temperature range of 727 to 951 K, they observed (A) the MW of the tar is lower than that of the extract, (B) the MW of atmospheric-tar is lower than that of vacuum-tar, and (C) the MW distribution of atmospheric-tar is very similar to that of the same tar that was re-evaporated. These observations are used to support the view that tars from softening coals are produced from selective evaporation of lighter components of extractable materials, and thus the rate of tar escape is significantly influenced by evaporation. However, the above observations also support the view that the internal mass transport may be the rate controlling step. For example, consistent with (A) is the fact that lighter species diffuse through the molten coal faster as they tend to have larger diffusion coefficients, e.g., the liquid-phase diffusion coefficient based on hydrodynamic theory is inversely related to the radius of the solute molecule (Reid et al., 1977). The observation (B) can also be explained by the fact that atmospheric-tar is more exposed to secondary reactions, which decrease MW (Serio, 1984). The observation (C) is difficult to interpret in terms of internal mass transport since sample conditions in the re-evaporation

experiment are likely to be different from those of the molten coal.

Also observed in the molecular weight studies was that tars from a wide variety of different coals (1 lignite, 2 HVB and 1 LVB coals) show "somewhat" similar MW distributions. This observation has been interpreted as to suggest that perhaps evaporation is also important for non-softening coals. But, the inverse relationship between the molecular diffusion coefficient [Eq.(3.2-8)] and a fractional power of tar MW (Reid et al., 1977), offers an alternative explanation for the observed behavior.

3.3. Experimental studies

Coal type, temperature-time history, reactor pressure, and particle size are the four main reactor variables in coal pyrolysis. In describing the influence of these variables on pyrolysis behavior, it is convenient to distinguish primary and secondary reactions, and further divide secondary processes into intra- and extra-particle reactions. Mass transport effects are coupled to secondary reactions as the rate of transport determines the secondary reaction residence time for reactive volatiles. The first two variables affect both the primary and secondary reactions, whereas the latter two variables affect mainly the secondary reactions.

3.3.1. Effect of coal type

Figure 3.3-1 compares literature data on product yields and distributions obtained from different coal types under similar operating conditions, where thinly spread small coal particles ($\tilde{<}$ 100 μm dia.) were pyrolyzed in a screen-heater type reactor under rapid

heating (≈1000 C/s) to $\tilde{<}$ 1000 C at pressures ranging from 'vacuum' ($\tilde{<}10^{-3}$ atm) to 69 atm. The rapid dilution and quenching of reactive volatiles presented minimal opportunity for extra-particle secondary reactions. Table 4.2-1 gives the elemental analysis of the coals compared in Fig.3.3-1. The general trends observed from the vacuum data (Fig.3.3-1a) are (1) carbon oxides and pyrolytic water yields decrease for higher rank coals, (2) methane and tar yields reach a maximum for coals with the elemental carbon content of 85-87 and 78-86 wt% daf respectively; (3) trends for other hydrocarbon gases are less clear. More experimental data are needed to establish trends at higher pressures.

Several investigators have attempted to relate pyrolysis product yields to coal properties. Neoh and Gannon (1984) observed that total volatile yields can be closely correlated to the reflectance and elemental composition of the coal. The yields were obtained under conditions representative of pulverized coal combustion. Using data from coal and biomass pyrolysis, Peters (1984) graphically compared total volatiles, carbon monoxide, and tar yields to values of certain elemental ratios in the coal, but established no quantitative correlations. Results from Suuberg (1977) suggest that carbon dioxide and pyrolytic water yields are linked respectively to the carboxyl and hydroxyl group contents in the coal. Based on CP/MAS ^{13}C NMR spectra measurements, Calkins et al. (1984 a,b,c,d) report that low molecular weight olefin yields are proportional to the amount of long-chain polymethylene structures present in the parent coal. Neavel et al. (1981) correlated liquid yields, from pyrolysis of vitrinite samples in a packed-bed type reactor, to the elemental hydrogen and organic

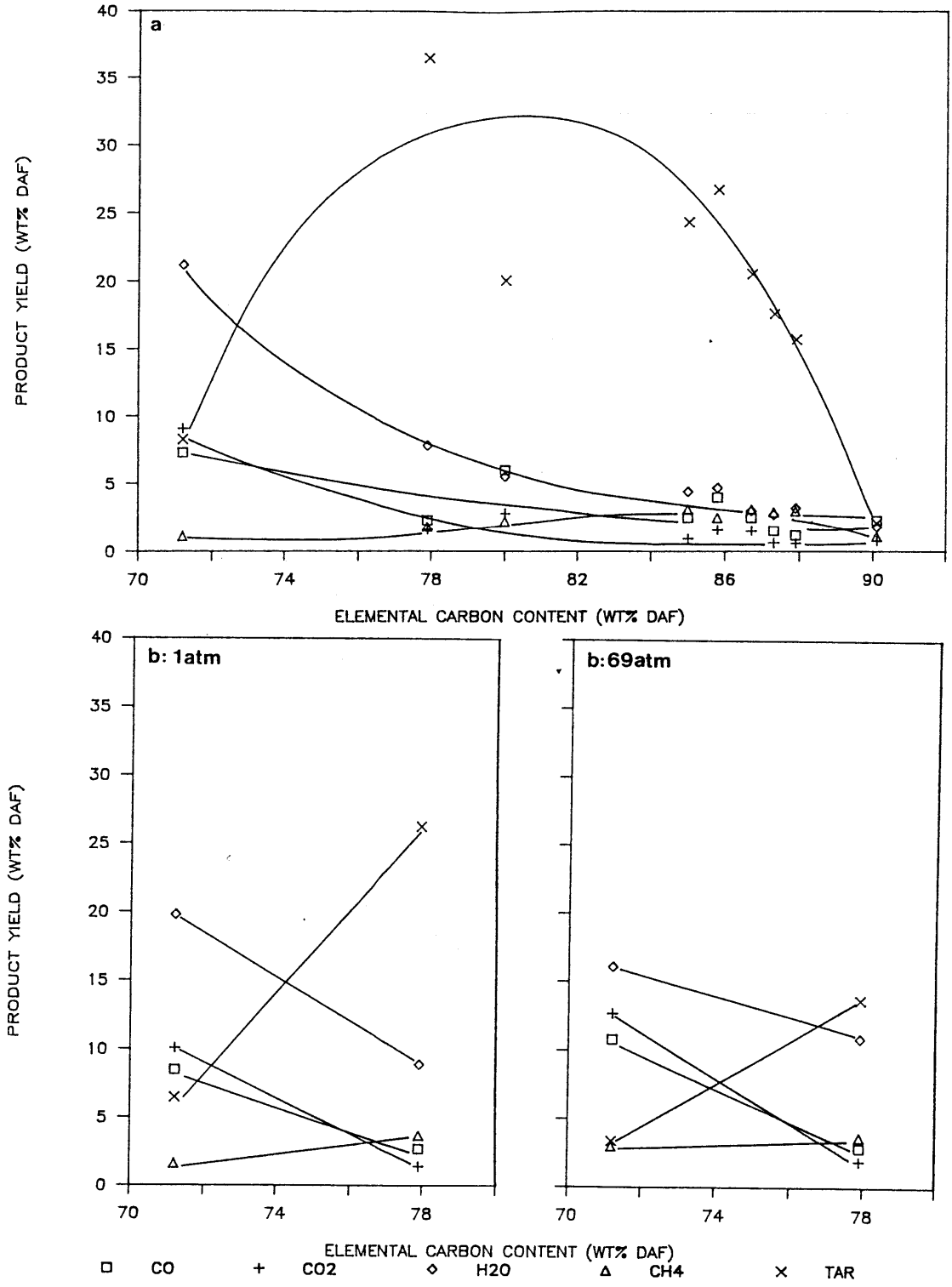

Figure 3.3-1 Comparison of product yields and distributions from different coal types: (a) vacuum, (b) 1 and 69 atm. [Data from Loison and Chauvin (1964) and Suuberg (1977).]

sulphur contents of the coal (Fig.3.3-2).

The effect of coal type on volatiles evolution rate is currently unclear. Kobayashi et al. (1977) showed that total weight loss data from both Montana lignite and Pittsburgh Seam bituminous coal can be described with the same set of model parameters, implying no apparent coal-type effect (Fig.3.3-3). The data were obtained at temperatures ranging from 700 to 1827 C, and heating rates from 180 to 10^6 C/s. The study assumed a competing reaction model consisting of two first-order single-reactions

$$\text{Coal} \xrightarrow{k_1} \text{Volatile 1 } (\alpha_1) + \text{Residue 1 } (1-\alpha_1)$$
$$\text{Coal} \xrightarrow{k_2} \text{Volatile 2 } (\alpha_2) + \text{Residue 2 } (1-\alpha_2)$$

k_1 and k_2 are pseudo Arrhenius rate constants, with a pseudo frequency factor/activation energy of $2\times10^5 s^{-1}$/25 kcal mol^{-1}, and $1.3\times10^7 s^{-1}$/40 kcal mol^{-1} respectively; α_1 and α_2 are the asymptotic volatile yields for each of the two reactions with values 0.3 and 1 respectively.

The rate of total weight loss for the two coals were also investigated by Anthony et al. (1974), but at lower temperatures and heating rates (400-1100 C, 10^2-10^4 C/s) than those employed by Kobayashi et al. (1977). Their results show some differences. For example, comparing the temperature at which the weight loss rate is maximum shows a difference of 60-85 C over the range of heating rates studied. The temperature is reached earlier for Pittsburgh Seam bituminous coal than for Montana lignite.

For individual products, the evolution rate appears to vary significantly among different coal types. For example comparing the

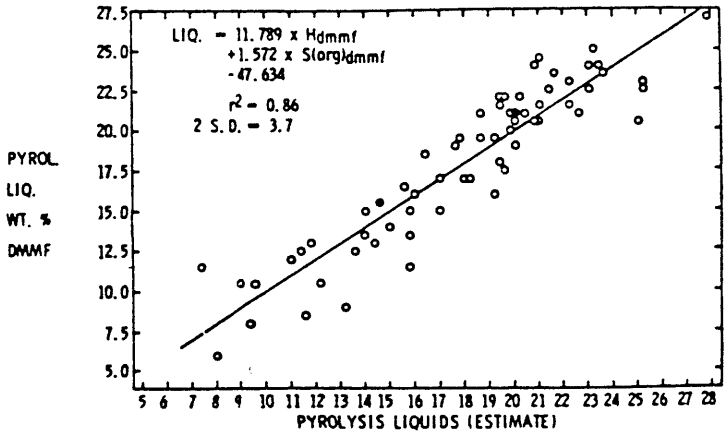

Figure 3.3-2 Comparison of experimental and predicted pyrolysis liquid yields from Neavel et al. (1982).

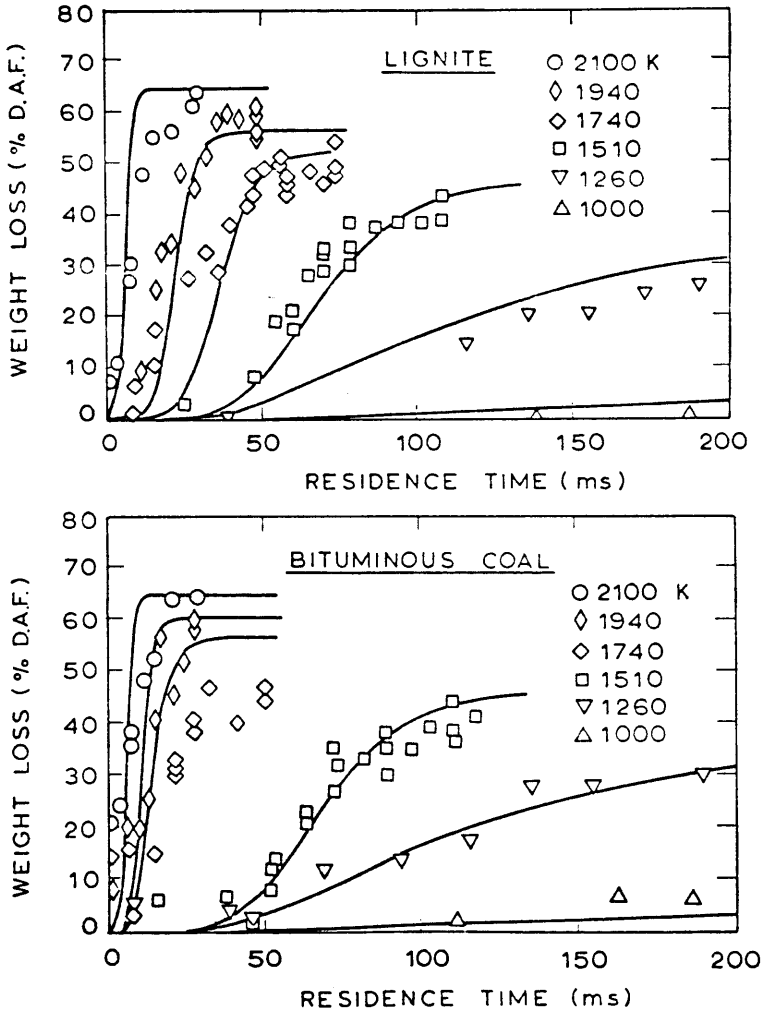

Figure 3.3-3 Comparison of calculated weight losses with experimental results. [Reproduced from Kobayashi et al. (1977).]

rate of hydrogen and pyrolytic water evolution between a Montana lignite and a Pittsburgh Seam bituminous coal using kinetic data from Suuberg (1977), revealed respectively over 100 and 200 C difference in the temperature at which the maximum rate occurs. Hydrogen evolved earlier from the lignite, whereas water evolved earlier from the bituminous coal. Differences in other products (CH_4,CO,tar) were somewhat less, below 100 C.

Some precautions need to noted in comparing literature data on apparent pyrolysis rates. First, direct comparisons of experimental rate data are valid only when the temperature-time history of the data sets being compared are completely identical, i.e., heating rates, final temperatures, holding times, and cooling rates. In many cases, such conditions are not fully satisfied among data sets from different investigators. Second, comparing model predictions under identical temperature-time histories is valid only within the range of conditions where model parameter values are valid. For example, predictions from commonly used global models such as the first-order single-reaction model, is only valid over a narrow range of heating rates from which the model parameters are derived (Howard et al., 1987b). Predictions from the multiple independent parallel reaction model are valid over a wide range of heating rates only when the range is covered by the data from which the model parameters are derived (Ko et al., 1988a).

Discerning coal-type effects is more difficult from low heating rate data reported in the literature since they often employ large sample sizes in a packed-bed type reactor (Juntgen and van Heek, 1977; Weimer and Ngan, 1979; Campbell and Stephens, 1976). As discussed below, significant contributions from extra-particle in-bed secondary

reactions are expected in such reactors. Results from fluidized bed reactors are also severely affected by in-bed secondary reactions, and thus are not discussed here.

3.3.2. Effect of pressure

Table 3.3-1 shows that for both Montana lignite and Pittsburgh Seam bituminous coal, rapid pyrolysis under higher pressures produces less tar, more char, and generally more gaseous products (Suuberg, 1977). This behavior has been attributed to the greater extent of intra-particle secondary reactions of tar --→ gas + char at higher pressures. Contributions from extra-particle secondary reactions are expected to be negligibly small because of rapid dilution and quenching of reactive volatiles in screen-heater type reactors.

Figure 3.3-4 shows the effect of pressure on the rate of volatiles production for Montana lignite and Fig.3.3-5 provides similar information for tar from Pittsburgh Seam bituminous coal. In both cases, no appreciable influence of pressure is seen for temperatures below 700 C; but above 700-800 C, noticeable effects of pressure on the apparent rate of product release are observed. The yields of tar and total volatiles from higher pressure runs 'leveling-off' at lower temperatures (Figs. 3.3-4a and 3.3-5), indicates a lower apparent overall activation energy behavior that is typically encountered under conditions of greater mass transport resistance. An opposite behavior for gas production rates at different pressures (Fig.3.3-4b,c) is explained by a greater extent of tar secondary reactions at higher pressures.

Table 3.3-1 Effect of pressure on pyrolysis product yields from Montana lignite and Pittsburgh Seam bituminous coal. [Reproduced from Howard (1981); data from Suuberg (1977).]

Average particle diameter, 74 μm; heating rate, 1000 C/s; peak temperatures, lignite, vacuum and 1 atm, 900-1035 C, all other cases, 850-1070 C; holding times at peak temperature, lignite, vacuum and 1 atm, 0.0 s, all other cases, 2-10 s.

	Yield, wt % of Coal (as-received)					
	Lignite			Bituminous		
Product	Vacuum[a]	1 atm	69 atm	Vacuum[a]	1 atm	69 atm
CO	6.1	7.1	9.0	2.0	2.4	2.5
CO_2	7.6	8.4	10.6	1.4	1.2	1.7
H_2O[b]	17.7	16.5	13.4	6.8	7.8	9.5
H_2	—[c]	0.50	—[c]	0.75	1.0	—[c]
CH_4	0.94	1.3	2.5	1.6	2.5	3.2
C_2H_4	0.43	0.56	0.55	0.45	0.83	0.46
C_2H_6	0.21	0.18	0.17	0.44	0.51	0.89
$C_1H_8+C_3H_8$	0.46	0.37	0.38	0.71	1.3	0.71
Other HC gases	0.60	[0.47]	0.21	0.98	1.3	1.6
Light HC liquids	0.81		1.1	1.6	2.4	2.0
Tar	6.9	5.4	2.8	31.9	23.0	12.
Char	55.2	58.7	59.0	48.5	53.0	62.4
	97.0	99.5	99.7	97.1	97.2	97.0
Error (loss)	3.0	0.5	0.3	2.9	2.8	3.0

[a] 6.6×10^{-5} atm He.

[b] Includes coal moisture (lignite, 6.8%; bituminous, 1.4%); may include some H_2S.

[c] Not measured.

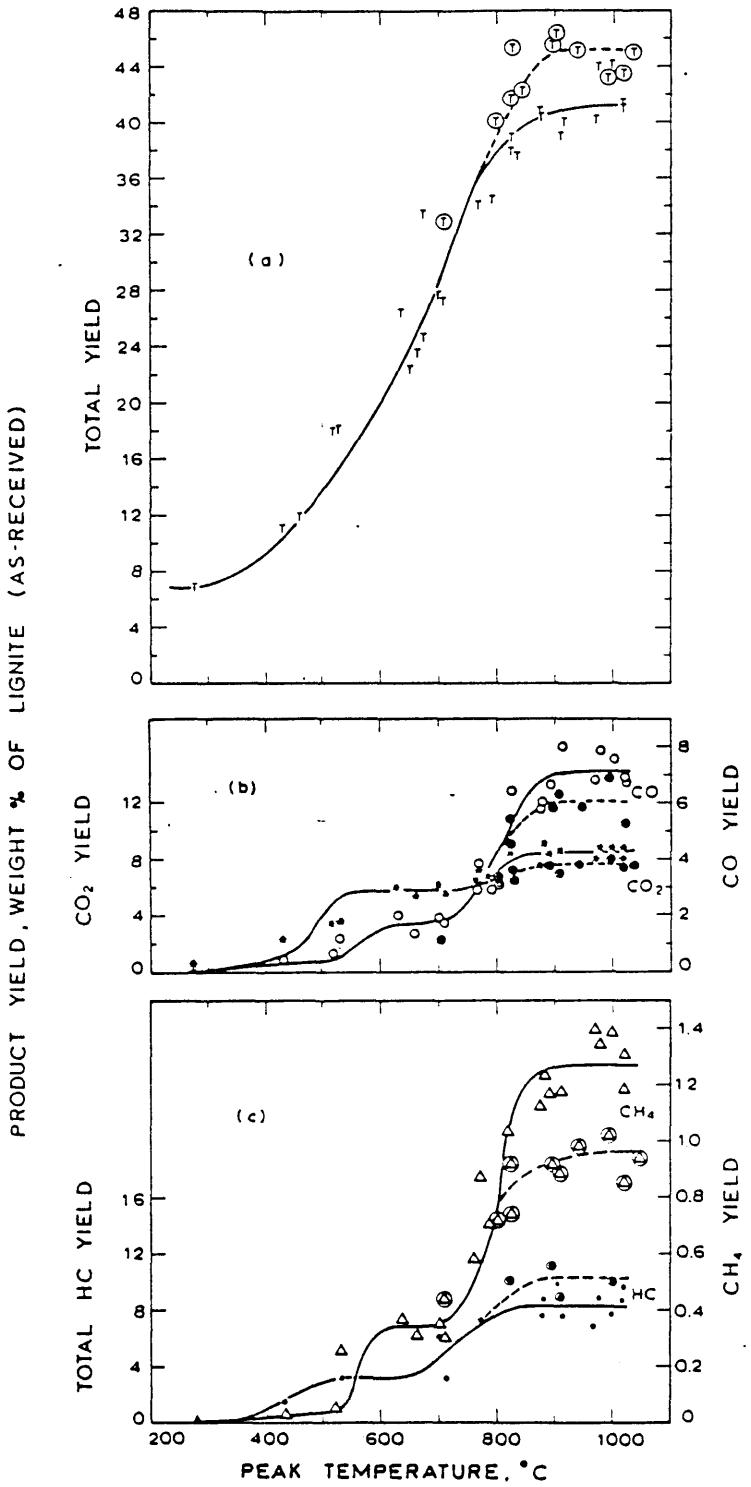

Figure 3.3-4 Effect of pressure on product yields from lignite pyrolyzed different peak temperatures. Pressures: 1 atm (single points and solid curves) and 6.6×10^{-5} atm (points in circles and dashed curves). Heating rate = 1000 C/s. Products: T = total (i.e., tar, all other HCs, H_2O, CO_2, and CO); open circles = CO; * = CO_2; open triangles = CH_4; solid circles = total HCs, including tar. [Reproduced from Howard (1981); data from Suuberg (1977).]

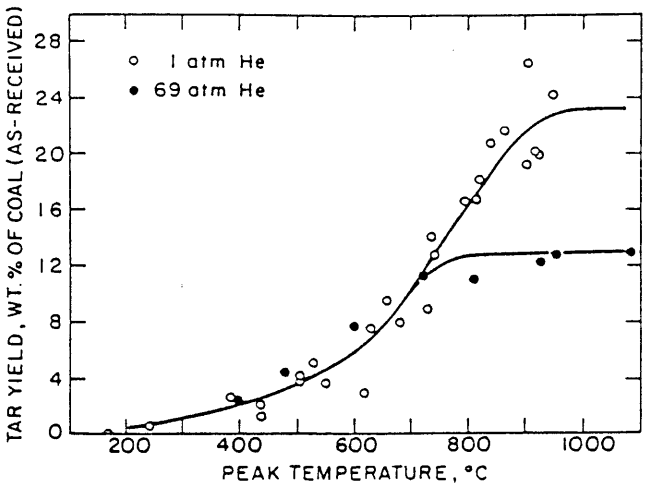

Figure 3.3-5 Effect of pressure on yield of tar from Pittsburgh Seam bituminous coal pyrolyzed at different peak temperatures. Helium atmosphere; heating rate, 1000 C/s; average particle diameter, 74 μm. [Reproduced from Howard (1981); data from Suuberg (1977).]

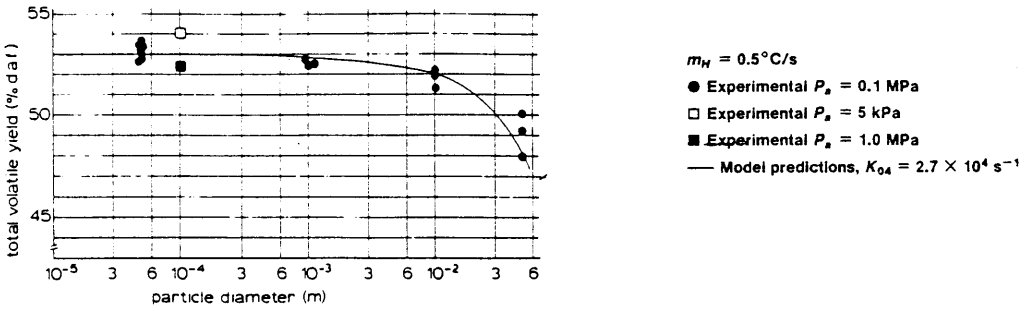

Figure 3.3-6 Total volatiles yield versus particle size for a German lignite. [Reproduced from Bleik et al. (1985).]

3.3.3. Effect of particle size

Table 3.3-2 shows that, on average for a Pittsburgh Seam bituminous coal, rapid pyrolysis of larger particles generally produces less tar, more gas, and more char (Suuberg, 1977). Figure 3.3-6 shows a similar trend for a German lignite pyrolyzed at a low heating rate (Bleik et al., 1985). This behavior has again been attributed to the enhancement of intra-particle secondary reactions of tar --→ gas + char for larger particles. Consistent with this explanation is the view that increasing particle size should not have significant effects in the range of pyrolysis temperatures where the secondary reaction is negligible (Ko et al., 1988a), $\tilde{<}$600 C for Pittsburgh Seam bituminous coal (Serio, 1984).

No experimental data are reported on how the rate of pyrolysis is influenced by the particle size. However, since both pressure and particle size affect the secondary reaction residence time, the pyrolysis rate behavior with changing particle size is expected to be similar to that reported for varying pressure (see Figs. 3.3-4 and 3.3-5).

Possible non-isothermality for large particles and segregation of macerals for different particle-size cuts complicate the analysis of particle-size data. The former complication can be checked by a set of criteria derived by Hajaligol et al. (1988), whereas the latter complication is currently being investigated by Griffin (1988).

3.3.4. Effect of temperature-time history

The effect of temperature-time history on pyrolysis behavior is most often studied by varying the heat-up rate of the sample. In

Table 3.3-2 Effect of particle size on pyrolysis product yields from Pittsburgh Seam bituminous coal. [Reproduced from Howard (1981); data from Suuberg (1977).]

Heating rate, 1000 C/s; peak temperature, 850-1070 C; holding time at peak temperature, 3-10 s; pressure, 1 atm.

	Yield, wt % of Coal (as-received)			
Product	53–88 μm (avg., 74 μm)	<300 μm[a]	300–830 μm	830–990 μm
CO	2.4	2.7	3.2	3.0
CO_2	1.2	1.1	1.2	1.3
H_2O[b]	7.8	5.4	5.3	7.2
H_2	1.0	—[c]	—[c]	0.99
CH_4	2.5	2.9	3.0	3.2
C_2H_4	0.83	1.0	1.1	1.3
C_2H_6	0.51	0.50	0.55	0.63
C_3's	1.3	0.92	0.84	1.1
Other HC gases	1.3	1.4	1.1	1.2
Light HC liquids	2.4	2.5	2.6	2.7
Tar	23.0	24.2	21.3	18.4
Char	53.0	57.1	56.5	55.8
	97.2	99.7	96.7	96.8
Error (loss)	2.8	0.3	3.3	3.2
Number of runs	20	1	2	3

[a] 830–990 μm sample ground to pass 297-μm sieve.
[b] Includes coal moisture (1.4%); may include some H_2S.
[c] Not measured.

general, one observes higher total volatiles yield under rapid heating conditions [$\tilde{>}$ 100 C/s, Loison and Chauvin (1964)] compared to slower heating carbonization conditions [$\approx$ 0.01-1 C/s, Peters and Bertling (1965)]. However, the effect of heating rate on the change in volatiles yield is difficult to discern from the data because of interferences from other experimental conditions, specifically the size and extent of dispersion of the sample. Rapid heating experiments typically employ small sample sizes thinly spread, whereas carbonization experiments employ much larger sample sizes in packed beds; thus, in the latter set-up, volatiles lost due to extra-particle secondary reactions contribute to the decrease in volatiles yield (Howard, 1981).

Even when the extent of extra-particle secondary reactions is minimized, the intrinsic heating-rate effect is still difficult to discern due to interferences from intra-particle secondary reactions. Experiments using thinly spread small coal particles ($\approx$70 μm dia.) under 1 atm reactor pressure report that the yield of total volatiles as well as individual products is generally independent of heating rates between 350 to 15,000 C/s (Anthony, 1974; Suuberg, 1977). The observations were made for both Montana lignite and Pittsburgh Seam bituminous coal. An exception is the slight increase ($\approx$2.5 wt% as rec'd) in the total weight loss for the bituminous coal when the heating rate was raised from 650-750 to 10^4 C/s (Anthony, 1974). In contrast, similar studies done under vacuum show noticeably higher volatiles yield as the heating rate is increased (Niksa, 1981); total volatiles yield from a Pittsburgh Seam bituminous coal increased from 41 to 52 wt% dmmf as the heating rate was raised from 100 to 10,000 C/s

at 1.3×10^{-4} atm pressure and 1000 C final temperature. Anthony's vacuum data show a slight increase in going from 650-750 to 3000 C/s, but no further from 3000 to 10^4 C/s (one data point at this heating rate).

The different heating-rate results at vacuum and atmospheric pressure may first appear contradictory. But, the results can be explained if the production of 'primary' volatiles is enhanced at higher temperatures, or heating rates if the heat-up is continuous. The extent to which primary volatiles further react (secondary reactions) depends on both the temperature and mass transport rate. Under vacuum, the transport rate is sufficiently fast for secondary reactions to be negligible over the range of heating rates studied. Thus, the vacuum data may be indicating an intrinsic heating-rate effect -- postulated here to enhance primary pyrolysis. At 1 atm, the mass transport resistance is expected to be small, but may be still sufficient for secondary reactions to obscure the intrinsic heating-rate effect. Thus, in this case, one may not observe the heating-rate effect because an increase in primary volatiles production at higher heating rates is 'off-set' by a greater extent of secondary reactions. This explanation suggests a competing reaction scheme between primary volatiles producing reactions and 'low-temperature' char forming reactions. Such a reaction scheme has been proposed by Kobayashi et al. (1977) (Section 3.3.1) and Niksa and Kerstein (1985) (Section 3.4.2), but their models are inadequate to fully explain the observed behavior because they do not explicitly include mass transport descriptions. A similar competing reaction concept was adopted in formulating the extended MIPR model (Section 6.2.1), which includes an explicit mass transport

description. Section 6.2.2 shows that quantitative predictions from the model are consistent with the experimentally observed heating-rate effects reported by Anthony (1974), Suuberg (1977), and Niksa (1981).

3.4. Modeling studies

Numerous coal pyrolysis models of various complexity currently exist. These models can be broadly classified into (1) global models, (2) detailed chemistry models, and (3) models with explicit description of mass transport. Each of these three classes of models are discussed below.

3.4.1 Global models

The multiple independent parallel reaction (MIPR) model (Hanbaba et al., 1968) and the functional group (FG) model (Solomon and Colket, 1978) are two commonly used coal pyrolysis global models to describe the evolution of individual products (tar: Serio, 1984; Ko et al., 1988a) (gases: Weimer and Ngan, 1979; Serio et al., 1987), and total volatiles (Anthony et al., 1974; Sprouse and Schuman, 1981). Under conditions where the effects of physical transport processes and secondary reactions are relatively unimportant but not negligible, both models approximate the complex chemical decomposition and any transport effects by global first-order decomposition reactions occurring uniformly throughout the particle. In addition, both models can also be used to represent only the chemical decomposition in descriptions that explicitly include mass transfer. Whether mass transport is treated explicitly or implicitly, a successful model must be able to predict reliable product evolution rates over a wide range of

temperature-time histories. This important criterion was examined by Ko et al. (1988a) by comparing tar evolution rates predicted from the two models to experimental data from Pittsburgh Seam bituminous coal over a wide range of heating rates (0.05 - 1000 C/s). The experimental conditions are limited to 1 atm pressure and small particle sizes where mass transport limitations are small.

The study found that the MIPR model can reliably predict tar evolution rates over the range of heating rates covered by the data from which the rate parameters used in the model were obtained, but generally not at heating rates outside this range. Thus, the range of applicability is substantial when the rate parameters are fitted from data collected at two or more widely different heating rates. For the FG model, several sets of parameter values have been published (Solomon et al., 1981; Solomon et al., 1982; Solomon and Hamblen, 1985; Serio et al., 1987) without always showing critical comparisons against data and without providing guidance as to which values are preferred for a given set of conditions. However, regardless of which of the published sets of parameter values is used, tar evolution rates predicted from the FG model do not generally agree well with the experimental data, especially at higher heating rates. Also large discrepancies are found between experimentally observed maximum tar yields and those predicted by the FG model. A reason for the poor performance of the FG model against Pittsburgh Seam coal tar evolution data may be that it employs the same rate parameters for the evolution of all products including tar for all coal types, regardless of whether the coal is softening or non-softening. The assertion that coal type has no effects on the kinetics of product evolution (Solomon et al., 1982; Solomon and

Hamblen, 1985), which forms the basis of the FG model, is investigated in Chapters 5 and 6.

The first-order single-reaction model is another global model widely used under conditions where the effects of physical transport processes and secondary reactions are relatively small. This model approximates the complex chemical decomposition and any transport effects by a single global first-order decomposition reaction. The model is most useful in applications where minimizing computational effort is important such as in large combustion or gasification models that fully describe fluid mechanics, heat and mass transport, and reaction kinetics; and in comprehensive devolatilization models that explicitly include the complex decomposition and secondary reaction chemistry, and multicomponent mass transfer in a gaseous or liquid phase environment. However, the model has a major weakness in that a different set of rate parameters is required at different heating rates. Thus, for a given set of rate parameters, the applicability of the model is confined to a narrow range of heating rates. A method developed by Ko et al. (1988b), extends the applicability of the model over a wide range of heating rates. The two rate parameters in the model, a preexponential factor and activation energy, are derived in the form of heating-rate dependent functions. Predictions using the heating-rate dependent rate parameters were compared with the total weight loss data from devolatilization of Montana lignite over heating rates from $\approx$0.1 to 10^4 C/s, and were found to agree well with the data. Two typing errors in the published paper (Ko et al., 1988b) need to be noted: (1) in Table 1, the printed σ values are lower than correct values by a factor of 10, e.g., 1.32 kcal/mole should read 13.2

kcal/mole, and (2) the y-axis label in Fig.2 should read wt fraction, not wt%.

The first-order competitive reaction model proposed by Kobayashi et al. (1977) has already been discussed in Section 3.3.1. A distinguishing feature of this model is that, through the competing reaction mechanism, it is able to predict the observed greater volatiles yield at higher heating rates/temperatures without having to adjust model parameters. Figure 3.3-3 shows that the model is capable of predicting total weight loss data from a Montana lignite and Pittsburgh Seam bituminous coal over a wide range of temperatures and heating rates.

3.4.2 Detailed chemistry models

The work of Gavalas and co-workers (1981a,b) provides a detailed approach to model the reaction chemistry in coal pyrolysis. Coal is represented as a collection of reactive functional groups whose concentrations are estimated from elemental analysis and NMR data. The chemical changes are described by 42 elementary reactions selected on the basis of chemical theory and information from model compound studies (Table 3.4-1). But, as pointed out by Gavalas, this large reaction set is by no means exhaustive as it excludes certain reactions that are known to be important at high temperatures ($\tilde{>}$ 700 C), and for coals of high oxygen content. For example the reaction set omits the formation of CO and H_2, which are speculated to evolve from phenolic, ring or ether oxygen, and from dehydrogenation of hydroaromatic rings respectively. It also neglects dissociation of ether type bonds (Ph-O-CH_2-Ph', Ph-O-CH_3), which are believed to be major constituents in low-

Table 3.4-1 Elementary reactions of coal pyrolysis. [Reproduced from Gavalas et al. (1981a).]

no.	X	reaction
		Bond Dissociation Producing Two Radicals
1	H	
2	CH_3	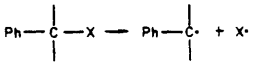
3	C_2H_5	
4		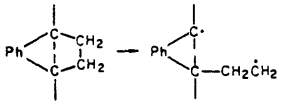
5		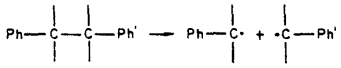
6		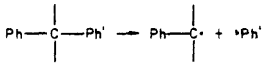
		Bond Dissociation Producing One Radical and One Double Bond
7		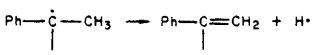
8		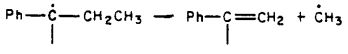
9		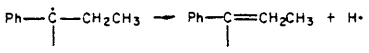
10		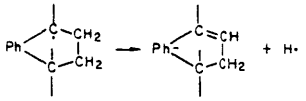
11	H	
12	CH_3	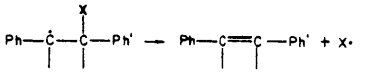
13	C_2H_5	
14		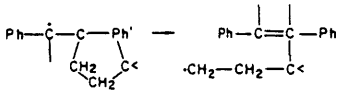
15	H	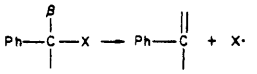
16	CH_3	
17	C_2H_5	(β represents $-\dot{C}H_2$ or $>\dot{C}H$ of) hydroaromatic structure
18		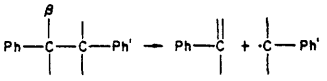
19		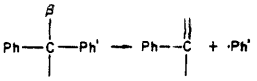
20		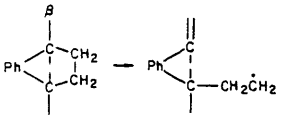
21		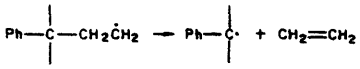
		α Radical Recombination
22		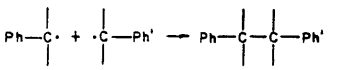
		Hydrogen Abstraction
23	H	
24	CH_3	$X\cdot + H_\alpha \longrightarrow XH + \alpha$ radical
25	C_2H_5	
26	H	
27	CH_3	$X\cdot + H_\beta \longrightarrow XH + \beta$ radical
28	C_2H_5	
29		$>\dot{C}H + H_\alpha \longrightarrow >CH_2 + \alpha$ radical (β radical)
		Addition-Displacement
30	H	
31	CH_3	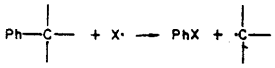
32	C_2H_5	(substituents on α carbon can be H, CH_3, C_2H_5)
33	H	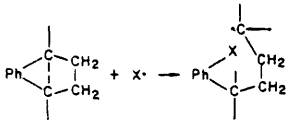
34	CH_3	
35	C_2H_5	(substituents on α carbon can be H, CH_3, C_2H_5)
36	H	
37	CH_3	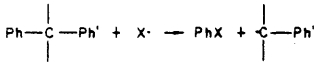
38	C_2H_5	(substituents on α carbon can be H, CH_3, C_2H_5)
		Phenolic Condensation
39		$Ph—OH + HO—Ph' \longrightarrow Ph—O—Ph' + H_2O$
40		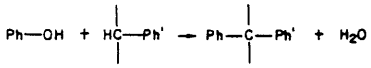
		Formation of Carbon Oxides
41		$Ph—COOH \longrightarrow PhH + CO_2$
42		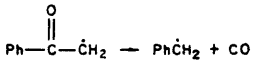

rank coals (e.g., lignites).

Testing the capability of the proposed reaction scheme is complicated by mass transport effects. Gavalas assumes no transport limitations for "small permanent molecules" such as H_2, CH_4, CO and H_2O since they have low reactivities and relatively large diffusion coefficients. Such assumption is less valid for large molecules like tar due to their larger sizes (≈10 Å) and reactive peripheral groups attached to the molecule's aromatic nucleus. To account for this effect in a simple manner, Gavalas assumes that the actual rate of generation of tar is Xr, where r is the rate of generation of tar molecules in the condensed phase and X is an empirical parameter adjusted to fit the experimental tar data.

Figure 3.4-1 shows a satisfactory agreement between the simulated and experimental weight loss, tar yield, and hydrocarbon gases for a bituminous coal. However, it needs to be pointed out that the simulated results were generated using kinetic parameter values that are considerably different from the best estimated values (Table 3.4-2) for some reactions as shown in Table 3.4-1. The author's explanation for this is that "the sets are different because many of the values used in the simulation were assigned rather arbitrarily before it was realized that they could be estimated by group additivity methods". In actual application of this approach, estimating the concentrations of the functional groups and kinetic parameters of the elementary reactions remains challenging because of the limited quantitative information on coal structure, and theoretical information on reaction chemistry. For example, Howard (1981) points out that the predicted total weight loss in pyrolysis at 500 C for 30 s drops by about 10%

Figure 3.4-1 Simulated and experimental (a) weight loss and tar yield, and (b) hydrocarbon gases from the pyrolysis of a bituminous coal. [Reproduced from Gavalas et al. (1981b).] 110

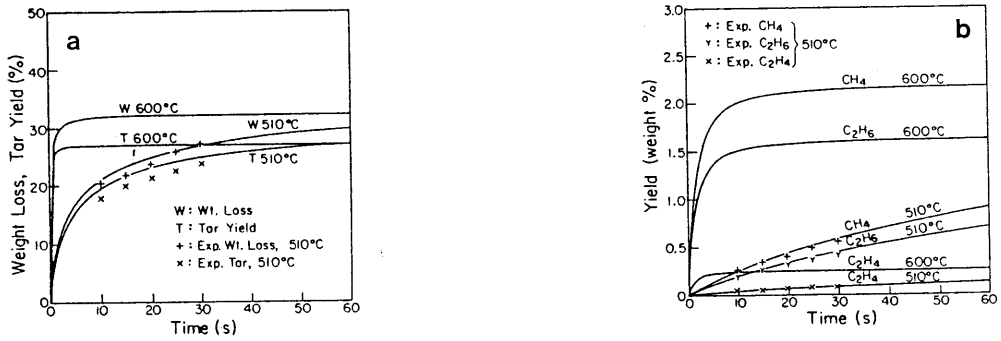

Table 3.4-2 Values of kinetic parameters used by Gavalas et al. (1981b) in their detailed chemistry model of coal pyrolysis [Reproduced from Gavalas et al. (1981b).]

	values used in simulation		best estimated – values	
reaction	log A	E, kcal/ g-mol	log A	E, kcal/ g-mol
1	15.5	84.0	14.9	81.3
2	15.3	65.0	15.3	68.4
3	14.9	63.0	15.4	65.0
4	14.9	63.0	15.4	65.0
5	14.4	52.0	13.9	50.4
6	14.4	68.5	14.3	76.7
7	12.8	50.0	15.1	55.7
8	12.8	48.0	14.4	49.0
9	12.8	50.0	15.1	56.0
10	12.8	50.0	15.1	55.7
11	12.0	38.0	12.8	54.2
12	12.0	37.0	12.1	47.5
13	12.0	37.0	12.1	47.4
14	12.0	38.0	12.1	47.4
15	12.3	38.0	12.8	34.3
16	12.3	38.0	12.1	23.6
17	12.6	35.0	12.1	20.8
18	13.6	35.0	13.0	7.0
19	13.6	35.0	13.0	57.6
20	12.4	35.0	12.1	20.9
21	12.4	36.0	14.2	13.5
22	8.0	10.0	-	-
23	11.1	10.0	10.0	2.3
24	8.0	10.0	7.5	8.0
25	8.0	10.0	7.0	8.9
26	11.1	10.0	10.3	9.7
27	8.0	10.0	7.8	10.8
28	8.0	10.0	7.3	13.4
29	8.0	20.0	-	-
30	11.0	15.0	10.4	2.0
31	7.0	15.0	7.8	7.0
32	7.0	15.0	7.3	9.0
33	11.0	10.0	10.4	2.0
34	7.0	10.0	7.8	7.0
35	7.0	10.0	7.3	9.0
36	11.0	10.0	10.4	2.0
37	7.0	10.0	7.8	7.0
38	7.0	10.0	7.3	9.0
39	8.5	35.0	-	-

(from ≈33 to ≈23%) if the activation energy for the cleavage of ethylene bridge ($Ph\text{-}CH_2\text{-}CH_2\text{-}Ph \dashrightarrow 2Ph\text{-}CH_2\cdot$) is raised by only 2 kcal/mole (from 48 to 50 kcal/mole). Such a small difference in the activation energy can easily be produced by structural factors that are not easily measured or accounted for. Extra free-radical stabilization from additional ring aromatics is approximately 2-4 kcal/mole (Stein, 1985), and from activating substitutions such as phenolic and ether groups is 2-5 kcal/mole (Gavalas et al., 1981a). These complications have been clearly acknowledged by Gavalas and co-workers in discussing the proposed reaction scheme. They state that, "In its present state the model should not be considered as final and ready to apply but rather as a source of mechanistic and kinetic information..." (Gavalas et al., 1981b).

Niksa and Kerstein (1985) present an alternative chemical description, where a large number of different chemical entities in the coal are classified into three groups consisting of bridges, aromatic units, and peripheral units. A unique feature of this model is that tar production occurs via a competitive reaction pathway involving stabilization or recombination of monomers. Monomers are produced by bridge scission reactions. According to the reaction scheme, assigning $E_{tar} > E_{char}$ favors tar production over char formation at higher temperatures when mass transport limitations can be neglected. This trend is consistent with experimental observations (Niksa, 1981) that greater volatiles yields are obtained at higher heating rates in pyrolysis of small particles under low pressures (vacuum). Including a mass transport description would enhance the range of applicability of the model.

3.4.3 Models with explicit description of mass transport

Separate intra-particle mass transport descriptions are required for non-softening and softening coals as their transport mechanisms are radically different. In the non-softening case, multicomponent mass conservation equations inside the particle generally consist of volatiles flux terms derived from the Dusty Gas Theory (Mason and Malinauskas, 1983), and global chemical kinetic terms describing formation and destruction of volatiles. In modeling hydropyrolysis of coal, Russel et al. (1979) considered a four component system consisting of reactive volatiles, non-reactive volatiles, hydrogen, and inert gas. In quantitatively formulating the model, they made significant simplifications in the general conservation equation by assuming (1) concentration and pressure profiles are at a pseudosteady state, (2) external mass transport resistance is negligible, (3) the coal particle retains its porous solid structure during all stages of pyrolysis, (4) binary diffusivities for all volatiles are equal, and (5) particles are spatially isothermal. Justifications for the first two assumptions are based on characteristic time analysis. The third assumption is valid only for non-softening coals. Improvements on the fourth assumption can be made by assigning separate diffusivities for high molecular weight (tars) and low molecular weight (gases) volatiles. The last assumption generally holds when small particles ($\tilde{<}$ 100 μm dia.) are pyrolyzed at moderately rapid heating rates ($\tilde{<}$ 1000 C/s) under atmospheric pressure. The predictive capability of the model is difficult to judge since the model is strictly applicable to non-softening coals, but predictions were compared to experimental data

The model proposed by Gavalas and Wilks (1980) considers a ternary system consisting of tars, gases and inert carrier gas, and as before, applies pseudosteady state conservation equations with negligible external mass transport resistance. A major advancement made in this work was that the model incorporates pore-size distribution information obtained from experimental measurements. Over the course of pyrolysis of a subbituminous coal, they observed only minor changes in the pore-size distribution, specifically slight pore enlargement. The model predicts that at low pressures, product yields depend on particle size only, while at high pressures, they depend on both pressure and particle size. These trends were shown to agree with limited experimental data from a subbituminous coal.

For a two component system consisting of gases and tars, Bleik et al. (1985) relaxed the pseudosteady state assumption, and formulated transient mass conservation equations coupled with a transient heat conservation equation. Negligible external mass transfer resistance is again assumed. In estimating physical parameters required in the Dusty Gas flux equations, Bleik et al. (1985) chose to use empirical correlations that relate the parameters to particle porosity, rather than to consider detailed pore structure. Justifications for this approach are based on findings that macroscopic transport of volatiles occurs predominantly through large pores (Gavalas and Wilks, 1980; Simons and Finson, 1979). For non-softening coals, predictions from the model compare well with experimental data over a wide range of temperature-time histories, pressures, and particle sizes. Including the heat transfer description significantly widens the range of

applicability of the model, especially for conditions of very rapid heating and/or large particles.

Two different directions have been taken in modeling pyrolysis of softening coals. One approach assumes that the rate of volatiles transport is controlled by evaporation from the surface of the molten coal and diffusion through a mass boundary layer, and neglects any internal transport resistance (Zacharias, 1979; Unger and Suuberg, 1981). The validity of this assumption is highly sensitive to which values of physical properties are chosen in computing the characteristic time scale for transport inside and outside the particle. It is not uncommon to see as much as an order of magnitude or more variation among values of some physical properties employed by different investigators, e.g., vapor pressures and liquid phase diffusivities (Oh, 1985). Further discussions on the experimental evidence cited to support the surface evaporation controlling assumption have been covered in Section 3.2.2. Predictions from the model generally agree well with experimental data at pressures $\geq$ 1 atm. The model is not directly applicable at lower pressures because evaporation becomes very rapid at pressures significantly less than 1 atm (Unger and Suuberg, 1981).

The second approach to modeling pyrolysis of softening coals includes internal mass transport effects via a mechanism of growth and escape of volatiles filled bubbles (Lewellen, 1975; Oh et al., 1988). The growth process occurs either by liquid-phase molecular diffusion of volatiles to nearest bubbles or by coalescence of two adjacent bubbles. The escape process is assumed to occur when a bubble reaches the particle surface. Although contributions are minor, a route for direct

escape of volatiles to the particle surface is also included in this approach. The bubble description requires a large number of physical properties, many of which are difficult to estimate or measure experimentally. An extensive effort was made by Oh et al. (1988) to overcome this inherent difficulty. The model predicted trends in volatiles yields, plasticity, and extent of swelling under various temperatures, pressures, particle sizes and heating rates, and they were in encouraging agreement with several literature measurements.

Six coals ranging from lignites to low-volatile bituminous coals were chosen in this study to investigate the effect of coal type on pyrolysis behavior. Main selection criteria in choosing the coals were fresh sample quality; good representation of coal rank and mine location; and commercial and scientific interest. Section 4.1 gives more information on the selection procedure, and the properties of the chosen coals.

An electrically heated screen-heater type reactor was used to measure the apparent evolution kinetics and the yield limit of volatile products for the six coals. This reactor type has been extensively used in past pyrolysis studies (Anthony et al., 1974; Suuberg, 1977; Fong, 1986), as it offers many advantages important in kinetic studies including reliable temperature measurement of the sample over a wide range of heating rates, rapid quenching and dilution of volatile products upon leaving the coal particle surface, and ability to work over a wide range of pressures. Section 4.2 gives a detailed description of the experimental apparatus.

Coal type, temperature-time history, pressure, and particle size are the main independent variables in coal pyrolysis. Section 4.3 specifies experimental conditions employed in this study.

Tars, light hydrocarbon gases, carbon oxides, and water are the major volatile products from coal pyrolysis. Tars are operationally defined as the sum of all volatile products (except water) that condense in the reactor at room temperature; typically, they consist of a complex mixture of molecules with molecular weights ranging from 100 to 1500. Light hydrocarbon gases include saturated and unsaturated

species up to about C_4. Section 4.4 describes the experimental procedure, including tar and gaseous product collection methods.

Additional liquid products can be obtained by solvent extraction of the solid residue of pyrolysis (char). The extract information is important in determining transport properties, swelling behavior, and agglomeration tendencies for softening coals (Fong, 1986). Also, the information is potentially valuable in elucidating the chemical and physical mechanism of tar production as tar is believed to originate from the extractable material. Molecular weight (MW) measurements on liquid products (tar and extract) are made by gel permeation chromatography (GPC). The MW data are essential input parameters to estimate transport properties (e.g., vapor pressures and diffusion coefficients). In addition, time-resolved MW data can provide valuable information in understanding the formation and depletion mechanism of liquids inside the coal particle. Extraction yield data and MW measurements for these products collected in this work are currently being analyzed by Sanchez (1988).

4.1. Coal selection

The six coals chosen for this study are:

1. Beulah Zap, ND (Lignite A)
2. Lower Wilcox, TX (Lignite A)
3. Smith Roland, WY (Subbituminous B)
4. Blue, NM (High-Volatile Bituminous C)
5. Illinois #6, IL (High-Volatile Bituminous A)
6. Lower Kittanning, PA (Low-Volatile Bituminous)

Table 4.1-1 gives the proximate and ultimate analysis of the selected

coals. All coals were obtained from the Advanced Coal Combustion Chemistry Research Program sponsored by the Department of Energy (DOE), Pittsburgh Energy Technology Center (PETC) and managed by United Technologies Research Center (UTRC). Whenever appropriate, the results obtained from this study are compared to those from a similar study on a Montana lignite and Pittsburgh Seam bituminous coal by Suuberg (1977); Table 4.1-2 gives the analysis of these two coals.

The main selection criteria were (1) fresh sample quality, (2) good representation of coal rank and mine location, and (3) commercial and scientific interest. Fresh coal samples are desired to minimize changes in their properties which may affect pyrolysis behavior. Weathered coals, for example, are known to produce lower tar yields (Jacab et al, 1985). The above coals were collected recently (all in 1985) and were carefully stored under inert atmosphere until they were ground and sieved. As shown in Table 4.1.1, the six coals have a wide variation in the elemental compositions (e.g., 56 wt% < C < 83 wt% dry basis) and volatile contents (16-42 wt% dry). Geographically, one coal is from the east (PA), one from the mid-west (IL), two from the west (WY,ND), one from the southwest (NM), and one from the south (TX). Zap lignite and Illinois #6 bituminous coal are of scientific interest since they have been widely used by other coal researchers (e.g., Serio et al., 1987; Darivakas, 1988; Suuberg et al., 1987). In addition, Illinois #6 is potentially important as a steam coal and in synthetic fuels processing. Smith Roland subbituminous (WY) coal and Lower Wilcox lignite (TX) are potentially important gasification feedstocks.

4.2. Experimental apparatus

Table 4.1-1: Ultimate and proximate analysis of the six selected coals in this study[a]

coal	Lower Wilcox	Beulah Zap	Smith Roland	Blue	Illinois #6	Lower Kittanning
coal-rank[b]	L	L	SB	HVB	HVB	LVB
Ultimate analysis wt%,dry						
C	56.0	60.2	62.0	74.9	67.4	82.5
H	4.2	4.0	4.6	5.0	4.4	4.5
N	1.1	1.0	1.0	1.4	1.3	1.3
S	0.7	1.1	1.1	0.8	3.9	1.2
O	19.9	21.6	19.5	13.7	8.7	2.4
ash	20.3	15.0	13.0	4.5	15.6	8.9
Proximate analysis wt%,dry						
moisture[c]	3.0	3.0	3.0	4.0	4.0	1.0
volatile matter	45.3	42.0	45.2	43.3	35.7	16.3
fixed carbon	34.4	43.0	41.8	52.2	48.7	74.8
ash	20.3	15.0	13.0	4.5	15.6	8.9

[a] analyzed by Huffman Laboratories, Inc.
[b] L = lignite, SB = subbituminous, HVB = high-volatile bituminous, LVB = low-volatile bituminous.
[c] partially vacuum dried.

Table 4.1-2: Ultimate and proximate analysis of the coals investigated by Suuberg (1977)[a]

coal	Montana	Pittsburgh Seam
coal-rank[b]	L	HVB
<u>Ultimate analysis</u> wt%,dry		
C	63.6	68.8
H	4.1	4.9
N	1.0	1.3
S	1.2	5.4
O[c]	19.5	8.1
ash	10.6	11.5
<u>Proximate analysis</u> wt%,dry		
moisture[d]	6.8	1.4
volatile matter	39.6	39.5
fixed carbon	49.8	49.1
ash	10.6	11.5

[a] analyzed by Huffman Laboratories, Inc.
[b] L = lignite, SB = subbituminous, HVB = high-volatile bituminous, LVB = low-volatile bituminous.
[c] by difference.
[d] as-received basis.

Figure 4.2-1 shows the reactor assembly, product collection apparatus, and data acquisition system. A screen-heater reactor, modified from a version originally constructed by Fong (1986), was used for 'vacuum' and atmospheric pressure runs. The rector vessel has a cylindrical casing made of two pyrex cylindrical pipes (Corning Pyrex, 22.86 cm x 22.86 cm) stacked vertically, and is closed at the top and bottom with a stainless steel plate (3/8" thick). The bottom plate has feedthroughs for gas inlet/outlet ports (recirculation pump, vacuum pump, gas sampler, He supply), and electrical ports (thermocouple, DC power supply). The top plate has a gas inlet/outlet port leading to the recirculation pump. In higher pressure runs, a high-pressure screen-heater originally constructed by Anthony (1974) and later modified by Griffin (1988) was used; it is similar to the low-pressure reactor described above except for the stainless steel casing (rated up to 200 atm at room temperature).

4.3. Experimental conditions

Coal type, temperature-time history, pressure, and particle size are the main experimental variables. The first two variables affect both the primary and secondary pyrolysis, whereas the latter two variables affect mainly the secondary process.

Table 4.3-1 summarizes experimental conditions employed in this study. The experiments varied coal type from lignites to low-volatile bituminous coals, and reactor pressure from 'vacuum' ($\tilde{<}10^{-3}$ atm) to 10 atm. Fixed variables were the particle size at 75-90 μm diameter, and temperature-time history at 1000 C/s heat-up, 200-1000 C/s cool-down, and 1050 C maximum temperature.

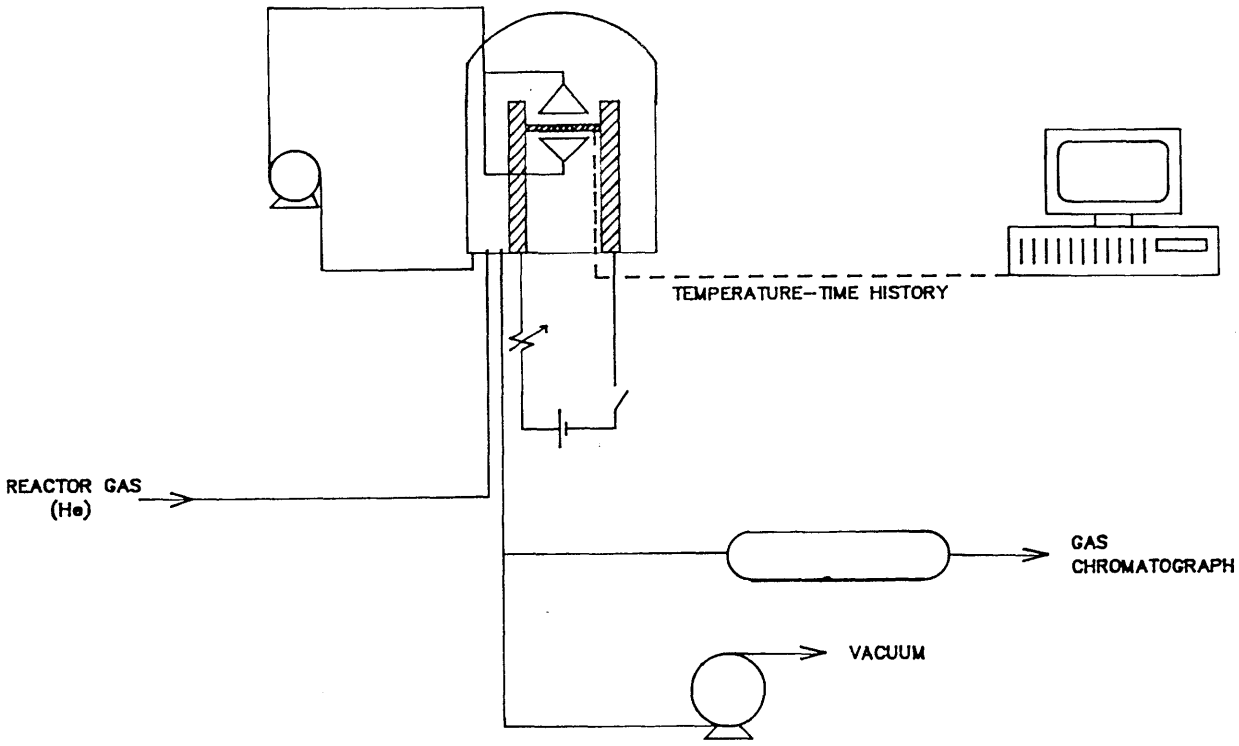

Figure 4.2-1 The reactor assembly, product collection, and data acquisition system.

Table 4.1-3: Summary of experimental conditions employed in this study

reactor variables:	coal type	temperature-time history	pressure	particle size
varied (v) or fixed (f)	v	f	v	f
range covered	lignites to low-volatile bituminous coals, elemental carbon content ranges 72-92 wt% dmmf.	1000 C/s heat-up, 200-1000 C/s cool down, 1050 C max. temperature.	10^{-3} - 10 atm	75-90 μm dia.

4.4. Experimental procedures

In a typical low pressure run (10^{-3} to 1 atm), about 20 mg of 75-90 μm diameter particles spread thinly in the central region of 10 cm x 5 cm, folded 400 mesh stainless steel screen (Fig.4.3-1) are devolatilized under a controlled temperature-time history. To ensure thin well dispersed coal particles, smaller sample sizes ($\approx$5 mg) had to be used in high pressure runs since smaller screens are used in the high pressure reactor. Digital timers connected to a 24 volt DC power supply control the heating, holding and cooling periods of the reacting material. The sample temperature is measured using a very thin Chromel-Alumel thermocouple (Omega K-2 type; 0.0005 in. foil) placed within the folded screen near the coal particles (Fig.4.3-1). Consistent temperature measurements require the gap between the two layers of the screen to be minimal; this is achieved by keeping the screen between the electrodes as tight as possible. The temperature-time history of each run is recorded using a Bascom Turner digital recorder (5 ms resolution), and is later transferred through an RS232 interface to an IBM PC/AT for use in kinetic analysis of the data. The reactor gas, ultra high purity He (99.999%), remains near room temperature, and provides rapid dilution and quenching of volatiles as soon as they are evolved from the coal surface, thus presenting minimal opportunity for extra-particle secondary reactions.

Reliable tar-yield measurements in screen-heater reactors are difficult. The conventional technique usually involves using a solvent-soaked tissue (e.g., CH_2Cl_2) to carefully wipe off the tar condensed on the inner surfaces of the reactor, followed by evaporating

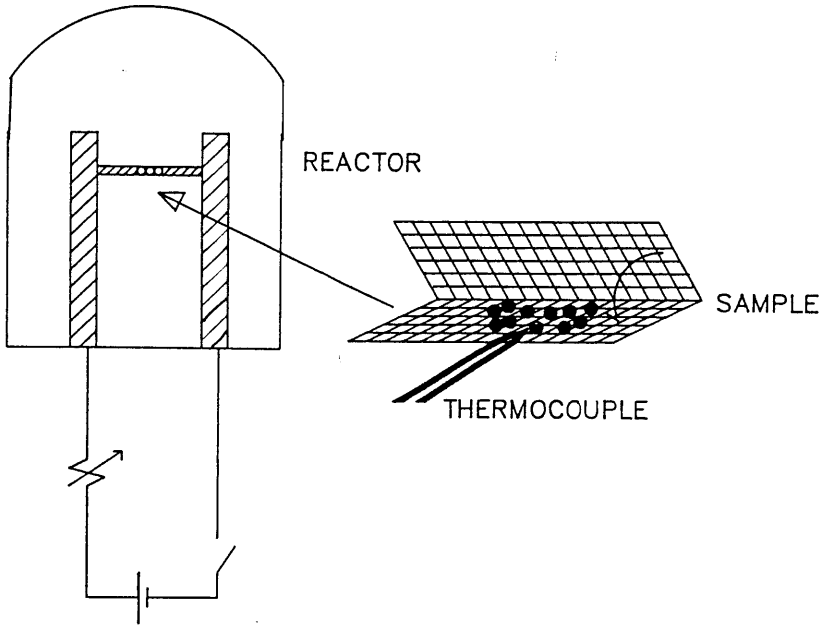

Figure 4.3-1 Details of the electrical screen-heater reactor.

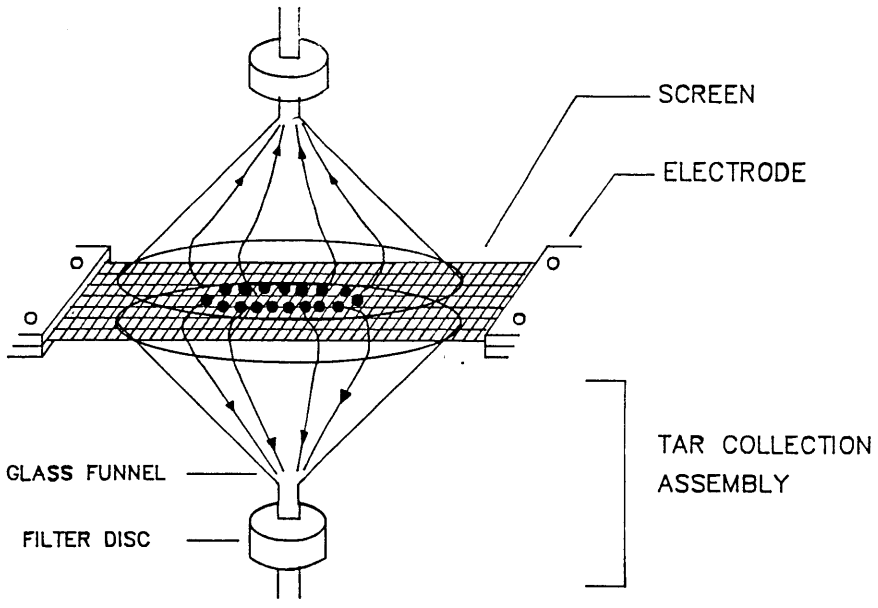

Figure 4.3-2 New tar collectors in electrical screen-heater reactor.

away the solvent (Bautista, 1984; Oh, 1985). Some major sources of error associated with this method are incomplete tar collection due to the fact that some tar condenses on reactor internals that are poorly accessible; incomplete evaporation of solvent arising from a partial miscibility between the solvent and the tar; and loss of more-volatile tar components during solvent evaporation (Bautista, 1984). Thus significant scatter and large experimental errors can typify screen-heater tar data.

The problems associated with the conventional tar collection technique were diminished in this work by developing a new tar collection system for screen-heater reactors. Figure 4.3-2 shows the tar traps, each consisting of a glass funnel connected at its stem to a small teflon filter disk (0.2 μm pore size). The mouths of the funnels completely cover the coal particles between the layers of the screen. Upon leaving the coal particle, tar, together with reactor gas, is convected into one of the two traps. The traps were weighed before and after the run, and the tar yield was taken as their combined weight increase. Convection into the traps was achieved during the run by reducing the pressure downstream of the traps using a small recirculation pump (Cole-Parmer Air Cadet) for atmospheric pressure runs, and a small vent from the trap to atmosphere for higher pressure runs (Griffin, 1988). As would be expected, a sufficient pressure differential could not be obtained across the trap in vacuum runs. In these experiments, the screen was virtually surrounded by tared sheets of aluminum foil to condense the tar as it evolved from the screen. The tar yield was taken as the increase in weight of the foils after the run. Tar yields measured using the tar traps were comparable to

those using the solvent-soaked tissue method, but the new method gave significantly better reproducibility.

Gaseous products from coal pyrolysis include CO, CO_2, H_2O, CH_4, C_2H_4, and C_2H_6. The gas yields were measured using a Perkin Elmer Sigma 2B Gas Chromatograph (GC), equipped with a spherocarb column, a thermal conductivity detector (TCD), and a flame ionization detector (FID). Helium was used as a carrier gas. Some C_3's and C_4+'s have been previously reported (Suuberg, 1977; Oh, 1985), but such species could not be identified using the current set-up. Hydrogen gas measurements were not attempted in this study because to do so would require another GC using a carrier gas with a thermal conductivity much different from that of H_2, typically Ar. But, the sum of these 'missing' gas species represents a small fraction of the overall mass balance ($\approx$ 1-4 wt% as rec'd basis).

Previous gas collection procedures also gave reliable measurements as indicated by good mass balances (Suuberg, 1977), but were slow since the entire reactor volume was purged out for as much as several hours (Oh, 1985). The large number of experimental runs planned for this study, demanded more rapid product collection. In the new method, a known volume of the reactor gas is withdrawn from the reactor using a gas sampler, and then is concentrated by purging the sampler through a cooled lipophilic trap where all light gases except hydrogen (and helium) are collected. The lipophilic trap consists of a stainless steel tube (1/4 in. O.D.) packed with Porapak QS, and is cooled by liquid nitrogen (b.p. -196 C). The total amount of gas in the reactor is computed from the volumes of the reactor and gas sampler.

Experimental studies to investigate the effect of coal type on pyrolysis product yields, compositions, and evolution rates were carried out using six coals ranging from lignites to low-volatile bituminous coals. Under reactor pressures ranging from 'vacuum' (10^{-3} atm) to 10 atm, coal particles with diameters of 75-90 μm were pyrolyzed in a screen-heater type reactor at a heating rate of 1000 C/s to a maximum temperature of 1050 C.

Sections 5.1, 5.2, and 5.3 respectively present coal-type effects on the evolution behavior of tars, individual gases, and total volatiles under 1 atm reactor pressure. The atmospheric pressure data for a given coal represent an overall pyrolysis behavior, that includes contributions from primary decomposition reactions, and from secondary reactions coupled with mass transport processes. In Section 5.4, pressure is varied to infer the extent of secondary reaction contributions in the overall pyrolysis behavior. Section 5.5 discusses magnitudes of uncertainties associated with experimental data.

5.1. Coal-type effects on tar production

5.1.1. Observed rate of tar production

Figure 5.1-1 shows the atmospheric tar yield versus peak and holding temperatures for the six coals studied. Heating and cooling rates in these runs were respectively 1000 and 200-1000 C/s with no holding time at final temperature. The maximum peak temperature was 1050 C. At higher temperatures, the fragmentation of more stable structures such as aromatic rings lead to further weight loss (Kobayashi et al., 1977). The lines through the data points in

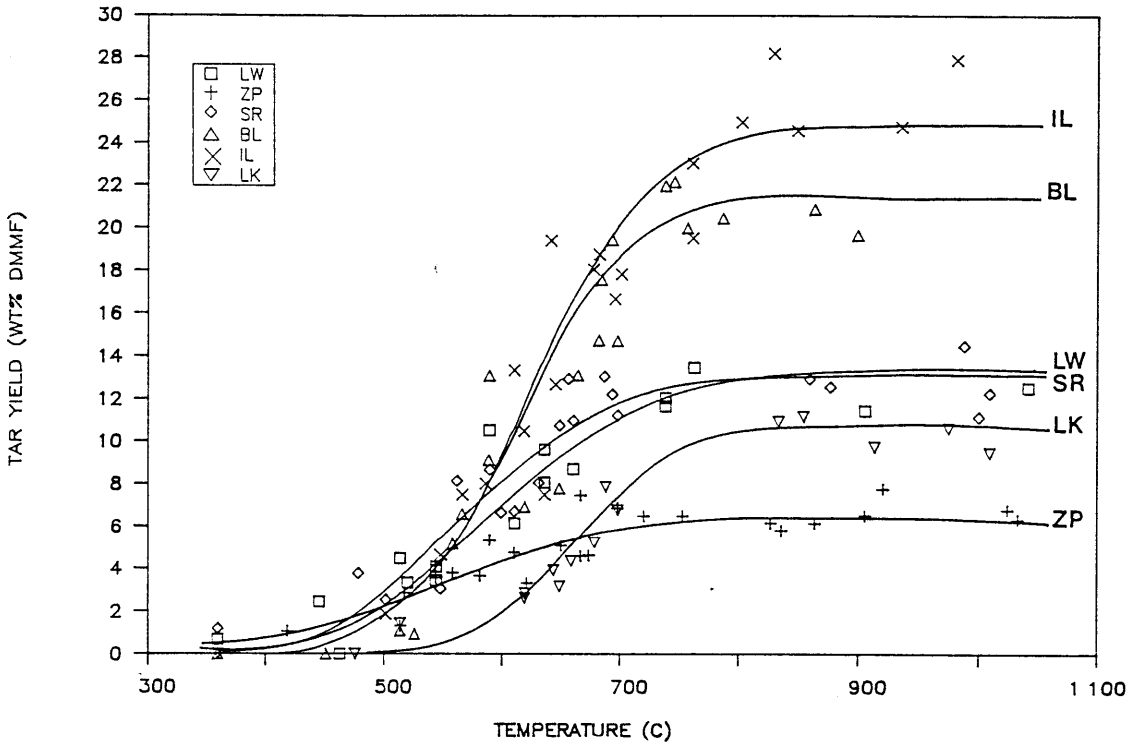

Figure 5.1-1 Experimental yields of pyrolysis tar versus peak temperature for the six coals selected in this study. Carbon: LW < ZP < SR < BL < IL < LK.

Abbreviations:

LW = Lower Wilcox lignite
ZP = Beulah Zap lignite
SR = Smith Roland subbituminous
BL = Blue high-volatile bituminous
IL = Illinois high-volatile bituminous
LK = Lower Kittanning low-volatile bit.

Fig.5.1-1 are hand-drawn to indicate trends. Individual plots with model predictions are given in Chapter 6 (Fig.6.1-1).

Qualitatively, the figure shows that there is a clear effect of coal type on both the apparent rate of tar production and the yield limit, defined as the asymptotic yield at high peak temperatures ($\tilde{>}$ 800 C). Low-rank coals (ZP,LW,SR) tend to initiate and achieve given extents of tar production at lower temperatures compared to higher rank coals (BL, IL,LK); abbreviations are defined in Fig.5.1-1.

These points are reinforced by quantitative observations on the apparent rate of tar production presented in Fig.5.1-2, which compares the temperatures at which the tar yield reaches 25% (T25), 50% (T50), and 75% (T75) of the yield limit for the six coals represented by their elemental carbon contents in wt% dmmf. The three characteristic temperatures were determined from the tar data fitted with the MIPR model (see Fig.6.1-1). The difference between T75 and T25 (T75-T25) represents an approximate spread of the yield curve, whereas T50 roughly corresponds to the temperature at which the observed tar evolution rate is maximum. Comparing T50 shows almost a monotonic increase with coal rank represented by the elemental carbon content of the coal, indicating a shift in the yield curve to higher temperatures for higher rank coals. T50 ranges from 545 C for ZP to 675 C for LK, an increase in the maximum difference of about 130 C among the coals studied. Comparing (T75-T25) shows a decreasing trend for higher rank coals, indicating less spread in the yield curve for higher rank coals. The difference ranges from 175 C for ZP to 85 C for LK, a reduction in the maximum difference of about 90 C.

A similar trend of greater T50 and smaller (T75-T25) as the coal

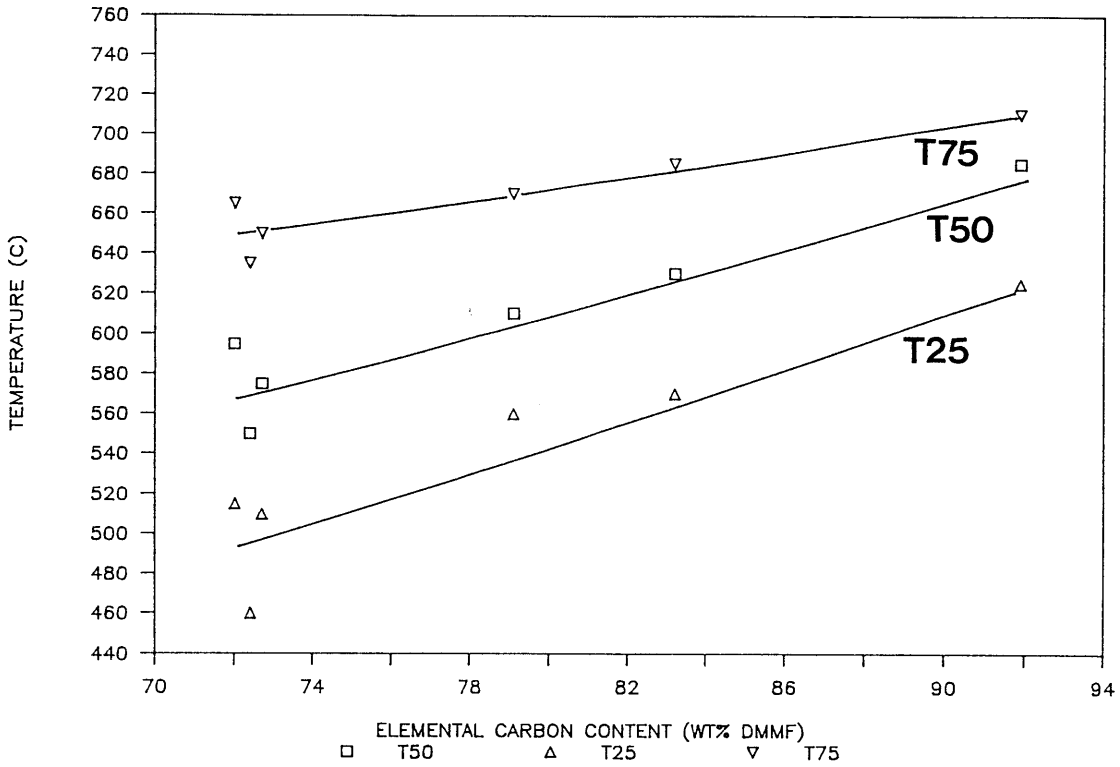

Figure 5.1-2 Characteristic yield temperatures for atmospheric tar production versus elemental carbon content for the six coals studied. [(a) T25, (b) T50, (c) T75 ; Tx denotes the temperature at which the yield reaches x% of the maximum yield]. Carbon: LW < ZP < SR < BL < IL < LK. Abbreviations: see Fig.5.1-1.

rank increases, has been reported in a previous study using a Montana lignite (ML) and a Pittsburgh Seam high-volatile bituminous coal (PB) (Suuberg, 1977). In relation to the coals studied here, these coals have elemental carbon contents in the order of LW < ML < ZP < SR < BL < PB < IL < LK. The elemental and proximate analysis of these two coals are given in Table 4.1-2. In going from Montana lignite to Pittsburgh bituminous coal, T50 increases from 570 to 675 C, and (T75-T25) decreases from 230 to 165 C. However, directly comparing these values to those from this work is not strictly valid due to somewhat different temperature-time histories employed in the two studies.

An exact description of the complex reaction chemistry and transport phenomena involved in tar production is currently not available. Thus, interpretation of the observed tar evolution rate behavior for different coal types, depends on the assumed mechanism for tar formation. A frequently assumed mechanism is the decomposition of 'tar precursors' in the coal via multiple first-order independent parallel reactions (Serio, 1984; Ko et al., 1988a)

$$\text{Tar precursors in coal} \xrightarrow[\text{transport}]{\text{first-order decomposition}} \text{Tar}$$

The fitted parameters for this global decomposition reaction are influenced by any physical transport effects. Under such a global description with the further assumption that all coals have the same preexponential factor in the Arrhenius rate constant, a higher T50 implies that tars are produced from reactions with greater apparent activation energies. Similarly, a larger (T75-T25) implies a wider distribution of apparent activation energies. Thus, under the assumptions of this global description, higher rank coals appear to

produce tars from reactions with apparent activation energies that have a higher mean but a narrower distribution.

5.1.2. Tar yield limit

Figure 5.1-1 shows that the tar yield limit increases from 7-13 wt% dmmf for the low-rank coals (LW,SR,ZP), to 21-25 wt% dmmf for the high-rank coals (BL,IL), and then drops to 11 wt% dmmf for the very high-rank coal (LK). Despite this general trend, however, a significant variation is also noted among coals of the same rank; e.g., almost a two fold variation for the low-rank coals. This observation along with other tar yield data reported in the literature, indicates that coal-rank information alone is not enough to quantitatively explain the observed trend.

A new approach to quantitatively relate the tar yield to measurable properties of the coal is to: (1) assume a chemical and physical mechanism of tar production, (2) identify the chemical structures that are important from the assumed mechanism, (3) formulate a coal-specific parameter based on the important chemical structures, and (4) relate the structures to (ideally readily) measurable properties of the coal (Ko et al., 1987, 1988c).

The correlation procedure discussed in detail below is tested against a large set of experimental data from this study and the literature, representing a wide range of coals (37 coals, ranging from lignites to anthracites) and pressures ('vacuum' to 90 atm). Table 5.1-1 gives the elemental analysis and measured tar yield under a specified pressure for each coal. The data represent the maximum amount of tar generated during devolatilization with minimal influence

from secondary reactions outside the coal particle. The following conditions support the fact that the tar data used here represent good estimates of the probable upper bounds on tar production at a given pressure:

- o All the data are from rapid devolatilization (100-1500 K/s) of small samples of coal particles (≈ 20 mg) in the 50-100 μm dia. size range, under constant pressures ranging from 0.0001 to 90 atm in screen-heater reactors. These conditions afford minimal opportunity for in-bed secondary reactions of newly evolved tars.
- o The screen-heater reactors provide rapid dilution and quenching of tar and other volatiles as soon as they are evolved from the coal surface, thus presenting minimal opportunities for extra-particle secondary reactions.
- o The final temperature and holding time ($\tilde{<}$1000 C and <10 s) are sufficient to drive devolatilization, including tar generation, essentially to completion.

Formulation of correlation: treatment of coal-type effects

(1) Chemical and physical mechanism of tar production

Tar is assumed to be generated via the global mechanism:

```
      [1] thermolysis                [2] transport
Coal ------------------> Metaplast ----------------> Tar
       of bridges
```

The above mechanism was first suggested by van Krevelen (1961), and similar versions have since been widely applied in many different pyrolysis models (Unger and Suuberg, 1981; Oh, 1985; Fong, 1986).

(2) Important chemical structures

The identities and numbers of bridges between aromatic clusters of the coal and the concentration of hydrogen available to stabilize the free radicals created by bridge scission reactions are important structural chemical factors in tar generation without transport effects. Since the structural features important in the latter process, [2] in the assumed mechanism, are not easily identifiable, the transport effect is correlated via empirical parameters obtained from best-fit analyses of existing data.

(3) Formulation of coal-specific parameter

A coal-specific parameter, X_{TAR}, proposed to correlate tar yields with coal type is

$$X_{TAR} = \frac{\text{(no. of labile bridges)(amt. of abstractable hydrogen)}}{\text{(no. of cross-linked bridges)}} \qquad (5.1\text{-}1)$$

(4) Estimation of identified structures

Since the necessary molecular structures are generally unavailable for most coals, reasonable estimates were made for each quantity based on currently available information.

Labile bridges are only aliphatic, and their concentration is assumed to be proportional to the aliphatic carbon content of the raw coal. This fraction $(1\text{-}f_a)$ also contains contributions from carboxyl, carbonyl, and ether carbons, but these are assumed to be small. Thus,

$$\text{(labile bridges)} = \{(1\text{-}f_a)[C]/12\}^{1.8} \qquad (5.1\text{-}2)$$

where [C] is the carbon content of the coal in wt% dmmf, and f_a is the aromaticity, estimated from a polynomial best-fit of f_a to [C] using data from Gerstein et al. (1982)

$$f_a = 0.830526 - 2.008147\ ([C]/100) + 2.241218\ ([C]/100)^2 \qquad (5.1\text{-}3)$$

The exponent of 1.8 in Eq.(5.1-2) is a best-fit parameter obtained by applying multivariable fitting routines to obtain the best correlation between experimental tar yields and X_{TAR}. An alternative and perhaps physically more appealing rationale for this exponent is to assume that X_{TAR} is proportional to (labile bridges)$^{1.8}$ and that (labile bridges) is linearly related to the aliphatic carbon content.

Cross-linked bridges consist only of ether and thioether structures, whose concentration is assumed to be proportional to the sum of elemental and organic sulphur contents of the raw coal. Thus,

$$\text{cross-linked bridges} = [O]/16 + [S_o]/32.066 \quad \text{if } [O]>3.5 \text{ wt\% dmmf,}$$
$$= 3.5/16 + [S_o]/32.066 \quad \text{if } [O]<3.5 \text{ wt\% dmmf} \tag{5.1-4}$$

where [O] and $[S_o]$ are elemental oxygen and organic sulphur contents in wt% dmmf respectively. A constant [O] was needed for coals with low elemental oxygen contents because the number of cross-linked bridge is highly sensitive to coal elemental oxygen contents below about 4 wt% dmmf, and uncertainties in oxygen measurement can easily exceed 1 wt% dmmf.

Abstractable hydrogen is the hydrogen attached to aliphatic carbons. Its concentration is assumed to be proportional to the amount of elemental hydrogen of the raw coal, minus a slight correction to account for experimental observations that -OH groups may compete for the abstractable hydrogen (Suuberg, 1977). Thus,

$$\text{abstractable hydrogen} = [H]/1 - [OH]/17 \tag{5.1-5}$$

where [H] is the elemental hydrogen content (wt% dmmf), and [OH] is the hydroxyl group content (wt% dmmf) obtained from Given (1976)

$$[OH] = 33.2 - 0.35\,[C] \tag{5.1-6}$$

Figure 5.1-3, a plot of the three key structural quantities computed from Eqs. (5.1-2,4,5) versus the elemental composition, offers a quick and convenient way to obtain X_{TAR} with minimal computational effort.

Formulation of correlation: treatment of pressure effects

Tar yield limit at a given pressure is linearly correlated with the coal-type parameter derived above:

$$\text{Tar yield limit (wt\% dmmf)} = \alpha(P) + \beta(P)X_{TAR} \qquad (5.1\text{-}7)$$

The pressure dependent coefficients α and β are obtained by best fitting experimental tar yield data either for specified pressures and pressure ranges or for all pressures. The results are given below.

The best-fit coefficient values for pressure-specific correlation are as follows:

For coals with $X_{TAR} < 15$,

$$\alpha(10\text{ Pa- }9\text{ MPa}) = 2 \qquad (5.1\text{-}8)$$

$$\beta(10\text{ Pa- }9\text{ MPa}) = 0. \qquad (5.1\text{-}9)$$

For coals with $15 \leq X_{TAR} \leq 31$,

$$\alpha(10\text{-}100\text{ Pa}) = -30.8125, \quad \beta(10\text{-}100\text{ Pa}) = 2.1825 \qquad (5.1\text{-}10,11)$$

$$\alpha(0.1\text{ MPa}) = -22.375, \quad \beta(0.1\text{ MPa}) = 1.625 \qquad (5.1\text{-}12,13)$$

$$\alpha(1\text{ MPa}) = -16.75, \quad \beta(1\text{ MPa}) = 1.25 \qquad (5.1\text{-}14,15)$$

$$\alpha(2.5\text{-}9\text{ MPa}) = -10.1875, \quad \beta(2.5\text{-}9\text{ MPa}) = 0.8125. \qquad (5.1\text{-}16,17)$$

For coals with $X_{TAR} > 31$,

$$\alpha(10\text{-}100\text{ Pa}) = 37 \qquad (5.1\text{-}18)$$

$$\alpha(0.1\text{ MPa}) = 28 \qquad (5.1\text{-}19)$$

$$\alpha(1\text{ MPa}) = 22 \qquad (5.1\text{-}20)$$

$$\alpha(2.5\text{-}9\text{ MPa}) = 15 \qquad (5.1\text{-}21)$$

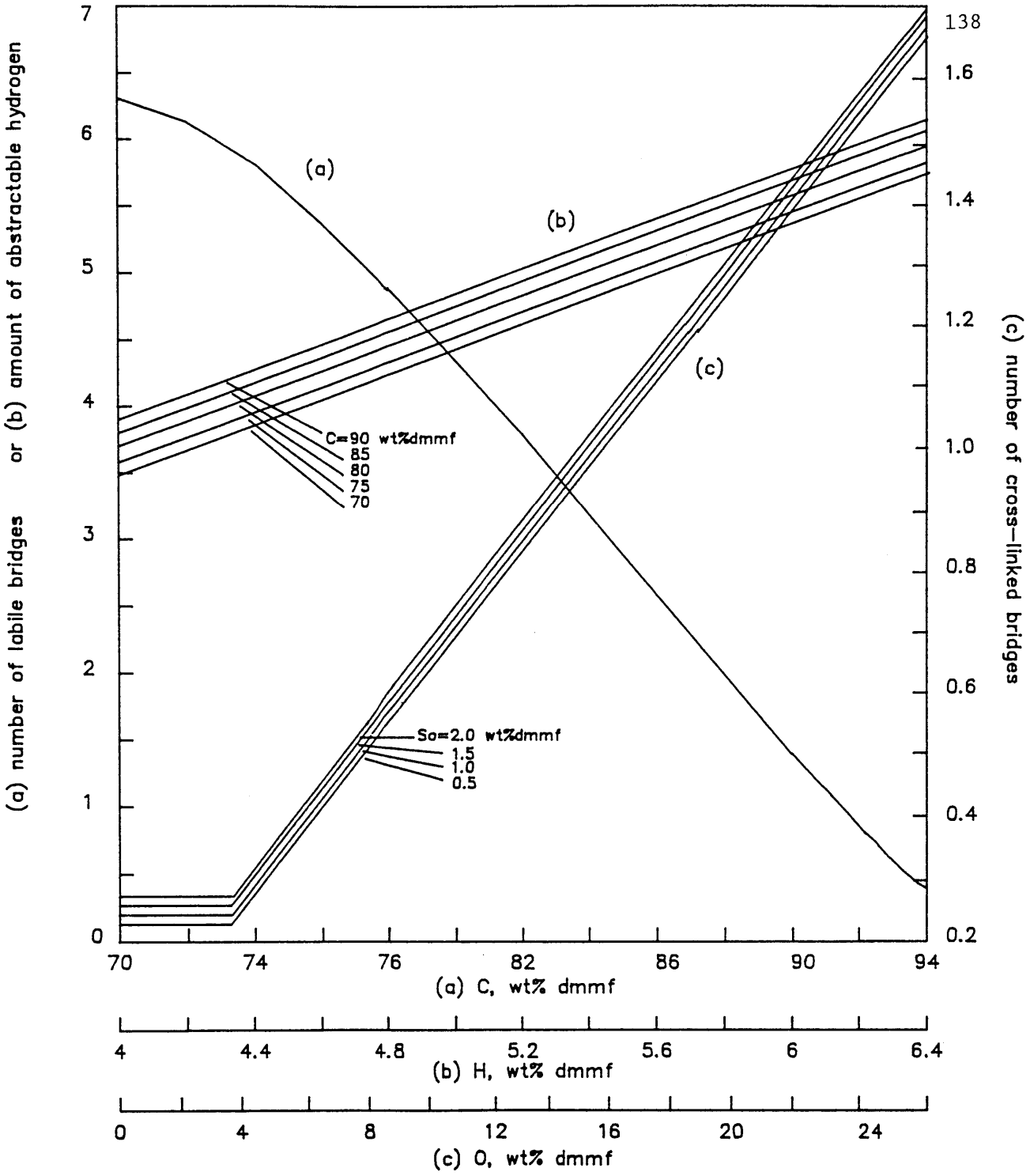

Figure 5.1-3 Estimates of the structural quantities in Eq.(5.1-1): (a) number of labile bridges vs. [C] computed from Eq.(5.1-2); amount of abstractable hydrogen vs. [H] from Eq.(5.1-5); (c) number of cross-linked bridges vs. [O] from Eq.(5.1-4).

$$\beta(10\ \text{Pa} - 9\ \text{MPa}) = 0. \qquad (5.1\text{-}22)$$

The best-fit coefficients applicable for all pressures are as follows:

For coals with X_{TAR} <15,

$$\alpha = 2 \quad , \quad \beta = 0. \qquad (5.1\text{-}23,24)$$

For coals with 15≤ X_{TAR} ≤31,

$$\alpha = 1/(0.021533 + 0.028651L_P) - 36 \qquad (5.1\text{-}25,26)$$

$$\beta = 0.508030 + 0.696487L_P - 0.06959L_P^2. \qquad (5.1\text{-}27,28)$$

For coals with X_{TAR} >31,

$$\alpha = 11.24071 + 9.743707L_P - 0.91326L_P^2 \qquad (5.1\text{-}29)$$

$$\beta = 0. \qquad (5.1\text{-}30)$$

$L_P = -\log_{10}P + 1$ with P=reactor pressure in MPa for P ≤ 2.5 MPa (1 MPa ≈ 10 atm), and P is fixed at 2.5 MPa for reactor pressure above 2.5 MPa. This was justified since pressure has negligible effects on tar yield above 2.5 MPa. Bautista (1984) observed that tar yield did not decline with increasing pressure above ≈2 MPa, and the present work (see Fig. 5.1-4 below) found close agreement between predictions and data using 2.5 MPa to represent pressures from 2.5-9 MPa.

Results and discussion

Figure 5.1-4 compares measured maximum tar yields with those predicted from Eq.(5.1-7) using the pressure-specific coefficients [Eqs. (5.1-8) through (5.1-22)]. The predicted yields are within ± 5 wt% dmmf of the observed values for all coals tested at the four pressures. The standard error of estimate of the prediction was 2.8 wt% dmmf. The standard error of estimate was computed using the definition

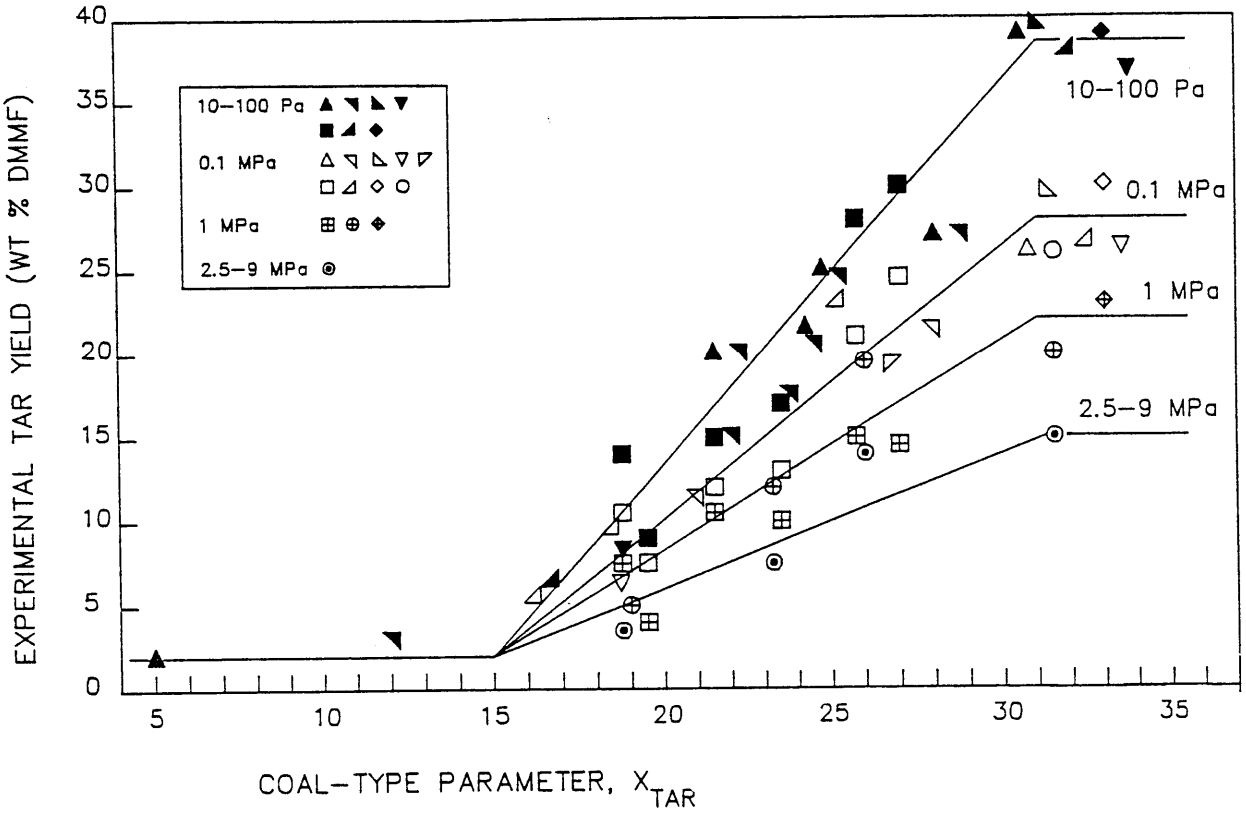

Figure 5.1-4 Correlation of tar yields at different pressures with X_{TAR}. Symbols: see Table 5.1-1. Lines are from Eq.(5.1-7) using the pressure-specific parameters from Eqs. (5.1-8)-(5.1-22).

$$\text{standard error of estimate} = \sum_{j=1}^{n} \left[\frac{(\text{Yield,j,exp'l} - \text{Yield,j,pre'd})^2}{n-k} \right]^{1/2} \quad (5.1\text{-}31)$$

where n is the number of data points (j), and k the number of best-fitted parameters used in the correlation.

Figure 5.1-5 compares experimental data for all pressures with predictions obtained from Eq.(5.1-7) using the pressure-correlated parameters [Eqs. (5.1-23)-(5.1-30)]. The predicted yields are within ±6 wt% dmmf for all coals. Use of the pressure correlated parameters has the advantage that it is applicable for all pressures between 10 Pa to 9 MPa, but suffers from a slightly greater standard error of estimate of 3.1 wt% dmmf.

The wide range of coal types ($4 \leq X_{TAR} \leq 34$) and pressures (10 Pa-9 MPa) covered in the present data base (Table 5.1-1) suggests that there should be little need to extrapolate the correlation outside the domains tested here. Predictions based on small extrapolations of X_{TAR} should be of comparable reliability to those from tested X_{TAR} values. As a rough guideline, X_{TAR} typically ranges from 4 to 12 for anthracites; 12 to 20 for low tar producing lignites and low-volatile bituminous coals; 20 to 30 for high tar producing lignites, and subbituminous and medium-volatile bituminous coals; and 30 to 34 for high-volatile bituminous coals. For applications to pressures above 9 MPa, the 2.5-9 MPa correlation is expected to give satisfactory predictions since pressure effects were observed to be negligible at pressures beyond ≈2.5 MPa.

Increasing pressure lowers tar yield by slowing tar transport rates, thus allowing additional time for tar conversion in secondary reactions. The decrease in tar yield with increasing pressure is less

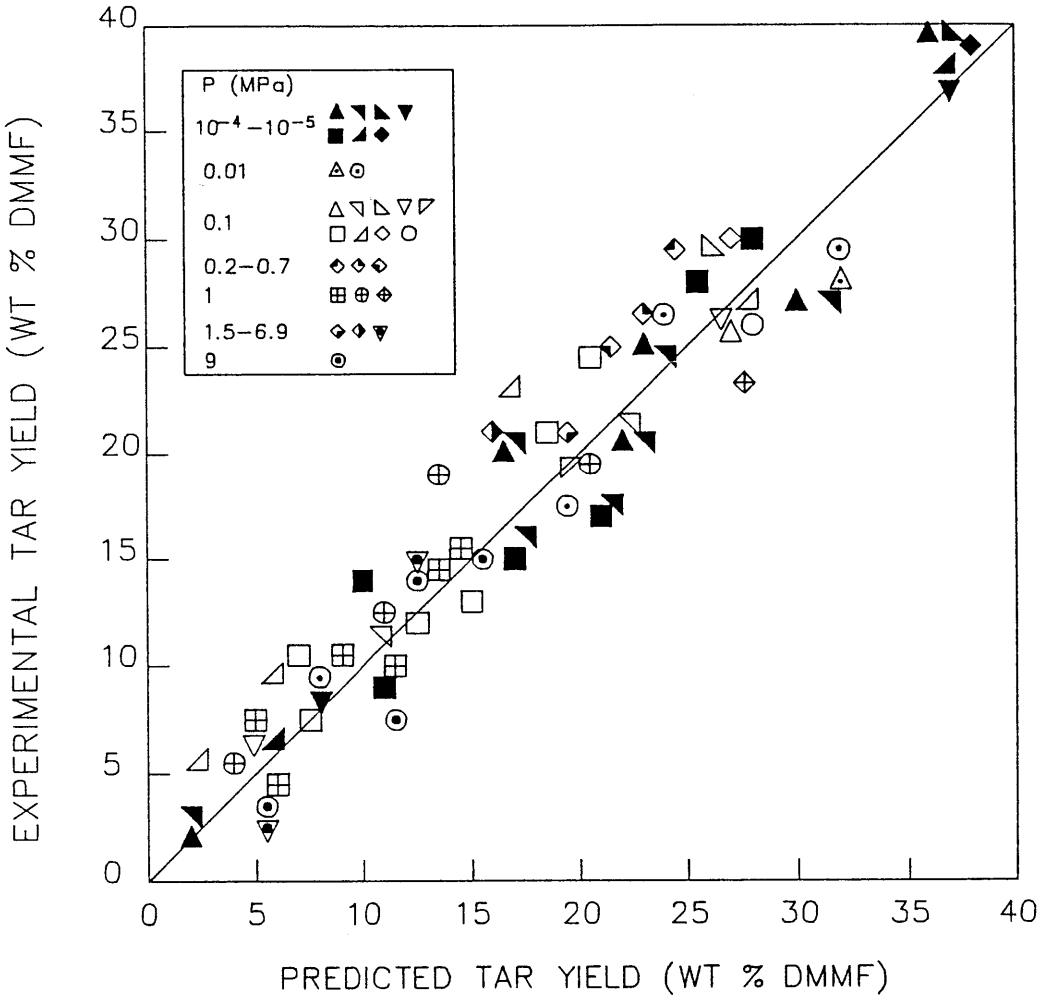

Figure 5.1-5 Comparison of experimental tar yields with those predicted by Eq.(5.1-7) using the pressure-correlated parameters from Eqs. (5.1-23)-(5.1-30). Symbols: see Table 5.1-1.

Table 5.1-1 Characteristics of coals and experimental tar yields used in the tar yield limit correlation.

Investigator	Coal[a]	Elemental Analysis (wt% dmmf) C	O[b]	H	So[c]	Tar yield (wt% dmmf; symbols used in Figs. 5.1-4 and 5.1-5) at pressures (MPa) of 10^{-4}-10^{-5}	0.01	0.1	1	6.9	9
Freihaut and Seery (1981)	Montana L	68.3	25.5	4.6	0.7	▲18.0[f]					
	Wyodak SB 1	75.4	18.1	4.9	0.4	▲20.0					
	Wyodak SB 2	75.5	17.0	5.2	0.6	▲21.0					
	Utah B	78.2	13.9	5.5	0.8	▲27.0					
	Colorado B	81.0	11.2	5.5	0.6	▲26.0[f]					
	Pittsburgh B	82.0	9.4	5.4	1.9	▲39.0					
	Alabama B	85.0	8.2	4.6	0.5	▲25.0					
	Anthricite	93.7	1.9	2.6	0.7	▲ 2.0					
Freihaut et al. (1982)	Colorado B	81.0	11.2	5.5	0.6		△19.8[d,f]	△19.2[f]			
	Pittsburgh B	82.0	9.4	5.4	1.9		△28.1[d]	△26.0			
Loison and Chauvin (1964)	Faulquemont B	80.8	12.8	5.1	0.5	◥20.0					
	Wendel III B	86.1	8.3	5.3	0.3	◥24.3					
	Lens-Lievin B	88.4	6.4	5.0	0.6	◥27.0					
	Emma B	88.5	5.4	4.7	0.5	◥20.5					
	Bergmannsgluck B	89.0	5.2	4.6	0.7	◥17.6					
	Maigre oignies B	91.9	4.4	3.8	0.4	◥15.1					
	Flenus de Bruay B	86.7	6.4	5.1	0.5	◥ 2.1					
Oh (1985)	Pittsburgh B	82.2	10.0	5.9	1.9	◥39.8		◺29.3			
Arendt and van Heek (1981)	Prosper II B	91.5	2.7	4.4	0.7		⊙ 9.9		⊕ 6.6		⊙ 3.7
	Schlaegel u. Eisen B	90.1	3.7	4.3	0.5		⊙17.7		⊕12.2		⊙ 7.5
	Wulfen B	87.6	5.7	4.7	0.6		⊙26.5		⊕19.3		⊙14.1
	Leopold B	84.2	8.4	5.7	0.9		⊙28.4	○25.7	⊕19.8		⊙15.2
Suuberg (1977)	Pittsburgh B	81.0	9.7	5.7	1.9	▼37.0		▽26.5		▽13.8	
Cosway (1981)	Montana L	72.2	22.0	4.6	0.8	▼ 8.4		▽ 6.5		▽ 3.2	
Reitzen (1978)	Wyodak SB	73.1	19.8	6.1	0.4			◹19.3			
	Sesser SB	82.9	10.3	5.4	0.4			◹21.5[e]			
	Colstrip L	76.8	17.4	4.9	0.5			◹11.5			
This Study	Lower Wilcox L	72.0	20.9	5.6	0.4	■16.8		□13.1	⊞ 9.9		
	Illinois B	83.2	9.8	5.4	2.0	■30.1		□24.8	⊞15.0		
	Blue SB	79.1	14.1	5.3	0.4	■27.7		□21.2	⊞14.5		
	Beulah Zap L	72.4	21.6	4.8	0.6	■ 9.1		□ 7.2	⊞ 4.1		
	Lower Kittanning B	91.9	1.7	5.0	0.6	■14.0		□10.7	⊞ 6.5[h]		
	Smith Roland L	72.7	20.9	5.3	0.5	■14.8		□12.9	⊞11.1		
Suuberg et al. (1987)	Pocahantas B	91.3	4.1	4.6	0.2			◹ 9.9			
	North Dakota L	74.5	20.5	4.1	0.5			◹ 5.6			
	Illinois B	78.6	14.6	5.4	2.0			◹22.8			
	Bruceton B	85.1	7.6	5.6	0.5			◹26.5			
Suuberg et al. (1985)	North Dakota L	75.4	19.1	4.1	0.5	◢ 6.7					
	Bruceton B	85.1	7.6	5.6	0.5	◢37.7					
Bautista (1984)	Pittsburgh B	84.7	7.9	5.8	0.7	◆38.6		◇30.0	◇29.7(0.2)[g]		
									◇26.5(0.4)		
									◇25.2(0.7)		
									◇23.7(1.0)[d]		
									◇21.1(1.5)		
									◆20.6(2.4)		

[a] B-bituminous; L-lignite; SB-subbituminous
[b] By Difference
[c] Estimated as half the total sulphur content when organic sulphur not reported (Loison and Chauvin, 1964; Arendt and van Heek, 1981; Cosway, 1981; Reitzen, 1978; Suuberg et al., 1985, 1987; Bautista, 1984; this study).
[d] Obtained by interpolation between 0.0007 and 0.013 MPa in Freihaut et al. (1982), and between 0.7 and 1.5 MPa in Bautista (1984).
[e] The tar yield (6.5 wt% dmmf) reported for Sesser SB seemed low and was substituted by the 21.5 wt% dmmf measured in this study.
[f] Colorado B and Montana L from Freihaut and Seery (1981), and Freihaut et al. (1982) were not used because possible errors in tar yield measurement are suspected.
[g] Indicates pressure in MPa.
[h] This value is slightly lower than the previously reported value (7.2 wt% dmmf) in Ko et al. (1988c).

severe for coals with lower X_{TAR}, becoming almost negligible for coals with X_{TAR} below 15 (Fig.5.1-4). Two possible explanations for this finding are: (1) tars from coals with higher X_{TAR} are more reactive to secondary reactions, and (2) faster rate of tar secondary reactions caused by higher concentrations of tars inside the coal particle for coals with higher X_{TAR}. Quantitative rationalization for this behavior must await further studies of tar reactivity.

Particle size is another important variable which affects tar yield. However, the small data base on particle-size effects (Suuberg, 1977; Bautista, 1984) suggests that the tar yield at 0.1 MPa is almost unaffected between 50 and 300 μm (dia.), and only slightly affected between 300 and 800 μm (dia.).

5.2. Coal-type effects on gas production

Figure 5.2-1 compares the yield limit of gaseous products versus the elemental carbon content for the six coals investigated in this study, and the two coals studied by Suuberg (1977) under similar but not identical experimental conditions. Higher rank coals generally produce less carbon oxides and pyrolytic water, but more methane; the ranges for CO, CO_2, H_2O, CH_4 are 0.9-11.0, 0.4-9.9, 2.4-16, 1.6-4.3 wt% dmmf respectively. The ethylene and ethane yields are small and their absolute yield values are less affected by coal type; they range from 0.6 to 1.6 wt% dmmf for ethylene and from 0.2 to 0.7 wt% dmmf for ethane. The higher carbon oxides and water yields have been associated with higher concentrations of carboxyl and hydroxyl groups respectively in lower rank coals (Suuberg, 1977). However, an exact reaction mechanism is not yet available to quantitatively rationalize the

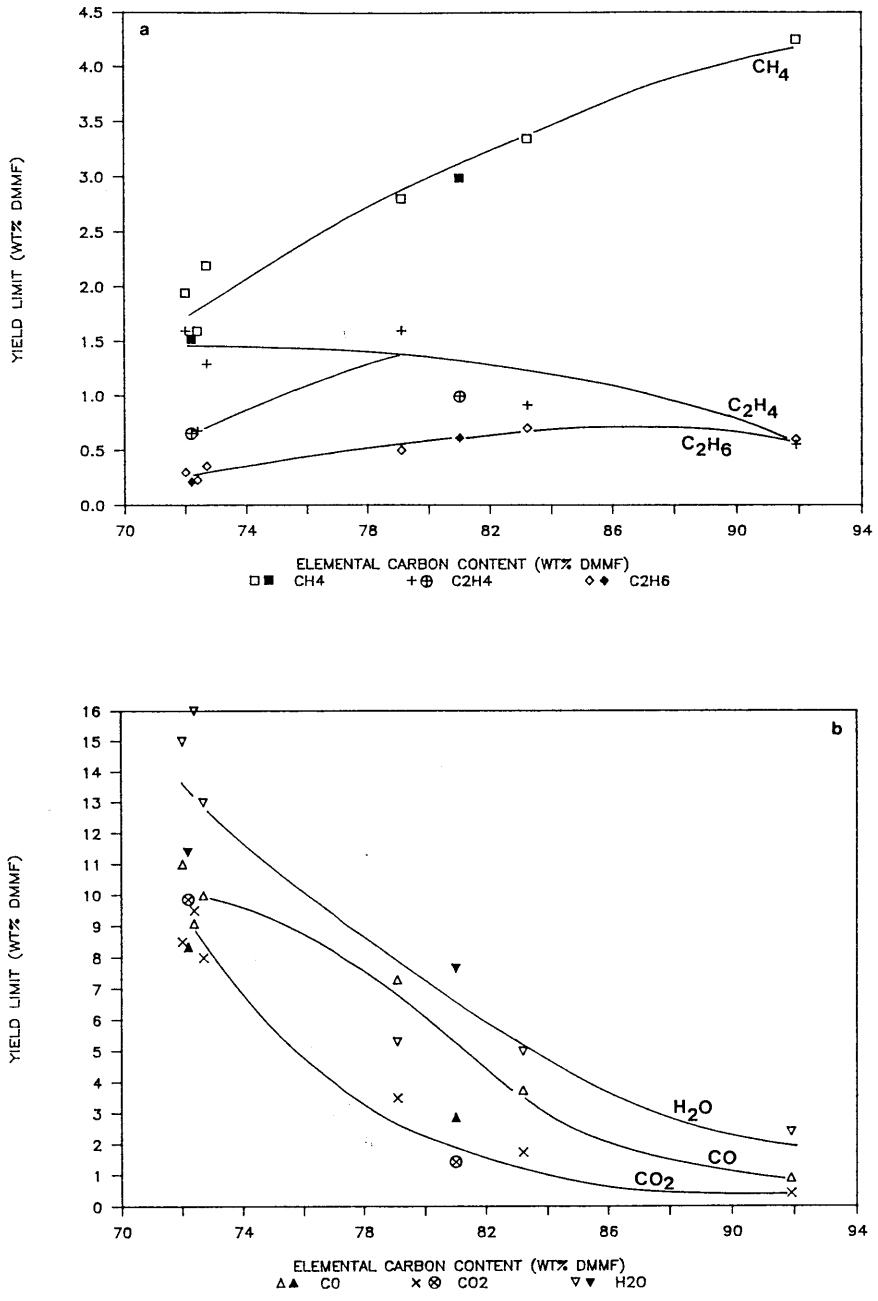

Figure 5.2-1 Comparison of the yield limit of gaseous products versus the elemental carbon content at ambient pressure: (a) hydrocarbons; (b) carbon oxides and pyrolytic water. Open or non-circled symbols are from this study; closed or circled symbols are from Suuberg (1977). Carbon: LW < ML < ZP < SR < BL < PB < IL < LK. Abbreviations: ML = Montana lignite, PB = Pittsburgh Seam high-volatile bituminous, see Fig.5.1-1 for others.

relationship. Methane production has been postulated to occur via bond dissociation of alkyl groups to yield methyl radicals, which upon abstracting hydrogen form methane (Gavalas et al., 1981a). But applying such a mechanism to explain the observed trend for methane yields is difficult due to the lack of the necessary quantitative structural information, e.g., in particular the concentration of alkyl groups.

Figures 5.2-2, 5.2-3, 5.2-4, 5.2-5, and 5.2-6 respectively compare the yields and apparent production rates of CH_4, C_2H_4, C_2H_6, CO, and CO_2 production for the six coals investigated. Each figure consists of (a) a combined plot of yield versus peak and holding temperatures for all six coals, and (b) a plot showing three characteristic yield temperatures (T25, T50, and T75; see Section 5.1.1 for definitions) versus the elemental carbon content of the coal. The lines in the figures are free-drawn trend lines. Model generated curves for yield versus peak holding temperatures for these products are given in Figs. 6.1-3 through 6.1-7 respectively. Comparing T50 shows a slightly increasing trend with coal rank for methane and ethane (Figs. 5.2-2 and 4), but almost no observable effect for ethylene and carbon oxides (Figs. 5.2-3,5,6). The spread of the yield curve as indicated by (T75-T25) appears to be unaffected by coal type for all gases, except for carbon dioxide, which shows a decreasing trend for higher rank coals.

Reasons for the lack of observable coal-type effects on the apparent rate of gas production are currently unclear. One hypothesis is that the kinetics of gas production are unaffected by coal type (Solomon and Hamblen, 1985). Gaseous products are claimed to evolve from decomposition of specific functional groups, e.g., carbon monoxide

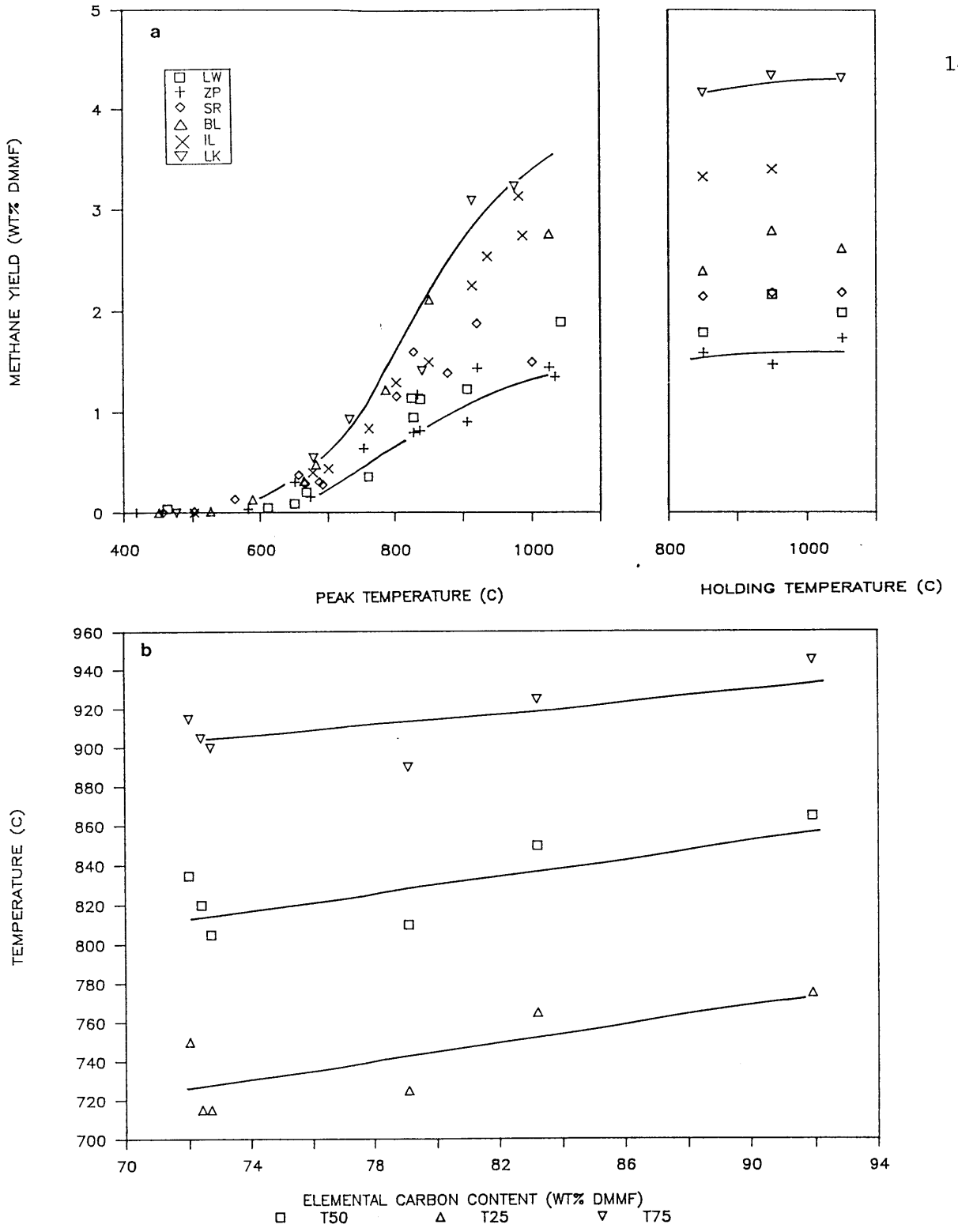

Figure 5.2-2 Comparison of methane production rate at 1 atm. (a) combined plot of yields versus peak and holding temperatures (5 s hold); (b) characteristic yield temperatures versus the elemental carbon content. Carbon: LW < ZP < SR < BL < IL < LK. Abbreviations: see Fig.5.1-1.

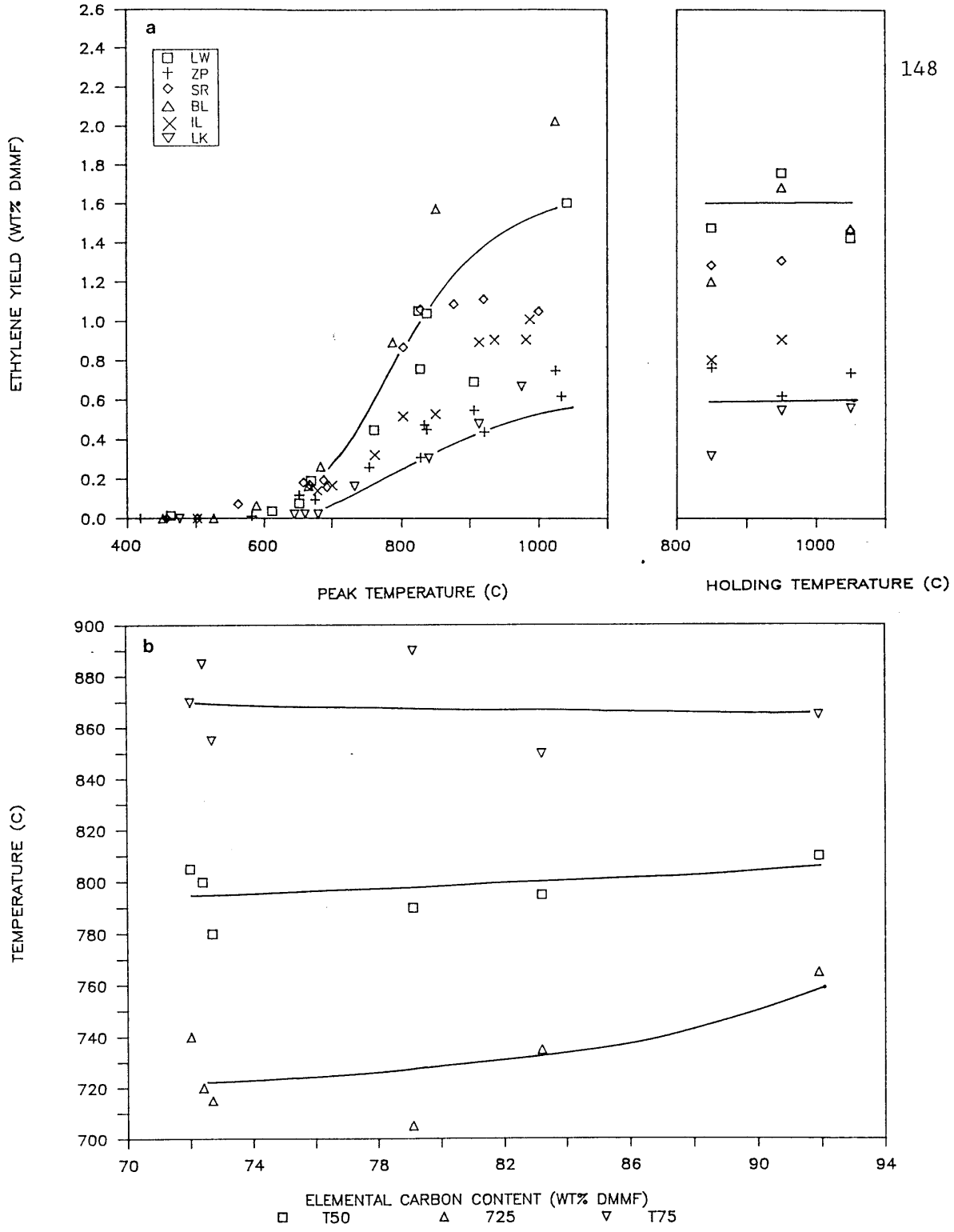

Figure 5.2-3 Comparison of ethylene production rate at 1 atm. (a) combined plot of yields versus peak and holding temperatures (5 s hold); (b) characteristic yield temperatures versus the elemental carbon content. Carbon: LW < ZP < SR < BL < IL < LK. Abbreviations: see Fig.5.1-1.

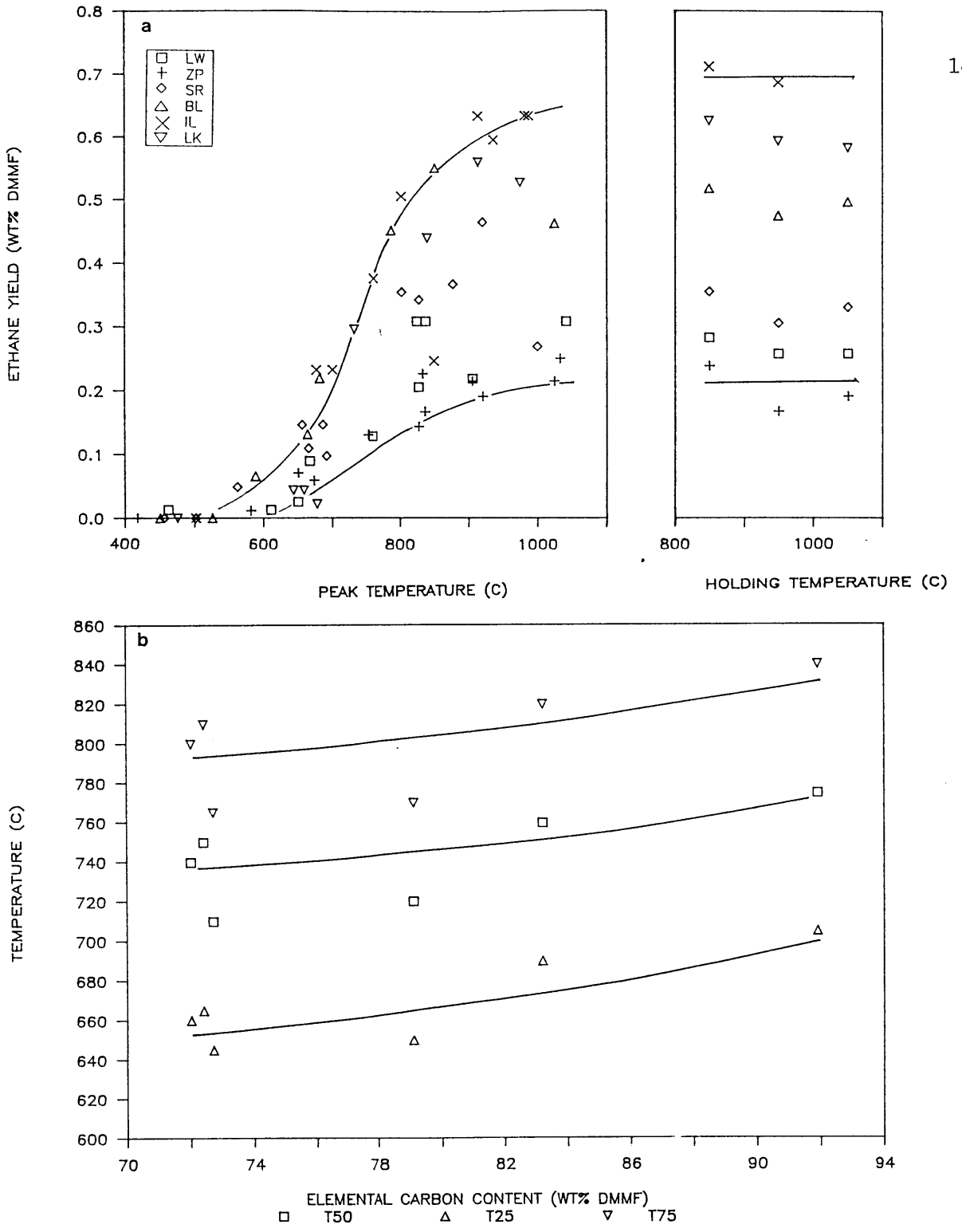

Figure 5.2-4 Comparison of ethane production rate at 1 atm. (a) combined plot of yields versus peak and holding temperatures (5 s hold); (b) characteristic yield temperatures versus the elemental carbon content. Carbon: LW < ZP < SR < BL < IL < LK. Abbreviations: see Fig.5.1-1.

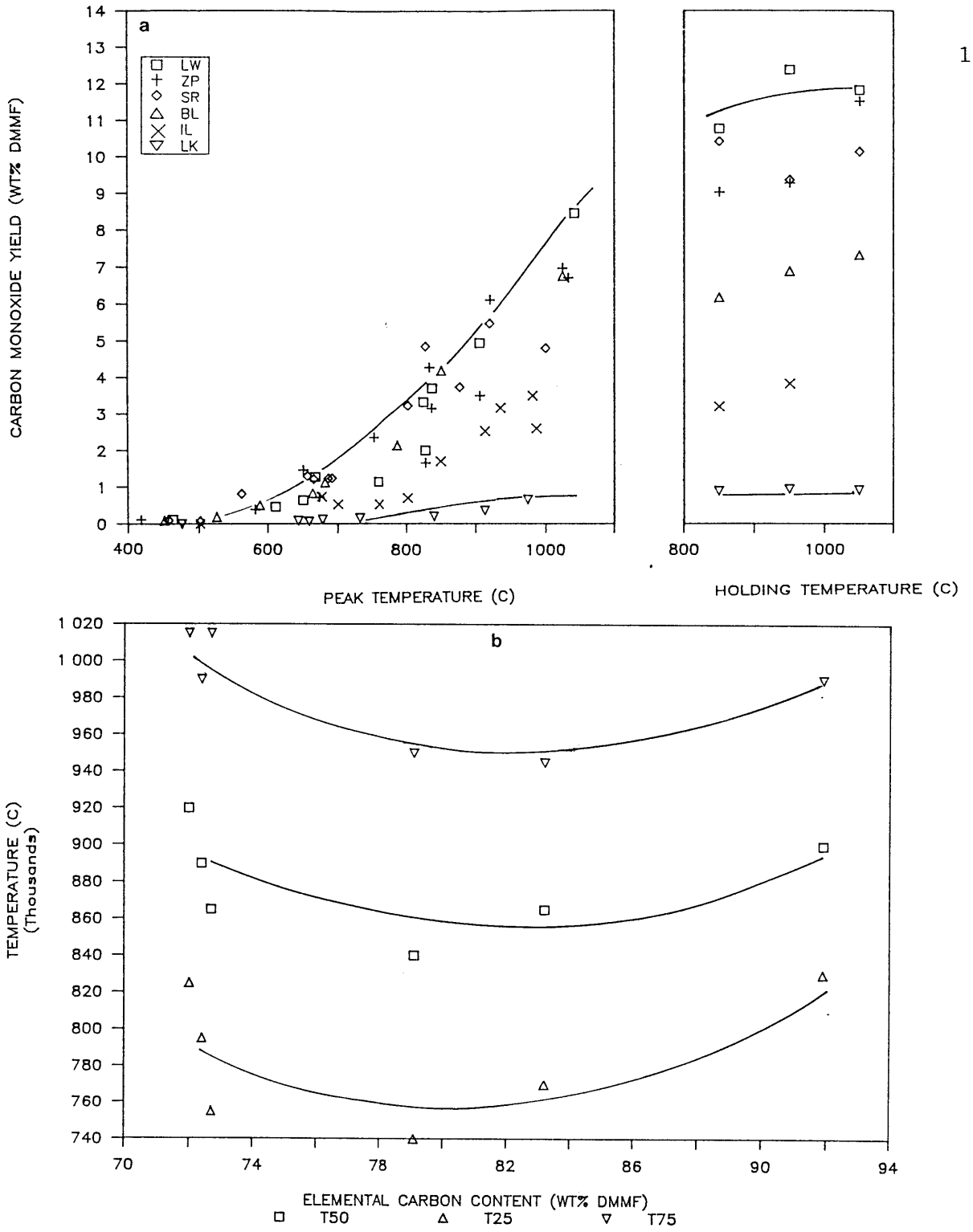

Figure 5.2-5 Comparison of carbon monoxide production rate at 1 atm. (a) combined plot of yields versus peak and holding temperatures (5 s hold); (b) characteristic yield temperatures versus the elemental carbon content. Carbon: LW < ZP < SR < BL < IL < LK. Abbreviations: see Fig.5.1-1.

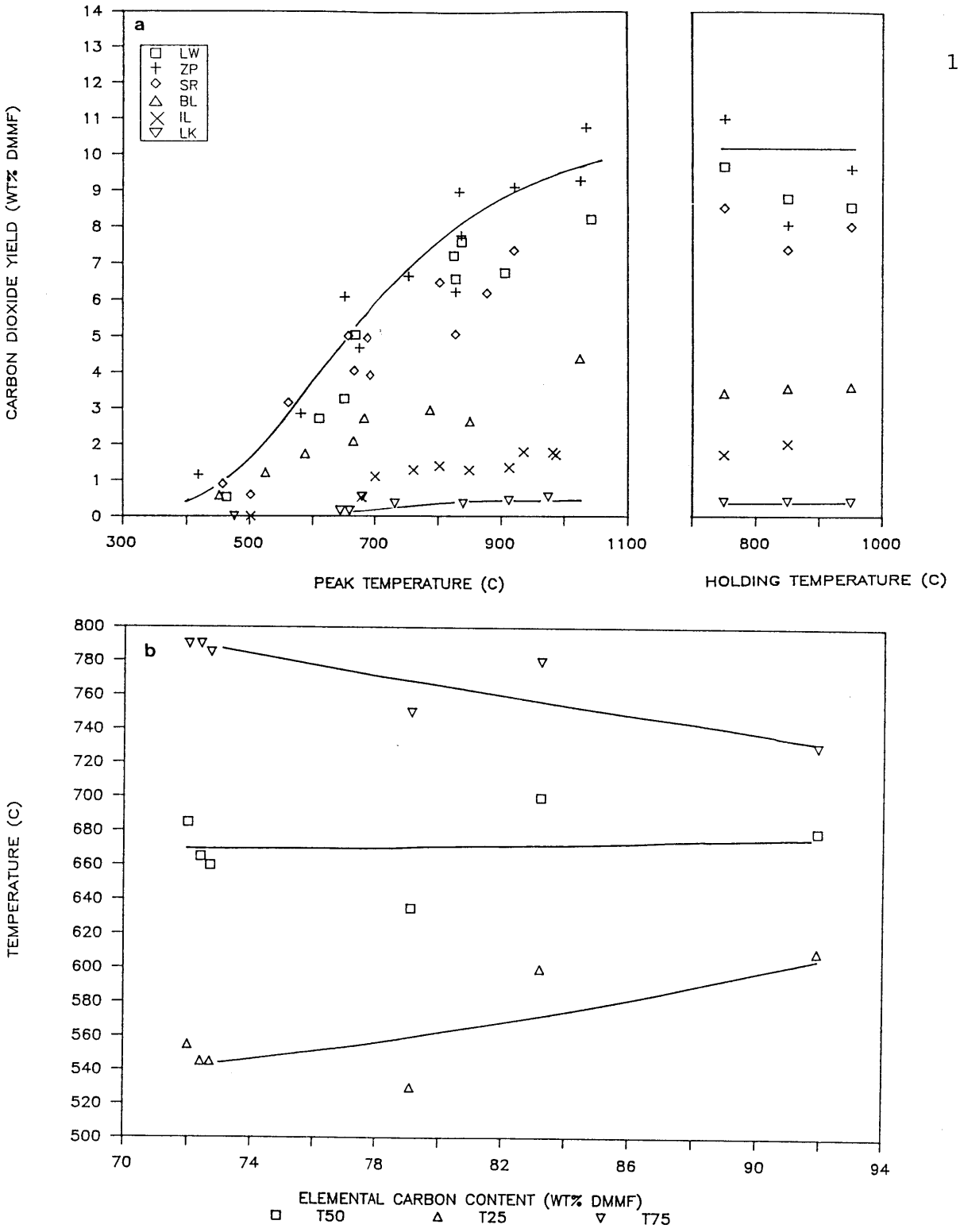

Figure 5.2-6 Comparison of carbon dioxide production rate at 1 atm. (a) combined plot of yields versus peak and holding temperatures (5 s hold); (b) characteristic yield temperatures versus the elemental carbon content. Carbon: LW < ZP < SR < BL < IL < LK. Abbreviations: see Fig.5.1-1.

is assumed to be produced from ether groups in the coal. The rate of gas production is assumed to depend only on the type of functional group, and thus is asserted to be independent of coal type. But a problem in such a simple picture is illustrated in the following example. Upon rapid pyrolysis at temperatures above 750 C, phenol decomposes along two parallel pathways, one of which gives CO and a C_5 moiety, and the other H_2O and benzene [Cypres and Bettens (1974), (1975a,b)].

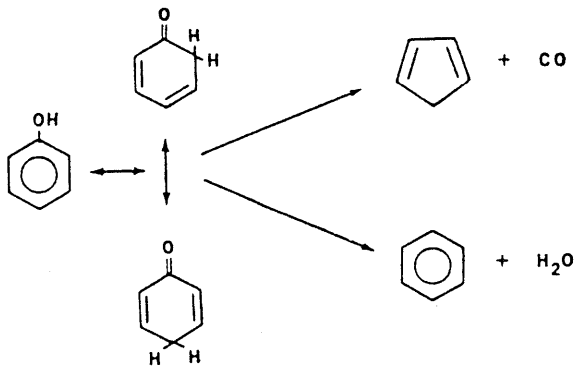

The former pathway is a base-catalyzed reaction, and thus is expected to be promoted by strong solid base materials from minerals in the coal such as CaO generated by calcite decomposition (Franklin et al., 1981). Thus, assuming this mechanism applies for decomposition of phenolic groups in coal, the phenol group can produce several different gas species, and the concentration of base-catalysts in minerals can strongly influence the relative extent of the two reaction paths. A more likely mechanism may be that gases are formed from a large set of complex elementary reactions involving, not just the structure initially present, but also many intermediate species that are formed

during coal decomposition, e.g., methyl radical side chains formed from scission of ethylene bridges. However, a better understanding of the reaction mechanism is needed to apply such a description to rationalize the observed gas production rate behavior among different coal types.

An alternative and more plausible explanation for the lack of observable coal-type effects in this study, is that differences in the apparent gas production rates are less than or comparable to scatter in the data caused by experimental uncertainties. Supporting evidence for this explanation comes from a recent study of Burnham et al. (1988), in which eight coals ranging from lignites to low-volatile bituminous coals were pyrolyzed at low heating rates ($\tilde{<}$ 1 C/s) under atmospheric pressure. They observed that T_{max} (T at which the evolution rate is maximum) generally increases with coal rank, with maximum differences ranging from 18 to 33 C among light hydrocarbons (CH_4, C_2H_4, C_2H_6). Such differences are more clearly resolved in the slow heating apparatus which is able to measure the sample temperature within ±5 C (Burnham et al., 1988). In rapid heating studies such as this one, uncertainties in the temperature measurement are much higher (≈±25 C), and are comparable to the reported differences caused by coal-type effects in the low-heating experiment. Rates for carbon oxides show multi-peaks, and thus are more difficult to compare among different coal types on the basis of T_{max}, though comparing the difference in the first peak (<500 C) of CO_2 production showed a difference of 86 C.

Pyrolytic water measurements in this study are highly uncertain. Despite an extensive effort to improve the accuracy of the water measurement technique, interference from atmospheric water vapor and condensation problems generated large scatter in the measured values.

Therefore, no comparisons are made for the rate of water production.

5.3. Coal-type effects on total volatiles production

Figure 5.3-1 compares the yield limit of total and 'reactive' volatiles versus the elemental carbon content for the six coals investigated in this study and the two coals studied by Suuberg (1977) under similar but not identical experimental conditions. Reactive volatiles are defined as total volatiles minus water and carbon dioxide yields. The total yield limit ranges from 41 to 55 wt% dmmf among lignites, and subbituminous and high-volatile bituminous coals, but drops to 22 wt% dmmf for the low-volatile bituminous coal. A useful quantity to compare is reactive volatile yields, which show that high-volatile bituminous coals (BL,PB,IL) produce significantly more than other coal types.

Figure 5.3-2 compares the characteristic yield temperatures of total volatiles production for the six coals. Plots of the total yield versus temperature for each of the six coals are shown in Fig.6.1-9. The characteristic temperatures tend to increase for higher rank coals, indicating a shift in the yield curve to higher temperatures. Comparing the spread of the yield curve, measured by (T75-T25), shows a small decreasing trend with increasing rank. These trends are consistent with the expected behavior from combining the observed coal-type effects on the rate of tar and gas production. Such a consistency together with a good product mass balance (Section 5.5), help to verify the experimentally observed coal-type effects on the apparent rate of product evolution.

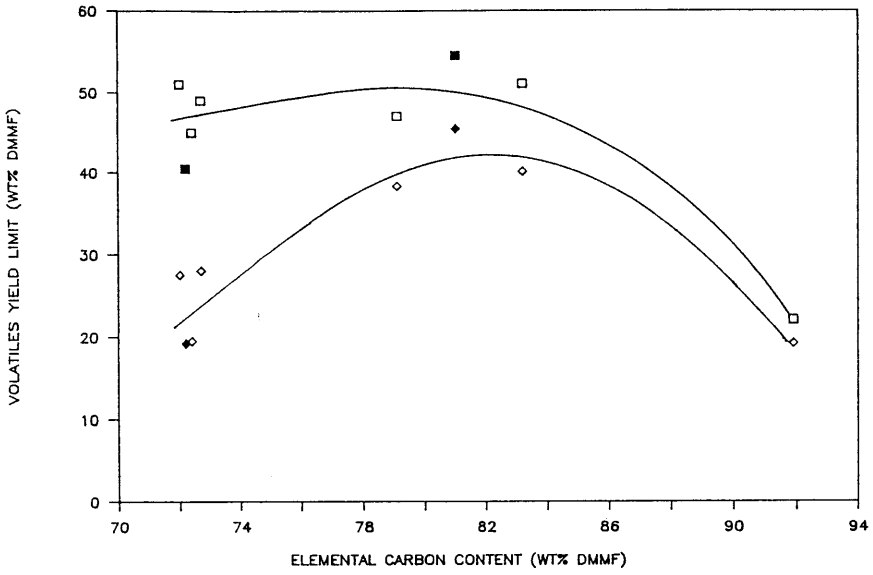

Figure 5.3-1 Comparison of total and reactive volatiles yield limit versus the elemental carbon content. Open symbols are from this study; closed symbols from Suuberg (1977). Carbon: LW < ML < ZP < SR < BL < PB < IL < LK. Abbreviations: see Figs. 5.1-1 and 5.2.1.

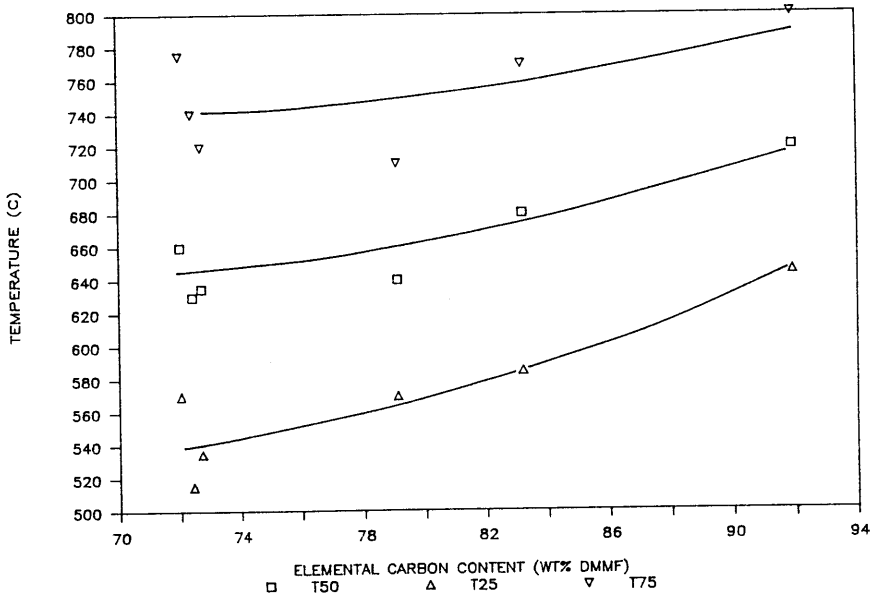

Figure 5.3-2 Comparison of characteristic yield temperatures for total volatiles production at 1 atm. Carbon: LW < ZP < SR < BL < IL < LK. Abbreviations: see Fig.5.1-1.

The aim of this pressure study is to determine the extent to which secondary reactions contribute in the overall pyrolysis behavior measured at atmospheric pressure. Changes in tar yields at different pressures are good indicators of the severity of secondary reactions. Figure 5.4-1 shows tar yield limits for the six coals over the pressure range of 10^{-3} to 10 atm; the yields from the two coals studied by Suuberg (1977) are also plotted in the figure to compare. For all eight coals, increasing the reactor pressure lowers the tar yield limit. Other investigators including Ardent and van Heek (1981) and Bautista (1984) have reported similar findings.

More quantitative observations on pressure effects can be made from Fig.5.4-2, which shows the % decrease in the tar yield limit at the indicated pressure relative to the vacuum yield limit. The yield at vacuum is least affected by pressure sensitive secondary reactions. For the coals investigated in this study (Fig.5.4-2a), the relative decrease at 1 atm ranges from 13 to 24 % of the vacuum value. The pressure effect is expected to be less at lower temperatures, i.e., before the yield limit is reached, since secondary reactions of tar are more severe at higher temperatures. The extent of the pressure effect is noticeably smaller for SR, and thus tars from this coal appear to be less prone to secondary degradation. However such differences can also be attributed to experimental errors associated with tar measurements, which can easily be ±10% of the vacuum yield limit for this coal. To be more conclusive, further studies are needed in reactors that are better suited to investigate tar secondary reactions, e.g., the two-stage flow-reactor (Serio, 1984). The results from Suuberg (Fig.5.4-

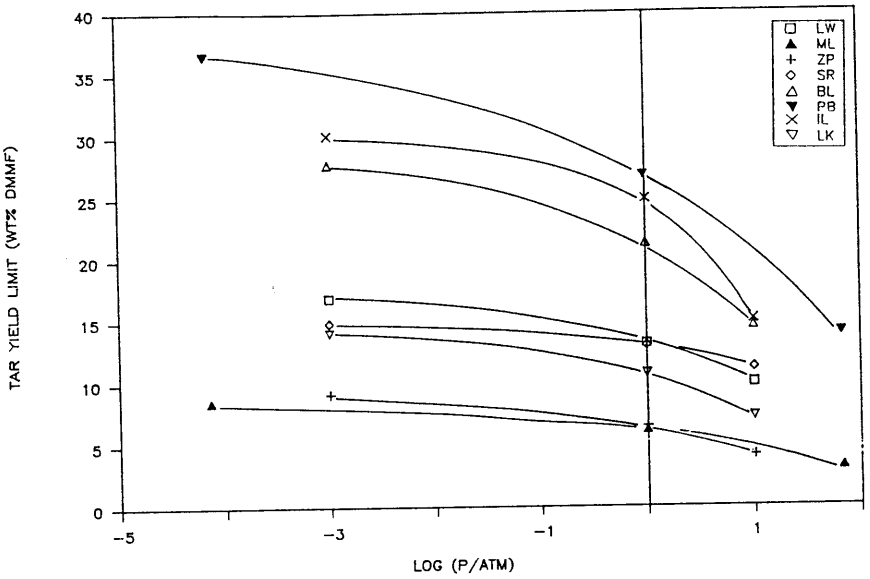

Figure 5.4-1 Effect of pressure on tar yield limit for different coals. Open symbols are from this study; closed symbols from Suuberg (1977). Carbon: LW < ML < ZP < SR < BL < PB < IL < LK. Abbreviations: see Figs. 5.1-1 and 5.2-1.

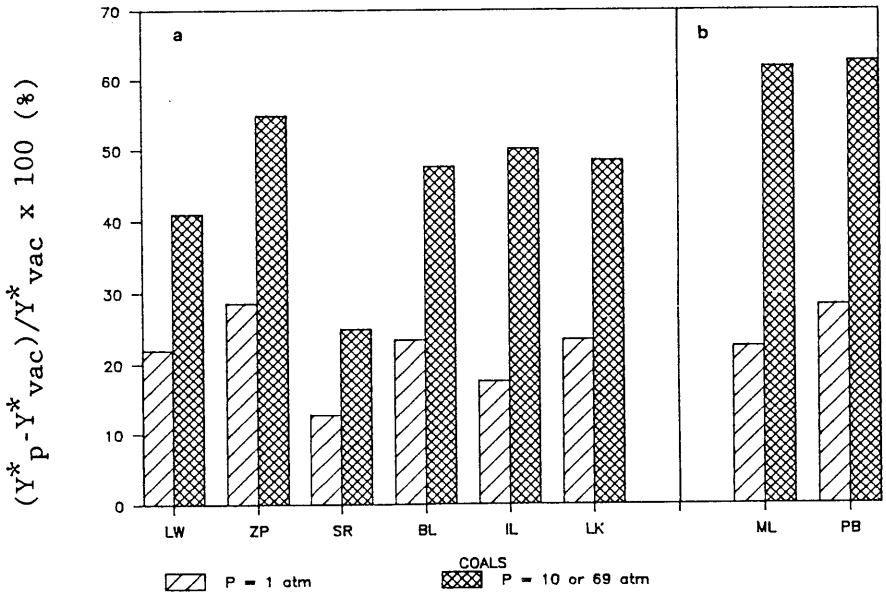

Figure 5.4-2 Decrease in the tar yield limit relative to the 'vacuum' yield. (a) coals from this study; (b) coals from Suuberg (1977). Y^*_{vac} = tar yield limit at 'vacuum', 10^{-3} atm in (a) and 6.6×10^{-5} atm in (b). Y^*_p = tar yield limit at a given pressure, p = 10 atm in (a) and 69 atm in (b). Carbon: LW < ML < ZP < SR < BL < PB < IL <LK. Abbreviations: see Figs. 5.1-1 and 5.2-1.

2b) show slightly larger pressure effects compared to those obtained in this study, but the larger effects may be rationalized by lower vacuum pressures attained in his study, 6.6×10^{-5} atm compared to 10^{-3} atm in this study.

Figure 5.4-3 shows total volatiles yields over the pressure range of 10^{-3} to 10 atm for the six coals of this study, and 6.6×10^{-5} to 69 atm for the two coals studied by Suuberg. Increasing the pressure reduces total volatiles yields as some of the tar is converted to produce solid char and gases. Although this study did not measure gas yields at pressures other than 1 atm, greater gas yields are expected at higher pressures. Figure 5.4-4 shows that for both Montana lignite and Pittsburgh Seam bituminous coal, increasing the pressure produced large gains in methane yields, but only small changes in carbon oxide yields. The trends for ethylene and ethane yields are less clear, but these species contribute very little to the overall gas production ($\tilde{<}$ 1 wt% as rec'd). Assuming a similar behavior for the coals studied here would suffice as a rough approximation.

Particle size is another variable that affects secondary reactions of tar. However the small data base on particle-size effects suggests that the 75-90 μm diameter particles used in this study are sufficiently small to avoid major contributions from particle-size induced secondary reactions. The tar yield at 1 atm is almost unaffected between 50 and 300 μm (dia.), and only slightly affected between 300 and 800 μm (dia.) (Suuberg, 1977; Bautista, 1984). Further studies on particle-size effects are currently being pursued by Griffin (1988).

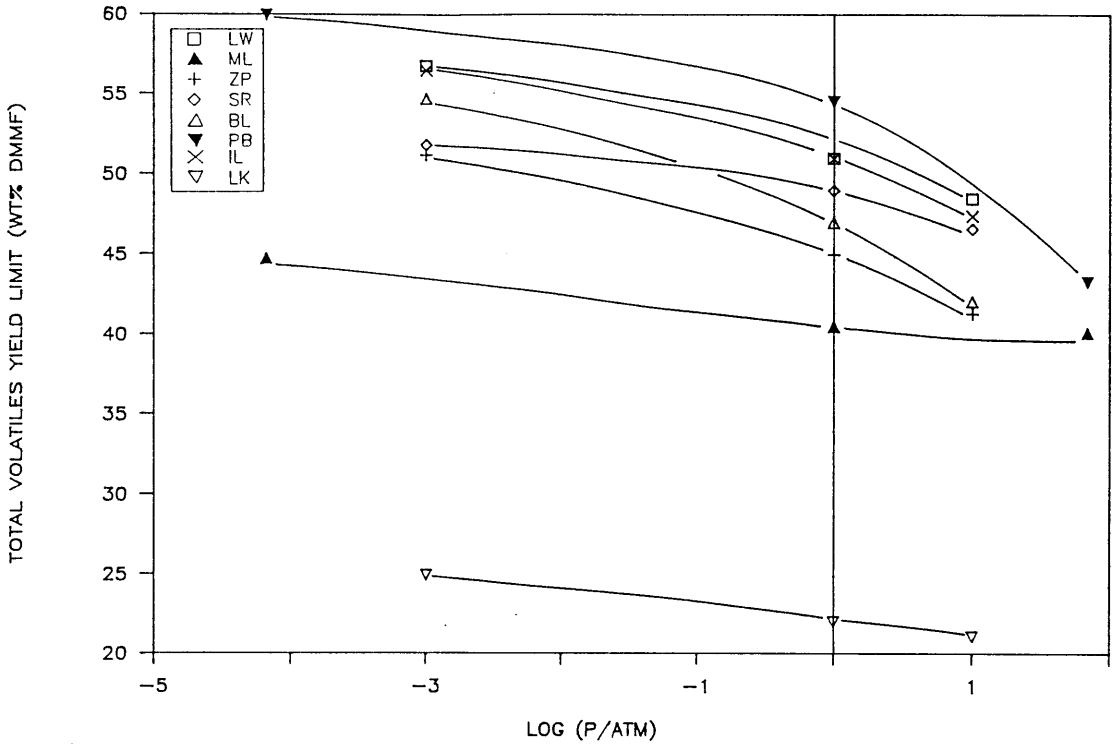

Figure 5.4-3 Effect of pressure on total volatiles yield limits for different coals. Open symbols are from this study; closed symbols from Suuberg (1977). Carbon: LW < ML < ZP < SR < BL < PB < IL < LK. Abbreviations: see Figs. 5.1-1 and 5.2-1.

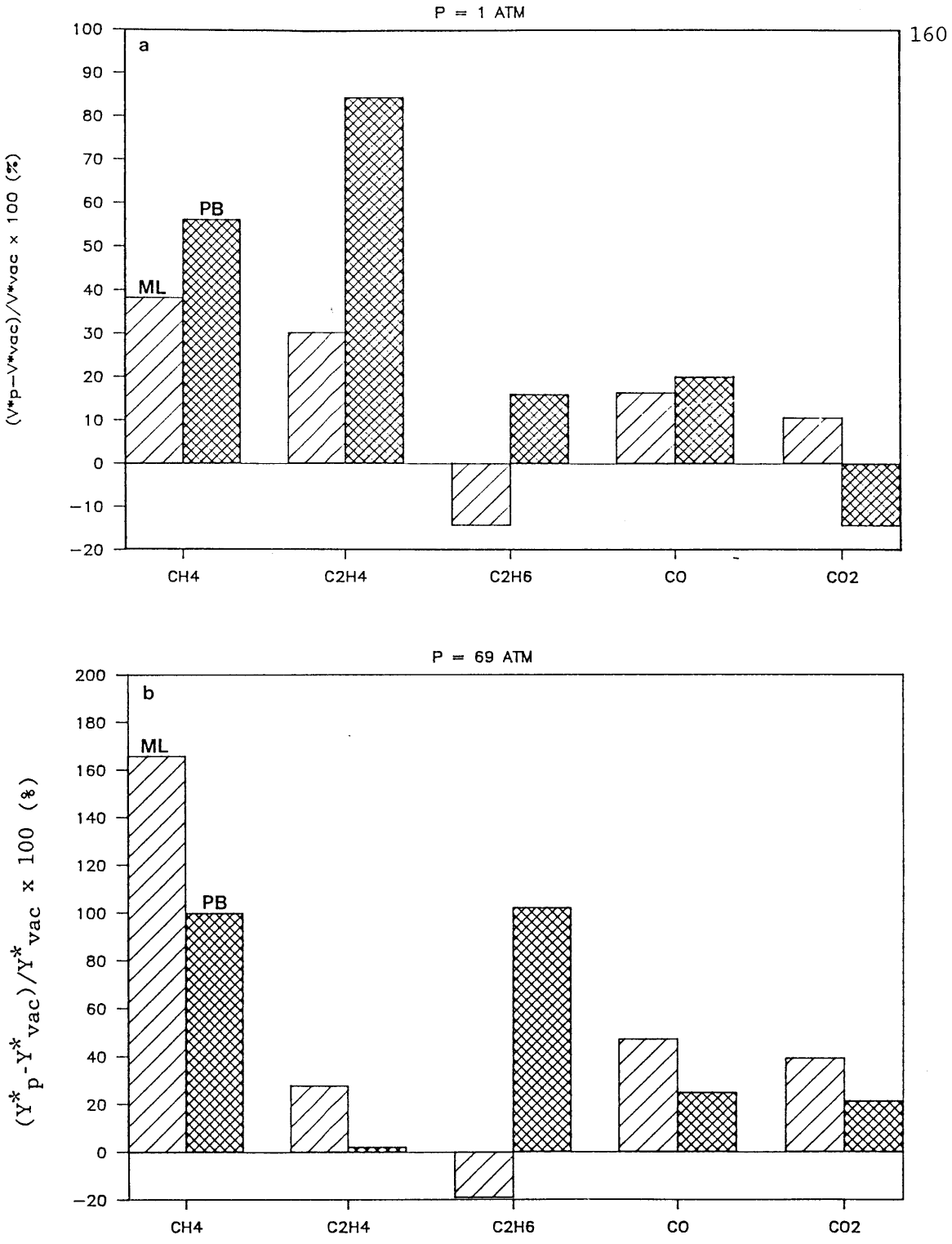

Figure 5.4-4 Effect of pressure on gas yield limits for Montana lignite (ML) and Pittsburgh Seam bituminous coal (PB). (a) p = 1 atm; (b) p = 69 atm. Data from Suuberg (1977). $Y^*_{i,vac}$ = yield of gas species i at 6.6×10^{-5} atm; $Y^*_{i,p}$ = yield of species i at pressure p.

Two main sources of experimental uncertainties arise from measurements of sample temperatures and product yields. To obtain consistent temperature measurements, it is crucial to (1) use small sample sizes, (2) spread the sample thinly, and (3) minimize the gap between the two layers of the screen. The first two criteria are satisfied by evenly spreading $\tilde{<}$ 20 mg samples on a 5 cm x 10 cm screen, whereas the last is satisfied by keeping the loaded screen between the electrodes as tightly as possible. Under such conditions, the sample temperature can be consistently measured within $\approx \pm 20$ C. Studies by Oh (1985) show that the particle temperature closely follows the screen temperature when small coal particles ($\tilde{<}$ 100 μm dia.) are pyrolyzed under atmospheric pressure at heating rates of $\tilde{<}$ 1000 C/s. Under such conditions, the coal particle can be assumed to be isothermal (Hajaligol et al., 1988). At pressures considerably lower than atmospheric, temperature measurements using the current technique are uncertain due to slower convective heat transfer from the hot screen to the coal particle (Oh, 1985). Thus, this study does not use any vacuum data to obtain kinetic information.

The magnitude of uncertainties from product yield measurements was estimated to be the maximum difference in the measurements from a set of 2-4 runs made under similar conditions. Based on these repeatability tests, the uncertainty for a given product is conservatively estimated to be

Products	Measurement uncertainties
tar	±2 wt% of unpyrolyzed coal, dmmf
char	±2 wt% of unpyrolyzed coal, dmmf
gases except H_2O	±0.05-0.5 wt% of unpyrolyzed coal, dmmf
H_2O	±3 wt% of unpyrolyzed coal, dmmf

For runs in which both tars and gases were collected, mass balances were calculated to be between 90 and 110 wt% of the original coal mass. A large portion of the uncertainty is due to large scatter in water measurements. Considerably better closures were obtained (typically 95-105 %) when mass balances are computed using an averaged value of pyrolytic water yield.

6. Modeling studies

This chapter derives kinetic information from the experimental data obtained in this study (Chapter 5) using two different models: the multiple independent parallel reaction (MIPR) model, and the extended MIPR model. The former model describes kinetics of product evolution under conditions where the effects of physical transport processes and secondary reactions are relatively unimportant. The latter model explicitly includes transport and secondary reaction effects, and thus is applicable over a wider range of operating conditions. Sections 6.1.1 and 6.2.1 give mathematical descriptions of the MIPR and extended MIPR models respectively; the kinetic information obtained with the two models is discussed in Sections 6.1.2 and 6.2.2 respectively.

6.1. Multiple independent parallel reaction (MIPR) model

The MIPR model has been widely used to describe the evolution rate of tar (Serio, 1984; Ko et al., 1988a), gaseous products (Weimer and Ngan, 1979; Serio, 1984), and total volatiles (Anthony et al., 1974; Ciuryla et al., 1979; Sprouse and Schuman, 1981). Since the model does not include an explicit description of mass transport, it is strictly valid only under conditions where mass transfer resistances are small. Under such conditions, the model is capable of describing volatiles evolution rates over a wide range of heating rates.

6.1.1. Mathematical description

The rate of volatiles evolution in the MIPR model is expressed as the sum of the contributions from a large number of first-order independent parallel reactions,

$$dY/dt = \sum k_{o\,i} \exp(-E_i/RT)\ (Y^*_i - Y_i) \qquad (6.1\text{-}1)$$

where i denotes one reaction. The same preexponential factor is used for all reactions, i.e., $k_{o\,i} = k_o$, and the activation energies are described by a Gaussian distribution function f(E) with mean E_o and standard deviation σ

$$f(E) = [\sigma(2\pi)^{1/2}]^{-1} \exp[-(E-E_o)^2/2\sigma^2] \qquad (6.1\text{-}2)$$

The probability of finding a reaction with activation energy between E and E+dE is given by f(E)dE, where for a large number of reactions, $f(E) = Y^*_i/Y^*$ and Y^* equal to the sum of the Y^*_i for all i. Integrating Eq.(6.1-1) for any temperature-time history gives

$$(Y^*-Y)/Y^* = \int_o^\infty \exp[-k_o \int_o^t \exp(-E/RT)dt]\ f(E)dE \qquad (6.1\text{-}3)$$

where Y^*, E_o, σ, and k_o are the input parameters required in the MIPR model, and in general temperature (T) is a function of time (t). The notation 'Y' here is equivalent to 'V' in earlier descriptions of this model (Anthony et al., 1974; Howard, 1981).

6.1.2. Results and discussion

This section discusses the effect of coal type on the MIPR model parameters for tar, gas, and total volatiles production.

Coal-type effects on tar production

Figure 6.1-1 compares the experimental and predicted tar yields from the MIPR model for the six coals investigated in this study. The model predictions were made with k_o fixed at 10^{14} s^{-1}, Y^* obtained from the measured maximum tar yield, and E_o and σ best-fitted to the experimental data using a multivariable non-linear regression routine

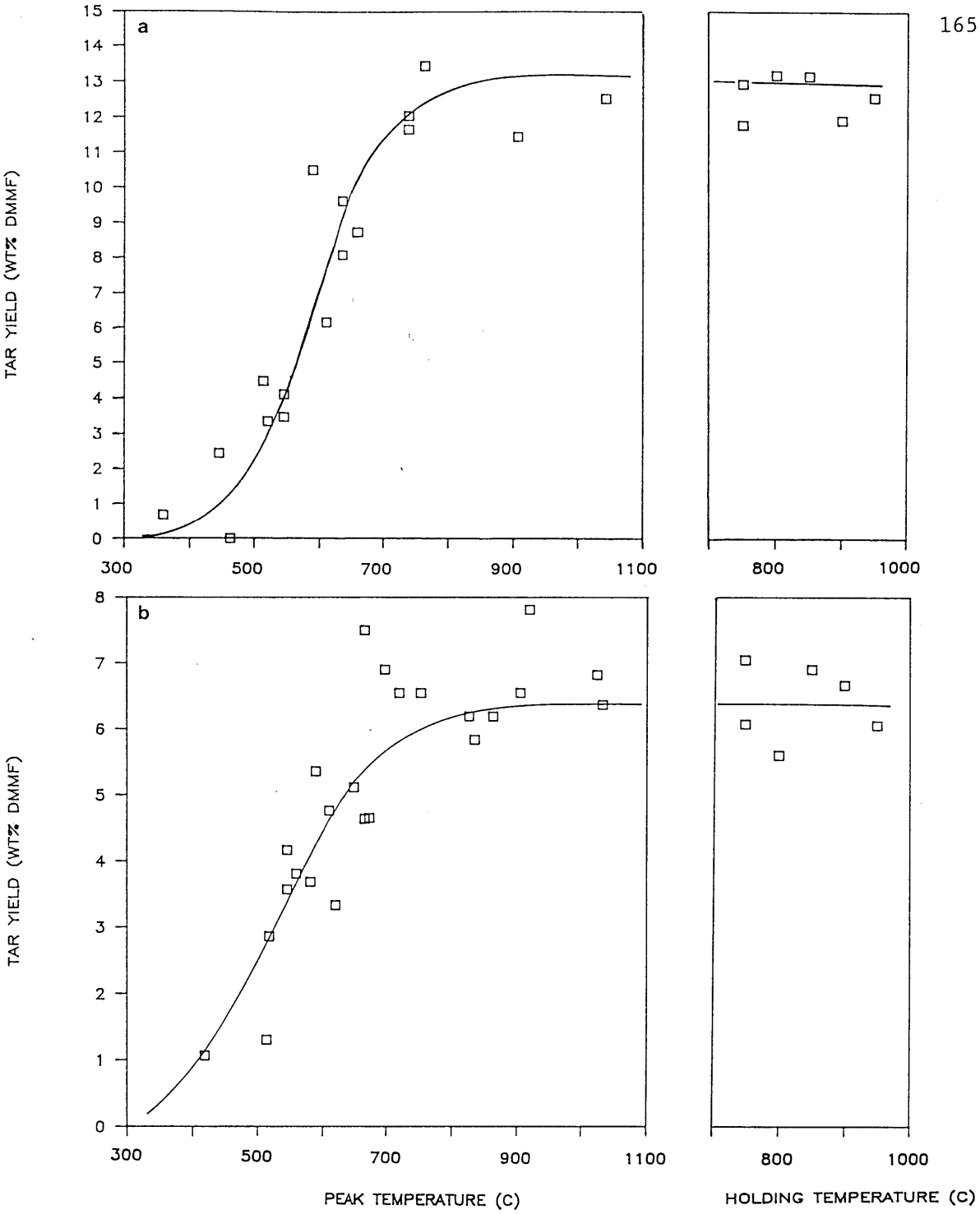

Figure 6.1-1 Tar yields versus peak and holding temperatures (5 s hold). Symbols represent experimental data; lines represent MIPR model predictions. (a) LW, Lower Wilcox lignte; (b) ZP, Beulah Zap lignite; (c) SR, Smith Roland subbituminous; (d) BL, Blue high-volatile bituminous; (e) IL, Illinois high-volatile bituminous; (f) LK, Lower Kittanning low-volatile bituminous.

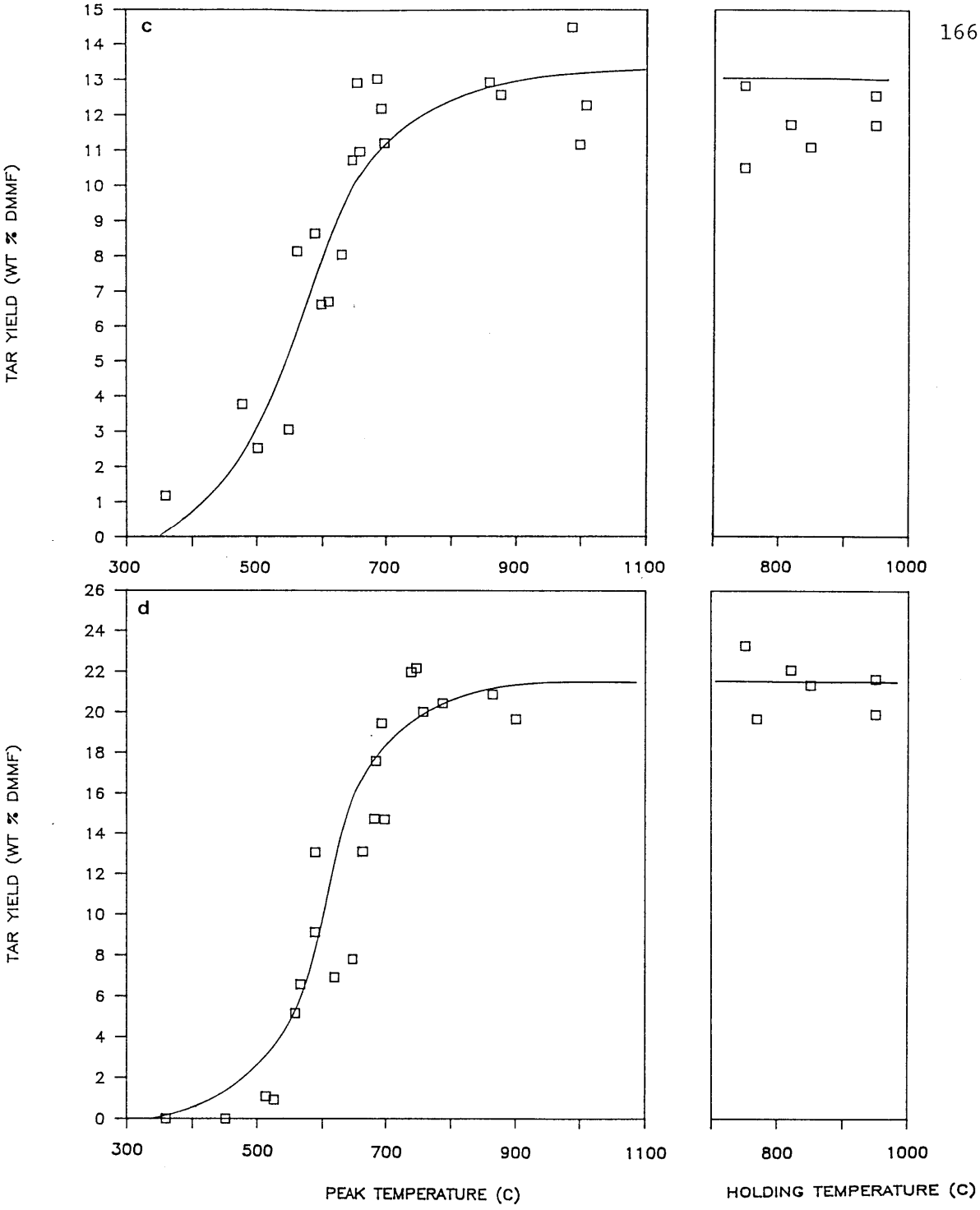

Figure 6.1-1 Tar yields versus peak and holding temperatures (5 s hold). Symbols represent experimental data; lines represent MIPR model predictions. (a) LW, Lower Wilcox lignte; (b) ZP, Beulah Zap lignite; (c) SR, Smith Roland subbituminous; (d) BL, Blue high-volatile bituminous; (e) IL, Illinois high-volatile bituminous; (f) LK, Lower Kittanning low-volatile bituminous.

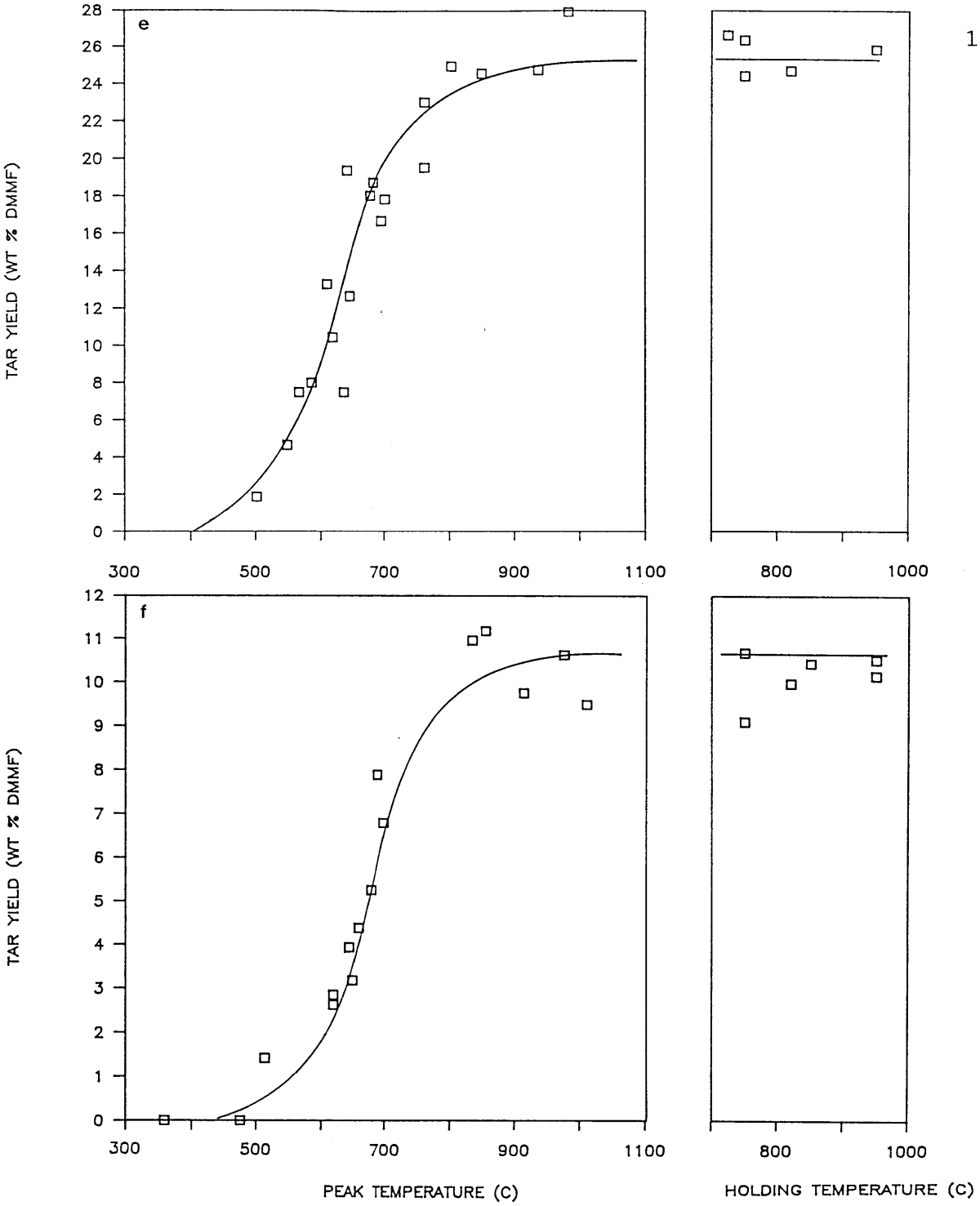

Figure 6.1-1 Tar yields versus peak and holding temperatures (5 s hold). Symbols represent experimental data; lines represent MIPR model predictions. (a) LW, Lower Wilcox lignte; (b) ZP, Beulah Zap lignite; (c) SR, Smith Roland subbituminous; (d) BL, Blue high-volatile bituminous; (e) IL, Illinois high-volatile bituminous; (f) LK, Lower Kittanning low-volatile bituminous.

(IMSL math library subroutine ZXSSQ). In all cases, the predicted yields agree well with the experimental values; the standard error of the estimate, as defined in Eq.(5.1-31), ranges from 6.5 to 10 % of the maximum tar yield.

Figure 6.1-2 plots the best-fitted values of E_o and σ versus the elemental carbon contents of the coal; numerical values are given in Table 6.1-1. These values are slightly different than those presented in an earlier report (Howard et al., 1988). The previously reported values were obtained with assumed approximate linear temperature-time histories, whereas the current values were obtained with more exact temperature histories and therefore are expected to be more accurate. The figure shows that higher rank coals, indicated by higher elemental carbon contents, generally gave greater values of E_o and smaller values of σ. Maximum differences in E_o and σ are 7.1 and 3.6 kcal/mole respectively. Such differences far exceed the variation explainable by experimental uncertainties, estimated to be approximately ±1 kcal/mole for both E_o and σ (see below). Therefore, under the conditions employed in this study, there appears to be a convincing coal-type effect on the MIPR model rate parameters for tar production.

Uncertainties associated with E_o (ΔE_o) and σ ($\Delta\sigma$) are estimated by independently considering experimental errors in temperature (ΔT) and yield (ΔY) measurements, and are assumed to be the maximum value generated from the two sources. For each individual product, the experimental error in the yield measurement is approximated as the standard error of the estimate [Eq.(5.1-31)]. The error in the temperature measurement is estimated as the average difference between the 'measured' and 'predicted' temperatures for given experimental

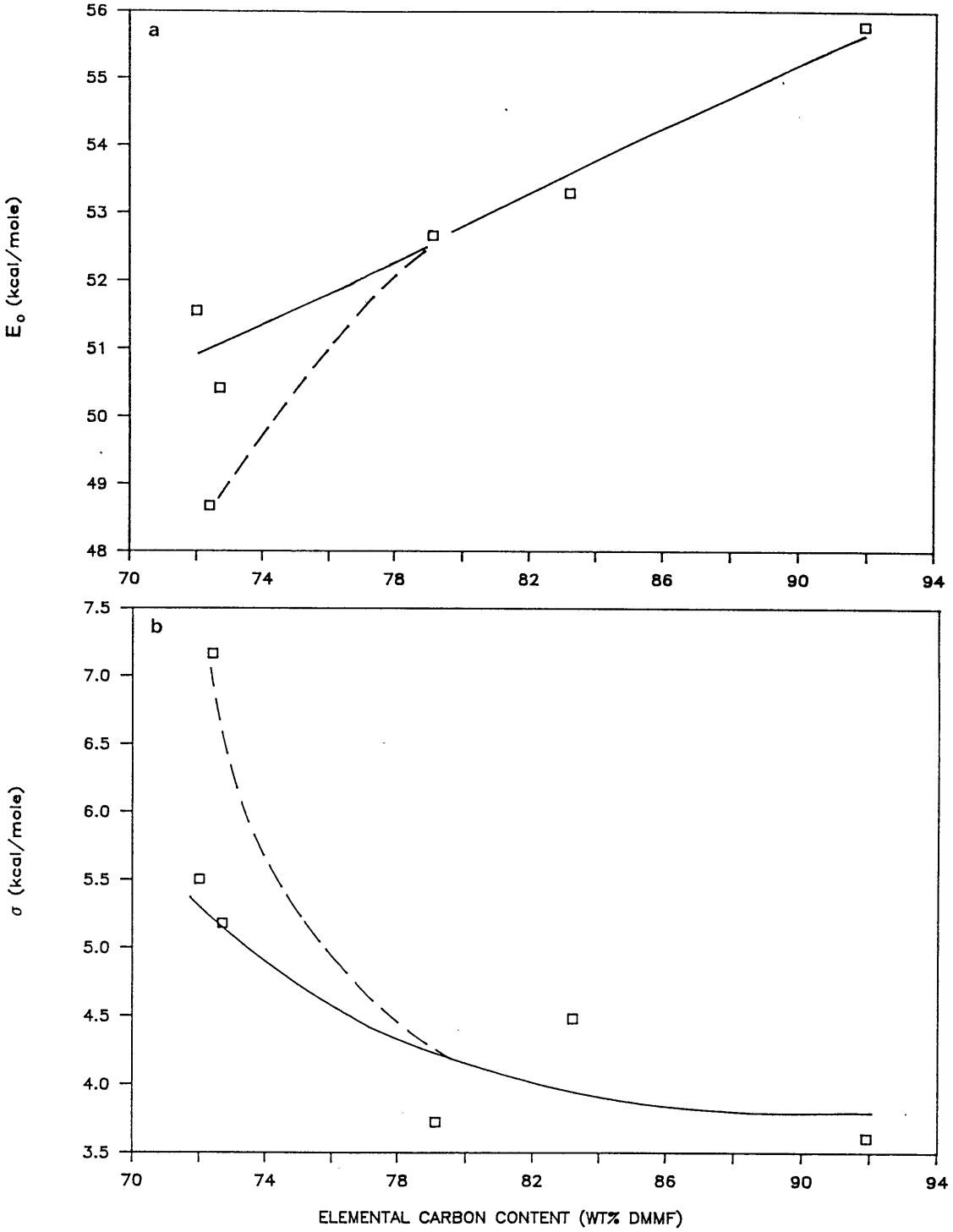

Figure 6.1-2 Best-fitted values of (a) E_o and (b) σ for predicting atmospheric tar evolution using the MIPR model versus the elemental carbon content of the coal. k_o was fixed at 10^{14} s^{-1} for all coals; Y^* was obtained from experimental data for each coal. Dashed lines for coals with [H] < 5 wt% dmmf; solid lines for [H] ≥ 5 wt% dmmf. Carbon: LW < ZP < SR < BL < IL < LK. Abbreviations: see Fig.6.1-1.

yields using total volatiles yield data, and is approximated to be about ±25 C. The data on total volatiles yields were chosen in estimating ΔT since they have the largest number of data points among measured products. The ΔE_o was estimated to be the maximum deviation from the best-fitted value of E_o caused by the estimated ΔT and ΔY; the deviation was computed at 50% of the final yield for cases where the temperature and the yield were consistently either too high or too low by $\Delta T/2$ and $\Delta Y/2$ respectively. Similarly, the $\Delta\sigma$ was estimated to be the maximum deviation from the best-fitted value of σ, and is computed at 25 and 75% of the final yield for cases where the temperature and the yield were consistently too high or too low by $\Delta T/2$ and $\Delta Y/2$ respectively to produce the most and the least spread in the yield curve.

The trends for both E_o and σ in Fig.6.1-2 appear to be more scattered among low-rank coals, where the Beulah Zap lignite shows a considerably lower E_o and higher σ compared to the Lower Wilcox lignite and Smith Roland subbituminous coal. A similar distinction is noted in the maximum tar yield (Y^*), where the Zap produced only about 7 wt% (dmmf) compared to about 13 wt% (dmmf) from the other two low-rank coals (Table 6.1-1). These consistent differences suggest that the information on coal rank alone is insufficient to explain the observed different behavior for coals within the same rank. One property that appears to distinguish the two types of low-rank coals is the elemental hydrogen content; in dmmf basis, the Zap has 4.8 wt% whereas the Lower Wilcox and Smith Roland have noticeably larger values of 5.6 and 5.3 wt% respectively. Therefore in estimating E_o and σ from Fig.6.1-2 in the low-rank region, the dashed curves are recommended for coals with

Table 6.1-1 Best-fitted values of E_o and σ of the MIPR model for tar production (k_o fixed at 10^{14} s^{-1} for all coals).

Coal[a]	Y* wt% dmmf	E_o kcal/mole	σ kcal/mole	Standard error of estimate wt% dmmf coal
Lower Wilcox L	13.1	51.6	5.5	1.3
Beulah Zap L	6.5	48.7	7.2	0.7
Smith Roland SB	12.9	50.4	5.2	1.4
Blue HVB	21.2	52.7	3.7	1.7
Illinois HVB	24.8	53.3	4.5	2.0
Lower Kittanning LVB	10.7	55.8	3.6	0.7

[a] Coals are listed in the order of increasing elemental carbon contents in dmmf basis. Elemental analysis is given in Table 4.1-1.

the elemental hydrogen content of < 5 wt% dmmf, and the solid curves for coals with the elemental hydrogen of ≥ 5 wt% dmmf.

Coal-type effects on gas production

Figures 6.1-3 through 6.1-7 compare the experimental and predicted gas yields from the MIPR model for the six coals investigated in this study. The model predictions were made using the same procedure as above for tar, with k_o fixed at 10^{14} s^{-1}, Y^* obtained from the measured maximum tar yield, and E_o and σ best-fitted to the experimental data using a multivariable non-linear regression routine. For all gas species, the agreement between the predicted and experimental yields is generally good; the standard error of the estimate ranges from 4 to 15 % of the maximum yield.

Figure 6.1-8 plots the best-fitted values of E_o and σ versus the elemental carbon contents of the coal; numerical values are given in Table 6.1-2. For hydrocarbon gases, methane and ethane show a small increase in E_o for higher rank coals, with maximum variations of about 2.7 and 3.9 kcal/mole respectively, whereas ethylene appears to be almost unaffected. Comparing σ of hydrocarbon gases shows a decreasing trend as the coal rank increases for methane and ethylene, with maximum variations of about 2 and 2.3 kcal/mole respectively, but no effects are observed for ethane. These variations in the rate parameters are small, and are only slightly greater than estimated errors produced from experimental uncertainties, which range from ± 0.5 to 1 kcal/mole for E_o and from ± 1 to 1.5 kcal/mole for σ. Large scatters in E_o and σ of ethane for the three low-rank coals are noted, and are attributed to very low yields among these coals (<0.4 wt% dmmf).

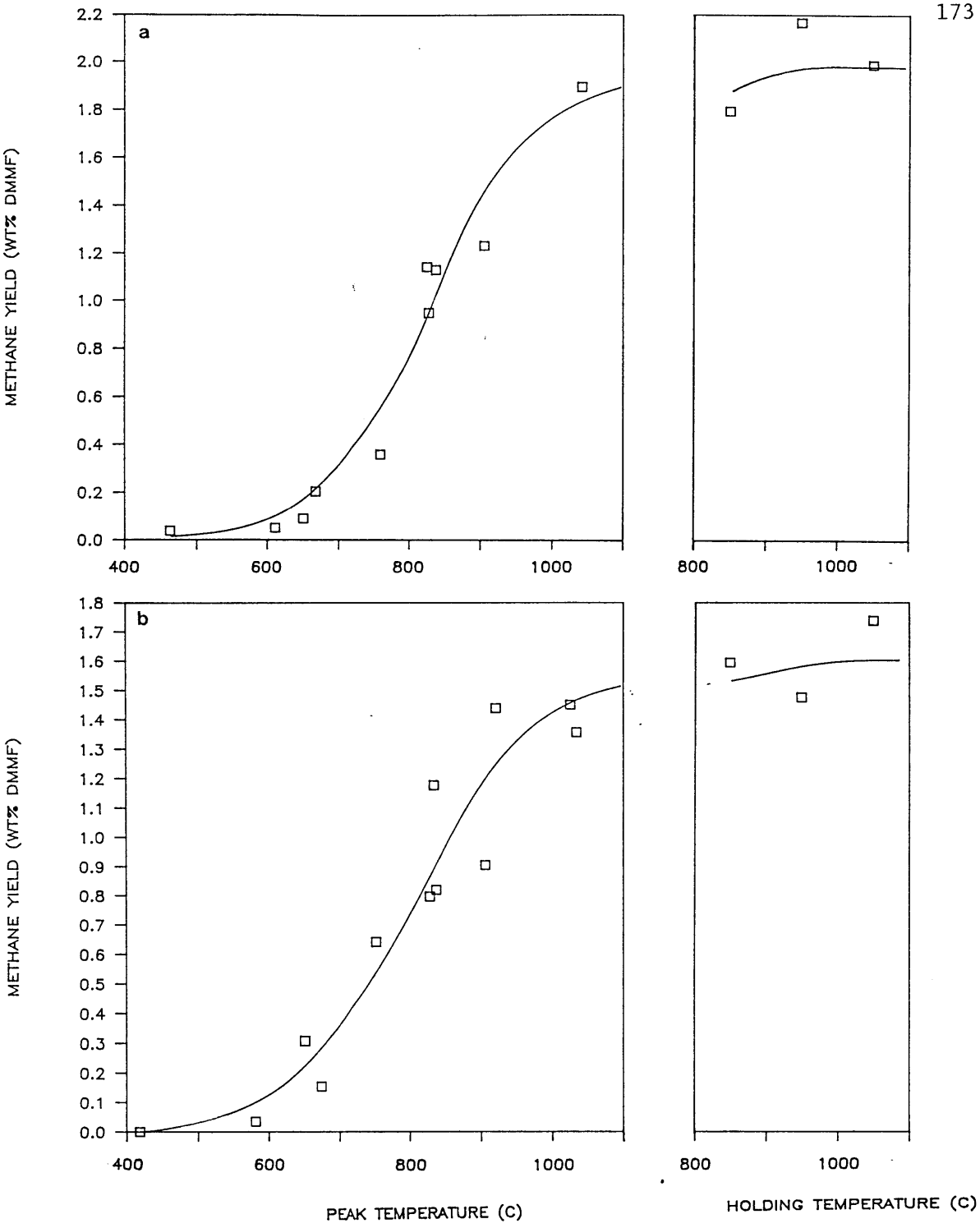

Figure 6.1-3 Methane yields versus peak and holding temperatures (5 s hold). Symbols represent experimental data; lines represent MIPR model predictions. (a) LW; (b) ZP; (c) SR; (d) BL; (e) IL; (f) LK. Abbreviations: see Fig.6.1-1.

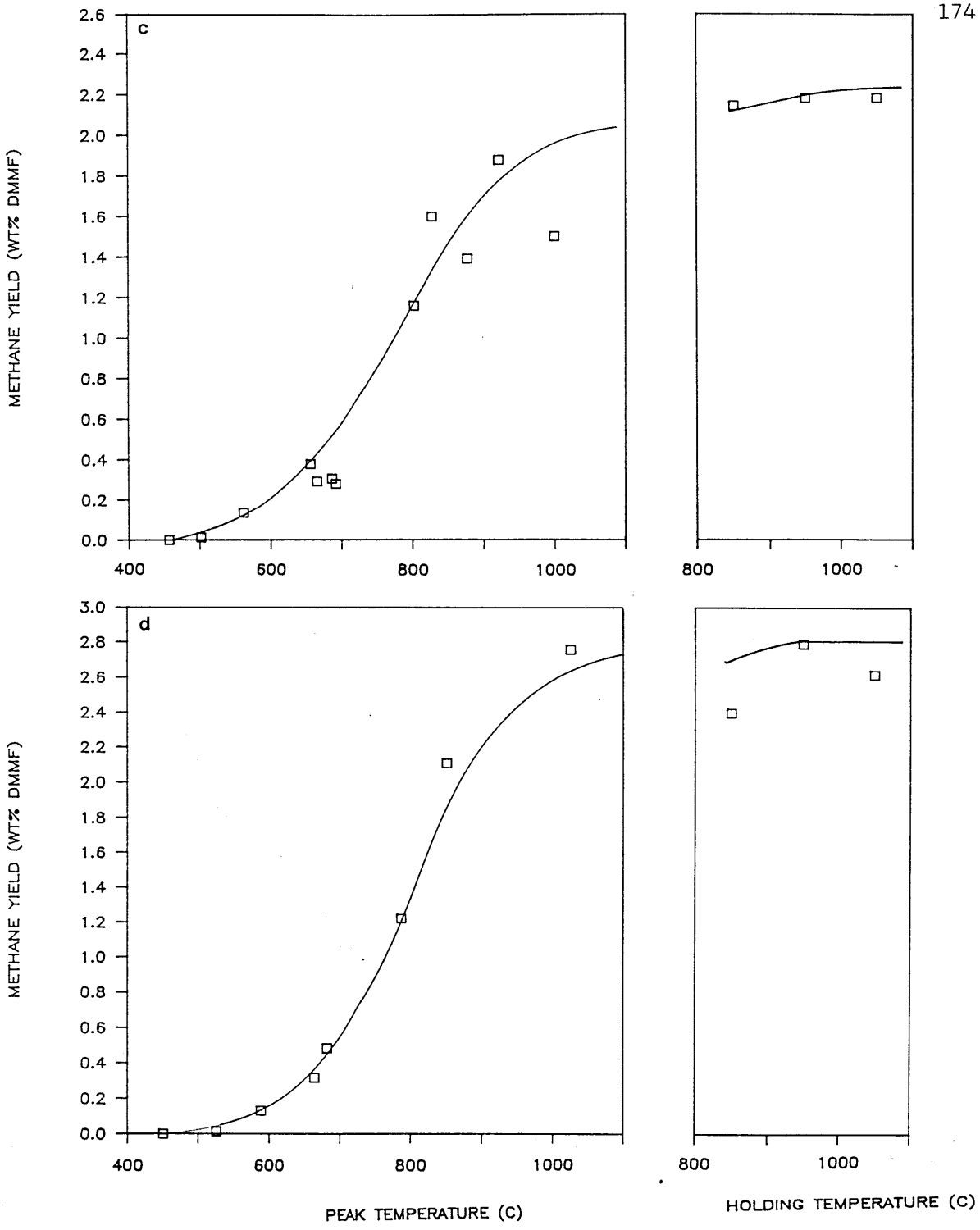

Figure 6.1-3 Methane yields versus peak and holding temperatures (5 s hold). Symbols represent experimental data; lines represent MIPR model predictions. (a) LW; (b) ZP; (c) SR; (d) BL; (e) IL; (f) LK. Abbreviations: see Fig.6.1-1.

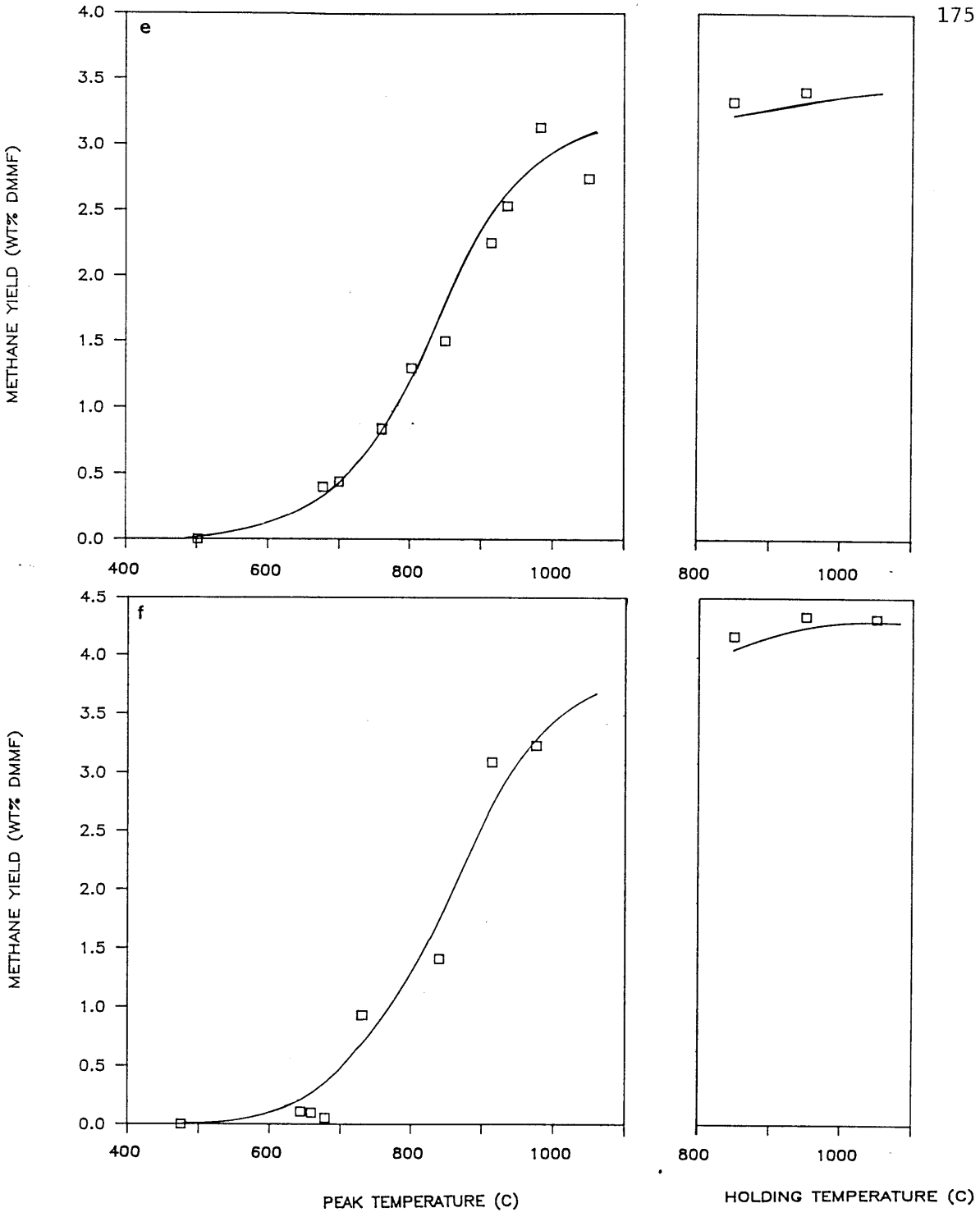

Figure 6.1-3 Methane yields versus peak and holding temperatures (5 s hold). Symbols represent experimental data; lines represent MIPR model predictions. (a) LW; (b) ZP; (c) SR; (d) BL; (e) IL; (f) LK. Abbreviations: see Fig.6.1-1.

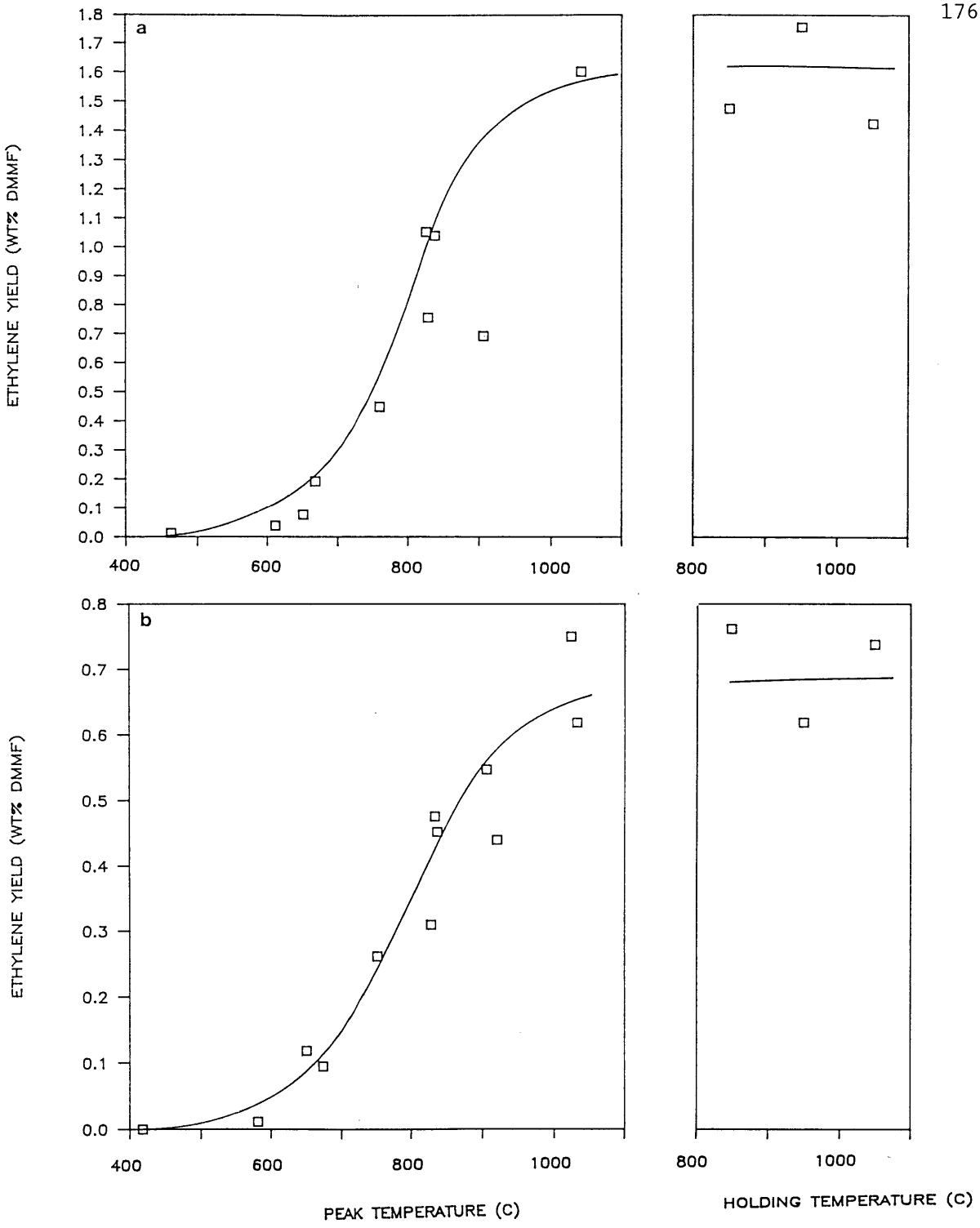

Figure 6.1-4 Ethylene yields versus peak and holding temperatures (5 s hold). Symbols represent experimental data; lines represent MIPR model predictions. (a) LW; (b) ZP; (c) SR; (d) BL; (e) IL; (f) LK. Abbreviations: see Fig.6.1-1.

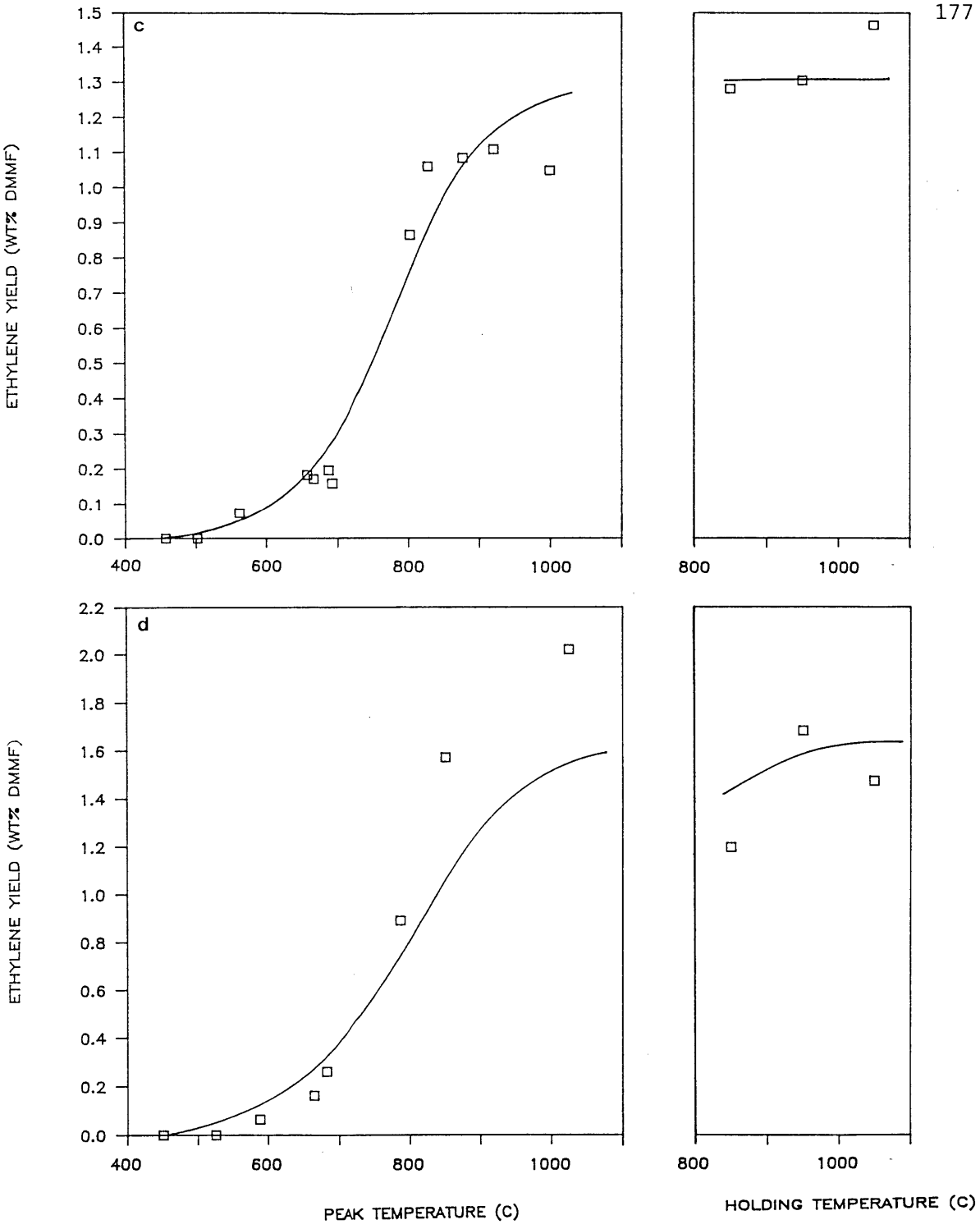

Figure 6.1-4 Ethylene yields versus peak and holding temperatures (5 s hold). Symbols represent experimental data; lines represent MIPR model predictions. (a) LW; (b) ZP; (c) SR; (d) BL; (e) IL; (f) LK. Abbreviations: see Fig.6.1-1.

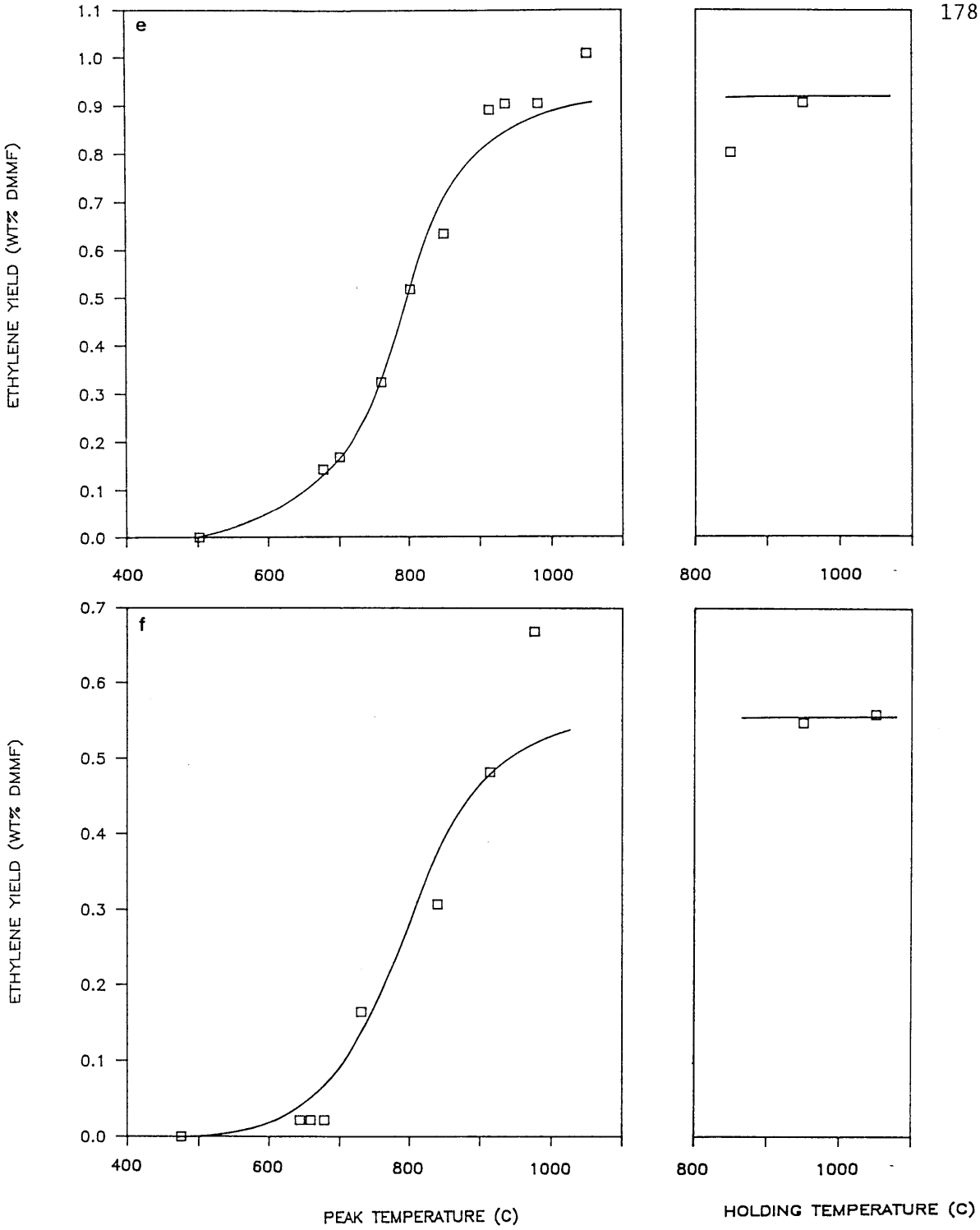

Figure 6.1-4 Ethylene yields versus peak and holding temperatures (5 s hold). Symbols represent experimental data; lines represent MIPR model predictions. (a) LW; (b) ZP; (c) SR; (d) BL; (e) IL; (f) LK. Abbreviations: see Fig.6.1-1.

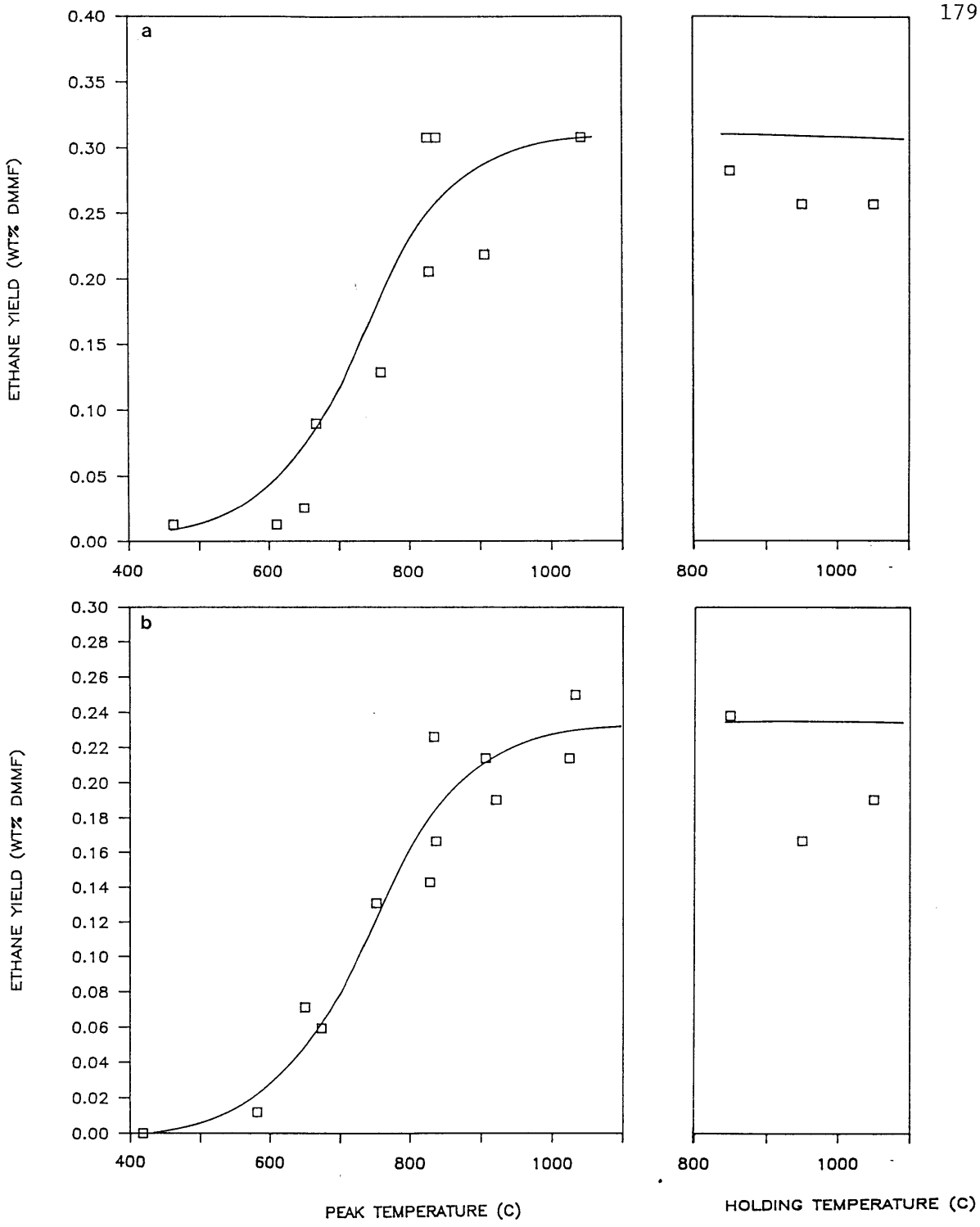

Figure 6.1-5 Ethane yields versus peak and holding temperatures (5 s hold). Symbols represent experimental data; lines represent MIPR model predictions. (a) LW; (b) ZP; (c) SR; (d) BL; (e) IL; (f) LK. Abbreviations: see Fig.6.1-1.

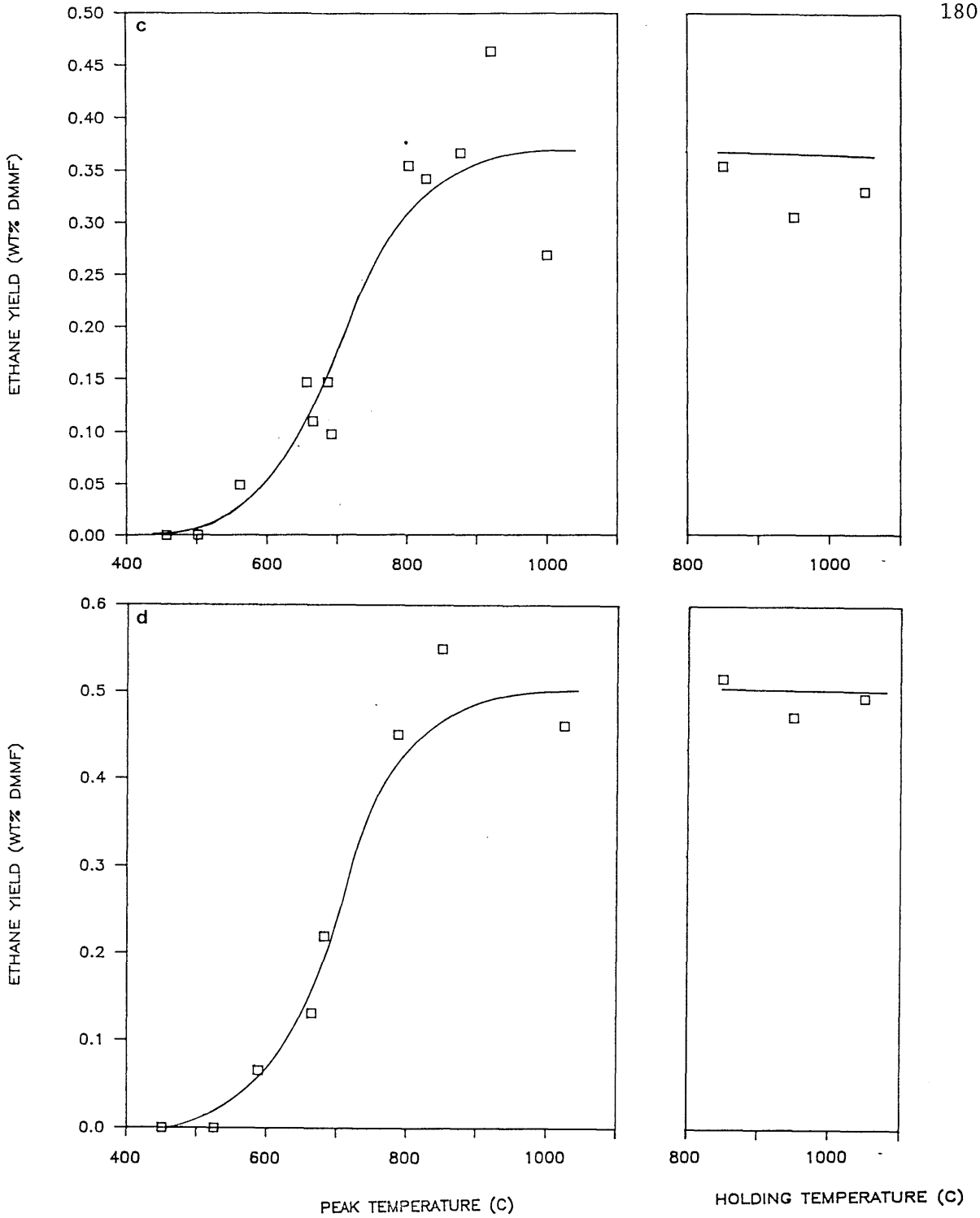

Figure 6.1-5 Ethane yields versus peak and holding temperatures (5 s hold). Symbols represent experimental data; lines represent MIPR model predictions. (a) LW; (b) ZP; (c) SR; (d) BL; (e) IL; (f) LK. Abbreviations: see Fig.6.1-1.

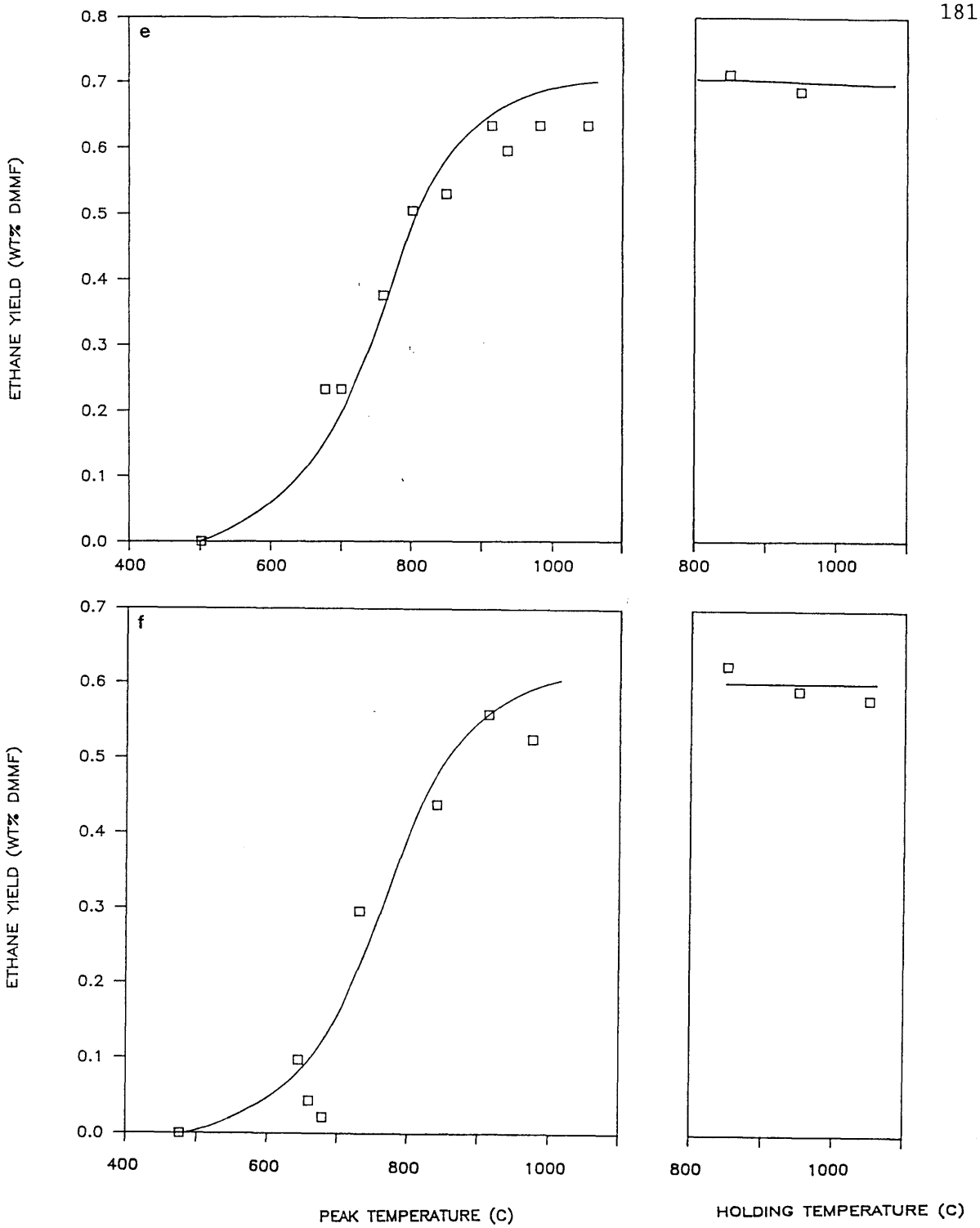

Figure 6.1-5 Ethane yields versus peak and holding temperatures (5 s hold). Symbols represent experimental data; lines represent MIPR model predictions. (a) LW; (b) ZP; (c) SR; (d) BL; (e) IL; (f) LK. Abbreviations: see Fig.6.1-1.

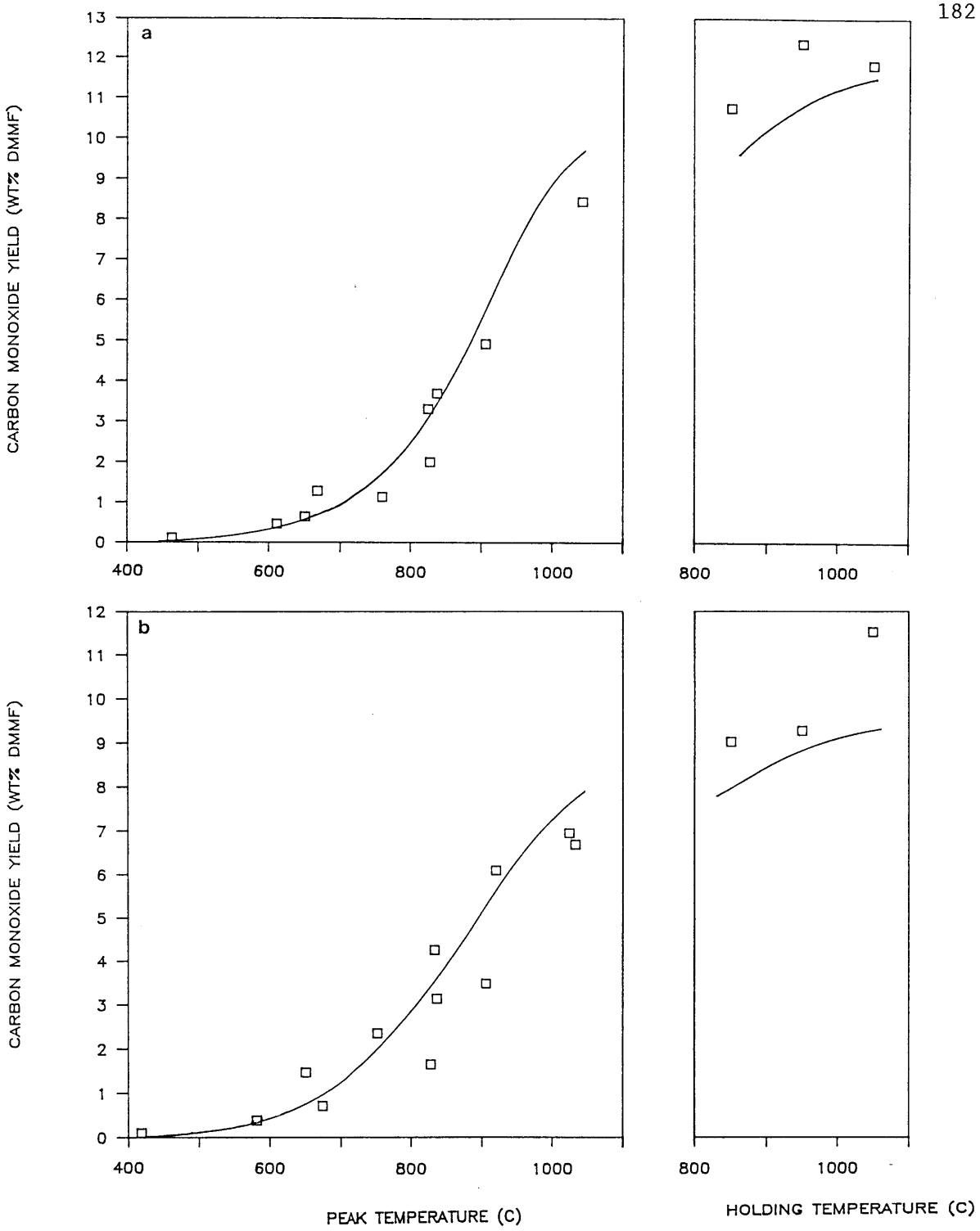

Figure 6.1-6 Carbon monoxide yields versus peak and holding temperatures (5 s hold). Symbols represent experimental data; lines represent MIPR model predictions. (a) LW; (b) ZP; (c) SR; (d) BL; (e) IL; (f) LK. Abbreviations: see Fig.6.1-1.

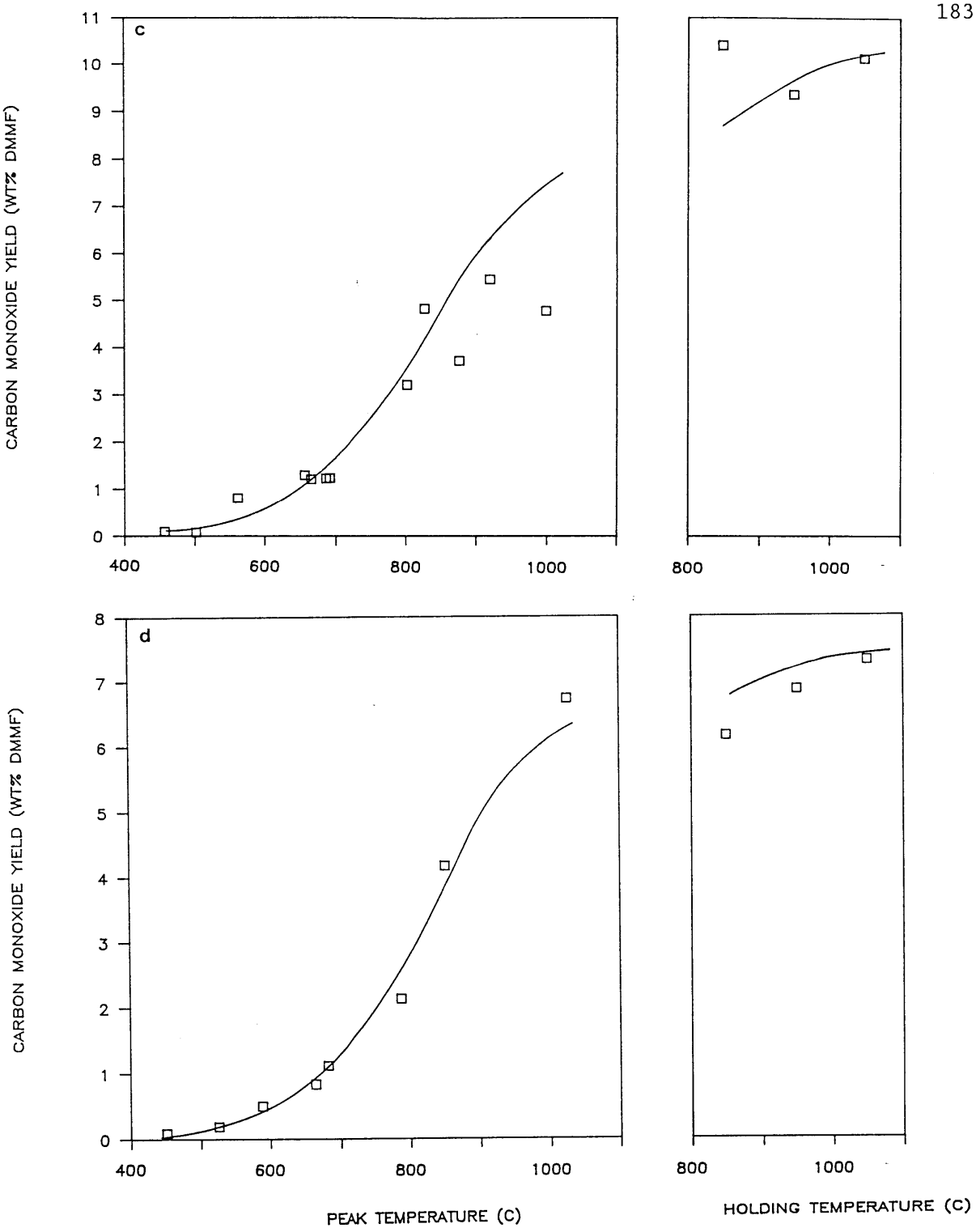

Figure 6.1-6 Carbon monoxide yields versus peak and holding temperatures (5 s hold). Symbols represent experimental data; lines represent MIPR model predictions. (a) LW; (b) ZP; (c) SR; (d) BL; (e) IL; (f) LK. Abbreviations: see Fig.6.1-1.

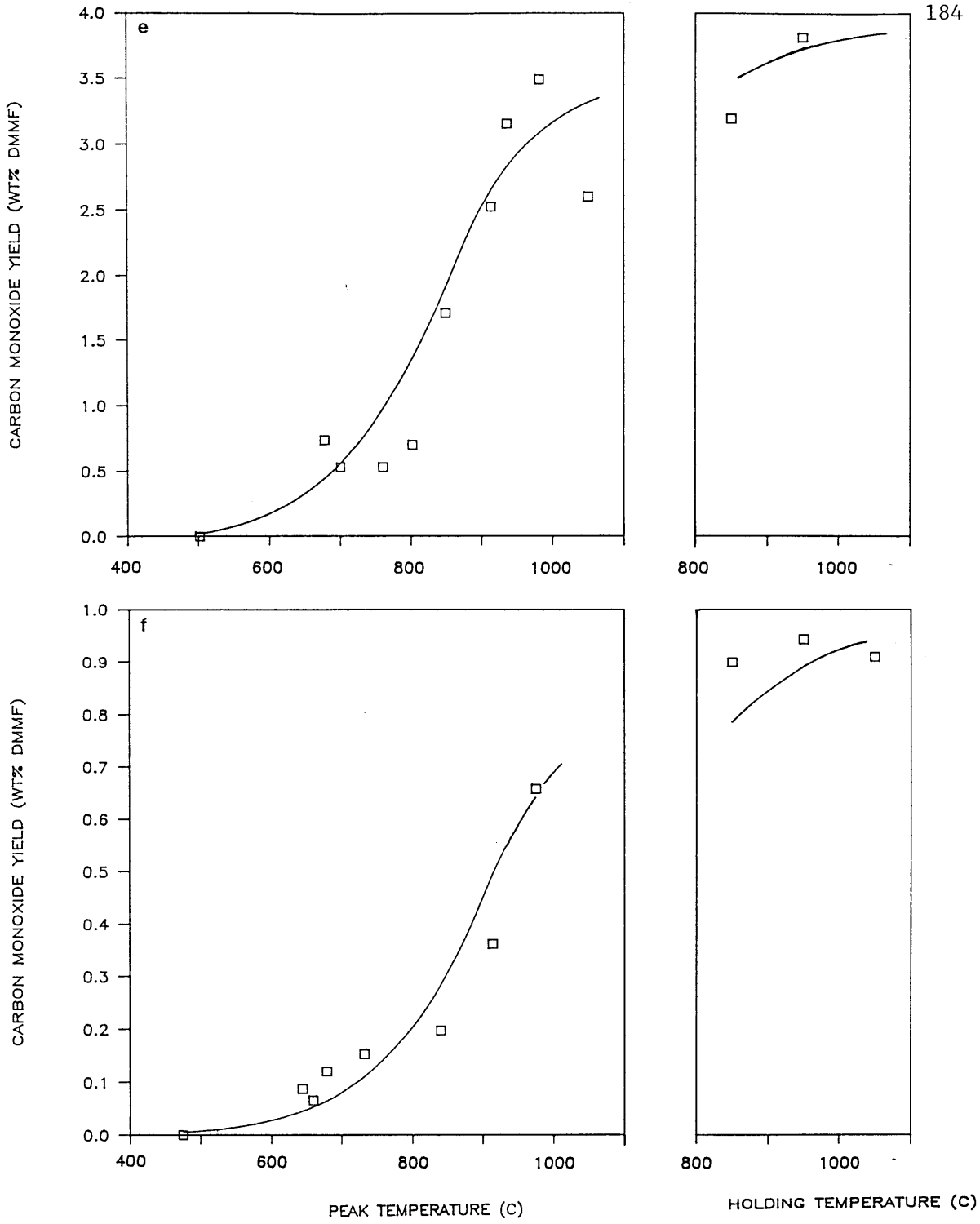

Figure 6.1-6 Carbon monoxide yields versus peak and holding temperatures (5 s hold). Symbols represent experimental data; lines represent MIPR model predictions. (a) LW; (b) ZP; (c) SR; (d) BL; (e) IL; (f) LK. Abbreviations: see Fig.6.1-1.

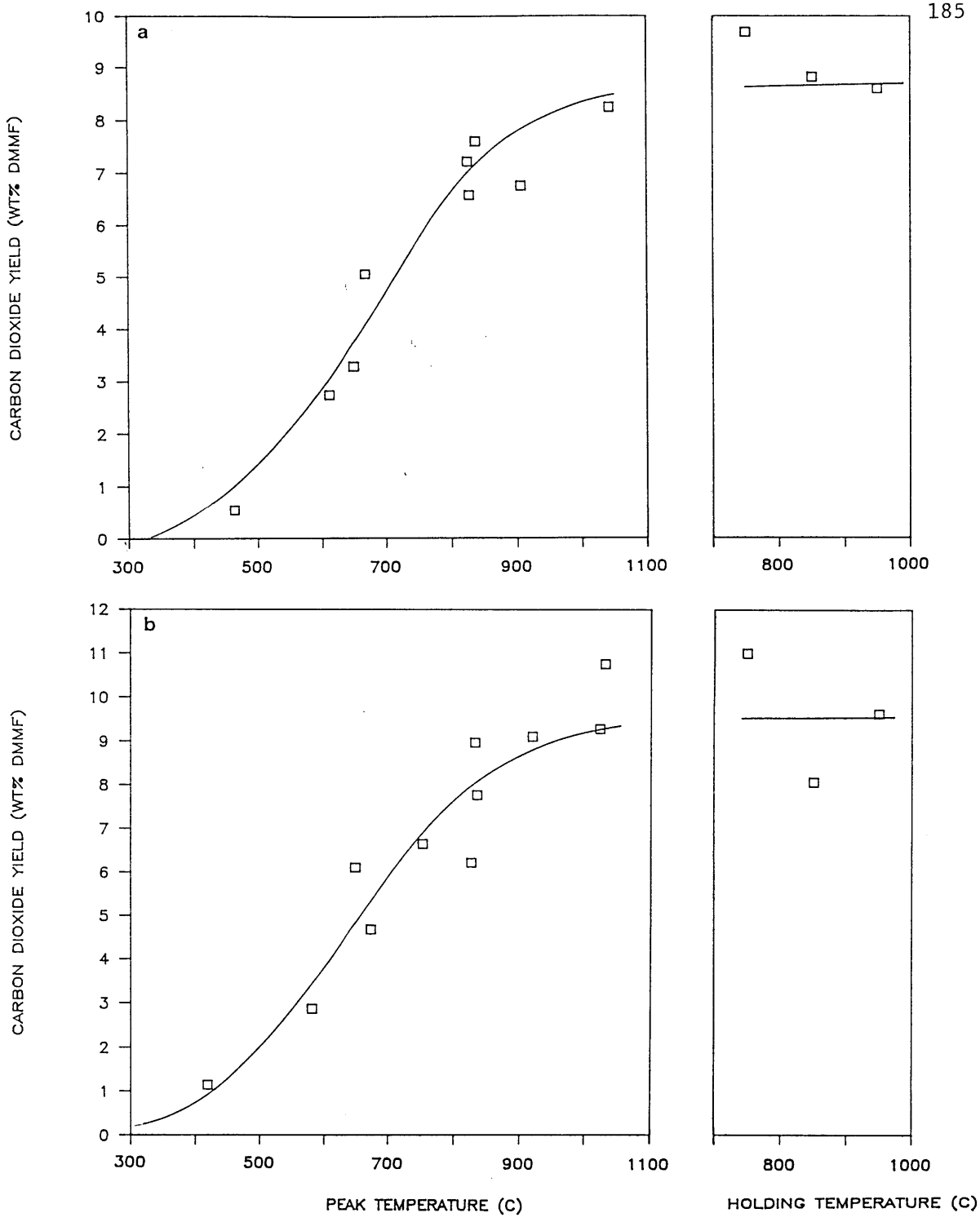

Figure 6.1-7 Carbon dioxide yields versus peak and holding temperatures (5 s hold). Symbols represent experimental data; lines represent MIPR model predictions. (a) LW; (b) ZP; (c) SR; (d) BL; (e) IL; (f) LK. Abbreviations: see Fig.6.1-1.

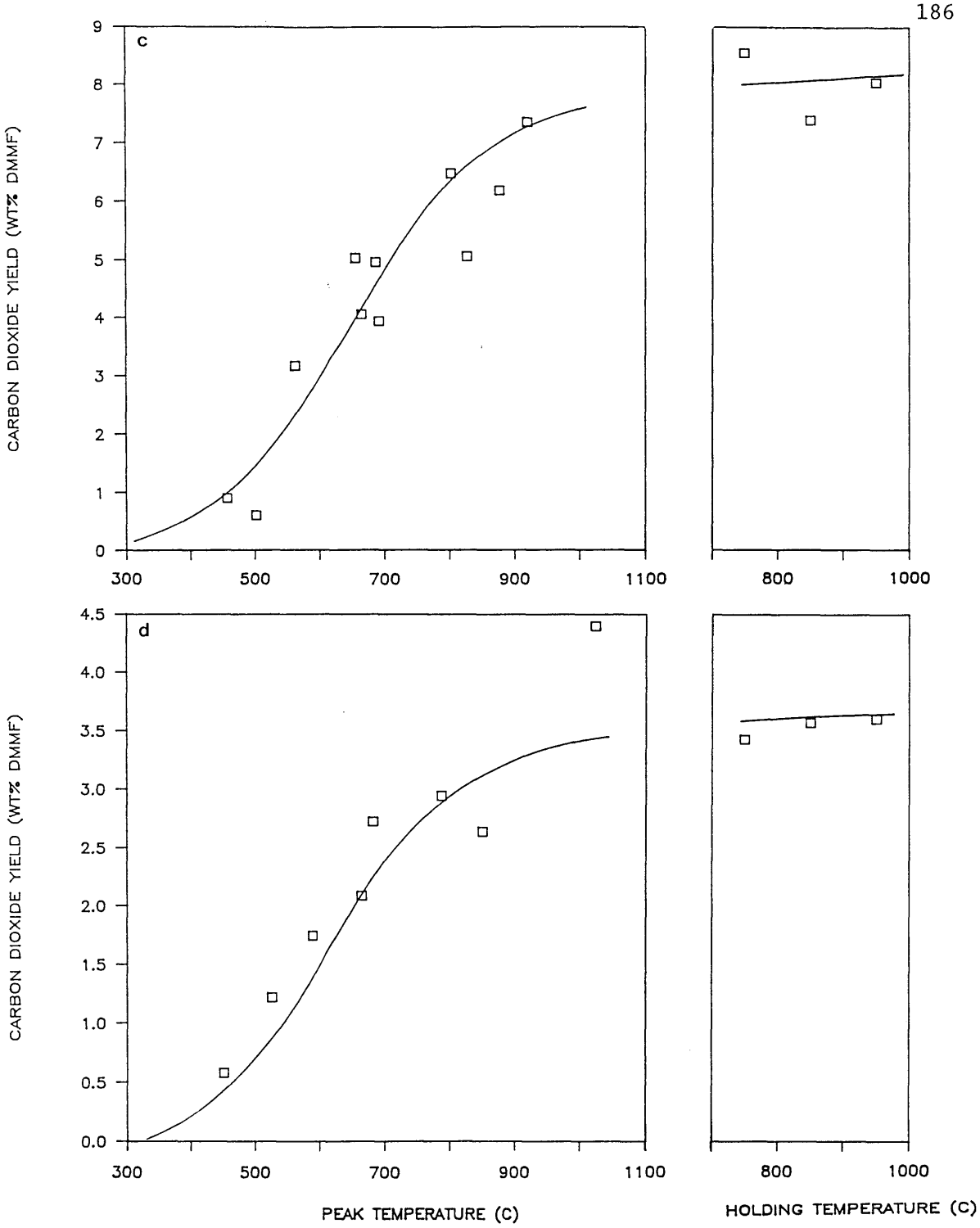

Figure 6.1-7 Carbon dioxide yields versus peak and holding temperatures (5 s hold). Symbols represent experimental data; lines represent MIPR model predictions. (a) LW; (b) ZP; (c) SR; (d) BL; (e) IL; (f) LK. Abbreviations: see Fig.6.1-1.

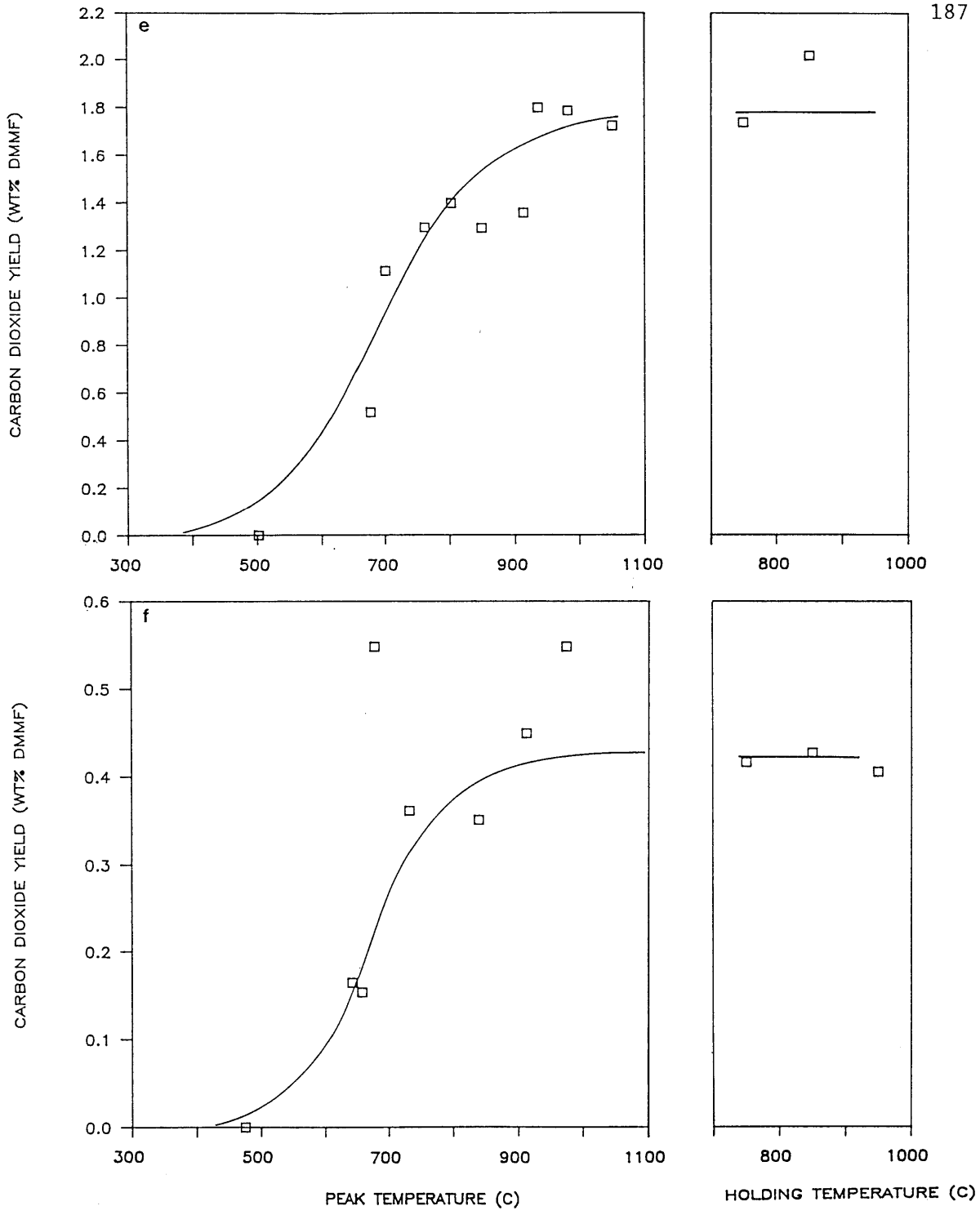

Figure 6.1-7 Carbon dioxide yields versus peak and holding temperatures (5 s hold). Symbols represent experimental data; lines represent MIPR model predictions. (a) LW; (b) ZP; (c) SR; (d) BL; (e) IL; (f) LK. Abbreviations: see Fig.6.1-1.

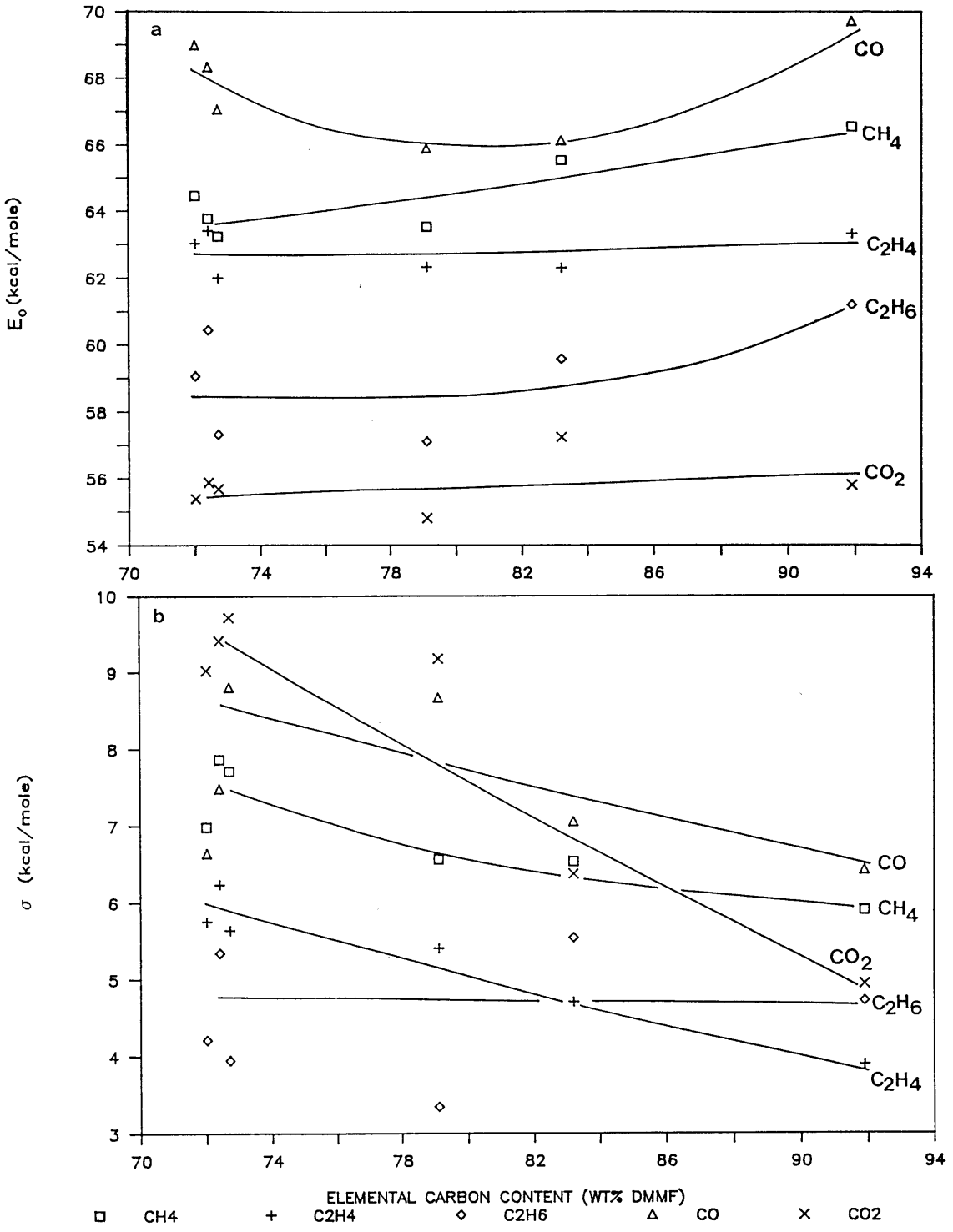

Figure 6.1-8 Best-fitted values of (a) E_o and (b) σ for predicting atmospheric pressure gas evolution using the MIPR model versus carbon contents of the coal. k_o was fixed at 10^{14} s^{-1} in all cases, and Y^* was obtained from experimental data for each coal. Carbon: LW < ZP < SR < BL < IL < LK. Abbreviations: see Fig.6.1-1.

Table 6.1-2 Best-fitted values of E_o and σ of the MIPR model for gas production (k_o fixed at 10^{14} s^{-1} for all coals).

(a) methane

Coal[a]	Y* wt% dmmf	E_o kcal/mole	σ kcal/mole	Standard error of estimate wt% dmmf coal
Lower Wilcox L	2.0	64.5	7.0	0.1
Beulah Zap L	1.6	63.8	7.9	0.2
Smith Roland SB	2.2	63.3	7.7	0.2
Blue HVB	2.8	63.5	6.6	0.2
Illinois HVB	3.4	65.5	6.5	0.1
Lower Kittanning LVB	4.3	66.5	5.9	0.4

[a] Coals are listed in the order of increasing elemental carbon contents in dmmf basis. Elemental analysis is given in Table 4.1-1.

(b) ethylene

Coal	Y* wt% dmmf	E_o kcal/mole	σ kcal/mole	Standard error of estimate wt% dmmf coal
Lower Wilcox L	1.6	63.0	5.8	0.1
Beulah Zap L	0.68	63.4	6.2	0.07
Smith Roland SB	1.3	62.0	5.6	0.09
Blue HVB	1.6	62.3	5.4	0.2
Illinois HVB	0.91	62.3	4.7	0.08
Lower Kittanning LVB	0.55	63.3	3.9	0.05

Table 6.1-2 (continued)

(c) ethane

Coal	Y^* wt% dmmf	E_o kcal/mole	σ kcal/mole	Standard error of estimate wt% dmmf coal
Lower Wilcox L	0.3	59.1	4.2	0.04
Beulah Zap L	0.23	60.5	5.3	0.03
Smith Roland SB	0.36	57.3	3.9	0.05
Blue HVB	0.5	57.1	3.3	0.06
Illinois HVB	0.7	60.0	5.5	0.07
Lower Kittanning LVB	0.6	61.2	4.7	0.05

(d) carbon monoxide

Coal	Y^* wt% dmmf	E_o kcal/mole	σ kcal/mole	Standard error of estimate wt% dmmf coal
Lower Wilcox L	11.0	69.0	6.6	1.0
Beulah Zap L	9.1	68.3	7.5	1.2
Smith Roland SB	10.0	67.1	8.8	0.8
Blue HVB	7.3	65.9	8.7	0.3
Illinois HVB	3.8	66.1	7.1	0.3
Lower Kittanning LVB	0.92	69.7	6.4	0.07

Table 6.1-2 (continued)

(e) carbon dioxide

Coal	Y^* wt% dmmf	E_o kcal/mole	σ kcal/mole	Standard error of estimate wt% dmmf coal
Lower Wilcox L	8.5	55.4	9.0	0.8
Beulah Zap L	9.5	55.9	9.4	1.0
Smith Roland SB	8.0	55.7	9.7	0.8
Blue HVB	3.5	54.8	9.2	0.5
Illinois HVB	1.8	57.3	6.4	0.2
Lower Kittanning LVB	0.42	55.8	4.9	0.03

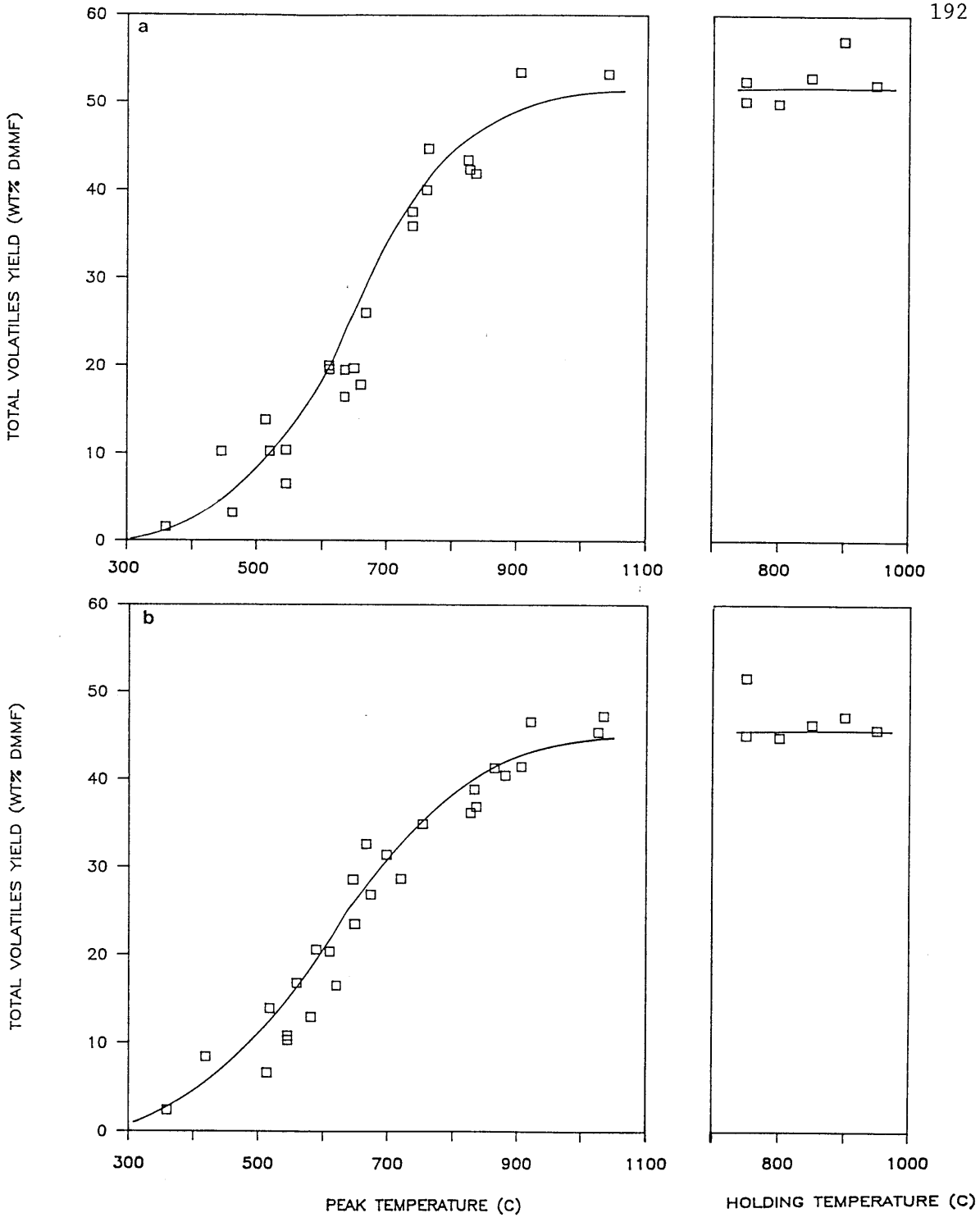

Figure 6.1-9 Total volatiles yield versus peak and holding temperatures (5 s hold). Symbols represent experimental data; lines represent MIPR model predictions. (a) LW; (b) ZP; (c) SR; (d) BL; (e) IL; (f) LK. Abbreviations: see Fig.6.1-1.

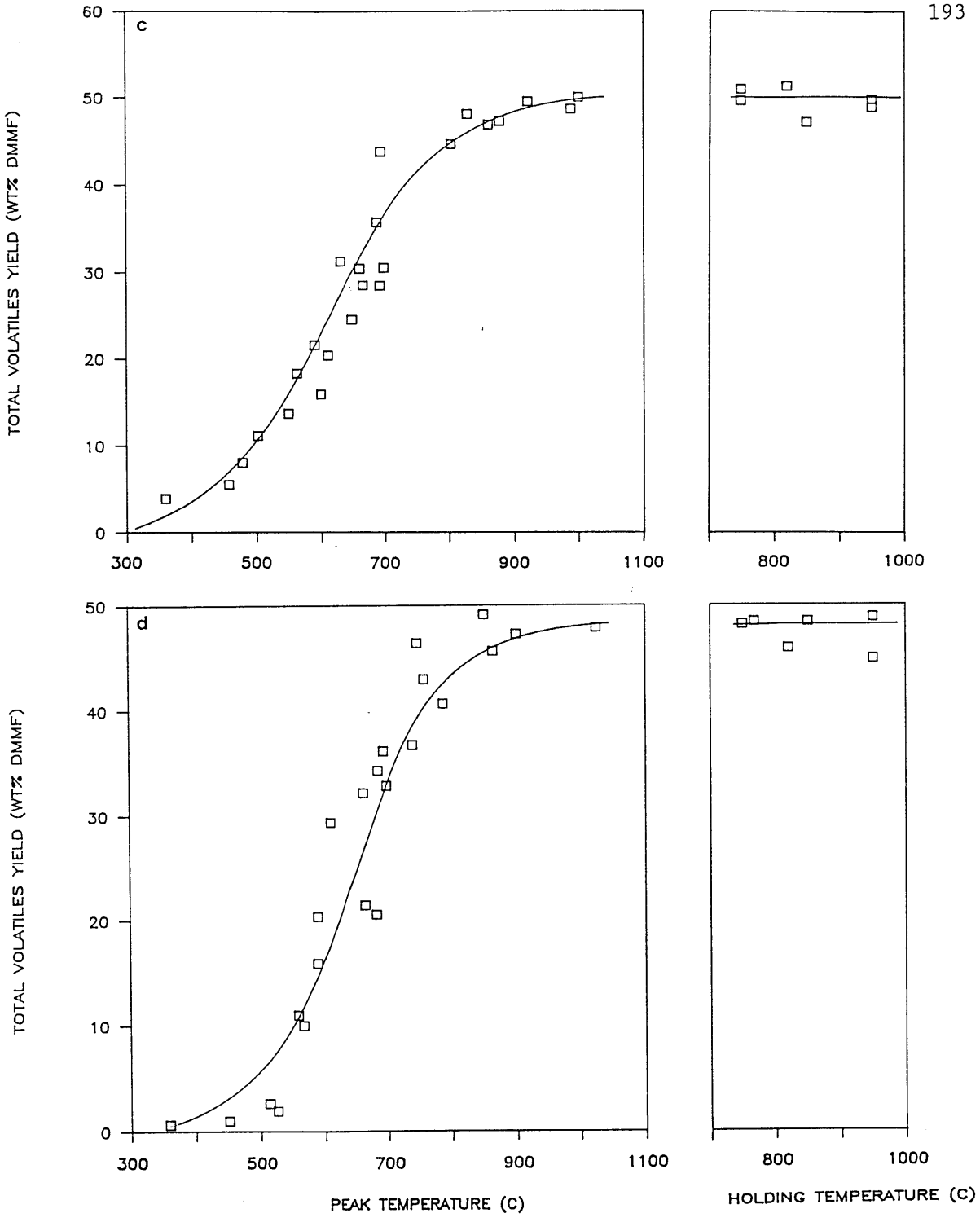

Figure 6.1-9 Total volatiles yield versus peak and holding temperatures (5 s hold). Symbols represent experimental data; lines represent MIPR model predictions. (a) LW; (b) ZP; (c) SR; (d) BL; (e) IL; (f) LK. Abbreviations: see Fig.6.1-1.

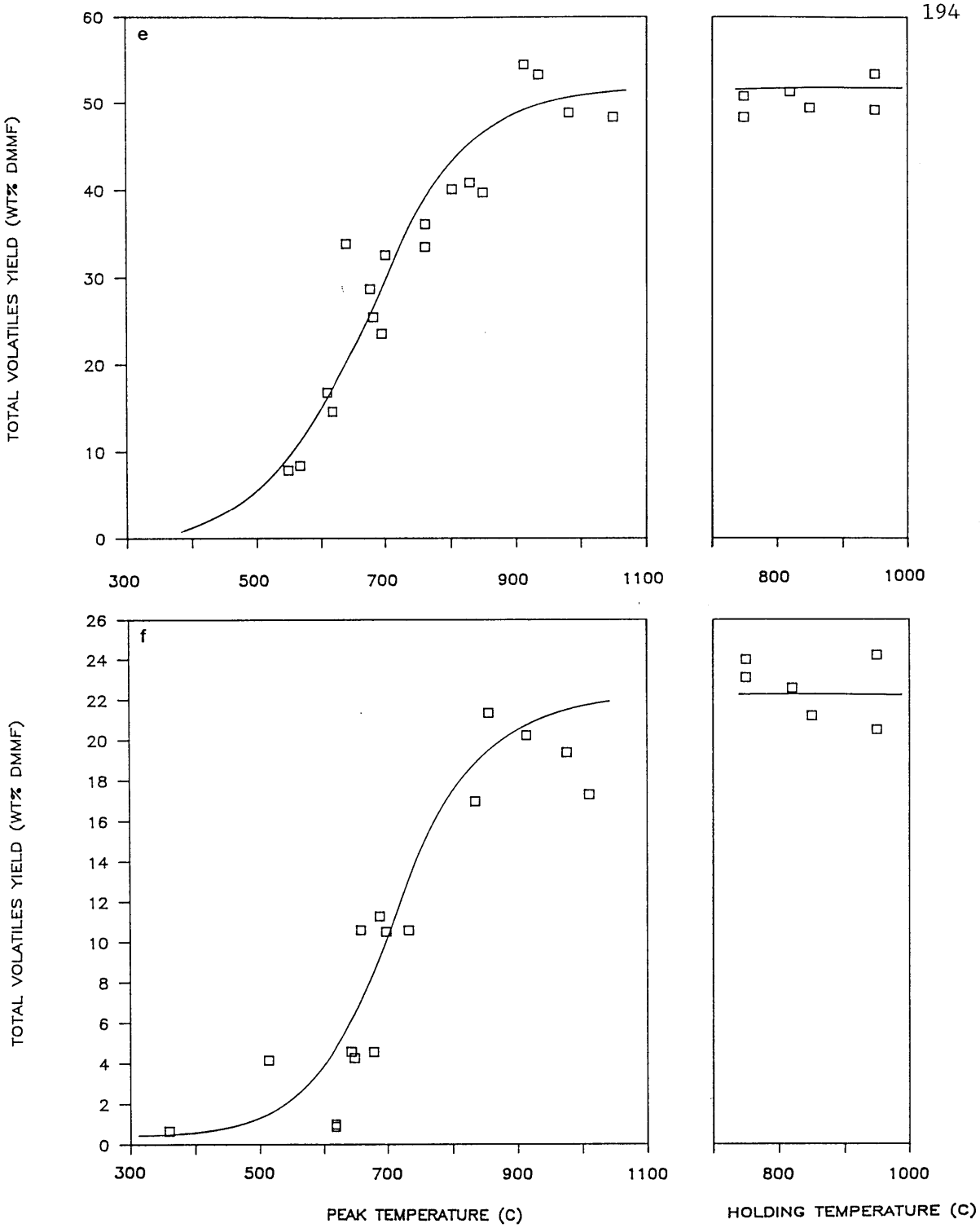

Figure 6.1-9 Total volatiles yield versus peak and holding temperatures (5 s hold). Symbols represent experimental data; lines represent MIPR model predictions. (a) LW; (b) ZP; (c) SR; (d) BL; (e) IL; (f) LK. Abbreviations: see Fig.6.1-1.

Comparing E_o of carbon monoxide shows a concave upward trend with a minimum near high-volatile bituminous coals. But the differences between the three low-rank coals and the two high-volatile bituminous coals are small, E_o = 67-69 kcal/mole for the former compared to $E_o \approx$ 66 kcal/mole for the latter. Such differences are small considering that about ± 1 kcal/mole deviations in E_o of carbon monoxide account for uncertainties from experimental errors. A modest increase to about 70 kcal/mole for the low-volatile bituminous coal is of less practical interest since the carbon monoxide yield for this coal is very small ($\lesssim$ 1 wt% dmmf). Comparing σ of carbon monoxide shows a slight decreasing trend for most coals as the coal rank increases, but the differences are within uncertainties produced from experimental errors, estimated to be about ±1.5 kcal/mole. The E_o of carbon dioxide shows almost no coal-type effect, whereas the σ shows a clear decreasing trend for higher rank coals, with a maximum difference of 4.5 kcal/mole. The uncertainties in the rate parameters of carbon dioxide are estimated to be comparable to those of carbon monoxide.

Coal-type effects on total volatiles production

Figure 6.1-9 compares the experimental and predicted total volatiles yields from the MIPR model for the six coals investigated in this study. The model predictions were made using the same procedure as above, where k_o was again fixed at 10^{14} s^{-1}, Y^* was obtained from the measured maximum total volatiles yield, and E_o and σ were best-fitted to the experimental data. In all cases, the predicted yields agree well with experimental values; the standard error of the estimate ranged from approximately 6 to 10 % of the maximum yield.

Figure 6.1-10 plots the best-fitted values of E_o and σ versus the elemental carbon contents of the coal; numerical values are given in Table 6.1-3. Generally, higher rank coals show increasing values of E_o with a maximum difference of about 6 kcal/mole. The E_o of Lower Wilcox lignite appears to be high compared to the other two low-rank coals, but is within estimated uncertainties of ±1 kcal/mole. Comparing the σ shows a decreasing trend for higher rank coals, but with much scatter. A maximum difference of 4 kcal/mole in σ is slightly greater than the estimated uncertainty of ±1.5 kcal/mole.

The trends in the rate parameters for independently measured total volatiles production confirm the trends observed for individual products. The relatively modest coal-type dependence of the MIPR rate parameters for total volatiles reflect the combined effects of a strong coal-type dependence for tars and a much weaker dependence for gases. Also, the general trends for all products are always consistent-higher E_o and lower σ for increasing coal rank.

Use of the MIPR model parameter values obtained in this study should be strictly confined to pyrolysis conditions similar to those employed in this study, where small coal particles (75-90 μm dia.) were rapidly pyrolyzed ($\approx$ 1000 C/s) to a maximum temperature of about 1000 C under atmospheric pressure with rapid dilution and quenching of volatile products. Under such conditions, the impact of secondary reactions inside the coal on the observed products evolution is expected to be small, although not negligible, and secondary reaction effects outside the coal are expected to be unimportant.

In applications employing coals other than those studied here, use of the model parameters obtained from the experimental data specific to

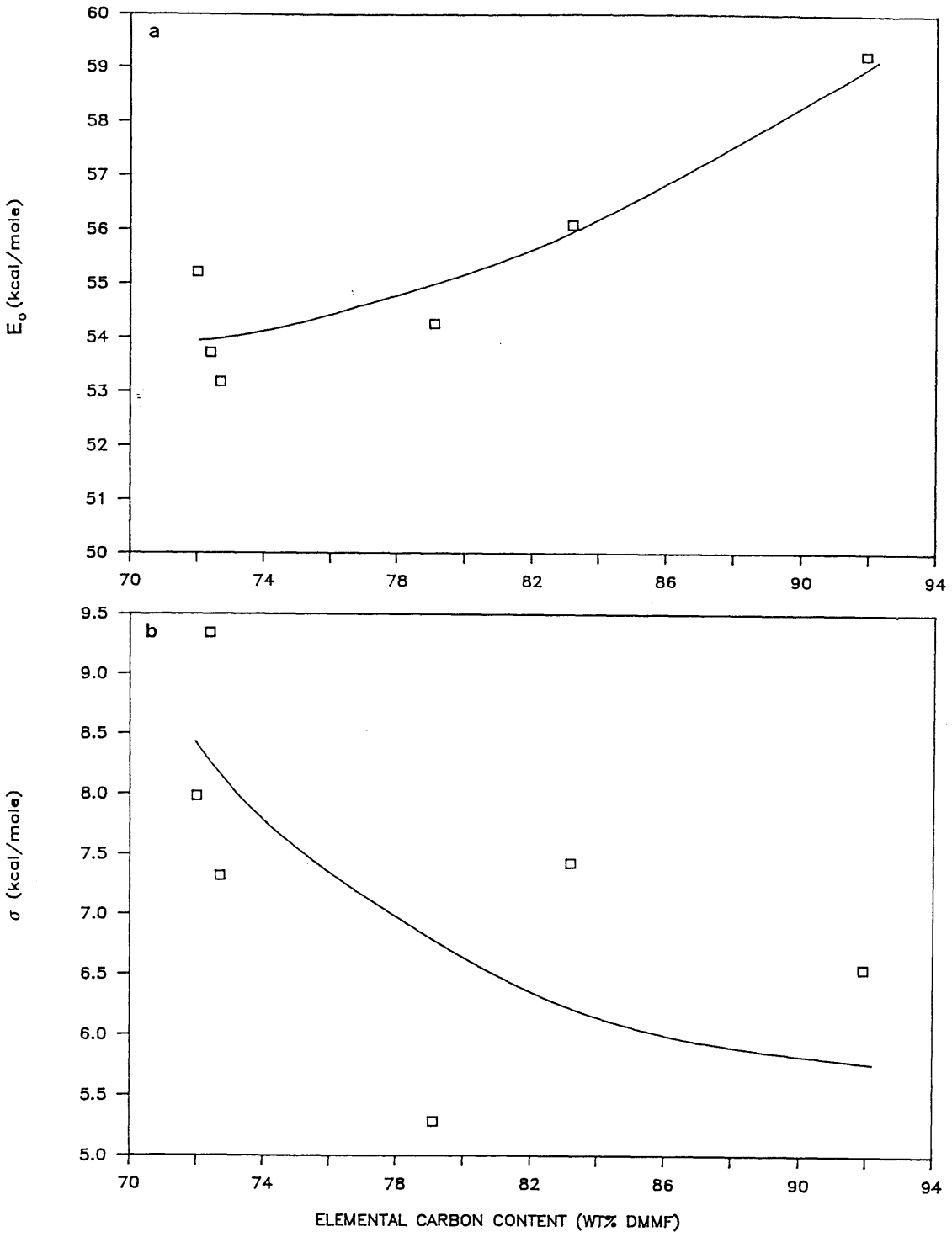

Figure 6.1-10 Best-fitted values of (a) E_o and (b) σ for predicting atmospheric pressure total volatiles evolution using the MIPR model versus carbon contents of the coal. k_o was fixed at 10^{14} s^{-1} in all cases, and Y^* was obtained from experimental data for each coal. Carbon: LW < ZP < SR < BL < IL < LK. Abbreviations: see Fig.6.1-1.

Table 6.1-3 Best-fitted values of E_o and σ of the MIPR model for total volatiles production (k_o fixed at 10^{14} s^{-1} for all coals).

Coal[a]	Y* wt% dmmf	E_o kcal/mole	σ kcal/mole	Standard error of estimate wt% dmmf coal
Lower Wilcox L	51	55.2	8.0	3.9
Beulah Zap L	45	53.7	9.3	2.9
Smith Roland SB	49	53.2	7.3	3.5
Blue HVB	47	54.3	5.3	4.2
Illinois HVB	51	56.1	7.4	3.9
Lower Kittanning LVB	22	59.2	6.5	2.3

[a] Coals are listed in the order of increasing elemental carbon contents in dmmf basis. Elemental analysis is given in Table 4.1-1.

the coal of interest would give the most reliable performance. If such experimental information is not available, use of the parameter values estimated from the coal-type dependent trends obtained in this study is expected to give the next best performance - Figs. 6.1-2 for tars, 6.1-8 for individual gases, and 6.1-10 for total volatiles. A note of caution in using the estimated values is that the trends were established from a fairly small number of coals (6), and thus there is a possibility that some 'unusual' coals may behave very differently from those studied here. In applications where one wishes to minimize the number of input parameters, use of an averaged value of the rate parameters is expected to give an adequate approximation over a narrow range of coal types for gases. But, such an approximation is generally not recommended for describing tar or total volatiles production.

6.2. Extended MIPR model

The extended MIPR model increases the range of applicability of the MIPR model by explicitly including descriptions of mass transport and secondary reactions.

6.2.1 Mathematical formulation

This section presents a chemical and physical mechanism of tar formation, and derives a quantitative model based on the mechanism. Figure 6.2-1 gives a schematic diagram of the proposed mechanism, where the solid arrows indicate reaction pathways leading to tar production and the dashed arrows indicate competing pathways leading to char and gas formation. The chemistry of the model assumes a hypothetical

molecular structure of coal deduced from the literature survey presented in Section 3.1.1 (Fig.3.1-1)

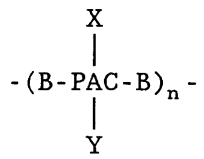

where PAC represents repeating nuclear units of polyaromatic and hydroaromatic clusters, B bridging molecules, X side groups suspected to be responsible for cross-linking, Y non-cross-linking side groups, and n the number of repeating units. The exact structures of these subunits are currently not known, but some qualitative information can be inferred from the literature survey in Section 3.1.1. The survey suggests bridging molecules are of polymethylene and polymethylene-ether type molecules; and side groups are molecules such as -OH, -COOH, $-CH_3$, and $-C_2H_5$, among which the oxygenated side groups are postulated to cross-link. The survey also indicates that the concentration of these structures is a strong function of coal type, but for most of these structures, reliable quantitative correlations are currently not available.

The model formulation is based on the mechanism shown in Fig.6.2-1, where the tar is produced via the sequential steps of **bridge scission**, **hydrogenation** and **transport**. Competing with the tar production pathway are **cross-linking**, **polymerization**, and **tar cracking reactions**, all of which lead the formation of char + gas. In the literature, the latter two reactions are often lumped together and globally referred to as the secondary reaction of tar (or metaplast). The importance of distinguishing the different competing reactions is described below, where each or a combination of these three competing reactions is shown

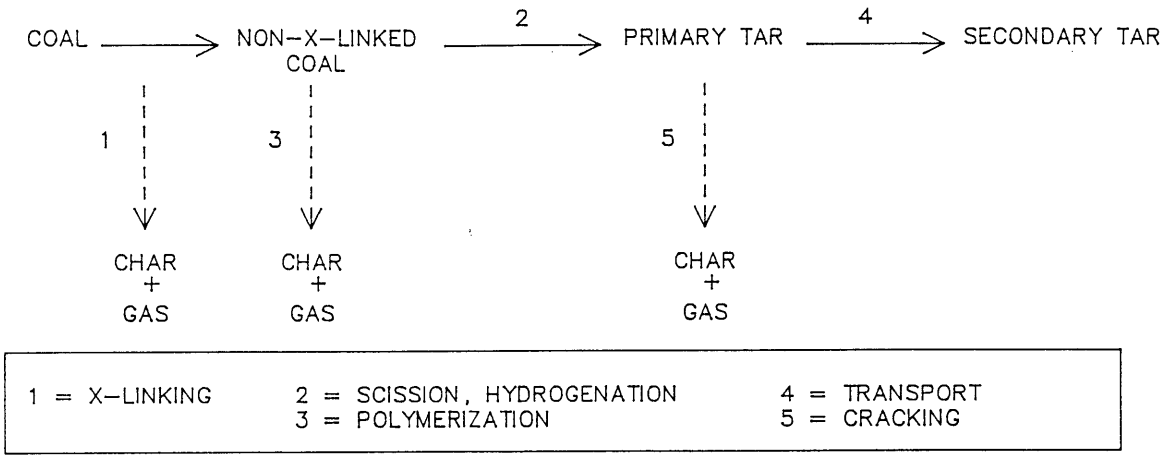

Figure 6.2-1 Chemical and physical mechanism of tar formation.

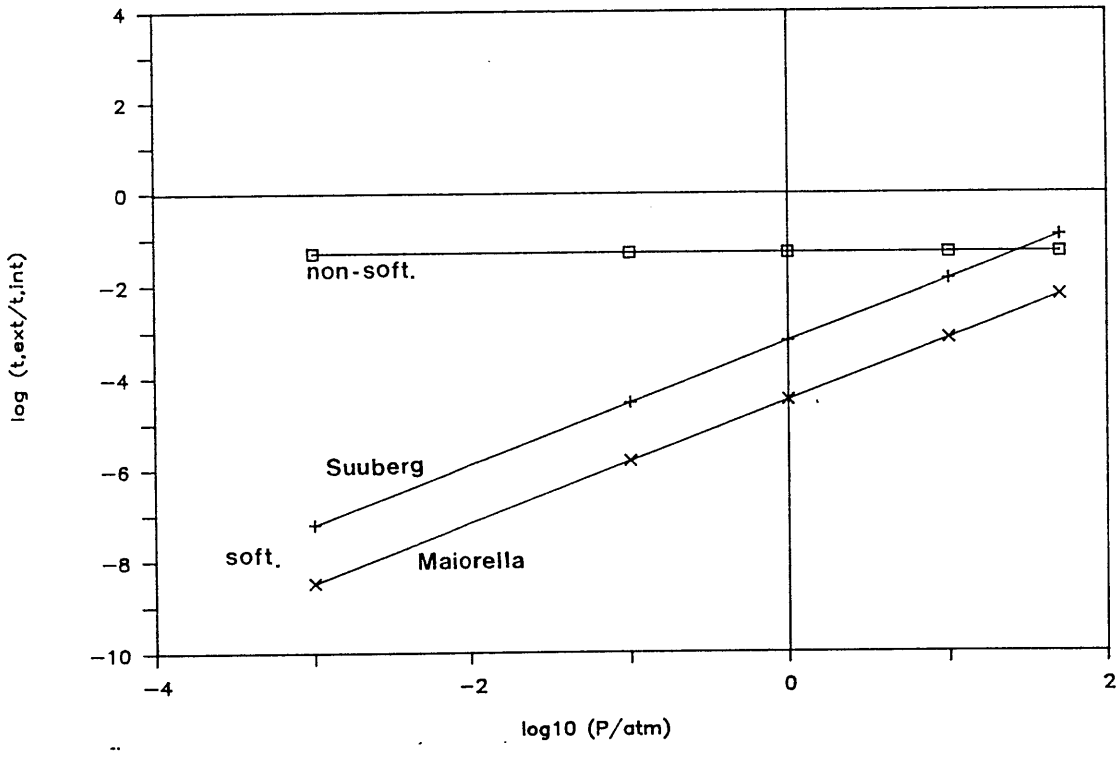

Figure 6.2-2 Comparison of the relative time scales for external and internal transport rates of tar.

to uniquely describe and explain the experimentally observed effects of main operating variables - coal type, heating rate, pressure, and particle size.

Cross-linking

The cross-linking in this work is defined as a reaction between side groups of two repeating units or nuclei to yield a coupled unit that is held together by a 'strong' bridge bond. We assume that the cross-linked molecule is too heavy to be volatile, and thus forms solid residue (char). Experimental evidence for this process comes from solvent swelling studies of pyrolyzed coals (Suuberg et al., 1987), where changes in the swelling ability is related to the degree of cross-linking. The observation that the cross-linking is more severe for lower rank coals that have higher -OH contents suggest, perhaps, dehydration between two -OH side groups plays an important role

$$\text{PAC-OH} + \text{OH-PAC} \dashrightarrow \text{PAC-O-PAC} + H_2O$$

The coupled molecule from the dehydration reaction is expected to be very stable due to the high activation energy ($\approx$ 70 kcal/mole) for the scission of the ether bond between the two phenyl groups. However, a lack of direct evidence supporting the dehydration mechanism suggests that the actual cross-linking reaction pathway is much more complicated than that shown above (Stein, 1988). Carbon dioxide is another potential by-product of cross-linking, but the fact that it can also be produced from unimolecular decarboxylation reactions makes this argument less appealing.

Define the fraction which survives cross-linking as V^*_{max}, and assume that this quantity depends only on the chemical structure of the

coal. Disregarding the kinetics of this process is justified since cross-linking occurs at relatively mild temperatures before other reactions proceed to any appreciable extent. A method to estimate V^*_{max} for a given coal is presented in Section 5.1.2 in form of an empirical correlation. Under the conditions of negligible polymerization and cracking reactions (steps 3 and 5 in Fig.6.2-1), all of V^*_{max} will evolve as tars. Experimentally, such a maximum yield is obtained by applying high heating rates ($\tilde{>}$ 100 C/s) to small particles ($\tilde{<}$ 100 μm dia.) under low pressures (P $\tilde{<}$ 10^{-3} atm). Rapid heating is postulated to minimize polymerization type reactions (Niksa and Kerstein, 1985), and low pressures and/or small particle sizes reduce transport limitations (step 4), thereby leaving little or no time for cracking reactions.

Scission/polymerization

Upon further heating, the non-cross-linked fraction of the coal (V^*_{max}) reacts via two competing pathways. One route is the scission of bridge bonds which release the PAC units in radical form from the macromolecular matrix. Various bridge bonds, each with its specific chemical bond strength, are assumed to be present in the coal molecule. To account for this, the thermal decomposition is assumed to occur by multiple independent parallel reaction, first-order with respect to the amount of reacting material remaining in the coal. The rate of scission is expressed as the sum of the contributions from all the reactions, each of which is described by,

$$dV_i/dt \text{ (scission)} = k_{s,i} \ (V^*_i - V_i) \qquad (6.2\text{-}1)$$

$$k_{s,i} = k_{os,i} \exp(-E_{s,i}/RT) \qquad (6.2\text{-}2)$$

where i denotes one reaction and V_i the cumulative amount of the reacted material by scission. The same preexponential factor is used for all the reactions, i.e., $k_{os,i} = k_{os}$, and the activation energies are described by a Gaussian distribution with mean E_{os} and standard deviation σ_s. Thus,

$$f(E) = [\sigma_s(2\pi)^{1/2}]^{-1} \exp[-(E-E_{os})^2/2\sigma_s^2] \qquad (6.2\text{-}3)$$

where $f(E) = V^*_i/V^*_{max}$ for a large i, and V^*_{max} is equal to the sum of the V^*_i for all i.

Competing with the scission pathway is the free-radical initiated polymerization type reaction assumed to occur first-order with respect to the amount of unreacted coal

$$dV_i/dt \text{ (polymerization)} = k_p\ (V^*_i - V_i) \qquad (6.2\text{-}4)$$

The polymerization pathway was postulated based on the experimental data of Serio (1984), Kobayashi et al. (1977), and Niksa (1981). Their data indicate that a fraction of tar (Serio) and coal (Kobayashi et al. and Niksa) reacts to form char at relatively low temperatures, and the activation energies derived from the data (Serio, 1984) are of the range for gas phase polymerization reactions of coal-related aromatic compounds (Gavalas, 1984).

Adding the two competing reactions, Eqs. (6.2-1) and (6.2-4), gives the total rate of disappearance for species i

$$dV_i/dt = (k_{s,i} + k_p)(V_i^* - V_i) \qquad (6.2\text{-}5)$$

$$= k_{t,i}(V^*_i - V_i)$$

where $k_{t,i} = k_{s,i} + k_p$. (6.2-6)

To convert quantities from weight fractions to molar basis, divide the quantity by the average molecular weight (MW_{avg}) of nuclei. All quantities in molar basis will be enclosed by a pair of square brackets

and will have the units of g-moles/g of raw coal.

Hydrogenation of the PAC radicals (PAC·) is assumed to be the main route to stabilize the radicals. We define these stabilized molecules as **primary tar**, and it is denoted YH. The rate of hydrogenation for species i is

$$dYH_i/dt = MW_{avg}\ k_h[AH][PAC\cdot]_i \qquad (6.2\text{-}7)$$

where [AH] represents the molar concentration of abstractable hydrogen, and k_h the bimolecular rate constant for hydrogenation. Applying a steady-state assumption to [PAC·] requires that the rate of hydrogenation be equal to the rate of scission. Equation (6.2-7) can thus be rewritten in the form of

$$dYH_i/dt = k_{s,i}\ (V^*_i - V_i) \qquad (6.2\text{-}8)$$

Repolymerization of PAC· is another possible depletion pathway, but including this reaction would substantially complicate the formulation and demand input parameters that are difficult to obtain, e.g., [AH], MW_{avg}. To get around this complication, we have arbitrarily assumed that the rate of scission given in Eq.(6.2-1) represents only the fraction that hydrogenates, and the fraction that repolymerizes is accounted for by the polymerization step.

The influence of polymerization on tar production can be more effectively described by expressing the rate of YH_i formation in terms of the total rate of disappearance of the non-x-linked fraction. First, define a quantity, $E_{p,i}$, as

$$E_{p,i} = \frac{\text{rate of scission}}{\text{rate of scission + polymerization}}$$

$$= k_{s,i} \,/\, (k_{s,i}+k_p) \qquad (6.2\text{-}9)$$

Then, combining Eq.s (6.2-5), (6.2-8), and (6.2-9) gives

$$dYH_i/dt = E_{p,i}\ k_{t,i}(V^*_i - V_i) \qquad (6.2\text{-}10)$$

Summing the above equation over all species i gives the total rate of primary tar production

$$dYH/dt = \sum E_{p,i}\ k_{t,i}(V^*_i - V_i) \qquad (6.2\text{-}11)$$

Under minimal transport limiting conditions (i.e., low pressures, small particles), Eq.(6.2-11) describes the rate of tar production for all heating rates. Mass transport effects are included next.

Transport/cracking

Upon hydrogenation, the primary tar is either physically transported away from the coal particle to yield secondary tar, or cracked to produce char plus gases. To rigorously model the former step would require a description of transient transport processes in a porous solid or liquid phase environment inside the particle, coupled with transport in the mass boundary layer outside the particle. This approach requires a large number of physical properties of both coal and tar, many of which are difficult to measure or estimate, e.g., transient pore-size distribution information for non-softening coals, vapor pressures of tars. Such limitations would be especially difficult to deal with in this study where we need to describe transport processes for different coal types, which include both softening and non-softening coals. In addition, the large computational effort often required in the rigorous approach can potentially restrict the use of such models in practical applications such as large combustion or gasification models that describe fluid mechanics, heat and mass transport, and reaction kinetics. Therefore, we felt a need to develop an approximate transport description that is able to capture the observed effects of pressure and particle size on

tar production, using as few input parameters as possible, and requiring minimal computational effort.

The first simplification made in formulating an approximate mass transport description is that, for both non-softening and softening coals, the transport resistance outside the coal particle is assumed to be negligibly small compared to that of inside. Comparing the characteristic times in the two domains shows that this assumption is valid over the range of operating conditions considered in this study. Figure 6.2-2 compares the relative time scales over a wide range of pressures for both non-softening and softening coals; the equations and the values of physical properties used to compute the time scales are given in Table 6.2-1. A similar simplification has been made in more rigorous models (Russel et al., 1979; Gavalas and Wilks, 1980; Bleik et al., 1985).

While escaping, some of the tar reacts to produce char plus gaseous products. Serio (1984) has shown that the rate of homogeneous tar cracking in the vapor phase can be modeled as a first-order reaction with respect to the vapor phase tar concentration; a possible catalytic effect of coal surface is presently poorly understood, and thus is not included. The rate of cracking reaction is then expressed as

$$\text{rate of tar cracking} = k_c YH_{avg} \qquad (6.2\text{-}12)$$

where k_c is the cracking reaction rate constant, and YH_{avg} the average mass fraction of primary tar inside the coal. The total rate of secondary tar, denoted as Y, leaving the particle surface is given as

$$dY/dt = \sum E_{p,i}\, k_{t,i}(V^*_i - V_i) - k_c YH_{avg} \qquad (6.2\text{-}13)$$

where YH_{avg} represents the average concentration of primary tar inside the coal. Derivations below relate YH_{avg} to the relative rates of

Table 6.2-1 Equations and physical properties used to compute the relative transport time scales shown in Fig.6.2-2.

Coals	time scales[a]	physical properties
Non-softening[b]:	$t_e/t_i = e/\tau$	$e \approx 0.1$ $\tau \approx 2$
Softening:	$t_e/t_i = (R_{eff}^2 D_L P)/(R_b^2 D_g P_{vap})$	R_{eff} = Eq.(6.2-26) with R of 50 μm R_b = boundary layer thickness[a] D_L = Eq.(6.2-29) with D_{oL} of 10^{-6} D_g = Eq.(6.2-28) P = reactor pressure P_{vap} = tar vapor pressure[c]

[a] Particle radius is assumed for the external boundary thickness. This approximation is comparable to the value computed from a rigorous flow description (Zacharias, 1979).

[b] e = void fraction, τ = tortuosity.

[c] Vapor pressure correlations of Maiorella (1978), and Unger and Suuberg (1983) were used.

Consider the mass transport in non-softening coals first. To meet the objective of developing a mathematically concise but effective transport description, the following assumptions were made:

(1) All of the primary tar enters macropores without encountering any appreciable configurational or Knudsen type diffusion resistances in the smaller pores.

(2) All of the primary tar enters macropores from the center of the particle.

(3) Neglect convective contributions.

(4) The concentration of the primary tar in the coal is at steady-state.

Supporting evidence for the first assumption comes from the analysis of Gavalas and Wilks (1980). The study indicates that most of volatiles are generated within the small pores (micro- and transition) and are transported to the outside via the large pores rather than directly. Thus although the diffusivity is extremely low in the small pores, the transport distance may be sufficiently short to make the transport resistance in these pores negligible. The second assumption is not strictly valid since tars enter from all points along the pore, not just from one end. But making this assumption considerably simplifies the mathematics without seriously hindering our ability to capture the effects of main operating variables. An important consequence of this assumption is that the apparent average residence time of primary tar inside the coal would be somewhat over-estimated, but one way to compensate for this effect would be to assign slightly higher diffusivity values. Evidence for the third assumption is based on the

observation that macropores can be approximated by a bimodal pore system with radii 0.05 and 0.5 μm, and that the larger pores are few in number and hence poorly inter-connected (Gavalas, 1984). The transport in the larger pores is much faster than the transport in the smaller pores due to greater convective contributions in the larger pores [$t_{diff}/t_{conv} \propto$ pore radius^2, Suuberg (1985)]. Thus, one can approximate the macropore system as having the two types of pores connected in series, where the resistance offered by the larger pores is negligible. Implicit in this approximation is that the effective diffusion path is now shorter than the particle radius, but the current description will allow this effect to be absorbed in the effective diffusivity term. The last assumption is valid if the particle radius (R) is much less than the square root of the effective gas phase diffusivity of tar inside the coal ($D_{g,eff}$) times a characteristic time scale for pyrolysis (t_{pyro})

$$R << (D_{g,eff}\ t_{pyro})^{1/2} \qquad (6.2\text{-}14)$$

$D_{g,eff}$ is related to the gas phase binary diffusivity of tar by

$$D_{g,eff} = e/\tau\ D_g \qquad (6.2\text{-}15)$$

where e and τ are the void fraction and tortuosity of pores in the coal respectively. For D_g = 0.1 cm^2/s, e = 0.1, τ = 2, and t_{pyro} = 1 s, the steady-state assumption holds for R << 700 μm, and thus is applicable in this study where the maximum particle radius is < 50 μm. With the above approximations, a material balance of YH across a thin cylindrical section of a macropore gives (< > indicates mass fraction/unit pore volume)

$$d^2<YH>/dx^2 - (k_c/D_{g,eff})<YH> = 0 \qquad (6.2\text{-}16)$$

where x is the coordinate along eh pore axis, and a general solution is

$$\langle YH \rangle = A_1 \exp(m_{ns} x) + A_2 \exp(-m_{ns} x) \qquad (6.2\text{-}17)$$

m_{ns} is equal to $(k_c/D_{g,eff})^{1/2}$, and A_1, A_2 are integration constants evaluated at the boundary conditions

$$\langle YH \rangle = 0, \quad \text{at } x = R \qquad (6.2\text{-}18)$$

$$d\langle YH \rangle/dx = - \sum E_{p,i}(V^*_i - V_i)/(N_p A_p R^2)\ (\underline{m}_{ns,i} R)^2, \quad \text{at } x = 0 \qquad (6.2\text{-}19)$$

where A_p, N_p are the cross-sectional area and the total number of macropores respectively, and $\underline{m}_{ns,i} = (k_{t,i}/D_{g,eff})^{1/2}$. The latter boundary condition has little physical meaning; the form was chosen to be consistent with the assumption (2) that the primary tar enters from the center of the particle. Solving for the integration constants gives

$$\langle YH \rangle = \frac{\sum E_{p,i}(V^*_i - V_i)(\underline{m}_{ns,i} R)^2 [\exp(-m_{ns} x) - \exp(-2m_{ns} R + m_{ns} x)]}{N_p A_p R\ [1+\exp(-2m_{ns} R)]} \qquad (6.2\text{-}20)$$

Integrating $\langle YH \rangle$ over the radius R and converting to mass fraction basis gives

$$YH_{avg} = \sum E_{p,i}(k_{t,i}/k_c)(V^*_i - V_i) \frac{[1+\exp(-2\underline{m}_{ns} R) - 2\exp(-\underline{m}_{ns} R)]}{[1+\exp(-2m_{ns} R)]} \qquad (6.2\text{-}21)$$

Substituting Eq.(6.2-21) into Eq.(6.2-13) gives the rate of tar (secondary) leaving the particle surface as

$$dY/dt = \sum E_{p,i}\ E_{c,ns}\ k_{t,i}(V^*_i - V_i) \qquad (6.2\text{-}22)$$

where

$$E_{c,ns} = \frac{\text{rate of tar production with transport limitation}}{\text{rate without transport limitation}}$$

$$= 2\exp(-m_{ns} R)/[1+\exp(-2m_{ns} R)] \qquad (6.2\text{-}23)$$

The quantity $m_{ns}R$ is the Thiele modulus for non-softening coals. The three multiplication factors in Eq.(6.2-22), V^*_{max} ($\sum V^*_i$), $E_{p,i}$, and $E_{c,ns}$, represent an important result of this model, as they respectively account for the effects of cross-linking, polymerization and cracking on tar production. Their values are each bounded between 0 and 1, where 0 represents the most severe limitation on tar production and 1 represents no limitation.

In <u>softening coals</u>, the liquid phase diffusion is assumed to be the dominant mode of transport inside the coal. The possibility of volatile bubbles enhancing the rate of tar escape is neglected based on the recent experimental evidence that at least in some cases most of the bubbling phenomena occur before any appreciable amount of tars are produced (Hsu, 1988; Griffin, 1988). Applying a similar derivation procedure as above for non-softening coals gives the rate of secondary tar escaping the particle surface as

$$dY/dt = \sum E_{p,i}\ E_{c,s}\ k_{t,i}\ (V^*_i - V_i) \qquad (6.2\text{-}24)$$

where

$$E_{c,s} = 2\exp(-m_s R_{eff})/[1+\exp(-2m_s R_{eff})] \qquad (6.2\text{-}25)$$

The quantity $m_s R_{eff}$ is the Thiele modulus for softening coals, where m_s equal to $(k_c/D_L)^{1/2}$; D_L represents the liquid phase diffusivity of tar in the molten coal; and R_{eff} is the effective diffusion length scale. Often, the molten coal has a shape of a cenospherical shell (Sung, 1978), prior to extensive tar release (Hsu, 1988). Thus an appropriate diffusion length scale for softening coals is assumed to be half of the shell thickness. For a Pittsburgh Seam bituminous coal with a particle radius of $\approx$40 μm pyrolyzed under atmospheric reactor

pressure, Griffin (1988) reports the shell thickness to be about 20% of the particle radius of the raw coal. This approximate value is assumed for the two softening coals in this study (Illinois HVB and Lower Kittanning LVB).

An exact explanation for the observed pressure and particle-size effect on tar production for softening coals, is currently unclear due to large uncertainties in physical parameter values of the molten coal (see Sections 3.2.2 and 3.4.3). In this formulation, excluding external and bubble transport effects leaves the possibility that the shell thickness is a function of pressure and particle size as the only viable explanation to describe the observed behavior. Until a more conclusive explanation becomes available, the present model will assume that the shell thickness is related to the pressure and particle size in the form of

$$R_{eff} = 0.1\ R \times 10^{-4}\ (P/1)^{1/3}(R/40)^{1/3}\ \text{cm} \qquad (6.2\text{-}26)$$

where R is the particle radius in μm, and P the reactor pressure in atm. The work of Griffin (1988) is currently seeking to provide quantitative experimental data to examine the effect of pressure and particle size on the shell thickness (6.2-26).

Model parameters for the extended MIPR model

For a given coal, the model requires a total of 9 input parameters: V^*_{max}, k_{os}, E_{os}, σ_s, k_{op}, E_p, k_{oc}, E_c, and $D_{g,eff}$ or D_L. In the discussions below, the kinetic parameters estimated by Gavalas (1984) are used in cases where no reliable experimental measurements are available. But, these estimated parameters are strictly valid for gas-phase reactions where the interference from neighboring molecules

(e.g., "cage" and solvation effects; Stein, 1981) can be neglected, and thus one may question the validity of applying these estimates to reactions occurring in a condensed phase environment such as in coal. Justifications for taking this approach are (1) solvent-molecule interaction effects decrease at higher temperatures (Stein, 1981) so that they may be small at typical coal conversion temperatures (400-1000 C); (2) experimentally measured homolysis rate constants in the gas and liquid phase are approximately the same, within a factor of 2 (Stein, 1981); and (3) no alternative methods are currently available.

The non-cross-linked fraction of the coal, V^*_{max}, is the experimental tar yield limit obtained with rapid heating under low pressures (vacuum). If experimental values are not available, the low-pressure tar correlation developed in Section 5.1.2 can be used; from just the elemental composition information of the coal, the correlation predicts V^*_{max} with a standard error of estimate of ±3 wt% dmmf.

In the scission reaction, $\log(k_{os}/s^{-1})$ was fixed at 14 for all coals; this value is within the range estimated by Gavalas et al. (1981a) for homolysis of ethylene (13.9) and methylene (14.3) bridges. Estimating a priori the two activation energy related parameters, E_{os} and σ_s, is more difficult because (1) unlike the preexponential factor the activation energy is highly sensitive to the bridge type, e.g., Gavalas et al. (1981a,b) estimates the dissociation activation energy for ethylene and methylene bridges between two unsubstituted phenyl groups to be 56.4 and 80.7 kcal/mole respectively; and (2) quantitative information on the type of bridges in the coal is currently lacking. Therefore, E_{os} and σ_s were best-fitted using the experimental tar data. The best-fitted values of E_{os} and σ_s respectively range from 51.7 to

56.8 and from 3.5 to 9.4 kcal/mole among the six coals studied. These values are within the range of expected values for the scission of bibenzyl type bridges (Ph-CH_2-CH_2-Ph) (Gavalas, 1984).

The activation energy for the polymerization reaction, E_p, was estimated to be approximately 35.5 kcal/mole and was assumed to the same for all coal types. This value was obtained from using the relationship (Rempp and Merrill, 1986)

$$E_p = E\ (\text{propagation}) + 1/2\ E\ (\text{initiation}) - 1/2\ E\ (\text{termination}) \qquad (6.2\text{-}27)$$

with activation energies for propagation, initiation, and termination steps assumed to be about 7.3, 56.4 and 0 kcal/mole respectively (Gavalas, 1984). The propagation reaction was assumed to occur by a radical addition to an unsaturated side group of a phenyl molecule, initiation by ethylene bridge scission, and termination by recombination of two benzyl radicals. The estimated E_p is very close to the 35.3 kcal/mole reported by Serio (1984) for the vapor phase secondary reaction of the most reactive fraction of tar (preexponential factor = 1.43×10^8 s^{-1}, modeled as a first-order single reaction). Applying the same procedure gave k_{op} of about 10^{12} s^{-1}, but using this value greatly over-predicted the extent of polymerization. When k_{op} was allowed to be best-fitted from the data, values ranging from $10^{6.8}$ to $10^{7.3}$ s^{-1} were obtained for the six coals studied. Such a variation is small, and thus k_{op} was fixed at 10^7 s^{-1} for all six coals.

The experimental information required to estimate k_{oc} and E_c for intra-particle tar cracking reactions is currently not available. Using Serio's (1984) data on homogenous extra-particle tar cracking reactions from Pittsburgh Seam bituminous coal, gave k_{oc} and E_c to be about 10^{14} s^{-1} and 69 kcal/mole respectively [first-order single-

reaction model was assumed, see Howard (1981) for description]. Among the three different reactive tar fractions distinguished by Serio, the moderately reactive fraction data were used to compute the kinetic parameters. The reaction rate for the most reactive fraction is in the range of the polymerization reaction, and that for the least reactive fraction is virtually negligible at temperatures below 1000 C. When used in the extended MIPR model, the estimated rate parameters substantially under-predicted the extent of secondary tar cracking reactions, implying that the rate of cracking reactions inside the coal is possibly much faster than that outside. Preliminary tests showed that lowering E_{oc} to 55 kcal/mole gave good predictions on the extent of tar cracking reactions, and thus this value was assumed for all six coals.

The diffusivity inside the non-softening coal is assumed to be (Suuberg et al., 1979; Froment and Bischoff, 1979)

$$D_{g,eff} = e/\tau \; 0.1 \; (T/273)^{1.5} \; (1/P) \; cm^2/s \qquad (6.2\text{-}28)$$

where e is the internal void fraction and τ the tortuosity factor. Since no measured values of e and τ are readily available for different coals, the ratio e/τ is best-fitted from the experimental tar yield data. The diffusivity inside the softening coal is assumed to be (Oh, 1985; Reid et al.,1977)

$$D_L = D_{oL} \; (T/298) \; cm^2/s \qquad (6.2\text{-}29)$$

where D_{oL} is of order 10^{-5} to 10^{-7} (Oh, 1985; Suuberg and Sezen, 1985), and inversely related to a fractional power of the viscosity of the molten coal. The exact value of D_{oL} for a given coal was obtained from applying best-fit regression routines with the experimental tar data.

Figure 6.2-3 compares the experimental and predicted tar yields from the extended MIPR model for the six coals investigated in this study. Table 6.2-2 gives the values of model parameters used to make the predictions. The four parameters assumed to vary with coal type are V^*_{max}, E_{os}, σ_s, and e/τ or D_{oL}. The V^*_{max} was inputted with experimentally measured tar yield limit at vacuum ($\lesssim$ 0.001 atm), and the remaining three parameters were best-fitted from the experimental tar data. The parameters, k_{os}, k_{op}, E_p, k_{oc}, and E_c were assumed not to vary significantly among different coal types. This assumption was mainly made because information necessary to assign coal-type dependent values for these parameters is currently not available, but we do not imply that these parameters are truly constant for all coal types. Any errors generated from this assumption will affect the values of best-fitted parameters. If the error cannot be sufficiently compensated by the fitted parameters, then the error will be reflected in the model's predictive capability.

Figure 6.2-3 shows a good agreement between the experimental and predicted tar yields at all three pressures - 0.001, 1 and 10 atm. An important observation to be made from the figure is the accurate prediction of the yield limits over a wide range of pressures. This result is especially encouraging since, unlike the MIPR model, the maximum yields are predicted without having to rely on experimentally measured values at different pressures, i.e., the extended MIPR model does not need a pressure-specific Y^*. Also, the predicted behavior in which the rate is unaffected by pressure at fairly low temperatures ($\lesssim$ 550 C), and that the yields 'level-off' earlier (i.e., at lower

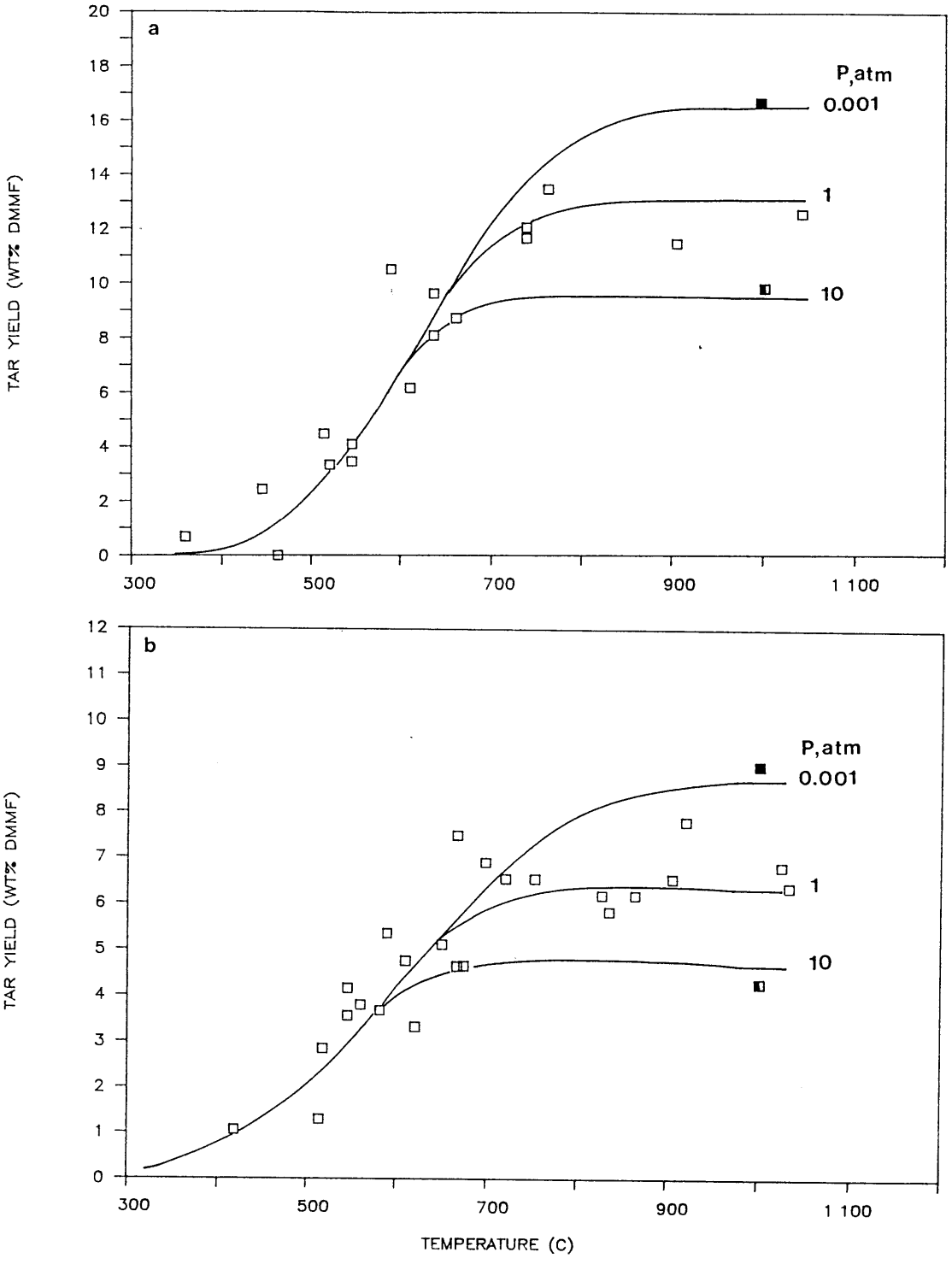

Figure 6.2-3 Tar yields versus peak temperatures. Symbols represent experimental data: ■ - 0.001 atm, □ - 1 atm, ◧ - 10 atm. Lines represent extended MIPR model predictions. 0.001 and 10 atm points represent averaged values from 1-3 runs. Coals: (a) LW, (b) ZP, (c) SR, (d) BL, (e) IL, (f) LK. Abbreviations: see Fig.6.1-1.

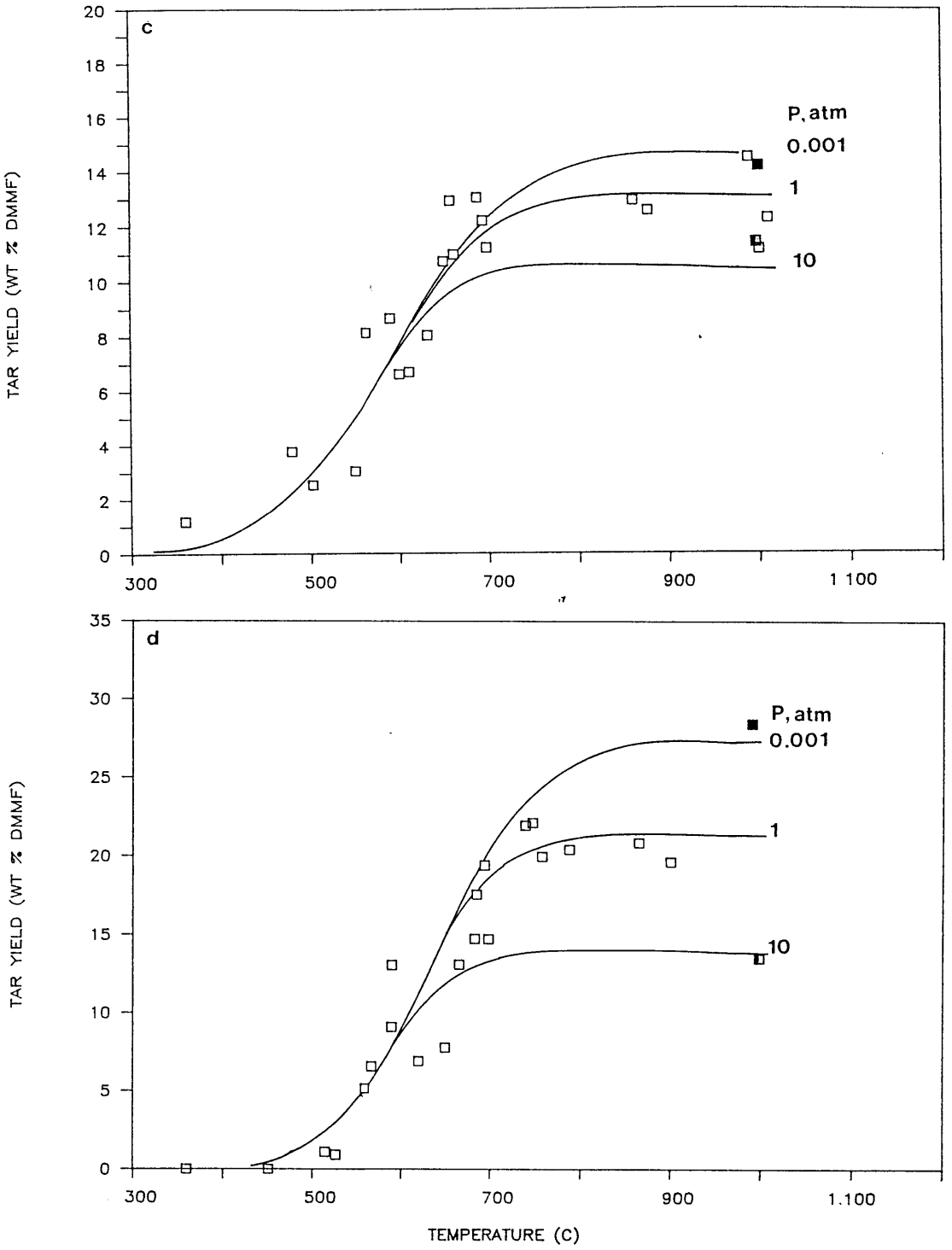

Figure 6.2-3 Tar yields versus peak temperatures. Symbols represent experimental data: ■ - 0.001 atm, □ - 1 atm, ◧ - 10 atm. Lines represent extended MIPR model predictions. 0.001 and 10 atm points represent averaged values from 1-3 runs. Coals: (a) LW, (b) ZP, (c) SR, (d) BL, (e) IL, (f) LK. Abbreviations: see Fig.6.1-1.

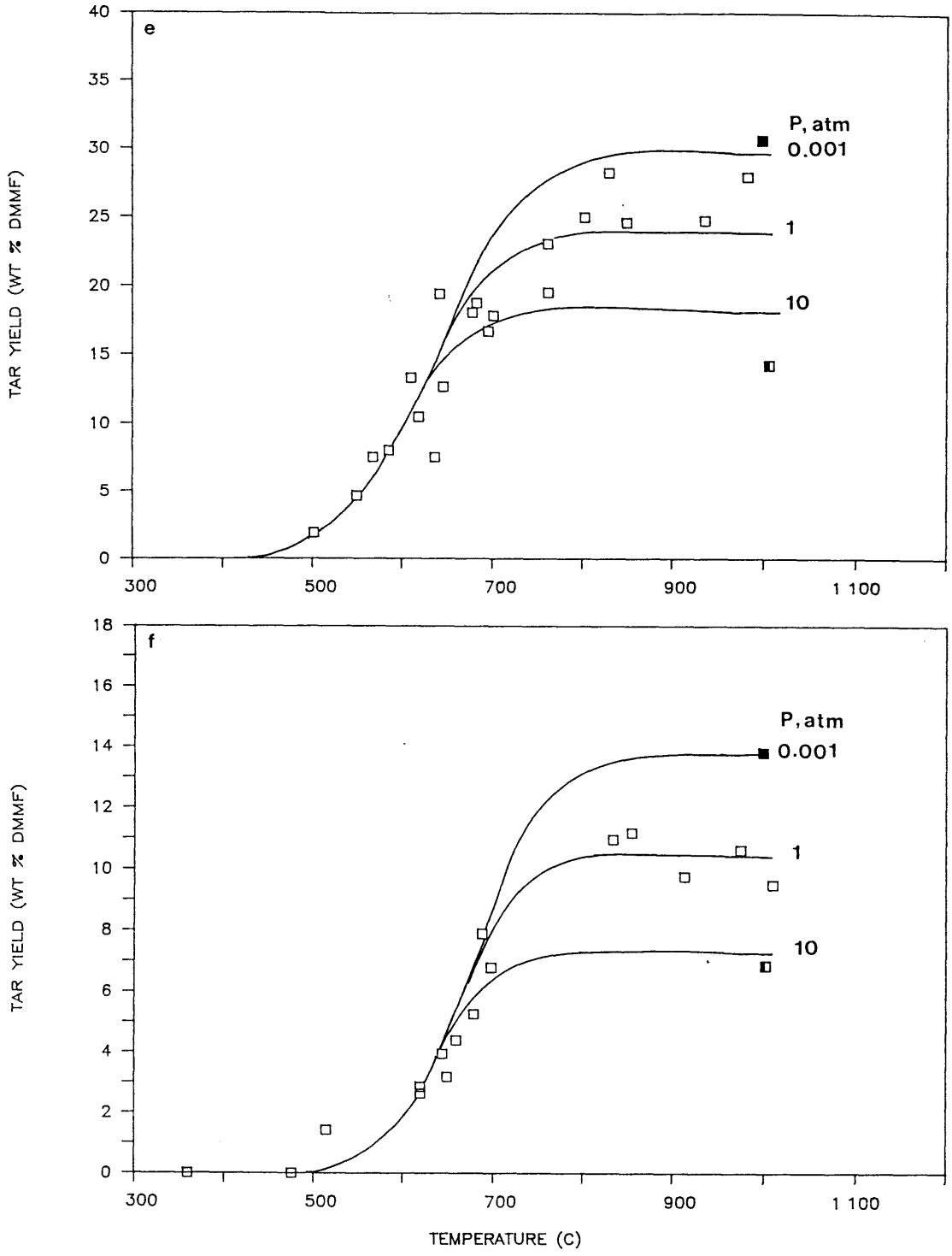

Figure 6.2-3 Tar yields versus peak temperatures. Symbols represent experimental data: ■ - 0.001 atm, □ - 1 atm, ◧ - 10 atm. Lines represent extended MIPR model predictions. 0.001 and 10 atm points represent averaged values from 1-3 runs. Coals: (a) LW, (b) ZP, (c) SR, (d) BL, (e) IL, (f) LK. Abbreviations: see Fig.6.1-1.

Table 6.2-2 Model parameters for the extended MIPR model.

(a) Coal-type dependent parameters:

Coal[a]	V^*_{max} wt% dmmf	E_{os} kcal/mole	σ_s kcal/mole	e/τ or	D_{oL}
Lower Wilcox L	16.8	53.8	7.0	$10^{-2.81}$	-
Beulah Zap L	9.1	52.8	9.4	$10^{-3.23}$	-
Smith Roland SB	14.8	51.7	6.3	$10^{-2.70}$	-
Blue HVB	27.7	54.6	5.3	$10^{-2.90}$	-
Illinois HVB	30.1	54.4	4.4	-	$10^{-5.67}$
Lower Kittanning LVB	14.0	56.8	3.5	-	$10^{-5.41}$

(b) Fixed parameters:

scission	k_{os}, s^{-1}	10^{14}	-	
polymerization	k_{op}, s^{-1}	10^{7}	E_p, kcal/mole	35.5
cracking	k_{oc}, s^{-1}	10^{14}	E_c, kcal/mole	55.0

[a] Coals are listed in the order of increasing elemental carbon contents in dmmf basis. Elemental analysis is given in Table 4.1-1.

temperatures) pressure is increased, closely resembles the experimentally observed behavior for tars [Suuberg (1977), Fig.3.3-5] and for total volatiles [Suuberg (1977), Fig.3.3-4a; Niksa (1981)].

Figure 6.2-4 helps to explain how the model works. The figure plots (a) $E_{p,avg}$, $E_{c,ns}$ and (b) $E_{p,avg}$, $E_{c,s}$ versus temperature, where $E_{p,avg} = \sum E_{p,i}\ f(E)\Delta E$. Recall that the rate of tar production for both non-softening [Eq.(6.2-22)] and softening coals [Eq.6.2-24)] is represented as the product of the total rate at which the non-x-linked fraction reacts and the two 'E' factors, and that the values of these E factors range between 0 and 1 [$E_{p,i}$, $E_{c,ns}$, $E_{c,s}$ are given in Eqs. (6.2-9), (6.2-23), (6.2-25) respectively]. The decrease in tar production at higher pressures is explained by the smaller $E_{c,ns}$ or $E_{c,s}$ as the pressure increases. At vacuum, $E_{c,ns}$ and $E_{c,s}$ are near 1 indicating negligible mass transport resistance; at high pressures ($\tilde{>}$ 10 atm), the values are much lower, indicating a substantial intra-particle transport resistance.

Another important feature of this model is that it is able to explain the experimentally observed heating-rate effects at vacuum and 1 atm. Recall from Section 3.3.4 that Niksa (1981) observed an increasing volatiles (implying tar) production at higher heating rates at vacuum, whereas Anthony (1974) and Suuberg (1977) observed negligible heating- rate effects at 1 atm. Figure 6.2-4 shows that the polymerization effect, indicated by $E_{p,avg}$, is more severe at lower temperatures. The non-x-linked fraction of coal reacts at higher temperatures as the heating rate is increased. Thus without mass transport effects, higher heating rates enhance tar production. At 1 atm, where mass-transport effects are not negligible, tars produced at

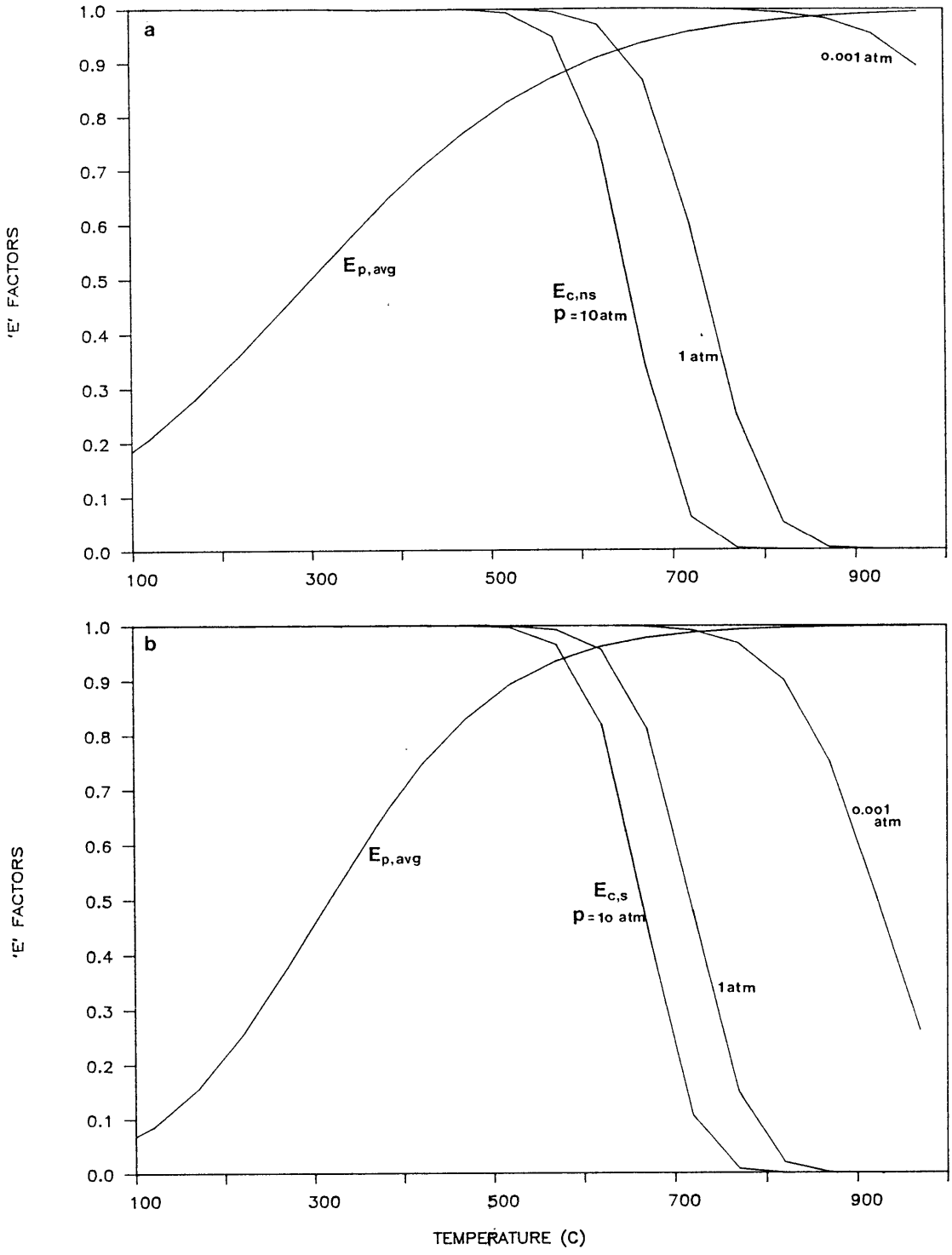

Figure 6.2-4 (a) $E_{p,avg}$ and $E_{c,ns}$ versus temperature for a non-softening coal (LW). (b) $E_{p,avg}$ and $E_{c,s}$ versus temperature for a softening coal (IL). $E_{p,avg} = \sum E_{p,i} f(E)\Delta E$, $E_{p,i}$ from Eq.(6.2-9), $E_{c,ns}$ and $E_{c,s}$ from Eqs. (6.2-23) and (6.2-25) respectively. Abbreviations: see Fig.6.1-1.

higher temperatures experience a greater extent of secondary tar cracking reactions. Thus, the increased tar production at higher temperatures is 'off-set' by more cracking reactions.

Figure 6.2-5 plots the best-fitted values of E_{os} and σ_s versus the elemental carbon contents of the coal. As before for the MIPR model (Fig.6.1-2), higher rank coals generally gave greater values of E_{os} and smaller values of σ_s, implying that bridging molecules of higher rank coals have bond dissociation energies with a greater mean and a narrower distribution. The noticeably larger E_{os} for LW compared to the other low-rank coals (ZP,SR), is more representative of higher rank coals (BL,IL); abbreviations are defined in Fig.6.1-1. A similar behavior has also been observed in describing the production of total volatiles using the MIPR model (Fig.6.1-10a). The higher σ_s for ZP among the low rank coals is similar to the trend observed in describing tar production using the MIPR model (Fig.6.1-2b), As discussed in Section 6.1.2, this may be a typical behavior for low-rank coals with small elemental hydrogen contents (<5wt% dmmf). For a given coal, the values of E_{os} are slightly but consistently greater than those of the global E_o for the MIPR model (tar). The difference is attributed to mass transport effects implicit in E_o, and confirms that the transport resistance at 1 atm is small but not negligible.

Figure 6.2-6 plots the best-fitted values of e/τ or D_{oL} versus the elemental carbon contents of the coal. For non-softening coals (LW,ZP, SR,BL), the best-fitted values of e/τ range from $10^{-3.23}$ to $10^{-2.70}$. These values imply that the tortuosity (τ) is about 100 assuming that the void fraction (e) is around 0.1. Such values for τ are at least an order of magnitude higher than typical values reported for porous

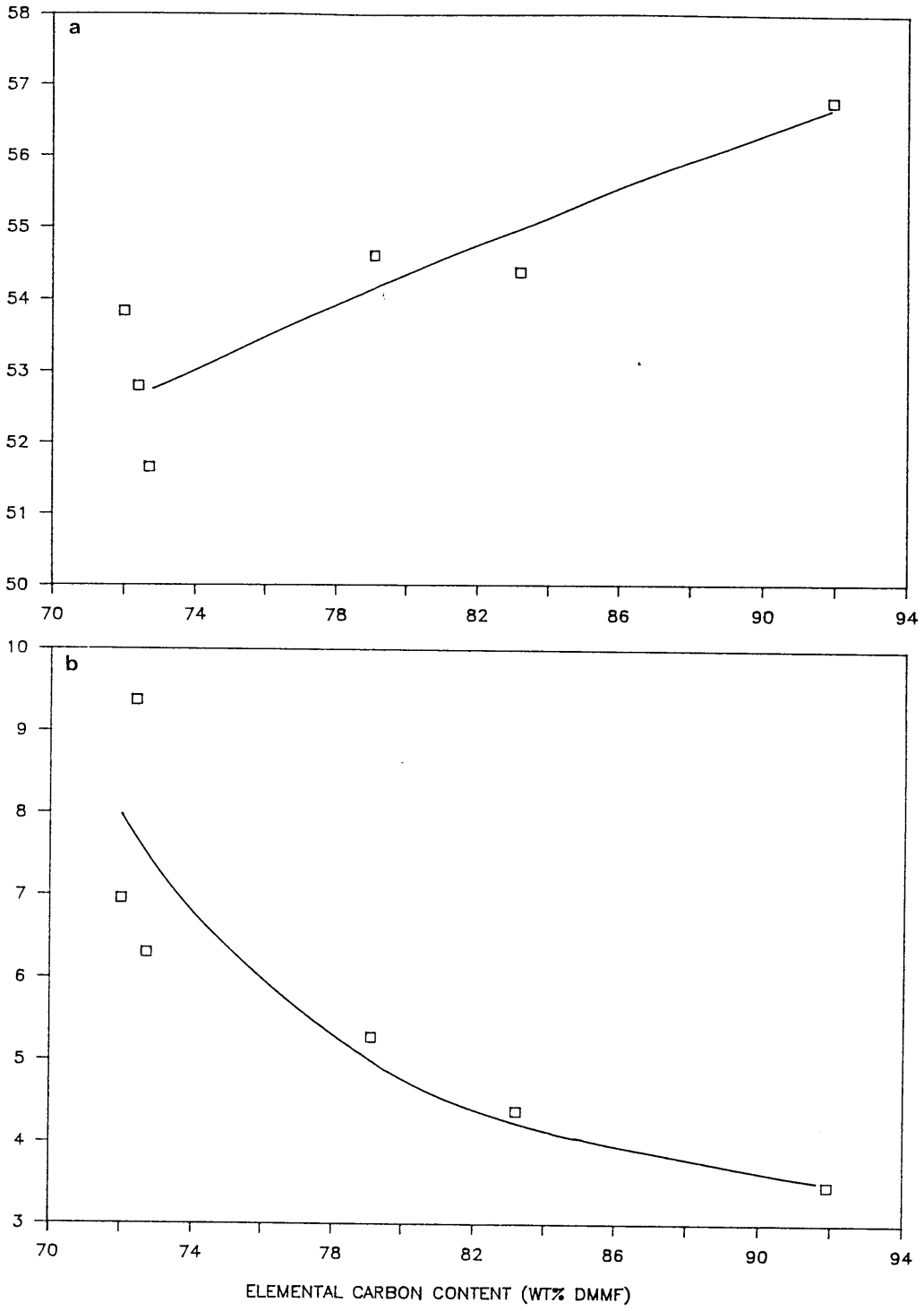

Figure 6.2-5 Best-fitted values E_{os} and σ_s for predicting tar evolution using the extended MIPR model versus the elemental carbon content of the coal. Carbon: LW < ZP < SR < BL < IL < LK. Abbreviations: see Fig.6.1-1. Other model parameters are given in Table 6.2.2.

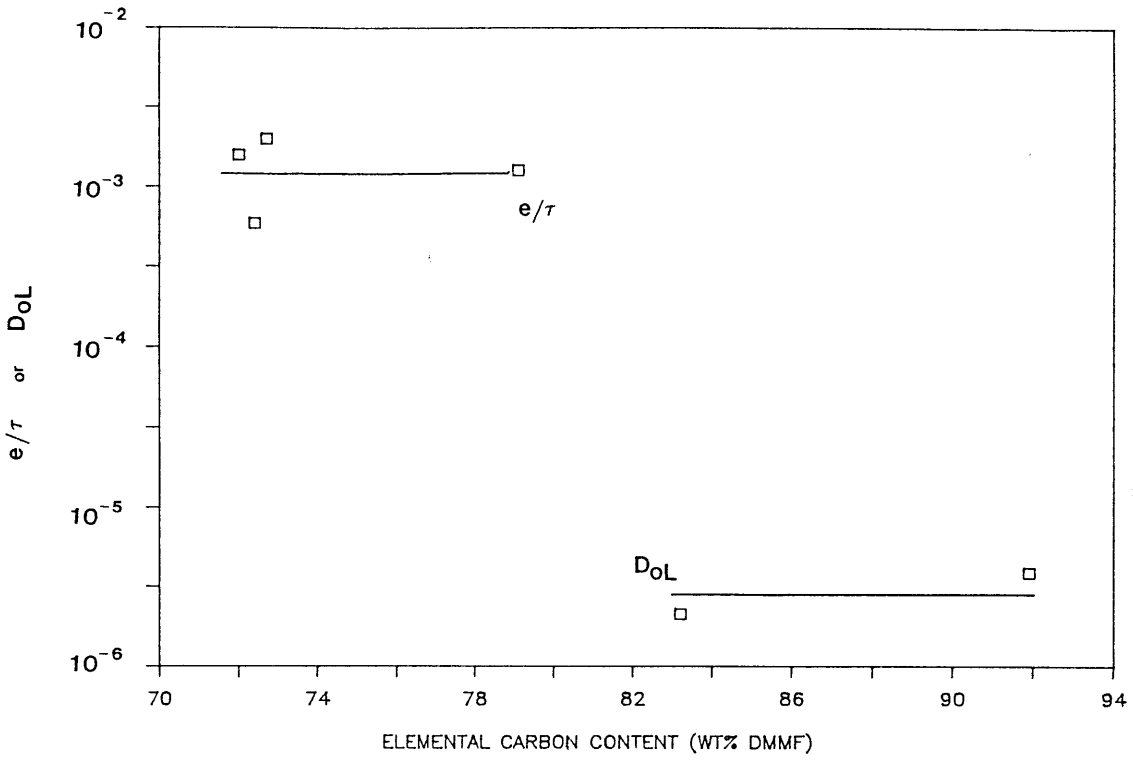

Figure 6.2-6 Best-fitted values of transport parameters for predicting tar evolution using the extended MIPR model versus the elemental carbon content of the coal. e/τ is for non-softening coals (LW,ZP,SR,BL), and D_{oL} is for softening coals (IL,LK). Carbon: LW < ZP < SR < BL < IL < LK. Abbreviations: see Fig.6.1-1. Other model parameters are given in Table 6.2.2.

solids (Froment and Bischoff, 1979). For softening coals (IL,LK), the best-fitted values of D_{oL} are between $10^{-5.41}$ and $10^{-5.67}$, which are within the range of expected values of $10^{-6\pm1}$. The best-fitted values of e/τ or D_{oL} assume that k_{oc} is about 10^{14} s^{-1}. Changing the value of k_{oc} will directly influence the values of the fitted transport parameters since the quantity that is actually fitted is the ratio $k_{oc}/(e/\tau)$ or k_{oc}/D_{oL}.

In applications employing coals other than those studied here, use of the model parameters obtained from the experimental data specific to the coal of interest would give the most reliable performance. If such experimental information is not available, use of the parameter values estimated from the coal-type dependent trends obtained in this study is expected to give the next best performance - Fig.6.2-5 for E_{os} and σ_s, and Fig.6.2-6 for e/τ or D_{oL}. As before for the MIPR model parameters, a note of caution in using the estimated values is that the trends were established from a fairly small number of coals (6), and thus there is a possibility that some 'unusual' coals may behave very differently from those studied here.

The objective of this study was to improve the understanding of coal-type effects in rapid coal pyrolysis. The experimental phase of this study examined the pyrolysis behavior of six coals ranging from lignites to low-volatile bituminous coals under conditions where mass transport resistances are small (1 atm pressure and $\tilde{<}$ 100 μm particle dia.). Selected high-temperature runs were also made at 0.001 and 10 atm. The modeling phase of this work derived kinetic information from the experimental data using the MIPR and extended MIPR models, and attempted to relate the kinetic information to measurable properties of the coal.

7.1. Conclusions

Tar production

1. Among the six coals studied, higher rank coals generally produced tars at higher temperatures, and over a narrower range of temperatures. Consequently, a larger mean and a narrower distribution of global activation energies were obtained using the MIPR model for coals of increasing rank.

2. High-volatile bituminous coals produced the most tar (21-25 wt% dmmf), followed by lignites and a subbituminous coal (7-13 wt% dmmf), and a low-volatile bituminous coal (11 wt% dmmf).

3. A quantitative correlation, developed to independently relate tar yield limits to coal type and pressure, was tested against a large set of experimental data representing a wide range of coals (37 coals, ranging from lignites to anthracites) and pressures ('vacuum' to 90 atm). Good agreement between the predicted and experimental yields

were obtained for all coals and pressures, with a standard error of estimate of ±3 wt% dmmf.

Gas production

4. In general, no discernable coal-type effects on the apparent rate of gas production were observed. A probable explanation for this is that variations in the rate caused by different coal types are comparable to those caused by uncertainties in experimental measurements. Consequently, kinetic parameters of the MIPR model parameters for measured gas species were only slightly affected by coal type.

5. Higher rank coals generally produced less carbon oxides and pyrolytic water, but more methane. The ethylene and ethane yields are small and their absolute yield values are less affected by coal type.

Total volatiles production

6. Total volatiles evolve at higher temperatures and over a narrower range of temperatures for higher rank coals. Thus as expected, a larger mean and a narrower distribution of global activation energies were obtained using the MIPR model for coals of increasing rank. The trends are consistent with the expected behavior from combining the observed coal-type effects on the rate of tar and gas production.

7. The total volatiles yield limit is fairly constant among the lignites, and subbituminous and high-volatile bituminous coals (41-55 wt% dmmf), but is significantly less for the low-volatile bituminous coal (22 wt% dmmf). The high-volatile bituminous coals produced significantly more reactive volatiles than other coals (38-45 versus

19-28 wt% dmmf); reactive volatiles are defined as total volatiles minus water and carbon dioxide yields.

Pressure effects

8. Increasing the pressure gave less tar and total volatiles for the coals investigated in this study. In absolute values, the pressure effect was more severe for coals that produced more tar.

Extended MIPR model

9. Predicted tar yields from the extended MIPR model agreed well with experimental values for a wide range of coal types (lignites to low-volatile bituminous coal; non-softening and softening) and pressures (0.001-10 atm).

10. For a given coal, the model requires just three adjustable input parameters (E_{os} and σ_s for bridge scission, and either a geometrical factor e/τ for non-softening coals or D_{oL} for softening coals), plus a quantity ,V^*_{max}, that is either directly obtained from experiment or estimated from the tar correlation developed in this study. The best-fitted values of E_{os} and σ_s for bridge scission are within the range of expected values for the scission of bibenzyl (Ph-CH_2-CH_2-Ph) type bridges. The best-fitted values of e/τ imply a tortuosity (τ) that is about an order of magnitude greater than typical values reported for porous solids, and those of D_{oL} are within the range of values reported in the literature.

7.2. Recommendations

1. More fundamental studies are recommended to improve the quantitative understanding of the coal structure, and the reaction mechanism in coal pyrolysis (e.g., studies using model compounds and chemically modified coals).

2. Analyze the MW and extract data collected in conjunction with this study to determine the effect of coal type on chemical changes of tar and extracts during pyrolysis.

3. Investigate the validity of the assumed relationship between the shell thickness of softening coals, and pressure and particle size [Eq.(6.2-26)].

4. Provide experimentally measured intra-particle tar secondary reaction rates to the extended MIPR model.

8. References

Anthony, D.B., "Rapid devolatilization and Hydrogasification of Pulverized Coal," Sc.D. Thesis, Dept. Chem. Eng., M.I.T., Cambridge, MA, 1974.

Anthony, D.B., Howard, J.B., Hottel, H.C., and Meissner, H.P., "Rapid Devolatilization of Pulverized Coal," Fifteenth Symp. (Int.) on Combustion, The Combustion Institute, Pittsburgh, 1303, 1974.

Arendt, P.A. and van Heek, K.J., "Comparative Investigations of Coal Pyrolysis Under Inert Gas and Hydrogen at Low and High Heating Rates and Pressures Up to 10 MPa," Fuel, 60, 779, 1981.

Bartle, K.D. and Jones, D.E., "NMR Spectroscopy" in Analytical Methods for Coal and Coal Products, Vol.2, Clarence Karr Jr., ed., 1978.

Bautista, J.R, "Time-Resolved Pyrolysis Product Distributions of Softening Coals," Ph.D. Thesis, Dept. Chem. Eng., Princeton University, Princeton, NJ, 1984.

Benjamin, B.M., Raaen, V.F., Maupin, P.H., Brown, L.L., and Collins, C.J., "Thermal Cleavage of Chemical Bonds in Selected Coal-related Structure," Fuel, 57, 269, 1978.

Benson, S.W., Thermochemical Kinetics, John Wiley, New York, 1976.

Bleik, A., van Poelje, W.M., van Swaaij, W.P.M., and van Beckum, F.P.H., "Effects of Intraparticle Heat and Mass Transfer During Devolatilization of a Single Coal Particle," AIChE J., 31, 1666, 1985.

Blom, 1960, taken from van Krevelen, D.S., Coal, Elsevier Publishing Co., Amsterdam, 1961.

Briunsma, O.S.L., Geertsma, R.S., R.S., Bank, P., and Moulijn, J.A., Fuel, 67, 327, 1988.

Burnham, A.K., Oh, M.S., and Crawford, R.W., "Activation Energy Distributions and Related Chemistry for Pyrolysis of the Argonne Premium Coals," submitted for publication in Energy and Fuels, 1988.

Calkins, W.H., Hagman, E., and Zaldes, H., "Coal Flash Pyrolysis 1. An Indication of the Olefin Precursors in Coal by CP/MAS ^{13}C NMR Spectroscopy," Fuel, 63, 113, 1984a.

Calkins, W.H., and Tyler, R.J., "Coal Flash Pyrolysis 2. Polymethylene Compounds in Low Temperature Flash Pyrolysis Tars," Fuel, 63, 1119, 1984b.

Calkins, W.H., "Coal Flash Pyrolysis 3. An Analytical Method for Polymethlylene Moieties in Coal," Fuel, 63, 1125, 1984c.

Calkins, W.H., Housepian, B.K., Dyrkez, G.R., Bloomquist, C.A.A., and Ruscic, L., "Coal Flash Pyrolysis 4. Polymethylene Moities in Coal

Macerals," Fuel, 63, 1226, 1984d.

Campbell, J.H., and Stephens, D.R. "Kinetic Studies of Gas Evolution During Pyrolysis of Subbituminous Coal," Am. Chem. Soc., Div. Fuel Chem. Prepr., 21 (7), 94, 1976.

Ciuryla, V.T., Weimer, R.F., Bivans, D.A., and Motika, S.A., "Ambient pressure thermogravimetric characterization of four different coals and their chars," Fuel, 58, 748, 1979.

Cosway, R.G., S.M. Thesis, Dept. Chem. Eng., M.I.T., Cambridge, MA, 1981.

Cypres, R., and Bettens, B., Tetrahedron, 1253, 30, 1974.

Cypres, R., and Bettens, B., Tetrahedron, 353, 31, 1975a.

Cypres, R., and Bettens, B., Tetrahedron, 359, 31, 1975b.

Darivakas, D.G., "Effects of Reaction Conditions and Pre-treatment Methods on Liquid Yields from Low Rank Coals," Ph.D. Thesis, Dept. Chem. Eng., M.I.T., Cambridge, MA, in preparation, 1988.

Deno, N.C., Curry, K.W., Jones, D.A., Keegan, K.R., Rakitsky, W.G., Ritcher, C.A., and Minard, R.D., "Linear Alkane Chains in Coals," Fuel, 60, 210, 1981.

Fong, W.S., "Plasticity and Agglomeration in Coal Pyrolysis," Sc.D. Thesis, Dept. Chem. Eng., M.I.T., Cambridge, MA, 1986.

Franklin, H.D., "Mineral Matter Effects in Coal Pyrolysis and Hydropyrolysis," Ph.D. Thesis, Dept. Chem. Eng., Cambridge, MA, 1980.

Franklin, H.D., Peters, W.A., Cariello, F., and Howard, J.B., "Effects of Calcium Minerals on the Rapid Pyrolysis of a Bituminous Coal," I&EC Proc. Des. & Dev., 20, 670, 1981.

Freihaut, J.D., and Seery, D.J., "An Investigation of Yields and Characteristics of Tars Released During the Thermal Decomposition of Coal," Am. Chem. Soc. Div. Fuel Chem. Prepr., 26 (2), 133. 1981.

Freihaut, J.D., Zabielski, M.F., and Seery, D.J., "A Parametric Investigation of Tar Release in Coal Devolatilization," Nineteenth Symposium (Int.) on Combustion, The Combustion Institute, Pittsburgh, 1159, 1982.

Froment, G.F., and Bischoff, K.B., Chemical Reactor Analysis and Design, John Wiley, New York, 1979.

Gan H., Nandi, S.P., and Walker Jr., P.L., "Nature of the Porosity in American Coals," Fuel, 51, 272, 1972.

Gavalas, G.R., and Wilks, K.A., "Intraparticle Mass Transfer in Coal Pyrolysis," AIChE J., 26, No.2, 201, 1980.

Gavalas, G.R., Cheong, P.H.K., and Jain, R., "Model of Coal Pyrolysis. 1.Qualitative Development," Ind. Eng. Chem. Fundam., 20, 113, 1981a.

Gavalas, G.R., Cheong, P.H.K., and Jain, R., "Model of Coal Pyrolysis. 2.Quantitative Formulation and Results," Ind. Eng. Chem. Fundam., 20, 122, 1981b.

Gavalas, G.R., Coal Pyrolysis, Elsevier Scientific Publishing Co., Amsterdam, 1984.

Gerstein, B.C., Murphy, P.D., and Ryan, L.M., "Aromaticity in Coal," in Coal Structure, R.A. Meyers, ed., Academic Press, New York, 1982.

Given, P.H., "The Organic Chemistry of Coal Macerals," Penn State Short Course on Coal, The Pennsylvania State University, June 1976.

Given, P.H., "What are the Important Characteristics of Coal?," Penn State Short Course on Coal, The Pennsylvania State University, Oct. 1977.

Griffin, T.P., "Intra-Particle Secondary Reactions in Coal Pyrolysis," Ph.D. Thesis, Dept. Chem. Eng., M.I.T., Cambridge, MA, in preparation 1988.

Hajaligol, M.R., Peters, W.A., and Howard, J.B., "Intra-Particle Heat Transfer Effects in Coal Pyrolysis," Energy and Fuels, in press 1988.

Hanbaba, P., Juntgen, H., and Peters, W., "Nicht-isotherme Reactionskinetik der Kohlenpyrolyse,Teil II. Erweiterung der Theorie der Gasabspaltung und Experimentelle Bestatigung an Steinkohlen," Brennstoff-Chemie, 49, 368-376, 1968.

Hirsch, P.B., "X-ray Scattering from Coals," Proc. Roy. Soc. London, A226, 143, 1954.

Howard, J.B.,"Fundamentals of Coal Pyrolysis and Hydropyrolysis," in Chemistry of Coal Utilization, 2nd Suppl. Vol., M.A. Elliott, ed., J. Wiley & Sons, New York, 1981.

Howard, J.B., Ko, G.H., and Peters, W.A., Quarterly Technical Progress Report submitted to DOE/METC, 1987a.

Howard, J.B., Fong, W.S., and Peters, W.A., "Kinetics of Devolatilization," in Fundamentals of the Physical-Chemistry of Pulverized Coal Combustion, Lahaye, J. and Prado, G., eds., Martinus Nijhoff Publishers, Dordrecht, 1987b.

Howard, J.B., Griffin, T.P., Ko, G.H., and Peters, W.A., "Fundamental Mechanisms of Coal Gasification", presented at the Eighth Annual Gasification and Gas Stream Cleanup Systems Contractors Review Meeting, 1988.

Hsu, J., Ph.D. Thesis, Dept. Chem. Eng., M.I.T., Cambridge, MA, in

preparation 1988.

Huston, J.L. and Studier, M.H., "Aromaticities of Various Coals Measured by Reaction with Fluorine and TGA-DTA studies of the Reaction Products," Fuel, 60, 1149, 1981.

Ignasiak, B.S. and Gawlak, M., "Polymeric Structure of Coal. 1.Role of Ether Bonds in Constitution of High-Rank Vitrinite," Fuel, 56, 216, 1977.

Jacab, E., McClennen, W.H., Hoesterey, B., Meuzelaar, H.L.C., and Hill G.R., "Weathering Effects on Yield and Composition of Pyrolytic Coal Tars," Am. Chem. Soc. Div. Fuel Chem. Prepr., 30 (3), 137, 1985.

Juntgen, H. and van Heek, K.H., "Research in the Field of Pyrolysis at Bergbau-Forschung during the Last Fifteenth Years," presented at the Meeting on Coal Fundamentals, Stoke Orchard, England, 1977.

Kerr, J.A. and Parsonage, M.J., Evaluated Kinetic Data on Gas Phase Hydrogen Transfer Reactions in Methyl Radicals, Butterworths, London, 1976.

Ko, G.H., Peters, W.A., Howard, J.B., "Correlation of Tar Yields from Rapid Pyrolysis with Coal Type and Pressure," Fuel, 66, 1118, 1987.

Ko, G.H., Peters, W.A., and Howard, J.B., "Comparison of Tar Evolution Rate Predictions in Coal Pyrolysis from Multiple Independent Parallel Reaction Model and Functional Group Model Over a Wide Range of Heating Rates," Energy and Fuels, in press 1988a.

Ko, G.H., Sanchez, D.M., Peters, W.A., and Howard, J.B., "Application of First-Order, Single-Reaction Model for Coal Devolatilization Over a Wide Range of Heating Rates," Am. Chem. Soc. Div. Fuel Chem. Prepr., 33 (2), 112, 1988b.

Ko, G.H., Sanchez, D.M., Peters, W.A., and Howard, J.B., "Correlations for Effects of Coal Type and Pressure on Tar Yields from Rapid Devolatilization," Twenty-Second Symposium (Int.) on Combustion, in press 1988c.

Kobayashi, H., Howard, J.B., and Sarofim, A.F., "Coal Devolatilization at High Temperatures," Sixteenth Symp. (Int.) on Combustion, The Combustion Institute, Pittsburgh, 411, 1977.

Kwan, J.T. and Yen, T.F., "Aromaticity Determination of Coal, Oil Shale and their Derivatives by X-Ray Diffraction," Am. Chem. Soc. Div. Fuel Chem. Prepr., 21 (7), 67, 1976.

Lewellen, P.C., "Product Decomposition Effects in Coal Pyrolysis," S.M. Thesis, Dept. Chem. Eng., M.I.T., Cambridge, MA, 1975.

Loison, R. and Chauvin, F., "Pyrolyse Rapide Du Charbon," Chem.Ind., (Paris), 91, 269, 1964.

Maiorella, B.L., "Behavior of Liquid Subbituminous Coal Tars Upon Heating, as it Relates to In-Situ Gasification," S.B. Thesis, Dept. Chem. Eng., M.I.T., Cambridge, MA, 1978.

Mason, E. A. and Malinauskas, A.P., "Gas Transport in Porous Media: The Dusty Gas Model." Chem. Eng. Monograph 17, Elsevier, Amsterdam, 1983.

Mayo, F.R., Huntington, J.B., and Kirshen, N.A., "Chemistry of Coal Liquefaction," in Organic Chemistry of coal, J.W. Larsen, ed., Am. Chem. Symposium Series No. 71, Am. Chem. Soc., 126, 1978.

Neavel, R.C., Smith, S.E., Hippo, E.J., and Miller, R.N., "Optimum Classification of Coals," Proc. of Int. Conf. on Coal Science, Dusseldorf, 1-9, Sept.1981.

Neoh, K.G. and Gannon, R.E., "Coal Volatile Yield and Element Partition in Rapid Pyrolysis," Fuel, 63, 1347, 1984.

Niksa, S.,"Time-Resolved Kinetics of Rapid Coal Devolatilization," Ph.D. Thesis, Dept. Chem. Eng., Princeton University, Princeton, NJ, 1981.

Niksa, S. and Kerstein, A.R., "The Distributed-Energy Chain Model for Rapid Coal Devolatilization Kinetics. Part I: Formulation, Part II: Transient Weight Loss Correlations," Sandia National Lab. Report, SAND84-8870, 1985.

Oh, M.S., "Softening Coal Pyrolysis," Sc.D. Thesis, Dept. Chem. Eng., M.I.T., Cambridge, MA, 1985.

Oh, M.S., Peters, W.A., and Howard, J.B., "A Mathematical Model of Softening Coal Pyrolysis," AIChE J., submitted for review for publication, 1988.

Peters, W.A., "Studies of the Pyrolysis Behavior of Condensed Phase Fuels with Applications to Fuel Conversion Technology," in Proc., Fifth Int. Symp. on Analytical Pyrolysis, K.J. Voorhees, ed., Butterworths, Borough Green, Seven Oaks, England, 340, 1984.

Peters, W. and Bertling, H., "Kinetics of the Rapid Degasification of coals," Fuel, 44, 317, 1965.

Poutsma, M.L., "Free Radical Model for Coal Conversions: Effect of Conversion Level and Concentration on Thermolysis of Bibenzyl," Fuel, 59, 535, 1980.

Reid, R.C., Prausnitz, J.M., and Sherwood, T.K., The Properties of Gases and Liquids, 3rd ed., McGraw-Hill, New York, 1977.

Reitzen, R.G., S.M. Thesis, Dept. Chem. Eng., M.I.T., Cambridge, MA, 1978.

Remmp, P. and Merrill, E.W., Polymer Synthesis, Huethig & Wepf Verlag,

Basel, 1986.

Retcofsky, H.L., Hough, M.R., Maguire, M.M., and Clarkson, R.B., Adv. Chem. Ser., 192, 37, 1981.

Retcofsky, H.G., "Magnetic Resonance Studies of Coal," in Coal Science, Vol.1, M.L. Gorbaty, J.W. Larsen, I. Wender, eds., 43, 1982.

Russel, W.B., Saville, D.A., and Greene, M.I., "A Model for Short Residence Time Hydropyrolysis of Single Coal Particles," AIChE J., 25, Vol.1, 65, 1979.

Sanchez, D.M., S.B. Thesis, Dept. Chem. Eng., M.I.T., Cambridge, MA, in preparation 1988.

Serio, M.A., "Secondary Reactions of Tar in Coal Pyrolysis," Ph.D. Thesis, Dept. Chem. Eng., M.I.T., Cambridge, MA, 1984.

Serio, M.A., Hamblen, D.G., Markham, J.R., and Solomon, P.R., "Kinetics of Volatile Product Evolution in Coal Pyrolysis: Experiment and Theory," Energy & Fuels, 1, 138, 1987.

Simons, G.A. and Finson, M.L., "The Structure of Coal Chars. 1: Pore Branching," Combst. Sci. and Tech., 19, 227, 1979.

Singer, J.G., Combustion Fossil Power Systems, Combustion Engineering, Inc., Windsor, CT, 1981.

Solomon, P.R. and Colket, M.B., "Coal Devolatilization," Seventeenth Symposium (Int.) on Combustion, The Combustion Institute, Pittsburgh, 113, 1978.

Solomon, P.R., Hamblen, D.G., and Carangelo, R.M., "Coal Pyrolysis," presented at AIChE meeting, New Orleans, Nov. 1981.

Solomon, P.R., Hamblen, D.G., Carangelo, R.M., and Krause, J.L., "Coal Thermal Decomposition in an Entrained Flow Reactor: Experiments and Theory," Nineteenth Combustion Symposium (Int.), The Combustion Institute, Pittsburgh, 1139, 1982.

Solomon, P.R. and Hamblen, D.G., Pyrolysis, in Chemistry of Coal Conversion, R.H. Schlosberg, ed., Plenum Press, N.Y., 1985.

Sprouse, K.M. and Schuman, M.D., "Predicting Lignite Devolatilization with the Multiple Parallel and Two-Competing Reaction Models," Combustion and Flame, 43, 265-271, 1981.

Stein, S.E. and Golden, D.M., J. Org. Chem., 42, 839, 1977.

Stein, S.E., "A Fundamental Chemical Kinetics Approach to Coal Conversion," in New Approaches in Coal Chemistry, Blaustein, B.D., Bockrath, B.C., Friedman, S., eds., Am. Chem. Soc. Symp. Ser. 169, 1981.

Stein, S.E., "Free radicals in Coal Conversion," in Chemistry of Coal Conversion, Schlosberg, R.H., ed., Plenum Publishing Co., 1985.

Stein, S.E., private communication, 1988.

Sung, W.F., "The Study of the Swelling Property of Bituminous Coal," S.M. Thesis, Dept. Chem. Eng., M.I.T., Cambridge, 1978.

Suuberg, E.M., "Rapid Pyrolysis and Hydropyrolysis of Coal," Sc.D. Thesis, Dept. Chem. Eng., M.I.T., Cambridge, MA, 1977.

Suuberg, E.M. and Sezen, Y., "Competitive Reaction and Transport Processes in Coal Pyrolysis," Proc. 1985 Int. Conf. Coal Science, Sydney, 913, 1985.

Suuberg, E.M., Lee, D., and Larsen, J.W., "Temperature dependence of crosslinking processes in pyrolysing coals," Fuel, 64, 1668, 1985.

Suuberg, E.M., "Mass Transfer Effects in Pyrolysis of Coals: A Review of Experimental Evidence and Models," in Chemistry of Coal Conversion, R.H. Schlosberg, ed., Plenum Press, New York, 1985.

Suuberg, E.M., Unger, P.E., and Larsen, P.E., "Relation between Tar and Extractables Formation and Cross-Linking during Coal Pyrolysis," Energy and Fuels, 1, 305, 1987.

Tingey, G.L. and Morrey, J.A., "Coal Structure and Reactivity," a Batelle Energy Program Report, Batelle Pacific Northwest Laboratories, Richland, WA, 1973.

Unger, P.E. and Suuberg, E.M., "Modelling the Devolatilization Behavior of a Softening Bituminous Coal," Eighteenth Symp. (Int.) Combustion, Pittsburgh, The Combustion Institute, 1203, 1981.

Unger, P.E. and Suuberg, E.M., Am. Chem. Soc. Div. Fuel Chem. Prepr. 28 (4), 278, 1983.

Unger, P.E. and Suuberg, E.M., "Molecular weight distributions of tars produced by flash pyrolysis of coals," Fuel, 63, 606, 1984.

Van Krevelen, , D.W., Coal, Elsevier Publishing Co., Amsterdam, 1961.

Weimer, R.F., and Ngan, D.Y., "Rates of Light Gas Production by Devolatilization of Coal and Lignite," Am. Chem. Soc. Div. Fuel Chem. Prepr., 24 (3), 129, 1979.

Whitehurst, D.D., "A Primer on the Chemistry and Constitution of Coal," in Organic Chemistry of Coal, J.W. Larsen, ed., Am. Chem. Soc. Symposium Series No. 71, Am. Chem. Soc., 1, 1978.

Whitehurst, D.D., Mitchell, T.O., and Farcasio, M., Coal Liquefaction-The Chemistry and Technology of Thermal Processes, Academic Press, New York, 1980.

Winans, R.E., Hayatsu, R., McBeth, R.L., Scott, R.G., and Botto, R.E., "Aromatic Structures in Whole Coals and Coal Macerals," Am. Chem. Soc., Div. Fuel Chem. Prepr., 33 (1), 407, 1988.

Wornat, M.J., "Pyrolysis-Induced Changes in the Composition of Polycyclic Aromatic Compounds from a Bituminous Coal," Ph.D. Thesis, Dept. Chem. Eng., M.I.T., Cambridge, MA, 1988.

Yarzab, R.F., Abdul-Baset, Z., and Given, P.H., "Hydroxyl Contents of Coals: New Data and Statistical Analysis," Geochim. et Cosauo Chim. Acta., 43, 281, 1980.

Yoshida, T., Tokuhashi, K., Narita, H., Hasegawa, Y., and Maekawa, Y., "Determination of Ether Oxygen in Coals by Carbon -13 CP/MAS NMR Spectrometry and Acetylation," Fuel, 63, 282, 1984.

Zacharias, M.W., "Analysis of Product Yields from Rapid Pyrolysis of Bituminous Coal," S.M. Thesis, Dept. Chem. Eng., M.I.T., Cambridge, MA, 1979.

APPENDIX 1: EXPERIMENTAL DATA

Note: 1. All data are in wt% dmmf basis.
2. Vacuum and 10 atm runs represent averaged values of 1-3 runs.

Coal type: Lower Kittanning

Atmospheric peak temperature runs:

T (C)	total wt. loss	tar	CO	CH_4	CO_2	C_2H_4	C_2H_6
476	0.0	0.0	0.00	0.00	0.00	0.00	0.00
644	4.6	4.0	0.09	0.11	0.16	0.02	0.10
678	4.6	5.3	0.12	0.05	0.55	0.02	0.02
659	10.6	4.4	0.07	0.10	0.15	0.02	0.04
732	10.6	-	0.15	0.93	0.36	0.16	0.30
975	19.4	10.6	0.66	3.23	0.55	0.67	0.53
840	-	-	0.20	1.41	0.35	0.31	0.44
913	20.3	9.8	0.36	3.09	0.45	0.48	0.56
1009	17.3	9.5	-	-	-	-	-
854	21.4	11.2	-	-	-	-	-
619	1.0	2.9	-	-	-	-	-
619	0.9	2.6	-	-	-	-	-
649	4.3	3.2	-	-	-	-	-
218	0.1	1.0	-	-	-	-	-
267	0.0	0.0	-	-	-	-	-
359	0.7	0.0	-	-	-	-	-
514	4.2	1.4	-	-	-	-	-
698	10.5	6.8	-	-	-	-	-
688	11.3	7.9	-	-	-	-	-
834	17.0	11.0	-	-	-	-	-

Atmospheric holding temperature runs (5 s hold):

T (C)	total wt. loss	tar	CO	CH_4	CO_2	C_2H_4	C_2H_6
850	23.1	10.7	0.90	4.17	0.42	-	0.62
950	21.2	10.4	0.94	4.34	0.43	0.55	0.59
1050	20.5	10.2	0.91	4.32	0.41	0.56	0.58
850	24.0	9.1	-	-	-	-	-
920	22.6	10.0	-	-	-	-	-
1050	24.2	10.5	-	-	-	-	-

0.001 atm runs (total wt. loss and tar only):

T (C)	total wt. loss	tar
1000	22.0	14.0

10 atm runs (total wt. loss and tar only):

T (C)	total wt. loss	tar
1000	21.1	7.2

Coal type: Lower Wilcox

Atmospheric peak temperature runs:

T (C)	total wt. loss	tar	CO	CH_4	CO_2	C_2H_4	C_2H_6
463	3.2	0.0	0.12	0.04	0.54	0.01	0.01
611	19.5	-	0.46	0.05	2.73	0.04	0.01
650	19.7	-	0.64	0.09	3.28	0.08	0.03
668	26.0	-	1.28	0.21	5.05	0.19	0.09
837	41.9	-	3.69	1.13	7.59	1.04	0.31
824	43.5	-	3.31	1.14	7.21	1.05	0.31
1042	53.2	12.5	8.45	1.90	8.23	1.60	-
760	40.0	-	1.14	0.36	-	0.45	0.13
827	42.4	-	2.00	0.95	6.56	0.76	0.21
906	53.4	11.5	4.92	1.23	6.74	0.69	0.22
520	10.3	3.3	-	-	-	-	-
445	10.3	2.4	-	-	-	-	-
545	10.4	3.5	-	-	-	-	-
545	6.5	4.1	-	-	-	-	-
661	17.8	8.7	-	-	-	-	-
739	37.6	11.7	-	-	-	-	-
739	35.9	12.1	-	-	-	-	-
267	1.5	0.0	-	-	-	-	-
359	1.5	0.7	-	-	-	-	-
514	13.9	4.5	-	-	-	-	-
590	27.2	10.5	-	-	-	-	-
763	44.7	13.5	-	-	-	-	-
636	16.4	8.1	-	-	-	-	-
636	19.5	9.6	-	-	-	-	-
610	10.0	6.2	-	-	-	-	-

Atmospheric holding temperature runs (5 s hold):

T (C)	total wt. loss	tar	CO	CH_4	CO_2	C_2H_4	C_2H_6
850	52.5	11.8	10.76	1.79	9.68	1.47	0.28
950	52.9	13.2	12.40	2.17	8.81	1.76	0.26
1050	52.0	12.6	11.81	1.99	8.58	1.42	0.26
850	50.1	13.0	-	-	-	-	-
1000	57.1	11.9	-	-	-	-	-
900	49.9	13.2	-	-	-	-	-

0.001 atm runs (total wt. loss and tar only):

T (C)	total wt. loss	tar
1000	56.8	16.8

10 atm runs (total wt. loss and tar only):

T (C)	total wt. loss	tar
1000	48.5	9.9

Coal type: Beulah Zap

Atmospheric peak temperature runs:

T (C)	total wt. loss	tar	CO	CH_4	CO_2	C_2H_4	C_2H_6
419	8.5	1.1	0.11	0.00	1.15	0.00	0.00
581	13.0	3.7	0.39	0.04	2.87	0.01	0.01
650	23.5	5.1	1.48	0.31	6.11	0.12	0.07
753	34.9	6.6	2.36	0.64	6.65	0.26	0.13
836	36.9	5.8	3.14	0.82	7.77	0.45	0.17
833	38.9	-	4.26	1.18	8.98	0.48	0.23
1024	45.4	6.8	6.95	1.45	9.29	0.75	0.21
906	41.5	6.6	3.49	0.90	-	0.55	0.21
674	26.9	4.7	0.71	0.15	4.68	0.10	0.06
1032	47.3	6.4	6.69	1.36	10.76	0.62	0.25
827	36.2	6.2	1.65	0.80	6.21	0.31	0.14
920	46.6	7.8	6.10	1.44	9.11	0.11	0.19
518	13.9	2.9	-	-	-	-	-
648	28.6	-	-	-	-	-	-
864	41.3	6.2	-	-	-	-	-
545	-	4.2	-	-	-	-	-
545	10.8	-	-	-	-	-	-
545	10.4	3.6	-	-	-	-	-
621	16.5	3.3	-	-	-	-	-
667	-	4.6	-	-	-	-	-
720	28.7	6.6	-	-	-	-	-
359	2.4	-	-	-	-	-	-
514	6.7	1.3	-	-	-	-	-
590	20.6	5.4	-	-	-	-	-
698	31.4	6.9	-	-	-	-	-
881	40.5	-	-	-	-	-	-
610	20.4	4.8	-	-	-	-	-
559	16.8	3.8	-	-	-	-	-
667	32.6	7.5	-	-	-	-	-

Atmospheric holding temperature runs (5 s hold):

T (C)	total wt. loss	tar	CO	CH_4	CO_2	C_2H_4	C_2H_6
850	45.1	7.1	9.02	1.60	11.00	0.76	0.24
950	46.3	6.9	9.27	1.48	8.07	0.62	0.17
1050	45.7	6.1	11.52	1.74	9.63	0.74	0.19
850	50.1	13.0	-	-	-	-	-
1000	57.1	11.9	-	-	-	-	-
900	49.9	13.2	-	-	-	-	-

0.001 atm runs (total wt. loss and tar only):

T (C)	total wt. loss	tar
1000	51.2	9.1

10 atm runs (total wt. loss and tar only):

T (C)	total wt. loss	tar
1000	41.3	4.1

Coal type: Blue

Atmospheric peak temperature runs:

T (C)	total wt. loss	tar	CO	CH_4	CO_2	C_2H_4	C_2H_6
451	1.0	0.0	0.09	0.00	0.58	0.00	0.00
589	15.9	9.1	0.51	0.13	1.75	0.07	0.07
665	21.4	13.1	0.84	0.32	2.09	0.16	0.13
682	20.5	14.8	1.12	0.48	2.73	0.26	0.22
1024	47.8	-	6.74	2.76	4.40	2.02	0.46
850	49.1	-	4.17	2.11	2.64	1.57	0.55
787	40.6	20.5	2.13	1.22	2.95	0.89	0.45
526	1.9	0.9	0.19	0.01	1.22	0.00	0.00
746	46.4	22.2	-	-	-	-	-
757	43.0	20.0	-	-	-	-	-
900	47.2	19.7	-	-	-	-	-
559	11.0	5.2	-	-	-	-	-
567	10.0	6.6	-	-	-	-	-
693	36.2	19.5	-	-	-	-	-
684	34.3	17.6	-	-	-	-	-
864	45.6	20.9	-	-	-	-	-
619	-	6.9	-	-	-	-	-
649	-	7.8	-	-	-	-	-
739	36.7	22.0	-	-	-	-	-
359	0.6	0.0	-	-	-	-	-
514	2.6	1.1	-	-	-	-	-
590	20.3	13.1	-	-	-	-	-
698	32.9	14.7	-	-	-	-	-
610	29.4	-	-	-	-	-	-
662	32.2	-	-	-	-	-	-

Atmospheric holding temperature runs (5 s hold):

T (C)	total wt. loss	tar	CO	CH_4	CO_2	C_2H_4	C_2H_6
850	48.1	23.3	6.16	2.40	3.43	1.20	0.52
950	48.4	21.4	6.87	2.79	3.57	1.68	0.47
1050	48.8	19.9	7.31	2.62	3.61	1.47	0.49
850	48.4	19.7	-	-	-	-	-
920	45.8	22.1	-	-	-	-	-
1050	44.9	21.7	-	-	-	-	-

0.001 atm runs (total wt. loss and tar only):

T (C)	total wt. loss	tar
1000		27.7

10 atm runs (total wt. loss and tar only):

T (C)	total wt. loss	tar
1000		14.5

Coal type: Smith Roland

Atmospheric peak temperature runs:

T (C)	total wt. loss	tar	CO	CH_4	CO_2	C_2H_4	C_2H_6
457	5.5	-	0.10	0.00	0.90	0.00	0.00
562	18.3	8.2	0.82	0.13	3.17	0.07	0.05
692	28.4	-	1.24	0.28	3.93	0.16	0.10
656	-	12.9	1.30	0.38	5.02	0.18	0.15
666	28.5	-	1.22	0.29	4.05	0.17	0.11
877	47.3	12.6	3.72	1.39	6.18	1.09	0.37
1000	50.0	11.2	4.78	1.50	-	1.05	0.27
827	48.1	-	4.83	1.60	5.05	1.06	0.34
802	44.7	-	3.21	1.16	6.48	0.87	0.35
687	35.7	13.0	1.23	0.30	4.95	0.20	0.15
502	11.1	2.5	0.07	0.01	0.60	0.00	0.00
1009	49.5	12.3	5.45	1.88	7.35	1.11	0.46
549	13.7	3.1	-	-	-	-	-
631	31.2	8.1	-	-	-	-	-
693	43.8	12.2	-	-	-	-	-
988	48.7	14.5	-	-	-	-	-
860	46.9	12.9	-	-	-	-	-
599	15.9	6.6	-	-	-	-	-
649	24.5	10.7	-	-	-	-	-
661	30.4	11.0	-	-	-	-	-
359	3.9	1.2	-	-	-	-	-
478	8.1	3.8	-	-	-	-	-
590	21.6	8.7	-	-	-	-	-
698	30.5	11.2	-	-	-	-	-
610	20.4	6.7	-	-	-	-	-

Atmospheric holding temperature runs (5 s hold):

T (C)	total wt. loss	tar	CO	CH_4	CO_2	C_2H_4	C_2H_6
850	49.6	10.5	10.40	2.15	8.55	1.28	0.35
950	47.1	11.1	9.35	2.18	7.39	1.30	0.30
1050	48.8	12.5	10.13	2.19	8.04	1.46	0.33
850	50.9	12.8	-	-	-	-	-
920	51.2	11.7	-	-	-	-	-
1050	49.8	11.7	-	-	-	-	-

0.001 atm runs (total wt. loss and tar only):

T (C)	total wt. loss	tar
1000	51.8	14.8

10 atm runs (total wt. loss and tar only):

T (C)	total wt. loss	tar
1000	46.6	11.1

Coal type: Illinois #6

Atmospheric peak temperature runs:

T (C)	total wt. loss	tar	CO	CH_4	CO_2	C_2H_4	C_2H_6
701	32.6	17.9	0.53	0.44	1.11	0.17	0.23
677	28.7	18.1	0.74	0.40	0.52	0.14	0.20
849	39.7	24.6	1.71	1.50	1.29	0.63	0.53
936	53.3	24.8	3.16	2.54	1.80	0.91	0.60
913	54.5	-	2.52	2.25	1.36	1.89	0.63
802	40.1	25.0	0.7	1.29	1.40	0.52	0.50
987	48.4	26.7	2.60	2.74	1.72	1.01	0.63
982	48.9	27.9	3.50	3.13	1.79	0.91	0.60
761	36.1	23.0	0.53	0.84	1.29	0.32	0.38
502	-	1.9	0.00	0.00	0.00	0.00	0.00
567	8.4	7.5	-	-	-	-	-
695	23.6	16.7	-	-	-	-	-
645	-	12.7	-	-	-	-	-
586	-	8.0	-	-	-	-	-
549	7.9	4.7	-	-	-	-	-
619	14.6	10.5	-	-	-	-	-
761	33.5	19.5	-	-	-	-	-
636	-	7.5	-	-	-	-	-
610	16.8	13.3	-	-	-	-	-
641	33.9	19.4	-	-	-	-	-
682	25.5	18.8	-	-	-	-	-
829	40.9	28.2	-	-	-	-	-

Atmospheric holding temperature runs (5 s hold):

T (C)	total wt. loss	tar	CO	CH_4	CO_2	C_2H_4	C_2H_6
850	48.3	26.4	3.20	3.32	1.73	0.80	0.71
950	49.4	-	3.82	3.40	2.02	0.91	0.69
1050	49.1	25.9	-	-	-	-	-
850	50.7	24.5	-	-	-	-	-
920	51.2	24.7	-	-	-	-	-
1050	53.3	-	-	-	-	-	-

0.001 atm runs (total wt. loss and tar only):

T (C)	total wt. loss	tar
1000	56.5	30.1

10 atm runs (total wt. loss and tar only):

T (C)	total wt. loss	tar
1000	47.4	15.0